# Identification and functional characterisation of potassium channels in mouse GI tract

**Ruolin Ma**

The thesis is submitted in partial fulfilment of the requirements for the award of the degree of Doctor of Philosophy of the University of Portsmouth

University of Portsmouth

School of Pharmacy and Biomedical Science

January 2019

# Abstract

Gastrointestinal (GI) motility disorders such as irritable bowel syndrome (IBS) occur when coordinated smooth muscle contractile activity is disrupted. Although much is known about the ionic conductances responsible for GI smooth muscle contraction, comparably little is known about the underlying potassium ($K^+$) channels responsible for suppressing smooth muscle contractility and promoting GI tract relaxation. Using a mouse model, quantitative real-time PCR was used to establish the expression profiles of 93 $K^+$ channel α- and β-subunit genes in ileum and colon. Immunostaining of selected $K_{2P}$ channel proteins, informed from the qPCR, revealed distinctive expression patterns. Specifically, the mechano-gated $K_{2P}$ channel, mTREK-1, was exclusively localised to smooth muscle of ileum and colon whereas the expression of related TREK-2 and TRAAK channel proteins was limited to enteric neurons. To assess the contribution of these $K^+$ channels to the regulation of longitudinal smooth muscle tone, ileum and colon tissues were exposed to a variety of $K_{2P}$ channels modulators including BL-1249, CDC and riluzole using an organ bath preparation. Activation of mechano-gated $K_{2P}$ channels resulted in significant relaxation of both KCl and CCh pre-contracted ileum and colon tissues and reduced the amplitude of spontaneous contractions. Relaxation occurred in the presence of TTX, indicating a direct smooth muscle action of the $K_{2P}$ modulators. Given their prominent role in determining GI tract smooth muscle contractility, mouse homologues of the mechano-gated subfamily of channels were investigated further. Cloned mouse TREK-1, TREK-2 and TRAAK channels exhibited similar biophysical properties to their human homologues, with comparable sensitivity to well-known $K_{2P}$ activators AA, CDC and BL-1249. In contrast to previous findings, I reveal the proposed TREK-1 blocker, spadin, to possess the pharmacological

characteristics of an antagonist. Spadin specifically antagonised the activation of cloned TREK-1 channels by the polyunsaturated fatty acid, arachidonic acid (AA), but not by other pharmacological activators. The generation of a chimera with the spadin insensitive mTREK-2 channel indicated that the mechanism of action of spadin does not involve the C-terminus directly, and likely works via an allosteric mechanism distinct from the AA binding site. This study has provided a new insight into the potassium channel subtype expression profile and function in mouse intestine, and highlights the mechano-gated $K_{2P}$ channel TREK-1 as a potential target for future drug development treating hypermotility GI disorders.

# Table of Contents

# Declaration

Whilst registered as a candidate for the above degree, I have not been registered for any other research award. The results and conclusions embodied in this thesis are the work of the named candidate and have not been submitted for any other academic award.

Thesis Word Count: 50,213

# List of Tables

## Chapter 1



## Chapter 2



## Chapter 3



## Chapter 5

# List of Figures

## Chapter 1



## Chapter 2

## Chapter 3



## Chapter 4

## Chapter 5



## Chapter 6

# Glossary of Terms

| | |
|---|---|
| 4-AP | 4-aminopyridine |
| 5-HT | Serotonin |
| AA | Arachidonic Acid |
| AC | Adenylate cyclase |
| ACh | Acetycholine |
| AChE | acetylcholinesterase |
| AD | Alzheimer's disease |
| AH | After-hyperpolarization |
| ANS | Autonomic nervous system |
| ATP | Adenosine Triphosphate |
| $Ba^{2+}$ | Barium |
| BK | Big conductance $K^+$ channel |
| $Ca^+$ | Calcium ion |
| cAMP | cyclic adenosine monophosphate |
| CB | Calbindin |
| CDC | Cinnamyl 1-3,4-dihydroxy-alpha-cyanocinnamate |
| cDNA | Complimentary Deoxyribose Nucleic Acid |
| ChAT | Choline acetyltransferase |
| ChTX | Charybdotoxin |
| CNS | Central nervous system |
| CR | Calretinin |

| | |
|---|---|
| CRH | Corticotropin-releasing hormone |
| DA | Dopamine |
| DAG | Diacyl glycerol |
| DHA | cis-4,7,10,13,16,19-Docosahexaenoic acid |
| DHP | Dihydropyridine |
| DMSO | Dimethyl sulfoxide |
| DPPs | dipeptidyl aminopeptidase-related proteins |
| dNTP | Deoxyribose Nucleoside Triphosphates |
| DRG | Dorsal root ganglion |
| EDTA | Ethylenediaminetetraacetic acid |
| ENS | Enteric nervous system |
| $E_{Rev}$ | Reversal potential |
| FFA | Flufenamic acid |
| GC | Guanylyl cyclase |
| GHK | Goldman-Hodgkin Katz |
| GI | Gastrointestinal |
| IBD | Inflammatory bowel disease |
| IbTX | Iberiotoxin |
| IBS | Irritable bowel syndrome |
| ICCs | Interstitial cells of Cajal |
| IK | Intermediate conductance $K^+$ channel |
| $IP_3$ | inositol 1,4,5-trisphosphate |
| IPANs | Intrinsic primary afferent neurons |

| | |
|---|---|
| $K^+$ | Potassium ion |
| KChIPs | Cytoplasmic $K_v$ channel interacting proteins |
| $K_{ir}$ | Inwardly Rectifying potassium Channel |
| KO | Knock out |
| $K_{rev}$ | $K^+$ reversal potential |
| $K_v$ | Voltage-gated potassium channel |
| $K_vS$ | electrically silent $K_v$ channels |
| $K_{2P}$ | Two-pore potassium channel |
| LB | Lysogeny Broth |
| LQT2 | Cardiac long QT syndrome |
| MLC | Myosin light chains |
| MLCK | Myosin light chain kinase |
| mRNA | Messenger ribonucleic acid |
| ms | Millisecond |
| mV | Millivolts |
| NA | Noradrenaline |
| $Na^+$ | Sodium ion |
| NCX | $Na^+/Ca^{2+}$ exchanger |
| NO | Nitric oxide |
| NOS | Nitric oxide synthase |
| PCR | Polymerase chain reaction |
| $PIP_2$ | Phosphatidylinositol 4,5-bisphosphate |
| PKA | Protein kinase A |

| | |
|---|---|
| PNS | Peripheral nervous system |
| PUFA | Polyunsaturated fatty acids |
| qRT-PCR | Quantitative reverse-transcriptase polymerase chain reaction |
| RMP | Resting membrane potential |
| RT-PCR | Reverse-transcription polymerase chain reaction |
| SD | Standard deviation |
| SDK | stretch-dependent potassium channel |
| SEM | Standard error of the mean |
| SERCA | sarcoplasmic/endoplasmic reticulum $Ca^{2+}$ ATPase |
| SK | Small conductance $K^+$ channel |
| SNS | Somatic nervous system |
| SR | Sarcoplasmic reticulum |
| SSRI | Selective serotonin reuptake inhibitors |
| TALK | Alkaline-activated $K_{2P}$ |
| TASK | Acid-sensitive $K_{2P}$ |
| TBS-Tx | Tris-buffered saline with Triton |
| TEA | Tetraethylammonium |
| TEVC | Two-electrode Voltage Clamp |
| THIK | Halothane-inhibited $K_{2P}$ |
| TM | Transmembrane spanning domains |
| TRAAK | TWIK-related arachidonic acid $K^+$ channel |
| TREK | TWIK-related $K^+$ channel 1 |
| TTX | Tetrodotoxin |

| | |
|---|---|
| VDCC | Voltage-dependent calcium channels |
| VIP | Vasoactive intestinal peptide |
| WT | Wild type |

# Acknowledgements

I would like to thank my supervisor Dr Anthony Lewis for his endless patience and support through these 4 years. Thanks you for believing in me and giving me the chance to fulfil my dream of becoming a researcher. Your guidance and encouragement has been truly invaluable, but I owe you a lot more than just this PhD, thank you for everything. I would also like to thank Dr Jerome Swinny and Dr James Brown, for all their help and guidance through my PhD.

Secondly I would like to express my immense gratitude to all members of my family, especially to my parents, my husband and my cousin. Without their love and support over the years none of this would have been possible. They have always been there for me and I am grateful for everything they have helped me achieve.

I would also like to thank my best friends and colleagues in my office. Mo, Ryan, Louise, Maria, Torquil, Arianna, Noor and Salman, thank you for your words of encouragement when experiments refused to comply and for being a constant source of amusement. You are all truly remarkable people and it has been a pleasure spending these years with you guys.

Moreover, I would like to thank bioresources unit staff, Scott Rodaway, Andy Milner, Angela Scutt, Alan Jafkins and Gretel Nicholson, as well as the pharmacology technicians, Stewart Gallacher, for all their help over the last four years.

Last but not least, thank you for reading my thesis, I worked really hard on it. You're either my supervisors, my viva examiners, a new student continuing my research, or just an extremely bored individual, but thanks anyway.

# Dissemination

## Publication

***Ma R***, Seifi M, Papanikolaou M, Brown JF, Swinny JD, Lewis A (2018). TREK-1 Channel Expression in Smooth Muscle as a Target for Regulating Murine Intestinal Contractility: Therapeutic Implications for Motility Disorders. Frontiers in physiology 9: 157.

## Manuscript in preparation

***Ma R***, et al. Spadin selectively antagonises arachidonic acid activation of mTREK-1 channels

## Conference presentations

1. *Oral Presentations*
    - Sep 2018, Europhysiology 2018, London, UK
    - July 2017, IBIS day, Portsmouth, UK (Best talk winner)
2. *Poster Presentations*
    - Dec 2015, British pharmacology 2015, London, UK
    - July 2016, Physiological society 2016, Dublin, Ireland
    - April 2017, Experimental Biology 2017, Chicago, US

# Chapter 1 – General Introduction

## 1.1 Gastrointestinal (GI) tract

### 1.1.1 Anatomy and function of the GI tract

The Gastrointestinal (GI) tract, also called the digestive tract, is a continuous pathway encompasses several organs within multicellular animals that allows the mixing and propulsion of intraluminal contents to enable efficient digestion of food, a progressive absorption of nutrients, and finally an excretion of residues. These functions are achieved through a series of organs with distinct roles from mouth to anus (**Figure 1.1**) (Greenwood-Van Meerveld et al., 2017). The mouth, also known as the oral cavity, is the beginning of the GI tract. There are many accessory organs such as tongue, teeth and salivary glands that results in the initial phase of food digestion. Teeth masticate the food into small pieces, moistened by saliva before the tongue and other muscles push the food into the pharynx. The oesophagus is a muscular tube that takes the food bolus from the pharynx to the stomach. The major role of the stomach is firstly to act as a storage tank for holding food, but also to churn and break down food particles using hydrochloric acid and digestive enzymes secreted from the stomach wall to continue the process of digestion of food. The rest of non-liquefiable remnants are released from the stomach and pass through the small intestines to be eliminated (Tortora and Derrickson, 2009). The small intestine can be anatomically subdivided into three distinct regions, including duodenum, jejunum and ileum, which are principally responsible for digestion and absorption, a process incorporating both physical and chemical mechanisms, and almost 90% of digestion and absorption occurs here. Moreover, the digestive enzymes used in small intestine are released by the pancreas and bile from the liver, which both organs act as the accessory organ of GI tract. The large intestine is the last part of our digestive system, containing

proximal colon and distal colon, which are primarily concerned with desiccation and compaction of waste, with storage in the sigmoid colon and rectum prior to elimination (Cheng et al., 2010).

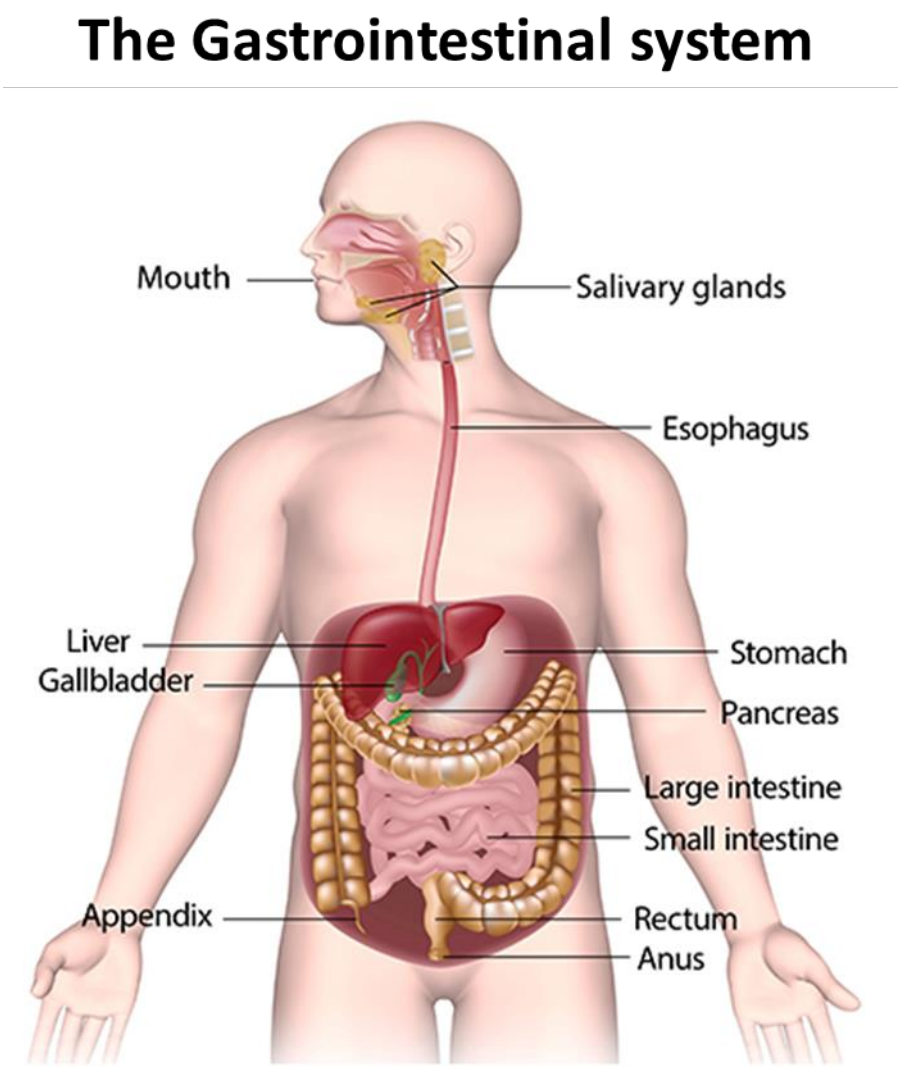


**Figure 1.1:** The anatomy of human GI tract**.**

### 1.1.2 Histology of the GI tract

There are four layers of tissue in the GI tract, including mucosa, submucosa, muscularis and serosa (**Figure 1.2**). The mucosa is a mucous membrane making up the innermost layer of

the gut wall, lining the entire GI tract and can be subdivided into epithelium, lamina propria and muscularis mucosa. The epithelium in the small intestine and large intestine are composed of simple columnar epithelial cells. The intestinal gland (also called intestinal crypt) are found in the intestinal epithelium and contains multiple types of the cells: stem cell, Paneth cell, goblet cell, Tuft cell, enterocytes and enteroendocrine cells. These cells secrete mucous and enzymes such as cholecystokinin and secretin, and other bio-chemicals such as anti-microbial peptides that either protect the mucosa or aid in digestion (Clevers, 2013). The submucosa is a connective tissue layer containing blood vessels, lymphatic vessels, submucosal glands and the submucosal plexus (also called the Meissner's plexus). The submucosal plexus is a network of nerves derived from the myenteric plexus, containing neuronal cells that influence the contraction and relaxation of the circular smooth muscle. The muscularis is a muscle layer consists of an outer longitudinal and an inner circular muscle layer (Reed and Wickham, 2009), sandwiching another nerve network called the myenteric plexus (also known as the Auerbach's plexus) which coordinates muscularis smooth muscle contractility (Furness et al., 2014). In addition, interstitial cells of Cajal (ICC), also known as pacemaker cells, are located around the circumference of the myenteric plexus, and through communication with enteric neurons and smooth muscle cells induce propagating electrical slow wave potentials leading to smooth muscle depolarisation, and thus helping to regulate the phasic contractile activity of GI smooth muscle that underlies peristalsis (Al-Shboul, 2013). The outermost layer of the gut wall is the serosa (or adventitia) containing a layer of connective tissue and a layer of cells that secrete serous fluid in order to reduces friction from muscle movement.

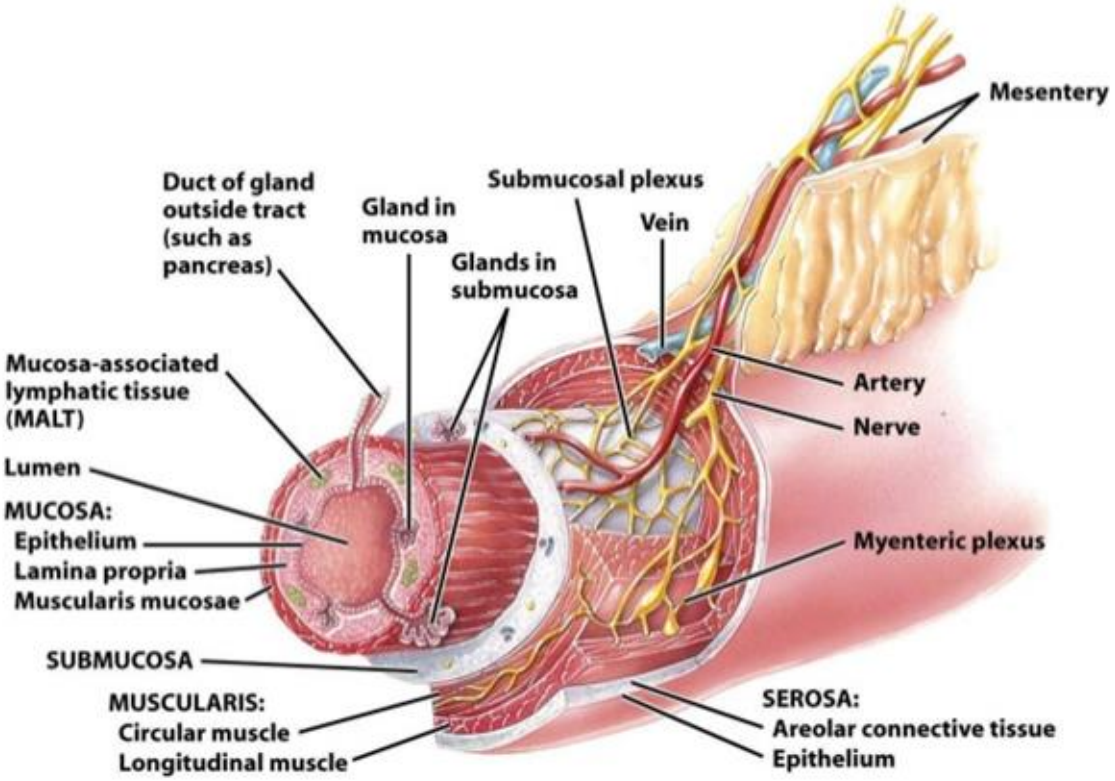


**Figure 1.2:** Diagram shows the layers of the GI tract identifying the sub-parts of the mucosa, submucosa, muscularis and serosa (Adapated from Tortora and Derrickson, 2009).

## 1.2 Enteric nervous system (ENS)

In vertebrates the nervous system consists of two main anatomical subdivisions, the central nervous system (CNS) and the peripheral nervous system (PNS). The CNS encompasses the brain and spinal cord, whereas the PNS can be divided into three subsystems; the somatic nervous system (SNS), the autonomic nervous system (ANS) and the enteric nervous system (ENS). The ENS is the largest and most complex unit of the PNS, and is the only substantial grouping of neurons that form a nervous system to generate activity independent of the CNS, unlike other autonomic neurons whose functions rely on signals transmitted from the CNS. Therefore, ENS is also referred to as the ‘‘second brain’’ in the body (Wood et al., 1999). However, ENS activity can be modulated by the CNS through the

influence of parasympathetic and sympathetic inputs. It is this coordinated bidirectional communication of the CNS and the ENS which is largely responsible for the neuronal control of GI motility and its secretory activity (Rao and Gershon, 2018).

Many properties of the ENS resemble the CNS and the conceptual model is the same (**Figure 1.3**). Similar to the CNS, the ENS consists of three major types of neurons which form neuronal microcircuits; sensory neurons (also referred to as intrinsic primary afferent neurons (IPANs)), interneurons and motor neurons. Sensory neurons have receptor regions responsible for detecting thermal, mechanical or chemical stimuli and translating them into signals, coded by action potentials, to other points in the nervous system. Interneurons are linked by synapses into networks that process information received from sensory neurons and control the kinetics of motor neurons. Motor neurons will finally transmit the response signal to the effector systems by initiating appropriate reflex control of motility, secretion and blood flow (Furness, 2007). This diverse ENS neuronal network innervates the GI tract, and thus provides the intrinsic neuronal control and integration of virtually all GI functions. As such, dysregulation of the ENS has been shown to be implicated in multiple GI disorders, such as Irritable Bowel Syndrome (IBS), gastroparesis and chronic intestinal pseudo-obstruction (Rao and Gershon, 2016). Furthermore, the ENS also communicates with many other cell types beyond muscular and secretory cells types, such as intestinal epithelial, endocrine and immune cells, to influence gut motility, intestinal infection and even in sites distal from an initial pathogen entry (Rao and Gershon, 2018).

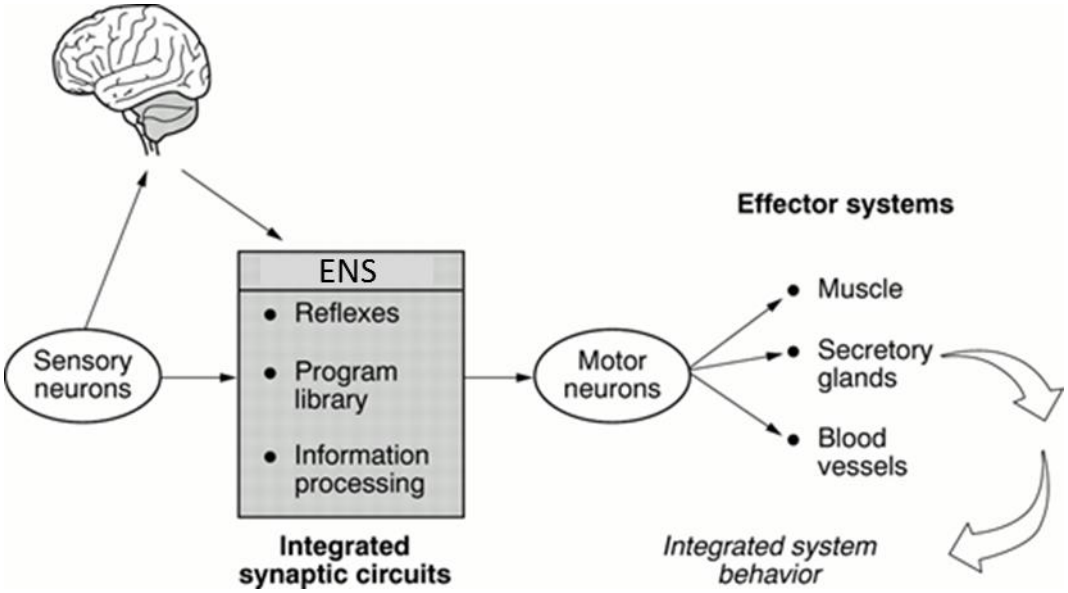


**Figure 1.3:** The conceptual model for the ENS is analagous to the CNS. Sensory neurons, interneurons and motor neurons are connected synaptically to form neuronal microcircuits. Information flow from sensory neurons to interneuronal integrative networks to motor neurons to effector systems ( Adapated from Wood et al., 1999).

### 1.2.1 Anatomy of the ENS

A vast amount of neurons are contained in the ENS, estimated to range between 200-600 million cells in humans, which are required for programmatic control of GI functions, and is comparable with the number of neurons estimated in the spinal cord (Furness, 2007, Wood, 2012). The ENS of the GI tract is formed of a number of interconnected signalling networks containing neurons, axons and enteric glial cells which are positioned inside the muscle wall of the GI tract. These neurons and glial cells are generally grouped into clusters, known as enteric ganglia, which in turn are connected by fibre tracts to form ganglionated plexuses. Interganglionic fibre tracts contain projections from ganglion cell bodies in one ganglion that connect synaptically with neurons in neighbouring ganglia (Furness, 2008). Moreover, the cell bodies of ENS neurons are not like other autonomic ganglia which form

in grape-like clusters, they can be observed histologically to lay edge-to-edge like a single layer of coins in a 2-dimensional plane (Hanani et al., 1998).

There are two major plexus in the ENS, the myenteric plexus located between the longitudinal and circular muscle layers, and the submucosal plexus located between the circular muscle and mucosa layer (**Figure 1.4**) (Furness, 2007). The network of the myenteric plexus is continuous around the circumference and along the GI tract, providing the neural regulation of contractions for both the longitudinal and circular smooth muscles, and thus primarily involved in the physiology of GI motility. In addition, most of the motor neurons that innervate the circular and longitudinal muscles cells which are located in the myenteric plexus (Brookes, 2001). Conversely, ganglion cells in the submucosal plexus mainly supply motor innervation to epithelial cells, secretory glands, blood vessels and inflammatory cells in the epithelial layer and also to the smooth muscle layer in the muscularis mucosae. As such, the submucosal plexus is mainly responsible for providing the neural regulation of mucosal function in the GI tract (Kunze and Furness, 1999). Furthermore, the submucosal plexus and myenteric plexus form an interplexus connection and reciprocally project to one another. For example, neurons in myenteric plexus project synaptic input from axons to the submucosal plexus, meanwhile received the fibres projecting from the submucosal plexus (Wood, 2012).

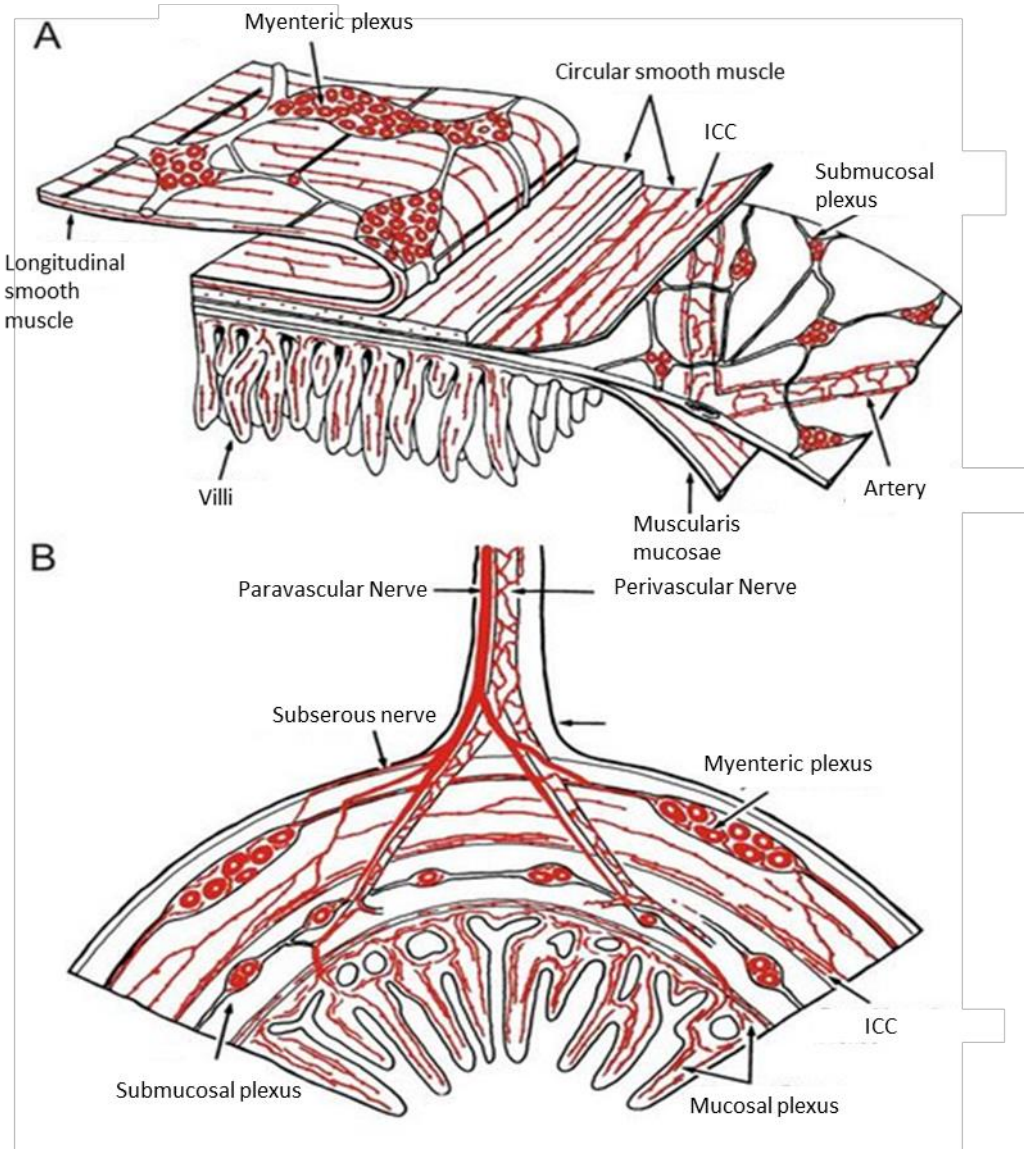


**Figure 1.4:** Anatomy of the enteric nervous system. Representation of the ENS in whole-mount section **(A)** and cross sections **(B)** ( Adapated from Furness, 2007).

## 1.2.2 Types of neurons in the ENS

The ENS of humans consists of over 500 million neuron cells which make it the largest collection of neurons outside of brain (Furness, 2007). ENS neurons are diverse in terms of their combinations of features, such as morphology, neurochemical properties and functional activities. ENS neurons with distinct roles in GI function can be classified as 1) excitatory and inhibitory motor neurons, 2) interneurons and 3) Intrinsic primary afferent

neurons (IPANs), based on their morphologies, their projections, and the primary neurotransmitters they utilise (**Figure 1.5 and Table 1.1**).

All the enteric neurons can be first sub-divided into 2 types by their morphology: Dogiel type I and Dogiel type II, as described by Jan von Dogiel in 1899 (Furness et al., 1998). Both types are present within the submucosal plexus as well as the myenteric plexus. Neurons with lamellar dendrites and a single axon are known as Dogiel type I neurons, which have been associated with motor neurons and interneurons. In contrast, Dogiel type II neurons have large round or oval cell bodies and multiple long axons and processes, which are processed by IPANs (Furness et al., 1998, Clerc et al., 1998, Costa et al., 2000).

Over 30 functionally distinct types of neurons have been discovered which communicate using more than 25 different neurotransmitters in ENS. Neurotransmitters are a type of chemical messenger which transmit signals across a chemical synapse from one neuron to another ‘‘target cell’’ such as neuron, smooth muscle cell or gland cell, and affect gut motility, nutrient absorption, GI innate immune system, and the microbiome. (Mittal et al., 2017). Moreover, the mechanism of chemically regulated synaptic transmission in the ENS is seemingly as complex as in the CNS. Enteric neurotransmitters include small molecules (e.g. acetylcholine (ACh) and glutamate), the mono-amine (e.g. noradrenaline (NA), serotonin (5-HT) and dopamine (DA)), large molecules (vasoactive intestinal peptide (VIP)), and gaseous signalling molecules (nitric oxide (NO) and carbon monoxide) (Lomax and Furness, 2000, Hansen, 2003). In general, neurons that secrete ACh and substance P (SP) are excitatory, which stimulate smooth muscle contraction, increase intestinal secretions,

release enteric hormones, and dilate blood vessels. In contrast, neurons that secrete NO and VIP are inhibitory, which stimulate smooth muscle relaxation (Nezami and Srinivasan, 2010).

Enteric neurons are also classified in terms of their function. IPANs function as sensory neurons and together with endocrine and immune cells establish a surveillance network which is essential for controlling digestion, the sensation of pain and energy and fluid homoeostasis in ENS (Holzer, 2002). Electrophysiological studies using intracellular recordings of myenteric neurons of the guinea-pig ileum indicate that there are two physiologically distinct enteric neuronal cell-types known as S (synaptic) and AH (after-hyperpolarization) neurons (Hirst et al., 1974, Nishi and North, 1973). IPANs are thought to be AH neurons, which as a component of the action potential is carried by $Ca^{2+}$ and a delayed and longer lasting after-hyperpolarizing (AHP) potential. Relatively, interneurons and motor neurons are known as S neurons, which have relatively high excitability and classified as tonically firing and are followed by a fast AHP (Furness, 2000, Smith et al., 1999). Regarding interneurons, there is one type of ascending and three types descending interneurons which have been characterised in the small intestine (**Table 1.1**), of which most are the descending type. Unlike descending interneurons which are associated with a complex of neurotransmitters including 5-HT, ACh, NO and VIP, ascending interneurons are mainly cholinergic (Kunze and Furness, 1999, Hansen, 2003). Finally, excitatory and inhibitory muscle motor neurons receive innervation signals from ascending or descending interneurons, leading to neurotransmitter release, provoking contraction or relaxation of longitudinal and circular smooth muscles (**Figure 1.5**).

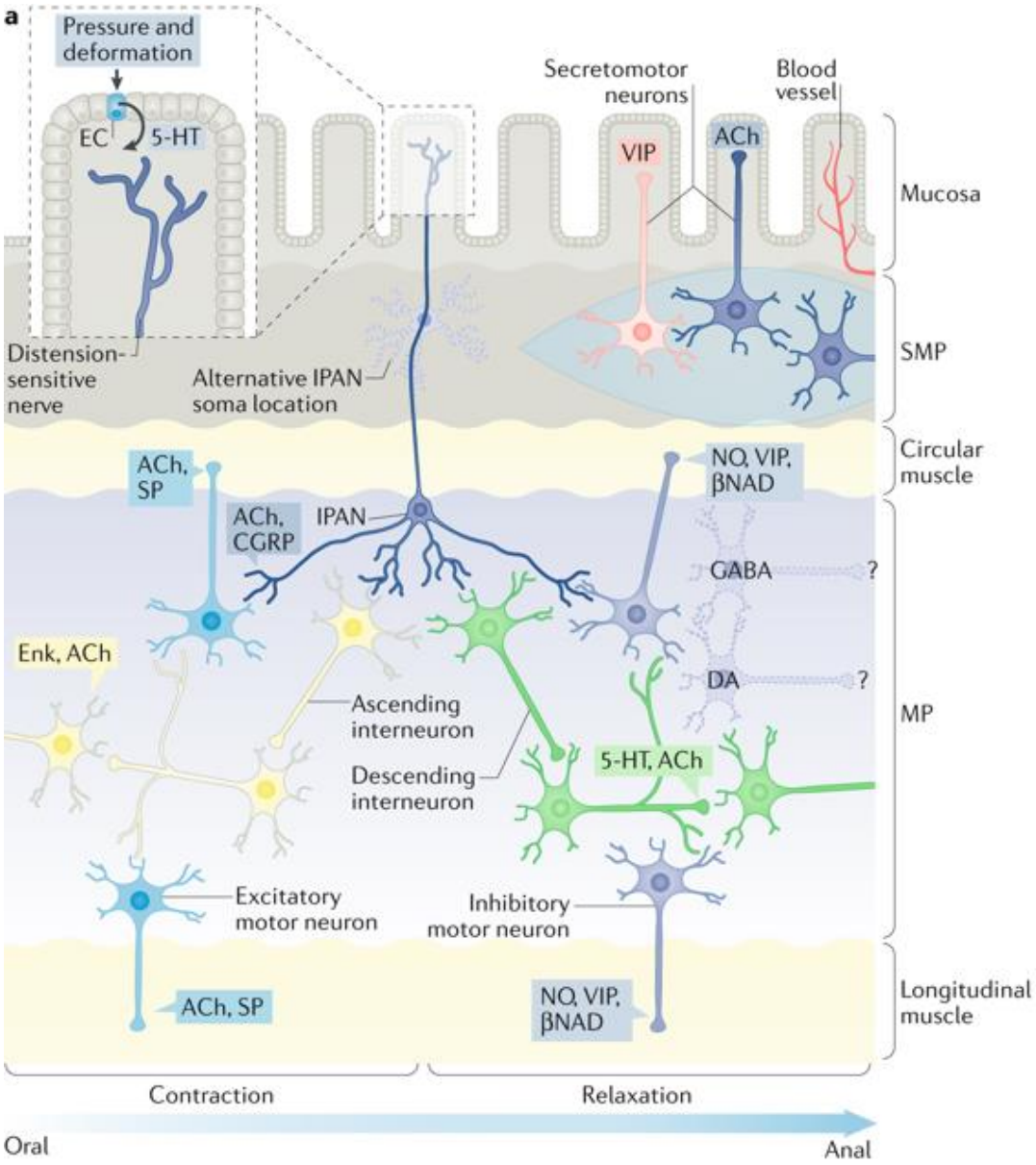


**Figure 1.5:** Schematic illustrating the major neuronal subtypes found in the enteric plexuses and highlighting the subset that forms the peristaltic reflex microcircuit. Luminal distention or mucosal deformation triggers direct activation of mechanoreceptive endings of intrinsic primary afferent neurons (IPANs) as well as indirect activation of IPANs upon serotonin (5-HT) release by enterochromaffin cells (ECs) in the epithelium. IPANs release acetylcholine (ACh) to activate ascending and descending interneurons, which excite excitatory and inhibitory motor neurons, respectively. Motor neuron activity results in oral contraction and anal relaxation of intestinal smooth muscle, which propels luminal contents in the proximal–distal direction. Ascending interneurons express enkephalin (Enk) and descending interneurons release ACh and 5-HT. Excitatory motor neurons secrete ACh and substance P (SP), whereas inhibitory motor neurons secrete nitric oxide (NO), vasoactive intestinal peptide (VIP) and the purine β-nicotinamide adenine dinucleotide (βNAD). Secretomotor and vasomotor neurons of the submucosal plexus (SMP) secrete ACh or VIP. Taken from (Rao and Gershon, 2018).

**Table 1.1:** Types of neurons in the enteric nervous system. This table lists the neuron types that are found in the guinea-pig small intestine, some of their defining characteristics, and percentage occurrence in each of the ganglionated plexuses. I have also listed three types of motor neuron that are found in other parts of the tubular digestive tract, marked by asterisks*. Taken from (Furness, 2000).

| | Proportion | Chemical coding | Function/comments |
|---|---|---|---|
| *Myenteric neurons* | | | |
| Excitatory circular muscle motor neurons (6) | 12% | *Short:* ChAT/TK/ENK/GABA<br>*Long:* ChAT/TK/ENK/NFP | To all regions, primary transmitter ACh, cotransmitter TK |
| Inhibitory circular muscle motor neurons (7) | 16% | *Short:* NOS/VIP/PACAP/ENK/NPY/GABA<br>*Long:* NOS/VIP/PACAP/Dynorphin/BN/NFP | Several cotransmitters with varying prominence: NO, ATP, VIP, PACAP |
| Excitatory longitudinal muscle motor neurons (4) | 25% | ChAT/Calretinin/TK | Primary transmitter ACh, cotransmitter TK |
| Inhibitory longitudinal muscle motor neurons (5) | ~2% | NOS/VIP/GABA | Several cotransmitters with varying prominence: NO, ATP, VIP, PACAP |
| Ascending interneurons (local reflex) (1) | 5% | ChAT/Calretinin/TK | Primary transmitter ACh |
| Descending interneurons (local reflex) (8) | 5% | ChAT/NOS/VIP±BN±NPY | Primary transmitter ACh, ATP may be a cotransmitter |
| Descending interneurons (secretomotor reflex) (9) | 2% | ChAT/5-HT | Primary transmitters ACh, 5-HT (at 5-$HT_3$ receptors) |
| Descending interneurons (migrating myoelectric complex) (10) | 4% | ChAT/SOM | Primary transmitter ACh |
| Myenteric intrinsic primary afferent (primary sensory) neurons (2) | 26% | ChAT/Calbindin/TK/$NK_3$ receptor | Primary transmitter TK |
| Intestinofugal neurons (3) | <1% | ChAT/BN/VIP/CCK/ENK | Primary transmitter ACh |
| *Motor neurons to gut endocrine cells | N/A | N/A | For example, myenteric neurons innervating gastrin cells. Neurons of this type may be in submucosal ganglia |
| *Submucosal neurons* | | | |
| Non-cholinergic secretomotor/vasodilator neurons (12) | 45% | VIP/GAL | Primary transmitter VIP. A small proportion of these have cell bodies in myenteric ganglia |
| Cholinergic secretomotor/vasodilator neurons (13) | 15% | ChAT/Calretinin/Dynorphin | Primary transmitter ACh |
| Cholinergic secretomotor (non-vasodilator) neurons (14) | 29% | ChAT/NPY/CCK/SOM/CGRP/Dynorphin | Primary transmitter ACh. A small proportion of these have cell bodies in myenteric ganglia |
| Submucosal intrinsic primary afferent (primary sensory) neurons (11) | 11% | ChAT/TK/calbindin | Calbindin-IR, seen with some antisera only. Primary transmitter assumed to be TK |
| *Excitatory motor neurons to the muscularis mucosae | N/A | N/A | Primary transmitter ACh |
| *Inhibitory motor neurons to the muscularis mucosae | N/A | N/A | Pharmacology of transmission appears to be similar to other enteric inhibitory muscle motor neurons |

## 1.2.3 Enteric glia

Enteric glia including enteric astrocytes, like their counterparts in the central nervous system provide structural and metabolic support for enteric neurons (Rao et al., 2015). There are two types of glial found in the enteric plexuses, the intramuscular glia, which are

interactive with nerve fibres coursing through the muscularis externa, and the mucosal glia, which located in the underneath the epithelium (Rao and Gershon, 2018). Recently, enteric glia have been suggested to be active contributors to the ENS and therefore GI tract functions, such as preventing inflammation and maintaining intestinal epithelial barrier integrity (Gulbransen and Sharkey, 2012). Furthermore, individual glia within the myenteric ganglion are electrically coupled to each other through gap junctions, allowing the cells to transmit $Ca^{2+}$ waves. It has been revealed that disruption of these $Ca^{2+}$ signals can modify GI motility, indicating glia are actively involved in GI functioning and homeostasis (Maudlej and Hanani, 1992, McClain et al., 2015).

## 1.3 Smooth muscle

Smooth muscle cells are found in the walls of various organs and tubular structures of the body, including blood vessels in cardiovascular system, the GI tract, airways in the respiratory system, and in the urogenital system. In the GI tract, smooth muscles are organized into two layers, the circular smooth muscle layer and the longitudinal smooth muscle layer. Both smooth and cardiac muscle tissue are usually activated involuntarily, whereas skeletal muscle is considered voluntary which can be made to contract or relax by conscious control (Tortora and Derrickson, 2009). Individual smooth muscle cells form both mechanical and electrical junctions with neighbouring cells to create a syncytium that underlies the coordination of contractions, forcing the food, water and waste to move though the gut, in a process called peristalsis (Sanders et al., 2012b). Peristaltic movement in GI tract comprises relaxation of circular smooth muscles, followed by their contraction to keep the substances from moving backward, then longitudinal contraction to push it

moving forward. These contractions manifest as either tonic and/or phasic contractions and are regulated by hormones, autonomic/involuntary nervous regulatory input and other local chemical signals (e.g. calcium ions). Moreover, smooth muscle contraction and relaxation is vastly slower and lasts much longer than skeletal muscle twitch or cardiac muscle contraction, and allows the muscle tone to retain partial contraction thereby sustain long-term tone. This property is important in controlling blood pressure in the cardiovascular system and functioning of the GI tract, where the walls of blood vessels called arterioles and intestine, which maintain a steady pressure of blood, and a steady pressure on the contents of the tract, respectively (Keynes et al., 2011, Tortora and Derrickson, 2009).

### 1.3.1 The role of interstitial cells

GI smooth muscles are ‘‘autonomous’’ and produce spontaneous pacemaker activity (electrical slow waves). This intrinsic pacemaker activity generated from interstitial cells of Cajal (ICC), which are electrically coupled to smooth muscle cells via gap junction resulting in depolarization which initiates $Ca^{2+}$ entry and contraction. A combination of intracellular timing of ICC and ion conductance generate the pacemaker currents which underlie slow waves and produces a continuous rhythmic cycle of depolarisation and repolarisation of smooth muscle cell membrane potential. This activity is characterised by spontaneous phasic contractions which are the foundation for peristaltic and segmental motility patterns (Koh et al., 2012, Sanders et al., 2016). Slow waves in the GI tract is independent of neural or hormonal inputs, although the frequency and force of contractions is highly dependent on neural and other regulatory inputs (Hennig et al., 2010). There are two types

of ICC found in the GI tract, myenteric ICC (ICC-MY) and intramuscular ICC (ICC-IM). ICC-IM pacemaker cells mediate the excitation of smooth muscle cells through receptor activation by neurotransmitters such as ACh and NO (Sanders et al., 2016, Sanders et al., 2006). Both inhibitory and excitatory neurons can regulate the amplitude of contractions, as basal spontaneous contractions have low amplitude contractions (Sanders et al., 2012b). As such, ICCs are hypothesised to be the cellular links between ENS neurons and intestinal smooth muscle cells (Sanders and Ward, 2006).

### 1.3.2 The mechanism of smooth muscle contraction

The contraction of smooth muscle is regulated mainly by external inputs from the autonomic nervous system via receptor activation or directly through mechanical stretch of the GI tract itself. These stimuli inducing a change in smooth muscle cell membrane potential permitting transmembrane influx of calcium ions ($Ca^{2+}$) through both TRPC channels (Tsvilovskyy et al., 2009) and voltage-dependent calcium channels (VDCC) such as L-type $Ca^{2+}$ channels (Ambudkar, 2009, Wegener et al., 2006). The mechanisms by which an increase in intracellular calcium stimulates GI smooth muscle contraction is illustrated in the **Figure 1.6**. Autonomic control of GI tract function occurs via neurotransmitter released from either parasympathetic nervous system (PNAS) or sympathetic nervous system (SNS) and receptor activation. Action potential induced exocytosis of acetylcholine (ACh) from parasympathetic post ganglionic neurons, triggers activation of G-protein coupled, metabotropic cholinergic receptors, the muscarinic receptor subtype 2 ($M_2$) and subtype 3 ($M_3$) located on post-synaptic smooth muscle cells. Stimulation of $M_2$ receptors cause activation of pertussis toxin (PTX)-sensitive $G_{i/o}$ proteins which opens TRPC4 channel

for $Ca^{2+}$ influx. While the $M_3$ is coupled to PTX-insensitive $G_{q/11}$ proteins that stimulate phospholipase C (PLC) and leads to hydrolyse phosphatidylinositol 4,5-bisphosphate ($PIP_2$) to diacyl glycerol (DAG) and inositol 1,4,5-trisphosphate ($IP_3$). This $IP_3$ signalling triggers intracellular $Ca^{2+}$ release from intracellular $Ca^{2+}$ stores called sarcoplasmic reticulum (SR) while DAG activates TRPC6 channels to cause $Ca^{2+}$ influx from extracellular fluid. The activation of TRPC4/6 channels (Beech et al., 2004, Tsvilovskyy et al., 2009) depolarises membrane potential and leads to activation of VDCC, allowing further $Ca^{2+}$ influx to the cell. The ensuing influx of $Ca^{2+}$ cause the formation of $Ca^{2+}$/calmodulin complex which activates myosin light chain kinase (MLCK), an enzyme that is capable of phosphorylating myosin light chains (MLC) in the presence of adenosine triphosphate (ATP). The myosin-binding subunit, when phosphorylated, inhibits the enzymatic activity of MLC phosphatase, allowing the light chain of myosin to remain phosphorylated, thereby promoting smooth muscle contraction. Finally, VDCC in the cell membrane will stay on opening in response to membrane depolarization that induced by mechanical stretch of the smooth muscle cells (Webb, 2003, Ambudkar, 2009).

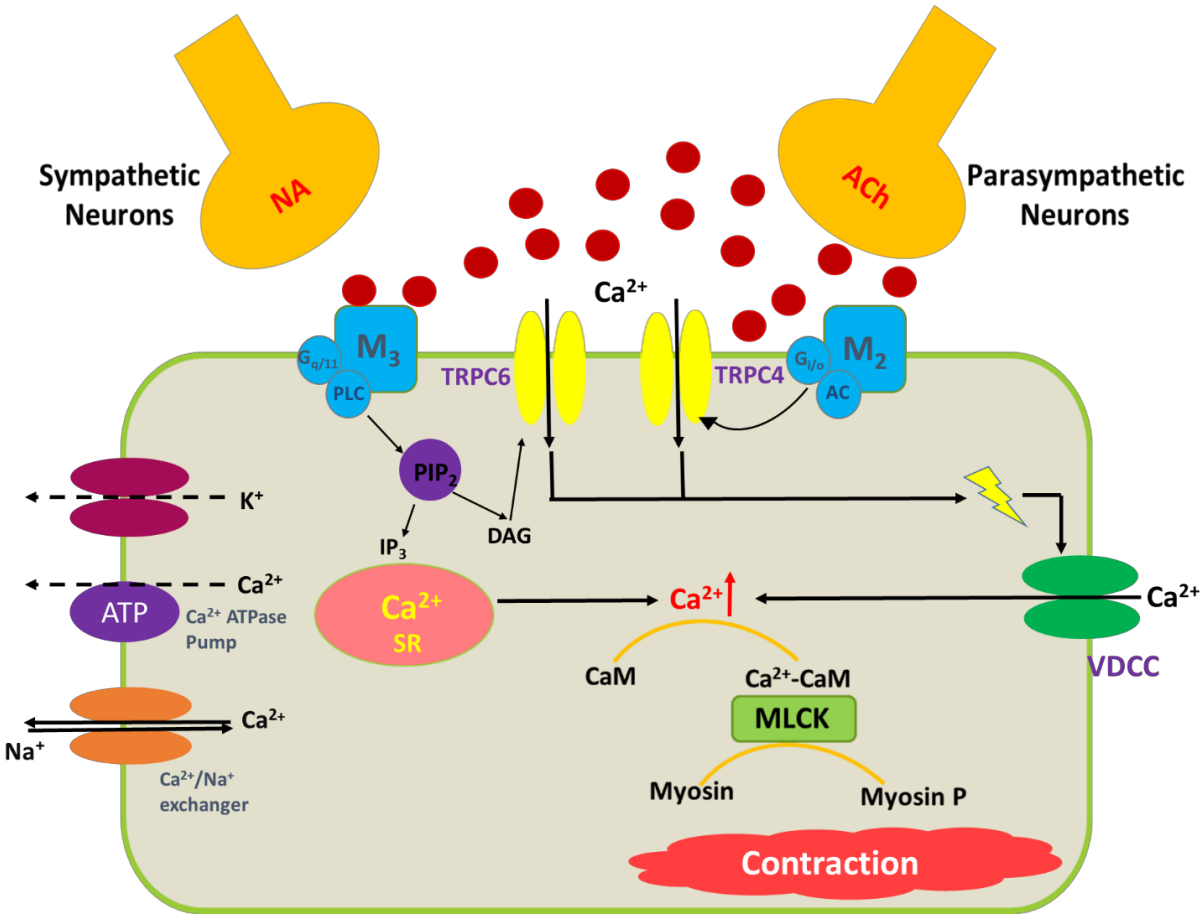


**Figure 1.6:** Mechanism pathway of GI smooth muscle contraction. Various agonists (neurotransmitters, hormones, etc.) bind to specific receptors to activate contraction in smooth muscle. Dotted lines indicates inhibition, solid lines indicates stimulation.

### 1.3.3 The mechanism of smooth muscle relaxation

Smooth muscle relaxation lead to a reduction of intracellular $Ca^{2+}$ concentration through closing of VDCC. However, direct regulation of VDCC is not typical in GI smooth muscle cells (Sanders et al., 2012a). As such, other conductance leading to membrane depolarization or hyperpolarization of GI smooth muscles are targeted by regulating opening of VDCC. Potassium ion ($K^+$) channels play an important role in regulating membrane potential. The fundamental purpose of $K^+$ channels is to regulate the intracellular concentration of $Ca^{2+}$ by controlling the closure of VDCC, thus promote smooth muscle relaxation. As shown in

**Figure 1.7,** activation of $K^+$ channels by cell membrane depolarisation leads to $K^+$ efflux from the cell, which causes membrane potential ($E_m$) to hyperpolarized towards resting membrane potential and the subsequent voltage-dependent closure of VDCC. This activity results in a reduced intracellular free $Ca^{2+}$ levels, causing the smooth muscle relaxation. Conversely, inhibition of $K^+$ channels would result in cell depolarization ($E_m$ becoming more positive), leading to the opening of VDCC and increased intracellular $Ca^{2+}$ levels, thus promoting smooth muscle contraction. Therefore, the potassium channels act as a major regulator of GI smooth muscle cells activity.

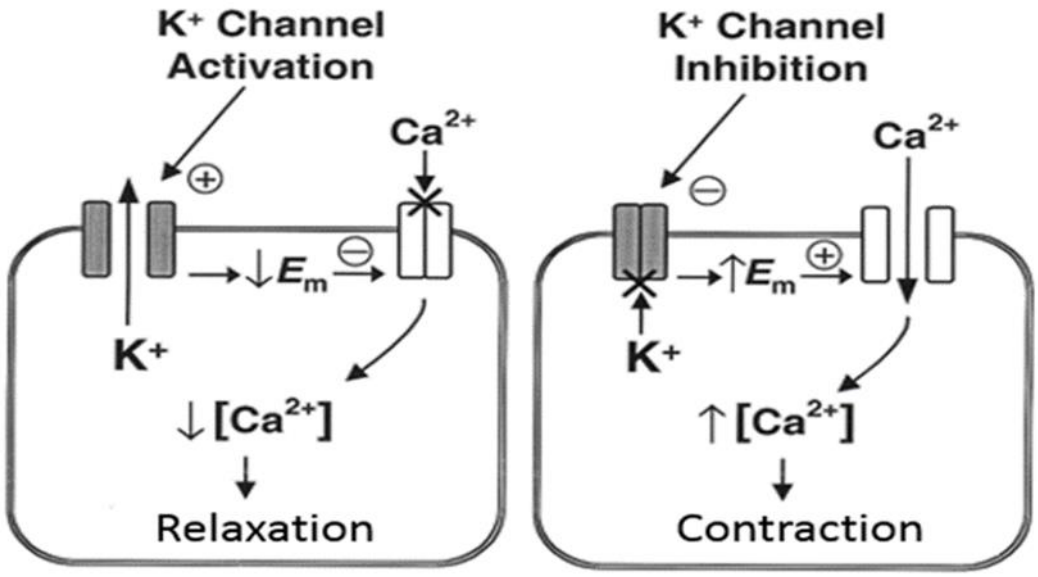


**Figure 1.7:** How $K^+$ regulates the smooth relaxation/contraction. Schematic illustration of the key events involved in the smooth muscle response to potassium ion channel activation (left) or inhibition (right) ( Adapated from Sobey, 2001).

The relaxation of smooth muscle also could be triggered directly via neurotransmitter released from SNS. Sympathetic neurons release noradrendaline (NA) that binds to β2-adrenergic receptor activating Gs protein leading to increased activity of adenylate cyclase (AC). Stimulation of AC converts adenosine triphosphate (ATP) to cyclic adenosine

monophosphate (cAMP) cause increase of intracellular cAMP, which activates protein kinase A (PKA). The activation of PKA leads to inhibition of $PIP_2$ hydrolysis, increased $Ca^{2+}$ uptake by internal store SR via SERCA pump, inactivation of myosin light chain kinase, and activation of cell membrane ion channels and transports such as $K^+$ channel and NCX. The net effect of these processed would be to reduce intracellular $Ca^{2+}$ concentration and thereby producing smooth muscle relaxation (Knox and Tattersfield, 1995, Billington et al., 2013). Furthermore, sympathetic transmission via nitric oxide (NO) from nitrenergic nerves in the GI tract could also induce smooth muscle relaxation. The release of NO from nitric oxide synthase (NOS) activates soluble guanylyl cyclase (GC) in smooth muscle cells that produce cyclic GMP (cGMP), triggers activation of $K^+$ channels and uptake intracellular $Ca^{2+}$ by internal store SR and NCX. This processes leads to a reduced intracellular free $Ca^{2+}$ levels and mimic smooth muscle cell membrane hyperpolarization, causing the smooth muscle relaxation (Toda and Herman, 2005).

### 1.3.4 GI motility disorders and current treatment

GI motility is a highly complex physiological process involving the coordinated contractions of the circular and longitudinal smooth muscle cells. Disruption to the natural rhythm of intestinal contractions can lead to common hypo- or hyper-motility pathologies such as Irritable bowel syndrome (IBS) (Beyder and Farrugia, 2012) which affects 1 in 5 people in the UK and 11% of the population globally, and is twice as common in woman as men (Canavan et al., 2014). IBS is a common functional GI disorder characterised by recurrent abdominal discomfort or pain, the onset of which is associated with abnormal defecation, alternating between constipation, diarrhoea and mixed symptoms (Curro, 2014). Although

IBS causes no pathological damage to the bowel wall, it can cause pain and affect a patient's quality of life significantly. As we discussed above, muscle contraction is a calcium dependent process, and thus ion channels are favourable targets given their prominent role in the contraction/relaxation process and their plasma membrane location. Calcium channels have already been targeted (such as nifedipine, verapamil and dilitaizem) (Opie, 1997) and given their targeting in other pathologies (neuronal and cardiac disorders) (Shaw and Colecraft, 2013, Ortner and Striessnig, 2016) present good potential drug targets in GI tract for GI disorders involving muscle dysfunction.

The aetiology of IBS has not been elucidated fully adding to the difficultly of directly curing the disorder, nonetheless it is believed environmental factors such as diet, stress, ageing and microbial flora may play a key role in effecting GI motility (Marynowski et al., 2015). Although there is no cure for IBS, treatment is mainly focused on preventing and relieving symptoms of pain, constipation, diarrhoea and discomfort. Dietary and lifestyle modification, such as high-fibre diet, regular exercise or drinking more water are usually recommended for treating mild symptoms (Camilleri and Ford, 2017). For pharmacotherapy, anticholingergics target, such as laxatives, is given to increase gut motility in patients suffering with constipation (Saha, 2014). Selective serotonin reuptake inhibitors (SSRI) antidepressants, such as fluoxetine (Prozac), are also commonly used to produce an antidepressant effect by blocking the neuronal reuptake of serotonin, in order to relief the abdominal pain and constipation (Talley, 2003). Moreover, an anti-diarrheal drugs like loperamide, an opioid receptor agonist which decreases the frequency of diarrhoea can be taken. Ion channel modulators, such as otilonium bromide, could either

inhibit the action of ACh at muscarinic receptors or block calcium channels on GI smooth muscle to alter contractility of GI smooth muscle (Camilleri and Ford, 2017).

Collectively, most of the currently identified therapeutic targets for the treatment of GI disorders within the ENS are neurotransmitter and hormone receptors (Furness, 2008), and thus some of these drugs have limited use due to their adverse effects, such as nausea, headache, dizziness and drowsiness. Therefore, a safer and more specific targets on smooth muscle contraction cycles could be a novel target to investigate. Given the important contribution of $K^+$ channels to the process of excitation contraction coupling and their plasma membrane location, they could be potential therapeutic targets for treating GI motility disorders such as irritable bowel syndromes, which have not been significantly targeted at present. For instance, $K^+$ channel activators could be used to relieve symptoms of GI tract hypermotility, and blockers could be used to relieve of symptoms of constipation. Before considering $K^+$ channels as a potential therapeutic target, their structural, functional and pharmacological diversity should be understand first.

## 1.4 Potassium ion channels

### 1.4.1 Ion channel signalling

Electricity plays an essential role in cell physiology. The movement of inorganic ions, including $Na^+$, $K^+$, $Ca^{2+}$, $Mg^{2+}$ $Cl^-$ and $H^+$, across cell membranes and constitutes an electrical current that produces a voltage difference across them, which leads to mediating a diverse range of processes in excitable cells, such as neuronal transmission, muscle contraction and cell proliferation (Kew and Davies, 2010). In excitable cells, fast electrical signalling is made possible by mechanisms that establish an asymmetric ionic distribution of various ions across the plasma membrane. This charge separation creates a chemical driving force for movement of ions across the membrane though ion channels following natural laws of thermodynamics. Though all ions are asymmetrically distributed across the membrane, only $K^+$ ions are permitted to cross the membrane at rest. There is an outflow of $K^+$ ions which tries to equilibrate the differential concentration difference across the membrane and leads to a negative resting membrane potential (the inside of the cell is less positive relative to the outside). The movement of $K^+$ ions continues until equilibrium is reached, where the tendency for ions to move down their chemical concentration gradient is offset by the matching electrical gradient (named the equilibrium potential) induced by the movement of $K^+$ ions themselves. Maintenance of ion concentration asymmetry across the membrane is achieved by active transport. This process is largely carried by the ATP-driven $Na^+/K^+$ pump, which constantly transport 3 $Na^+$ out of the cell, and 2 $K^+$ ions into the cell, and thus, indirectly, plays a critical role in maintaining the resting membrane potential (Hille, 2001, Kew and Davies, 2010, Dubyak, 2004).

When the cell has been stimulated, these specialized electrical signalling produce the action potential, a distinctive and rapid electrical signal that is propagated along the nerve fibre (Hille, 2001, Rasband, 2010). The action potential is made by a rapid feedback process involving the direct action of voltage changes due to the passive diffusion of charged ions through gated ion channels. As shown in **Figure 1.8**, a change in membrane potential induced by an external stimulus causes opening of voltage-gated $Na^+$ channels. This allows $Na^+$ ions to flow passively down their electrochemical gradient into the cell. This influx of cations into the interior of the cell creates an increasingly more positive electrical environment (less negative) relative to the outside of the cell, a process known as depolarization. The extent of this depolarisation is limited by two processes; firstly, the continuation of $Na^+$ conductance across the plasma membrane through voltage-gated sodium channels is halted via the rapid onset of an intrinsic gating mechanism called inactivation (Hille, 2001), secondly the delayed (compared to sodium channel activation) opening of voltage-gated $K^+$ channels causes $K^+$ ion efflux from the cell down its own electrochemical gradient resulting in a re-establishment of a negative electrical environment (relative to the outside of the cell), a process known as repolarization. This repolarisation of the membrane potential may be extended more negatively beyond the normal homeostatic level of resting membrane potential, a hyperpolarisation of the membrane potential. During this period, voltage-gated potassium channels close, sodium channels recover in a time- and voltage-dependent manner from their inactivated state and constitutively open background/leak potassium conductances along with active processes allow an equilibration of potassium ions across the membrane back to homeostatic levels equalling the $K^+$ reversal potential ($K_{rev}$) (Yellen, 2002, Goldstein et al., 2001). The action potential is the basis for transmitting signals in excitable cells, for

example to initiate muscle contraction or hormone/neurotransmitter release. Therefore, potassium ion channels, constitute the physical substrates that underlie neuronal and muscular signalling.

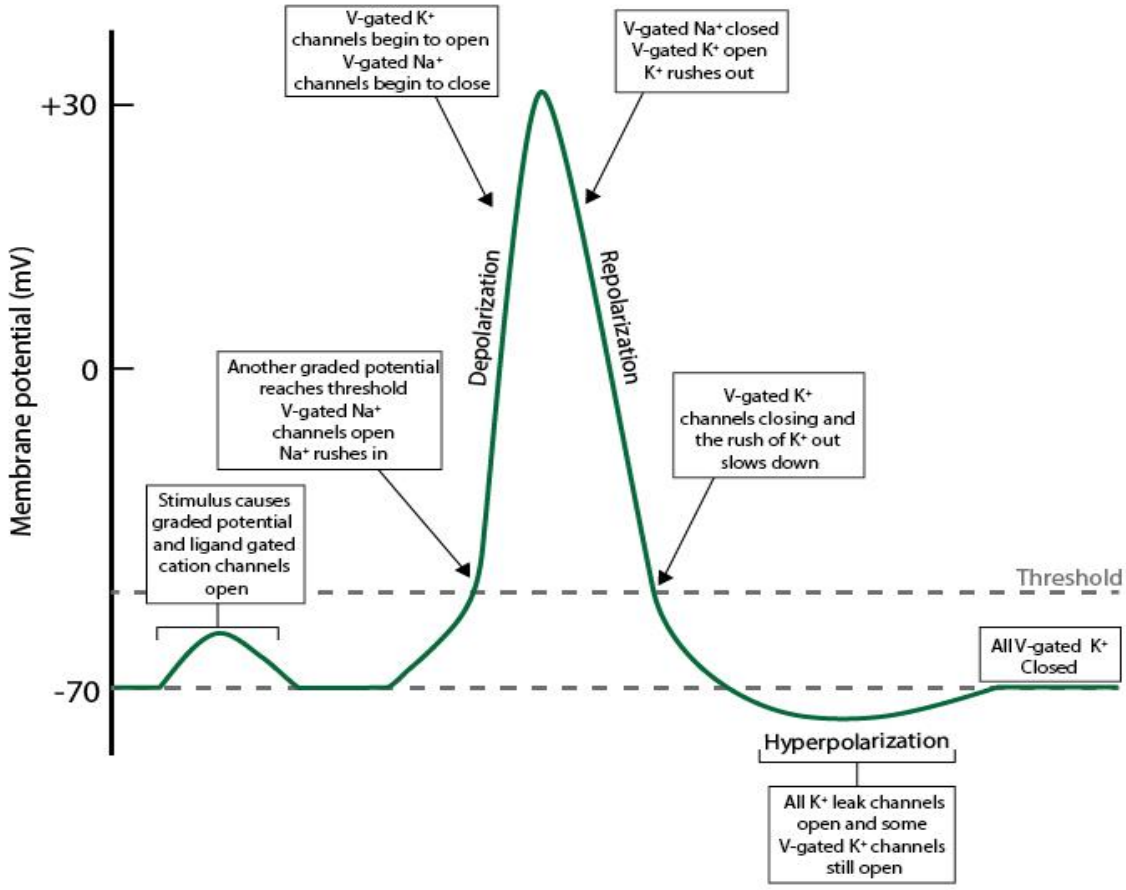


**Figure 1.8:** A ‘‘Schematic’’ diagram of action potential. The membrane potential starts out at −70 mV. When stimulus is applied, the membrane potential increase above the threshold potential. Followed by the opening of voltage-gated $Na^+$ channels triggers rapid depolarization of the cell membrane. This is followed by a transient outward repolarization induced by activation of voltage-gated $K^+$ channels. After this, $K^+$ conductances return the membrane potential to hyperpolarized values, where the balance of depolarizing and hyperpolarizing stimuli will determine the next action potential.

### 1.4.2 $K^+$ channel superfamily

$K^+$ channels form the largest family of ion channels, with more than 90 genes in the human genome. $K^+$ channels allow the selective and passive movement of $K^+$ ions into or out of the cell along their electrochemical gradients. $K^+$ channels are formed as multimeric complexes via the assembly of principle (α) subunits containing various transmembrane spanning domains (TM) with intracellular facing n and c termini, and a semi-hydrophobic loop (P) that partially spans the lipid bilayer. Some $K^+$ channels are also formed with auxiliary β subunits which can alter channel structure, function, pharmacology and regulation (Tian et al., 2014). Structurally, α subunits can be classified into the following three main families: 2TM-1P, 6/7TM-1P and 4TM-2P (**Figure 1.9**). As expected, $K^+$ channels belonging to the same family present similar structure and biophysical activities, and thus they can also be categorised based on functional attributes such as how they open and close (referred to as "gating") which can be regulated by variety of stimuli including changes in pH, temperature, membrane voltage, ligands and mechanical stretch. Structural and functional analyses of $K^+$ channels, particularly crystallisation, have elucidated a much deeper understanding of the molecular mechanisms behind ion selectivity, conduction and gating.

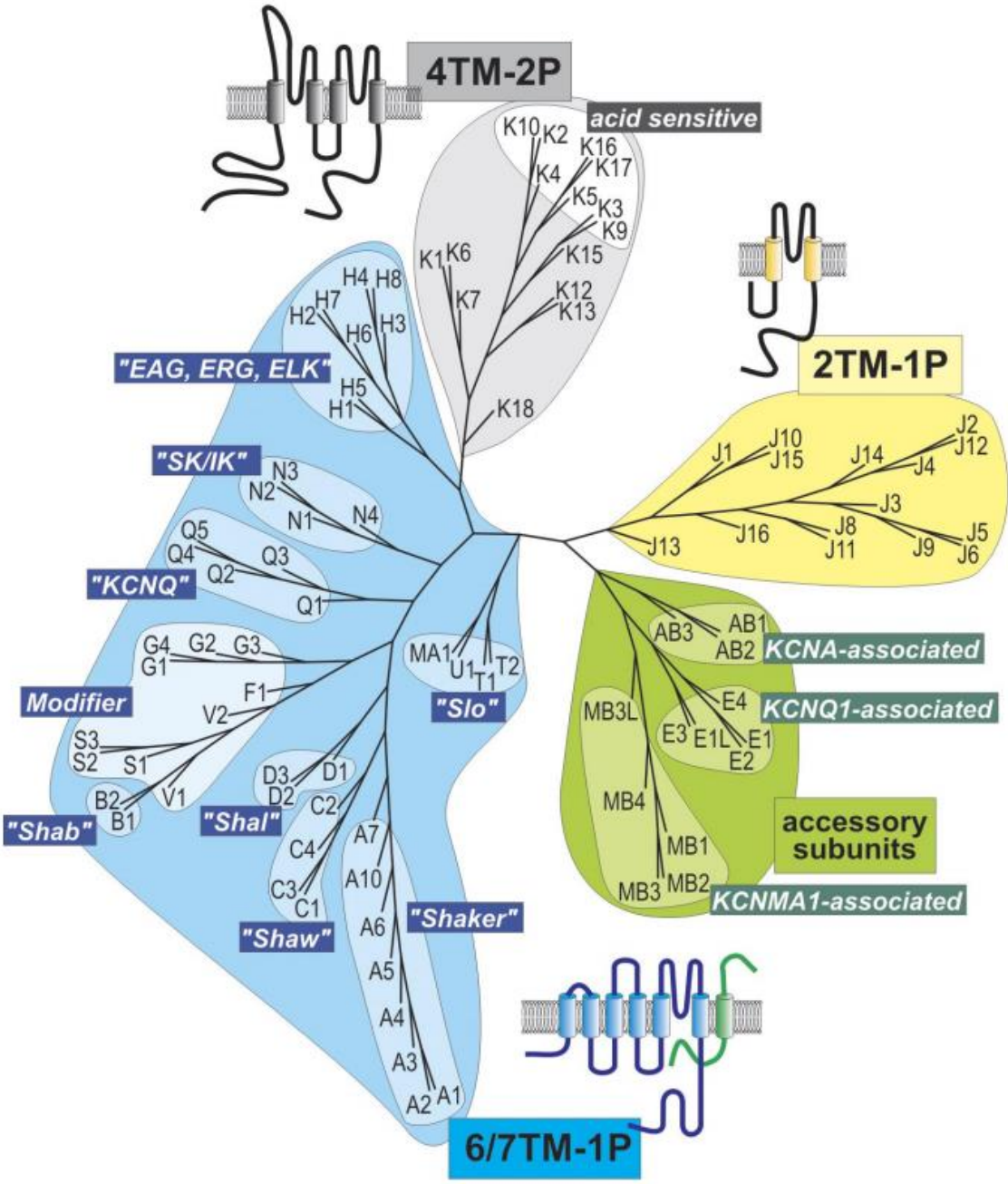


**Figure 1.9:** $K^+$ channel families. Phylogenetic tree of human $K^+$ channels. The insets correspond to the typical structure presented by subunits of each of the tree families. For simplicity, the letter code for $K^+$ channels (KCN) has been omitted (e.g., KCNA1 is depicted as A1), the ‘‘words’’ refer to different subtype of $K^+$ channels (e.g., ‘‘KCNQ’’ indicates the $K_v$ 7 subfamily) (Heitzmann and Warth, 2008).

### 1.4.3 Selectivity filter of $K^+$ channels

$K^+$ channels possess a unique structural hallmark, which singularly defines its functional phenotype, the selectivity filter sequence. A common feature present at their pore-lining P-loops of $K^+$ channels which is a conserved sequence of amino acids known now as the ''$K^+$ channel sequence signature'' (Yellen, 2002). Mutation of these amino acids disrupts the ability of the channel to distinguish between $K^+$ and $Na^+$ ions (Heginbotham et al., 1994) or indeed to pass ions at all. $K^+$ ions can pass through the selective filter at an extremely fast rate, around $10^7$ to $10^8$ $K^+$ ions per second (Morais-Cabral et al., 2001). These high diffusion rates are essential during rapid opening and closing channel transitions, since a typical action potentials in neurons requires millions of ions to flow in a millisecond timescale (Yellen, 2002, Doyle et al., 1998). To catalyse $K^+$ ion flow through the pore almost as fast as they are able to diffuse up to it, the energetic barriers in the channel have to be very low or equal to $K^+$ ions diffusing through water. This is all achieved while discriminating between $K^+$ ions, which have an atomic radius of 1.33Å and $Na^+$ ions with an atomic radius of 0.95Å (MacKinnon, 2004).

Crystallisation of the bacterial ion channels KcsA generated the first accurate structure of selectively filter and led to confirmation of how $K^+$ channels discriminate between $K^+$ and $Na^+$ ions at such high conductance rates. The ion pathway of KcsA was found to be long and wide, with a length in 18Å and a cavity in the region of 10Å in diameter (Doyle et al., 1998). Each α subunit was found to direct the negatively charged C-terminal end of its pore loop towards a $K^+$ ion thereby the pore helices are stabilising the $K^+$ ion in the cavity (**Figure 1.10A**) (Roux and MacKinnon, 1999). **Figure 1.10B** shows the structure formed by the

selectively filter, which present in their pore-lining P-loops located towards the extracellular face of the ion conduction pathway. It consists of a consensus amino acid signature sequences ‘‘TxGxG’’ (Heginbotham et al., 1994), where the x between the two glycines (G) is usually an aromatic tyrosine (Y), phenylalanine (F) or a hydrophobic leucine (L) (Heginbotham et al., 1994, Schewe et al., 2016). The glycine residues provide the dihedral angles, the threonine residues provides the hydroxy oxygen atom to coordinates the $K^+$ ion and the tyrosine and valine side-chains provide geometric constraint (Roux and MacKinnon, 1999). This features allows their main chain carbonyl oxygen atoms to the inside and towards the ions, which forms a narrow tube with 4 equally spaced $K^+$ binding sites with eight oxygen atoms (MacKinnon, 2004). The oxygen atoms surrounding the $K^+$ ions in the selectivity filter mimic the environment of $K^+$ in an aqueous solution. Therefore, the ability of $K^+$ channels to discriminate between $K^+$ and $Na^+$ ions is a results of the binding sites compensating the energetic cost of the dehydration of the $K^+$ ions, which cannot be accomplished for $Na^+$ as it is too small (Zhou et al., 2001b, Morais-Cabral et al., 2001).

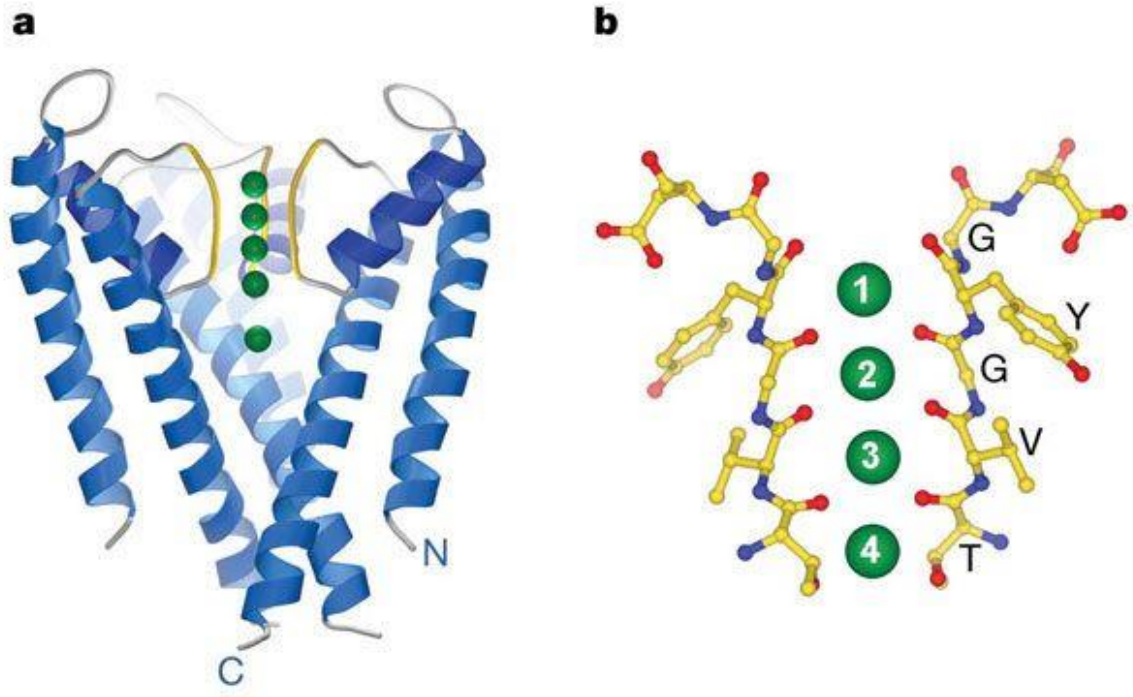


**Figure 1.10:** Schematic of the KcsA K+ channel. **(a)** Molecular structure representation of the KcsA channel. $K^+$ (green) bind at four locations in the selectivity filter (yellow). **(b)** Close-up view of the selectivity filter in ball-and stick representation. $K^+$ are numbered as 1-4 to indicate the location of binding sites in the filter. Position 1 is closest to the extracellular solution and position 4 is closest to the cavity. Taken from (Morais-Cabral et al., 2001).

### 1.4.4 2TM-1P channel family

Inwardly rectifying channels ($K_{ir}$) represent the simplest architecture among $K^+$ channels, comprising two transmembrane spanning domains separated by a single pore loop domain and flanked by cytoplasmic amino and carboxyl terminal domains (**Figure 1.11a**). Functional channels are formed by homo or heteromeric tetramerisation of subunits. There are 15 $K_{ir}$ genes expressed in humans encoding 15 different alpha subunits. Homotetrameric assembly leads to 7 different subfamilies ($K_{ir}$1-7) that can be further classified into four general functional groups: 1) classical $K_{ir}$ channels ($K_{ir}$2.x), 2) G-protein gated ($K_{ir}$3.x), 3) $K^+$-

transport channels ($K_{ir}$1.x, $K_{ir}$4.x, $K_{ir}$5.x, and $K_{ir}$7.x), 4) ATP-sensitive $K^+$ channels ($K_{ir}$6.x) (Kew and Davies, 2010).

Heteromerisation of channel subunits normally occurs between channels of the same subfamily, for instance $K_{ir}$2.1 can form functional subunits with any other $K_{ir}$2.x family member (Preisig-Muller et al., 2002). However, some subfamilies, such as $K_{ir}$4.1 have been reported to assemble functional channels with other families, such as $K_{ir}$5.1 (Hibino et al., 2004). The characteristic inward rectification of $K_{ir}$ channels results primarily from a voltage-dependent chronic pore obstruction by intracellular polyamines and charged $Mg^{2+}$ ions, which physically blocks the conduction pathway during depolarization, thereby impending the outward flow of $K^+$. This pore block is relieved at negative potentials allowing voltage-independent large inward $K^+$ currents at potentials negative to $E_k$ (where there is no block and influx overcomes block) compared to the smaller $K^+$ currents at potential more positive to $E_K$ (where intracellular block overcomes outward ionic flux; see **Figure 1.11b & c**) (Hille, 2001, Osawa et al., 2009). Thus, the voltage at which rectification occurs is controlled by the equilibrium potential for $K^+$, which is defined by transmembrane $K^+$ concentration gradients, and therefore not by voltage *per se* (fig 1.13c). Due to these properties, $K_{ir}$ channels are predominantly responsible for maintaining the resting membrane potential of the cell, and are particularly active at hyperpolarised potentials, and in regulation of the action potential duration and receptor-dependent inhibition of cellular excitability (Osawa et al., 2009).

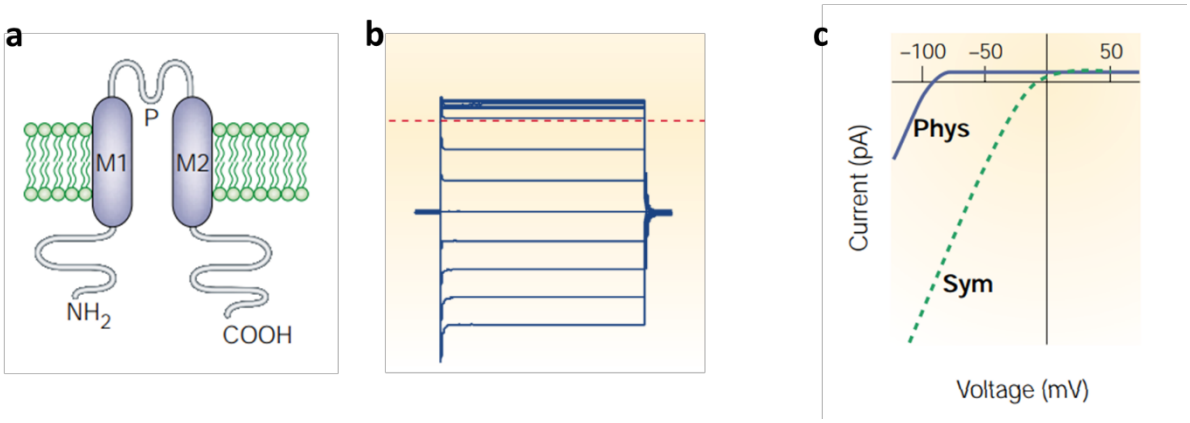


**Figure 1.11:** Characterisation of 2TM-1P channels. **(a)** Membrane topology of a typical 2TM-1P family. Transmembrane domains are labelled M1-M2, with the pore loop labelled P. **(b)** Example current traces based on $K_{ir}4.2$. **(c)** Current-voltage relationship for $K_{ir}$ channels under physiological $K^+$ concentration (blue line) and symmetrical $K^+$ concentration (dotted green line). Taken from (Goldstein et al., 2001).

$K_{ir}$ channels have various functions in multiple cell types including macrophages, cardiac myocytes, endothelial cells and CNS cells. For example, in cardiac myocytes, $K_{ir}2.x$, $K_{ir}3.x$ and $K_{ir}6.x$ with SUR subunits (also known as $K_{ATP}$) subfamilies are important for maintenance of prolonged action potential by slowing membrane repolarisation (Anumonwo and Lopatin, 2010). In endothelial cells, vascular smooth muscle cells and pericytes, $K_{ir}2.1$ and $K_{ATP}$ channels participate in dilation, induced by elevated extracellular $K^+$ (Jackson, 2005). In pancreatic β cells, $K_{ATP}$ channel activity is inversely correlated with insulin secretion, conditions tending to reduce channel activity will stimulate insulin secretion above normal leading to hypoglycaemia, while increasing channel activity will attenuate insulin secretion, leading to hyperglycaemia (Kew and Davies, 2010). Furthermore, $K_{ir}2.x$, $K_{ir}3.x$ and $K_{ATP}$ subfamilies are also expressed GI tract. Activation of $K_{ir}$ currents would lead to reduce the amplitude of conducting slow waves and reduce the tendency of slow waves to initiate $Ca^{2+}$ action potentials in smooth muscle cells (Koh et al., 2012).

Blockers most commonly used for $K_{ir}$ channels are $Ba^{2+}$ and $Cs^{+}$ (Franchini et al., 2004, Hagiwara et al., 1976), while tetraethylammonium (TEA) and 4-aminopyridine (4-AP) are known as the classic blockers for $K_v$ channels, but have little effect on $K_{ir}$ channels (Oonuma et al., 2002, Hagiwara et al., 1976). There are also other compounds available that can affect particular types of $K_{ir}$ channels. A small-molecule named as VU590 has been reported that potently block $K_{ir}1.1$ and $K_{ir}7.1$ channels by crossing the membrane to access an intracellular binding site (Lewis et al., 2009). Tertiapin is a toxin that was isolated from honey bee venom which blocks G-protein gated $K_{ir}$ ($K_{ir}3.x$) and $K_{ir}1.1$ channels (Jin and Lu, 1998). The oxidation-resistant tertiapinQ blocks G-protein gated $K_{ir}$ current, but not $K_{ATP}$ current (Hibino et al., 2010). The majority of reagents affecting $K_{ATP}$ channel activity react on the auxiliary pancreatic sulfonylurea receptor (SUR) subunits. A number of chemically diverse agents are able to bind to SUR and activate $K_{ATP}$ channels, including diazoxide, cromakalim, pinacidil and aprikalim (Kew and Davies, 2010). Moreover, $K_{ir}$ channels could be also modified by regulatory factors. For instance, the phosphatidylinositol 4,5-bisphosphate ($PIP_2$) has been reported that activate the $K_{ir}$ channels by activation of ATP-dependent lipid kinases (Hilgemann and Ball, 1996, Hilgemann et al., 2001), which are thought to bind to positively charged residues along the C-terminus (Huang et al., 1998, Lopes et al., 2002). In addition, some $K_{ir}$ channels (such as $K_{ir}1.1$, $K_{ir}2.3$ and $K_{ir}4.1$) are regulated by pH levels of intracellular or extracellular (Dahlmann et al., 2004), while others such as $K_{ir}3.2$ and $K_{ir}3.4$ can be regulated by intracellular $Na^{+}$ (Ho and Murrell-Lagnado, 1999, Zhang et al., 1999).

### 1.4.5 6TM-1P channel family

6TM-1P channels represent the largest sub-family of $K^+$ channels, encoded by at least 40 different genes in human genome, with additional diversity produced by alternative splicing and heteromultimerization (Yellen, 2002). 6TM-1P channel subunits consist of a series of six transmembrane spanning domains with a single semi-hydrophobic loop between TM5 and TM6, and intracellular facing N and C terminus. Their hallmark is a voltage-sensing domain formed by TM1-TM4 with the forth TM acting primarily as the voltage sensor. TM4 has conserved positively charged residues (lysine or arginine) at every third or fourth position that allow a mechanical response to changes in transmembrane potential to trigger channel opening (**Figure 1.12 a**) (Goldstein et al., 2001, Hille, 2001). Fully assembled 6TM-1P channel are formed by homo- or heterotetramers of α-subunits, with the four pore loop domains of each subunit coming together to form the four-fold symmetric conduction pathway across the bilayer. The functional 6TM-1P channel can often be further functionally, biophysically and pharmacologically diversified through association with accessory subunits, also called auxiliary subunits or β-subunits (Heitzmann and Warth, 2008). The opening of $K^+$ channels leads to currents that tend to drive the membrane potential towards the equilibrium potential for $K^+$, and thus in general are inhibitory. Physiologically, these voltage-dependent $K^+$ channels are activated by membrane depolarization, and play a fundamental role in repolarization of membrane potential, a critical signalling process in excitable tissues comprising neurons or muscle (**Figure 1.12 b & c**).

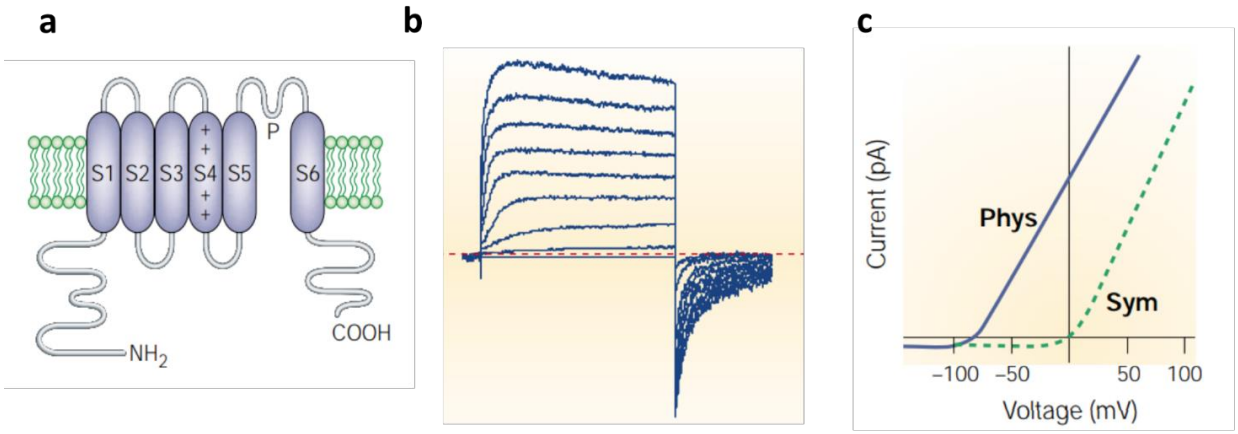


**Figure 1.12:** Characterisation of 6TM-1P channels. **(a)** Membrane topology of a typical 6TM-1P family subunit. Transmembrane domains are labelled S1-S6, with the pore loop labelled P. The channels are noted for their positively charged TM4 (S4) that acts as the primary voltage sensor for detecting changes in the membrane potential. **(b)** An example current trace based on KCNQ1. **(c)** Current-voltage relationship for $K_v$ channels under physiological $K^+$ concentration (blue line) and symmetrical $K^+$ concentration (dotted green line). Taken from (Goldstein et al., 2001).

The α-subunits of 6TM-1P $K^+$ channels can be divided into 12 classes within 3 major groups of proteins, according to their functional attributes and sequence homology. These groups are: 1) $K_v1$–$K_v6$ and $K_v8$-$K_v9$ subfamilies, which are components of voltage-gated $K^+$ channels with fast kinetics; 2) $K_v7$ subfamily (often called the KCNQ family) which are pore-forming subunits of voltage-gated $K^+$ channels with slow kinetics; 3) $K_v10$-$K_v12$ subfamilies (also known as EAG family), like $K_v7$ subfamily, that activate relatively slowly upon membrane depolarization (Kew and Davies, 2010). For example, the subunits of the $K_v7$ subfamily form the M-type $K^+$ channels responsible for M current ($I_M$), which is activated at a lower-threshold membrane potential than would normally activate neuronal cells, hyperpolarizes the cell membrane, and consequently reduces the firing of action potential (Santini and Porter, 2010). The protein of EAG family, such as $K_v11.1$, contribute to the cardiac current ($I_{Kr}$), which is important for cardiac repolarization.

### 1.4.5.1 $K_v$ 1-4 channels

$K_v$ 1.x, $K_v$ 2.x, $K_v$ 3.x and $K_v$ 4.x are homologues to the *Drosophila melanogaster* (fruit fly) genes as *shaker, shab, shaw and shal* respectively (Covarrubias et al., 1991). There are 8 genes in $K_v$1 subfamily: $K_v$1.1–$K_v$1.8. All $K_v$1 proteins are capable of forming heteromeric channel complex. In addition, most native $K_v$1 channel complex may include at least one type of $K_v$β subunit. This β-subunits binds to the domain where located in the N-terminal region of the channel pore-forming subunits, constructing channel complexes of eight polypeptides, which play diverse roles in modulating the gating, stability, and trafficking of $K_v$1 channels (Long et al., 2005a). For instance, crystallisation of $K_v$1.2 channel complex exhibits a tetramer of $K_v$1.2 pore-forming subunits associated with a tetramer of $K_v$β proteins (Long et al., 2005b). Moreover, in cultured hippocampal neurons, $K_v$β subunit co-expression led to axonal targeting of $K_v$1.2, recapitulating the $K_v$1.2 localization observed in many brain neurons (Campomanes et al., 2002). $K_v$1 channels can be delayed rectifiers channels that show different degrees of inactivation, except $K_v$1.4 which fully inactivates creating an A-type current due to fast voltage-dependent inactivation by an N-terminal blocking peptide. $K_v$1.4 channels also show a slow recovery from inactivation (MacKinnon et al., 1993). All $K_v$1 subunits are voltage-dependent channels that tend to activate faster and at lower membrane potentials than other $K_v$ channel subfamilies. They produce significant current at voltages below spike threshold (between -50 and -55 mV), and thus are thought to be associated with the subthreshold activity of neurons (Kew and Davies, 2010). The expression of $K_v$1 are widely distributed throughout the body, mainly in brain, but some subunits with important roles in immune cells ($K_v$1.3) (Kazama, 2015), in heart ($K_v$1.4 and $K_v$1.5) (Matsubara et al., 1993), and in smooth muscle ($K_v$1.5) (Yuan et al., 1998). Furthermore, all $K_v$1 channels are highly sensitive to 4-AP with $IC_{50}$ ~ 500 μM, except $K_v$1.8

which exhibit inhibition effects with $IC_{50}$ above 1 mM (Kew and Davies, 2010), whereas the voltage-gated channel blocker TEA does not inhibit the $K_v$1.x channel activity (Hopkins, 1998).

$K_v$2 channels constitute $K_v$2.1 and $K_v$2.2 subunits and are delayed rectifiers that play a significant role in membrane excitability, particularly the repolarisation of action potentials in neurons (Peng and Wu, 2007). $K_v$2 subunits are unique in that they are able to form functional heteromeric channels with other $K_v$ subunits, including $K_v$5, $K_v$6, $K_v$8 and $K_v$9. These associations influence the voltage-dependence and dynamics of activation, deactivation and inactivation, as well as their pharmacological characteristics (Kew and Davies, 2010). For example, co-expression of $K_v$2.1 with $K_v$9.1 slows the rate of activation, leads to a hyperpolarizing shift in the voltage-dependence of activation and inactivation and changes sensitivity to TEA, compared to $K_v$2.1 channel alone (Richardson and Kaczmarek, 2000). The expression of $K_v$2.1 and $K_v$2.2 are both largely expressed across brain tissue (Hwang et al., 1993). $K_v$2 channels are blocked by high concentrations of the classical $K^+$ channel pore blocker TEA ($IC_{50}$: 5-10 mM) but are less-sensitive to 4-AP (Shieh and Kirsch, 1994).

$K_v$3 channels are predominately expressed in CNS neurons, particularly interneurons and are responsible for generating high firing frequencies. $K_v$3.1 and $K_v$3.2 activate and deactivate very fast, with little or no inactivation, a prerequisite feature for fast neuronal firing. $K_v$3 channels have also been suggested to play an essential role in neurotransmitter release due to their distribution in axons and presynaptic terminals of neurons (Brooke et

al., 2004, Ishikawa et al., 2003). Moreover, the activity of $K_v3$ channels become more apparent at more positive potentials in comparison to other $K_v$ channels, not really becoming apparent until potentials more positive than -20 - -10 mV. Interestingly, $K_v3.4$ channels, which show significant inactivation are rarely expressed in the neurons where the other three $K_v3$ genes ($K_v3.1$-3.3) are usually expressed (Weiser et al., 1994), instead they have been shown to have important roles in skeletal muscle physiology (Abbott et al., 2001). $K_v3$ channels are blocked by classical $K^+$ channel blocker TEA ($IC_{50}$: 0.1-0.3 mM) and 4-AP ($IC_{50}$: 0.6-1 mM) (Kew and Davies, 2010), and also blood depressing substance (BDS) toxin BDS I and BDS II with high sensitive with $IC_{50}$ ~ 1 μM (Yeung et al., 2005).

$K_v4$ channels are defined by their fast inactivation and recovery from inactivation, and are known as A-type $K^+$ currents. These features make these channels (particularly those formed by $K_v4.2$ and $K_v4.3$ subunits) key components of the transient outward $K^+$ currents in human heart (Wettwer et al., 1993, Nadal et al., 2001). $K_v4$ channels may associate with specific β-subunits: cytoplasmic $K_v$ channel interacting proteins (KChIPs) and membrane-spanning dipeptidyl aminopeptidase-related proteins (DPPs) (Nadal et al., 2003, An et al., 2000, Barghaan et al., 2008). KChIPs slow $K_v4$ current decay kinetics, promote recovery from inactivation and shift the voltage dependence of steady-state inactivation to more positive potentials (An et al., 2000). DPPs promote both current inactivation and recovery kinetics and shift both activation and inactivation curves of $K_v4$ channels to more negative potentials (Nadal et al., 2003). All members from $K_v4$ subfamily are sensitive to 4-AP (5-10 mM) and display differential sensitivity to block by toxins (e.g. phrixotoxins and stromatoxin) (Kew and Davies, 2010, Diochot et al., 1999, Escoubas et al., 2002).

### 1.4.5.2 $K_v$ 5, 6, 8 and 9 channels

$K_v$ 5, 6, 8 and 9 channels are collectively referred to as electrically silent $K_v$ ($K_vS$) channels because they fail to generate functional ion channel protein by themselves. There are 10 $K_vS$ subunits that have been identified to date: $K_v5.1$, $K_v6.1$-6.4, $K_v8.1$, $K_v8.2$, and $K_v9.1$-9.3, which all display three features in common; 1) they are unable to form functional channels at the plasma membrane as homotetramers or heterotetramers within the $K_vS$ family because of retention in the endoplasmic reticulum, 2) they only associated with $K_v2.x$ as heterotetramers to form functional channels and not with members of the $K_v1.x$, $K_v3.x$ and $K_v4.x$ subfamilies, and 3) they can modulate the biophysical properties of $K_v2$ channels. Therefore, $K_v2/K_vS$ heterotetramers display shifts in the voltage-dependence of activation and/or the voltage dependence of inactivation; changes in the activation, deactivation, and/or inactivation kinetics; and alterations in the current density in comparison with $K_v2$ homotetramers (Bocksteins, 2016). In addition, $K_v6.1$ has been shown to decrease the TEA sensitivity when co-expressed with $K_v2.1$ (Post et al., 1996).

### 1.4.5.3 $K_v$ 7 channels

The $K_v7$ channel subfamily consists of five subunits, $K_v7.1$ to $K_v7.5$. They can form functional homomeric and heteromeric channels within the $K_v7$ subfamily. $K_v7.1$, also known as KCNQ1 or $K_v$LQT1 because of it is association with a form of long QT syndrome, forms the functional basis for the slowly activating $K^+$ ($I_{ks}$) current in the heart (Barhanin et al., 1996). The other members of $K_v7$ ($K_v7.2$-7.5 or KCNQ2-5) are expressed throughout the central and peripheral nervous system (Kew and Davies, 2010). Unlike $K_v7.1$ which forms preferentially homomeric channels, other $K_v7$ channel members co-associate to form

physiologically important currents. $K_v7.2$, $K_v7.3$ and $K_v7.5$ (through co-assembly with $K_v7.3$) are thought to be the molecular correlate for the neuronal M-current (Wickenden et al., 2001, Wang et al., 1998). Mutations to either $K_v7.2$ or $K_v7.3$ are suspected to play a significant role in the hereditary form of juvenile epilepsy (Robbins, 2001, Biervert et al., 1998). Moreover, $K_v7.4$ and $K_v7.5$ have been reported to be expressed in vascular and intestinal smooth muscle cells, and also play an important role in regulating the smooth muscle contractility (Jepps et al., 2009, Greenwood and Ohya, 2009, Stott et al., 2014). Members of the $K_v7$ family have been documented to interact with accessory subunits encoded by KCNE genes. There are five KCNE genes that have been identified, KCNE1-KCNE5. These genes encode proteins with a single transmembrane domain, intracellular N-terminus and an extracellular C-terminus and can significantly affect the activation of threshold $K_v7$ channels (Dedek and Waldegger, 2001). Message for both $K_v7.1$ and KCNE1 (also known as minK) have been detected in epithelial cells of gut and exocrine pancreas (Heitzmann and Warth, 2008). Meanwhile, the $K_v7.1$/KCNE3 complex forms a leak channel in crypt cells of the intestine which is constitutively open at resting potentials (Schroeder et al., 2000).

Regarding their pharmacology, $K_v7$ channel currents are sensitive to the classic potassium channel blockers TEA and $Ba^{2+}$ (Kew and Davies, 2010). XE991 and linopidine are known $K_v7$ channel blockers, and are selective over other $K_v$ channel complexes. Chromanol 293B is a selective blocker for $K_v7.1$ subunits, but displays less sensitivity on $K_v7.2$-7.5 channel currents (Seebohm et al., 2001, Schroeder et al., 2000). Retigabine is an anti-epileptic drug that has been showed to selectively activate $K_v7$ channels (Tatulian et al., 2001). However,

*Stott et al.* (2014) has reported that $K_v$7.1 has lower sensitivity to retigabine-induced enhancement compared to $K_v$7.2-$K_v$7.5, due to the absence of a critical, conserved tryptophan residue in TM6 which forms part of the binding pocket for the drug.

### 1.4.5.4 $K_v$ 10, 11 and 12 channels

$K_v$10, $K_v$11 and $K_v$12 channels are encoded by eight different genes, collectively referred to as the *ether-a-go-go* (eag) $K^+$ channel family and designated KCNHx for the human forms. These three channel types can be characterised by their different biophysical properties. $K_v$10 channels are identified by very rapid activation and lack of inactivation. $K_v$12 channels are characterized by more slowly activation compared with $K_v$10 channels, and may ($K_v$12.1) or may not ($K_v$12.2) exhibit inactivation. $K_v$11 channels display slowest activation properties in these three channel types, but it can be rapidly inactivated (Kew and Davies, 2010), leading to what appears to be an inwardly rectifying current voltage relationship. However, during repolarisation, the channels pass back through the open state to return to the closed state, a phenomenon that results in a large repolarising current. This biophysical phenotype is unique and is central to regulation of cardiac cell excitability. Like $K_v$7 channels, mutations to erg channels induce pathologies such as cardiac long QT syndrome (LQT2) (Sanguinetti and Tristani-Firouzi, 2006). Epilepsy (Li et al., 2016), along with schizophrenia (Calcaterra et al., 2016) and cancer (Asher et al., 2010).

The classic potassium channel blockers such as TEA, quinine, quindine and 4-AP display weakly inhibition in $K_v$10 channels. E-4031 is a cardiac drug that blocks $K_v$11 channels with high-affinity (Zhou et al., 1998) and also blocks $K_v$10 channels (Gessner and Heinemann,

2003) but does not affect $K_v12$ channels (Shi et al., 1998). Human $K_v11$ (hERG) channels remains a critical pharmacological target for therapeutics used in human disease. hERG is universally blocked by many different structurally unrelated chemical compounds ranging from anti-histamines to antibiotics to anti-epileptics. The reason for this appears to be related to the absence of a pivotal conserved proline residue in TM6 that is present across the $K_v$ channel family inducing a widening of the inner cavity of the channel, combined with presence of two aromatic residues (per subunit) that point into the internal cavity of the hERG channel and create a non-specific binding site for many different types of compounds (Mitcheson et al., 2000). Recently several activators have been identified for $K_v11$ channels, such as RPR260243 (Kang et al., 2005b) and NS1643 (Hansen et al., 2006).

### 1.4.5.5 $K_{Ca}$ channels

Calcium-activated $K^+$ channels ($K_{Ca}$) are gated by either voltage and $Ca^{2+}$ combined or $Ca^{2+}$ alone and their activity is directly related to the intracellular $Ca^{2+}$ concentration. The subfamily of $K_{Ca}$ channels contains 8 members and according to their biophysical and pharmacological properties can be subdivided into three groups; small conductance (SK) channels, intermediate conductance (IK) channels and big conductance (BK) channels. SK and IK subunits have the same structure as voltage-gated $K^+$ channels with 6 transmembrane domains and 1 pore loop domain, however they are not voltage-activated. Instead they possess a calmodulin binding domain located in the C-terminus. This calmodulin binding site is utilised for $Ca^{2+}$ sensing that directly induces activation and inactivation of these channels. In contrast, BK channels uniquely have 7 transmembrane domains, possessing an extra TM domain (TM0) prior to the voltage sensor domain, and

therefore an accompanying extracellular N-terminus. The BK channel can be gated by voltage, although weakly compared to other voltage-gated channels, and intracellular calcium ions (Gueguinou et al., 2014, Kew and Davies, 2010). Calcium binding serves to right-shift the apparent voltage activation threshold/sensitivity of the channel. The BK channel can work alone or as a complex with a modulatory β subunit (**Figure 1.13**). BK channels are especially important in smooth muscle cells, where they are maximally activated at the peak of the action potential and participate in the repolarization phase (Vogalis, 2000). Therefore, BK channels are able to sense in an integrative way the changes in both membrane voltage and intracellular $Ca^{2+}$ levels and to respond by mediating an outward hyperpolarizing $K^+$ current. These features award to BK channels remarkable functional roles in excitable cells, such as the regulation of neurotransmitter release and smooth muscle contractility.

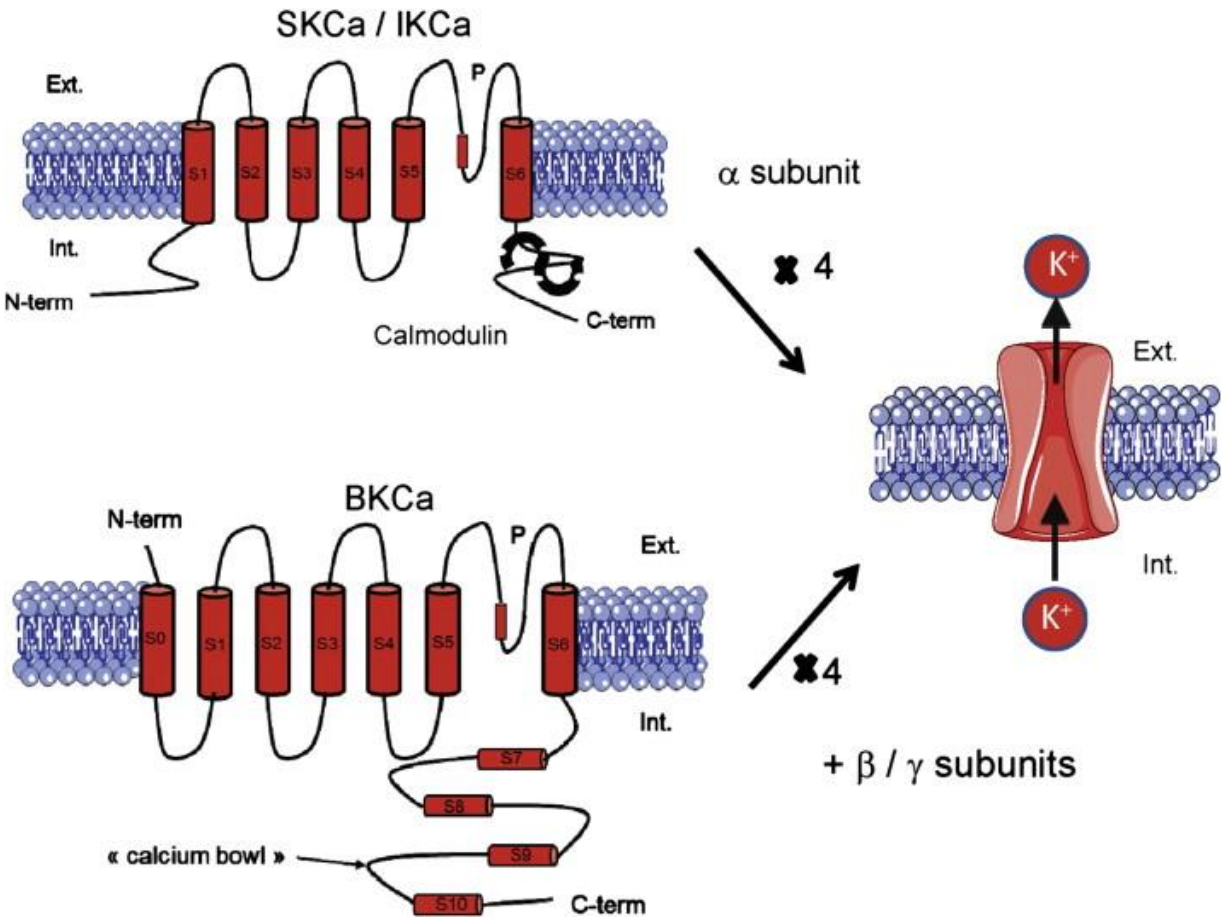


**Figure 1.13:** Characteristics of $K_{Ca}$ channels. $K_{Ca}$ channels are divided into 3 families that include large conductance (BK) channels, intermediate conductance (IK) channels and small conductance (SK) channels. The α-subunit associate to form tetramers for SK and IK, with β subunit for BK or without known auxiliary subunit for SK and IK channels (Gueguinou et al., 2014).

$K_{Ca}$ channels are widely distributed throughout the nervous system. SK and BK channels are expressed in CNS, while IK channel is mainly expressed in PNS. Both BK and SK channels have been identified in intestinal smooth muscle cells, which are essential to the regulation of smooth muscle contractility (Tang et al., 2015, Wang et al., 2010). Unlike for SK and BK channels, the expression of IK subunits is largely non-neuronal, for example in the salivary glands, the placenta and the lungs, and are suggested to play an essential role in lymphocyte activation (Gueguinou et al., 2014). Furthermore, $K_{Ca}$ channels have been

found in various tumour cell lines, including prostate cancer, breast cancer, gliomas, and melanoma colon cancer. Here they are thought to play a functional role in regulating cancer cell migration and proliferation (Gueguinou et al., 2014, Bulk et al., 2015, Potier et al., 2006).

Pharmacology of $K_{Ca}$ channels has traditionally been centred on various peptide toxin blockers or small organic molecules that either inhibit by a pore-blocking mechanism or act as positive or inhibitory modifiers of the gating processes. Apamin has been revealed to be a selective blocker of SK channels with the affinity in SK2 > SK3 > SK1. IK channels can be inhibited by several scorpion toxins such as charybdotoxin, maurotoxin and margatoxin (Kew and Davies, 2010). There are two well characterised peptide inhibitors of BK channels, iberiotoxin (IbTX) and charybdotoxin (ChTX). A number of non-peptide compounds also inhibit BK channels, such as TEA with $IC_{50}$ ~0.14 mM and paxilline with $IC_{50}$ ~ 1.9 nM (Kew and Davies, 2010). SKA-31 is an activator for SK1, SK2 and IK channels, displaying a higher affinity for IK than to SK channels (Sankaranarayanan et al., 2009). Furthermore, a small molecules known as NS309 has been shown activate both IK and SK channels but displays no activity towards BK channels (Strobaek et al., 2004, Morimura et al., 2006).

### 1.4.5.6 Gating mechanisms of voltage-gated $K^+$ channels

As previously stated, signal transduction in excitable cell requires an extremely rapid mechanism for opening and closing (gating) the ion channel pore. In voltage-gated potassium channels, open/closed transitions are created at the level of the TM6 (S6) domain. As shown in **Figure 1.14**, this gating mechanism involves rotation of the TM6 of

each subunit of the channel thereby, like an iris of a camera, shutting the intracellular entrance to the channel. This rotation of the TM6 domains occurs in response to movement of the voltage sensing apparatus, and is therefore directly coupled to changes in transmembrane potential. There are also two further mechanism that control the viability of the conduction pathway, through a process known as inactivation. Here the intracellular TM6 (S6) gate remains open but the channel is no longer able to conduct ions. Firstly, the narrowest portion of the conduction pathway, the selectivity filter, may collapse, pinching shut the conduction pathway and is also known as C-type inactivation. This mechanism is prominent in A-type channels such as $K_v4$ channels, where transmembrane voltage changes are sensed by the voltage sensing apparatus, causing their subsequent realignment and mechanically inducing opening of the TM6 gate, which is swiftly followed by a collapse of the selectivity filter. It is argued that the C-type inactivation mechanism is allosterically coupled to TM6 gate transitions such that opening of the intracellular gate initiates inactivation of the filter gate (Bahring et al., 2012, Yellen, 2002). Finally, there is an alternative process of inactivation, called N-type inactivation. Again the intracellular (TM6) gate remains open, but here the entrance to the intracellular face of the conduction pathway is plugged by the binding of an auto-inhibitory peptide, attached to the N-terminus of the channel subunit, to the cavity of the channel. This type of inactivation by a ball peptide occurs in a voltage-dependent manner in $K_v1.4$ channels, but can also be provided by ball peptides intrinsic to auxiliary β subunits (Yellen, 2002, Zhou et al., 2001a).

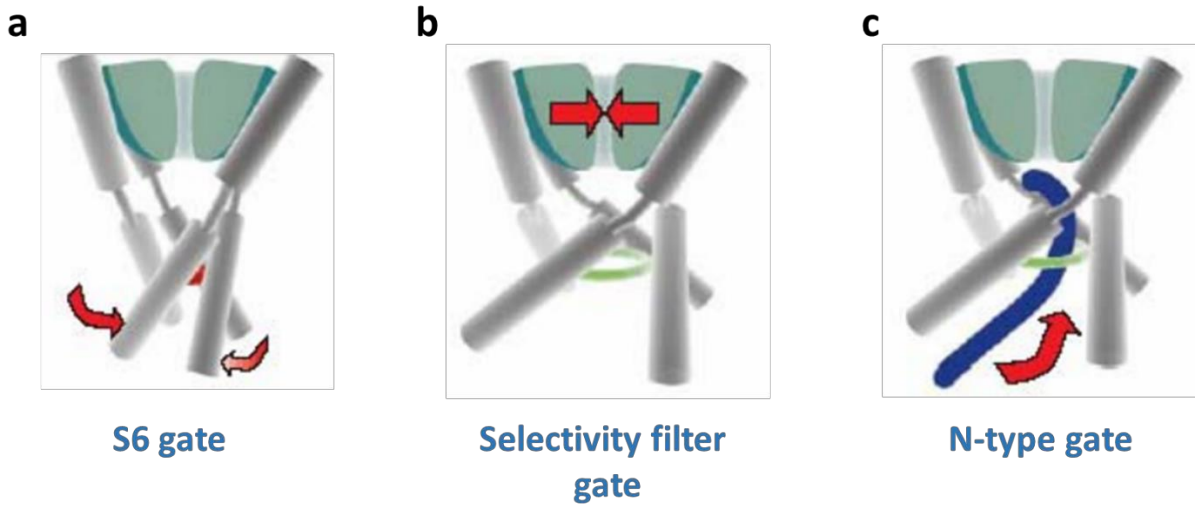


**Figure 1.14:** The conformational changes that gate the $K^+$ channel pore. **(a)** Shows a closed $K^+$ channel, on the basis of the KcsA structure. The four TM6 (S6) transmembrane segments swing together to produce a secure closure at the bundle crossing. This prevents ion flow and can also trap organic channel blockers in the enclosed cavity. Alternatively, the channel may be inactivated at the selectivity filter **(b)**, or by binding of an auto-inhibitory peptide **(c)** when a binding site in the pore is revealed by opening of the S6 gate (Yellen, 2002).

### 1.4.6 4TM-2P channel family

4TM-2P (two-pore domain or $K_{2P}$) channel subunits consist of four transmembrane domains, and two pore-forming regions between TM1 and TM2, and also between TM3 and TM4 (**Figure 1.15a**). Therefore functional channels are a result of subunit dimerisation as opposed to the tetramerisation required of $K_v$ and $K_{ir}$ channel subunits. $K_{2P}$ channels lack voltage dependency and specific ligand gating requirements and as such contribute to background potassium conductance across all voltages. Their outward rectification under physiological conditions arises from the asymmetric $K^+$ gradient across the membrane as predicted by the Goldman-Hodgkin-Katz (GHK) (Goldstein et al., 2001). These features allow $K_{2P}$ channels to play an important role in excitable cells (such as neurons and muscle cells) because they not only set and regulate resting membrane potential but also

contribute significantly to repolarization in many cell types. (Schewe et al., 2016). Historically, the first recognised two pore $K^+$ channel ($K_{2P}$) was discovered in the baker's yeast *Saccharomyces Cerevisiae* in 1995 and was called TOK (Ketchum et al., 1995). This channel had subunits that possess 8TM and 2P domains and led to the identification of related two pore channel subunits from the fruit fly Drosophila melanogaster (KCNKO) in 1996 (Goldstein et al., 1996). A few month later, the first mammalian $K_{2P}$ channel homologues, a weak inward rectifying $K^+$ channel (TWIK-1 also known as KCNK1) were cloned (Lesage et al., 1996).

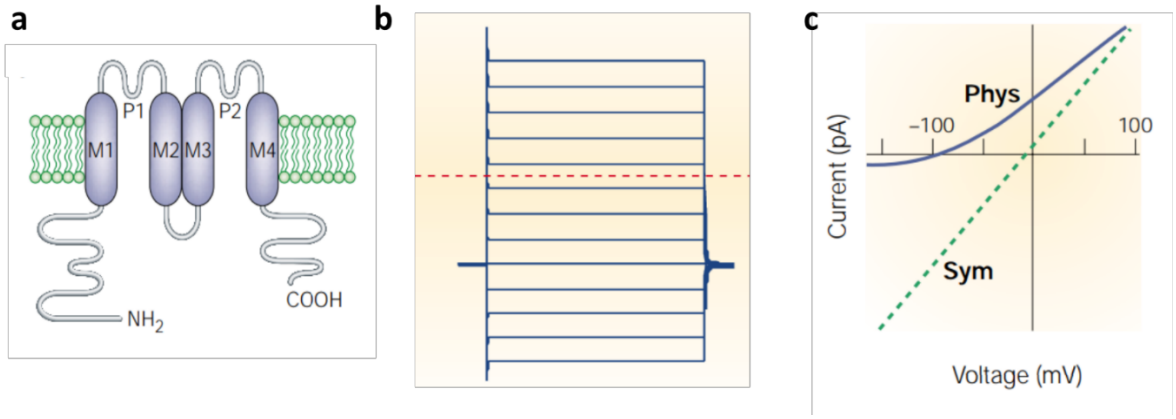


**Figure 1.15:** Characterisation of 4TM-2P channels. **(a)** Membrane topology of a typical 4TM-2P family. Transmembrane domains are labelled M1-M6, with the pore loop labelled P1 & P2. **(b)** The example current traces based on KCNK0. **(c)** Current-voltage relationship for $K_{2P}$ channels under physiological $K^+$ concentration (blue line) and symmetrical $K^+$ concentration (dotted green line). Taken from (Goldstein et al., 2001).

## 1.5 Two-pore-domain $K^+$ channels

The human genome encodes 15 $K_{2P}$ family subunits, which can be divided into following 6 subfamilies by their different biophysical and pharmacological properties (**Figure 1.18**): TWIK, TASK, TREK TALK, THIK and TRESK. Although each $K_{2P}$ subunit displays same structure, they share rather low sequence similarity outside the pore domains (Sanders & Koh, 2006). In addition, $K_{2P}$ channel gating can be modulated by voltage, changes in oxygen tension, temperature, pH levels and membrane stretch (Kang et al., 2005a, Lewis et al., 2001, Maingret et al., 1999), but insensitive to classic $K^+$ blocker TEA and 4-AP (Lotshaw, 2007, Enyedi and Czirjak, 2010).

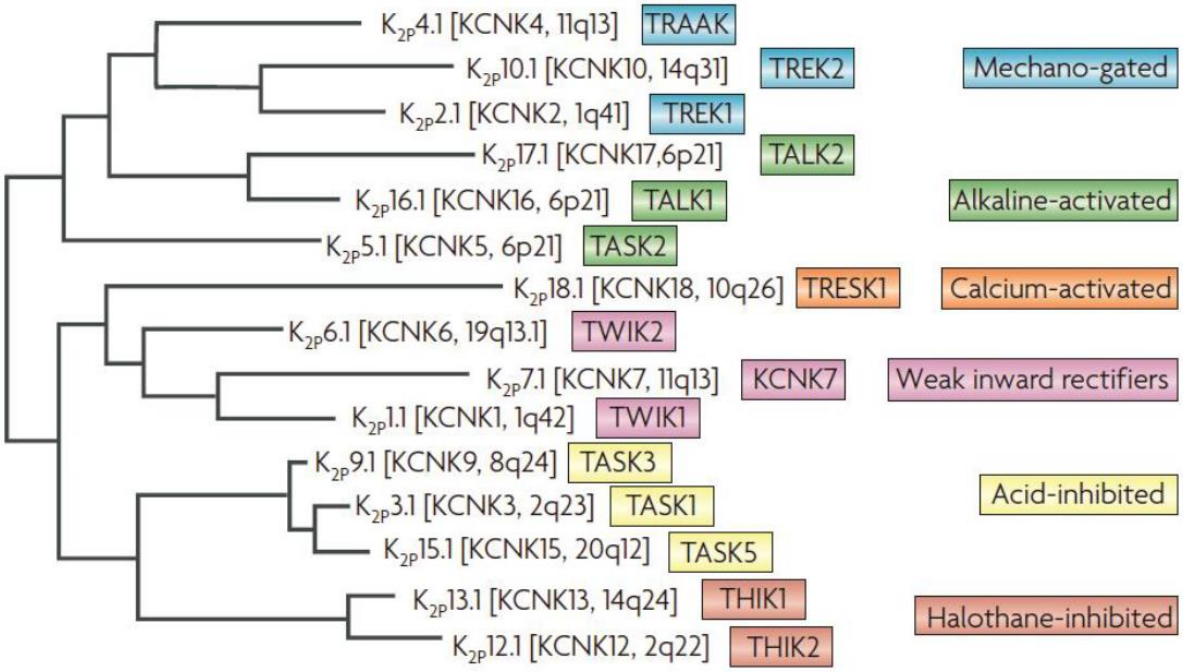


**Figure 1.16:** Phylogenetic tree of human $K_{2P}$ channels. The nomenclature according to the International Union of Pharmacology ($K_{2P}$ X.X) and the HUGO (KCNKX) are presented, together with the chromosomal localization and functional characteristic of each channel subfamily (Honore, 2007).

### 1.5.1 Weak Inward rectifier TWIK subfamily

The TWIK subfamily comprises the first mammalian member of $K_{2P}$ channel family to be discovered, KCNK1 (TWIK-1), as well as KCNK6 (TWIK-2) and the silent subunit KCNK7 (TWIK-3) (Lotshaw, 2007). Both TWIK-1 and TWIK-2 display weak inwardly rectifying currents, which are sensitive to cytosolic pH levels, inhibited by intracellular acidification (Lesage et al., 1996). Unfortunately, the electrophysiological characterization of TWIK subfamily members has been obstructed by their low or absent functional expression in heterologous systems, thought to be due to suppression by a small ubiquitin-like polypeptide, SUMO. However, either deSUMOylation of expressed channels using a SUMO-selective protease or mutation of the predicted SUMOylation site K274 to a glutamic acid can prevent SUMOylation and increase functional expression (Rajan et al., 2005). Interestingly, TWIK-1 is the only member in TWIK subfamily that subject to SUMOylation, since TWIK-2 lacks lysine within its C-terminus while the lysine in TWIK-3 does not appear to reside within any known variations of the SUMOylation sequence (Lotshaw, 2007). In addition, TWIK-1 has been reported to form functional channels upon heteromeric assembly with other $K_{2P}$ subunits, such as TASK-1, TASK-3 and TREK-1 (Hwang et al., 2014, Berg et al., 2004a, Plant et al., 2012).

Pharmacological characterization of TWIK family is still very limited by virtue of its poor functional expression. There are no selective pharmacological modulators available for either TWIK-1 or TWIK-2. Both $Ba^{2+}$ and quinidine have been shown to have an inhibitory effect on TWIK-1 channel (Lesage et al., 1996). However, human TWIK-2 was identified to

be insensitive to both $Ba^{2+}$ and quinidine (Chavez et al., 1999) while rat TWIK-2 was significantly inhibited by both $Ba^{2+}$ and quinidine (Patel et al., 2000).

### 1.5.2 Mechano-gated TREK subfamily

The TWIK-related $K^+$ channel (TREK) family is comprised of KCNK2 (TREK-1) (Fink et al., 1996), KCNK10 (TREK-2) (Lesage et al., 2000) and the closely related TWIK-related arachidonic acid activated $K^+$ channel KCNK4 (TRAAK) (Fink et al., 1998). The TREK subfamily have been demonstrated to contribute to the cellular mechanisms of apoptosis, vasodilatation, anesthesia, pain, neuroprotection and depression (Noel et al., 2011). Characterisation of TREK-1 identified showed it to be outwardly rectifying (Fink, Lesage et al. 1998), with the presence of physiological $Mg^{2+}$ or $Ca^{2+}$ saturating the unitary conductance observed in symmetrical $K^+$ at negative potentials (Kim et al., 2001a, Patel et al., 1998). While the amplitude of TREK-2 and TRAAK channel currents is not influenced significantly by the presence of extracellular $Mg^{2+}$ (Bang et al., 2000, Kim et al., 2001a, Lesage et al., 2000). These channels present a low, weakly voltage-dependent open probability that can be activated by both chemical and physical stimuli, including mechano-stretch (Patel et al., 1998, Lesage et al., 2000, Kim et al., 2001a), polyunsaturated fatty acids (PUFA) (Patel et al., 1998, Kim et al., 2001b, Kim et al., 2001a), temperature increasing (Maingret et al., 2000a, Kang et al., 2005a) and cytosolic acidification, except TRAAK which activated by cytosolic alkalinisation (Lesage et al., 2000, Kim et al., 2001b, Kim et al., 2001a). For instance, regarding their mechano-sensitivity, TREK channels are activated by laminar and shear stress due to membrane cup formation, whilst they are inhibited by shrinkage of the cell which induces membrane crenation (Patel et al., 1998). Furthermore, these

mechano-gated TREK channels have been identified to be functionally coupled to G-protein signalling pathways and activation of the Gs/cAMP/PKA and the Gq/PLC/DAG/PKC signalling pathways indirectly inhibit TREK-1 channels by phosphorylating defined serine residues on the C-terminal tail (Enyedi and Czirjak, 2010, Lesage et al., 2000).

TREK-1 subunits were the first members of the TREK subfamily to be identified, (Fink et al., 1996). TREK-1 shares 63% sequence identity and 78% homology with TREK-2 (Noel et al., 2011), which was firstly cloned from human brain by Lesage *et al* (2000). While human TRAAK share 38% sequence identity to human TREK-1 and 40% sequence identity to human TREK-2 (Fink et al., 1998). The identity falls to 45% and homology to 69% with TRAAK and to 50–55% homology with the other K2P subunits (Noel et al., 2011). Previous studies reported that mouse TREK-1 is widely expressed in brain, lung, kidney, heart as well as GI tract (Fink et al., 1996, Koh et al., 2001, Talley et al., 2001b), while human TREK-1 is abundantly expressed in brain and GI tract (Meadows et al., 2000, Medhurst et al., 2001). TREK-2 was abundantly expressed in human kidney, pancreas, brain and GI tract, overlapping with TREK-1 expression in many brain regions as well as in peripheral organs (Lesage et al., 2000, Medhurst et al., 2001), whereas TRAAK is present exclusively in brain, spinal cord and retina (Fink et al., 1998)

Regarding their pharmacology profile, TREK-1 and TRAAK can be inhibited by the classical pore blocking ion, $Ba^{2+}$ at high concentration ~1 mM (Ma et al., 2011, Fink et al., 1998). The serotonin reuptake inhibitors such as fluoxetine and its active metabolite norfluoxetine have been reported as a blocker of TREK-1 (Kennard et al., 2005) and TREK-2 (Dong et al.,

2015). Recently, an endogenous peptide called Spadin has been reported as a selective blocker to TREK-1 with $IC_{50}$ ~ 100nM (Mazella et al., 2010), but had effect to TREK-2 and TRAAK channel currents (Moha Ou Maati et al., 2012). The neuroprotective agent riluzole has been reported as an activator of TREK channels at concentration ~100 µM (Duprat et al., 2000). Fenamates, non-steroid anti-inflammatory drugs, including BL-1249 and FFA (flufenamic acid) have been revealed to directly and reversibly activate all three channels (Veale et al., 2014), but BL-1249 displays selectively among the TREK subfamily, activing TRAAK around 10 fold less potently than TREK-1 (Pope et al., 2018). Also, the caffeic acid derivative and lipoxygenase inhibitor cinnamyl 1-3,4-dihydroxy-alpha-cyanocinnamate (CDC) has been revealed to activate TREK-1 (Danthi et al., 2004).

### 1.5.3 Acid-sensitive TASK subfamily

The TWIK-related acid-sensitive $K^+$ channel family (TASK) comprises of three channels, TASK-1 (KCNK3), TASK-3 (KCNK9) and non-functional TASK-5 (KCNK15) (Duprat et al., 1997). The non-functional TASK-5 channels share high sequence similarity with the other two members thereby has been classified into TASK subfamily. TASK-1 and TASK-3 are closely related with similar biophysical activities as well as overlapping pharmacological phenotypes. Both functional channels are strongly inhibited by extracellular acidification such that only about 10% of the current remains following a reduction of pH from 7.3 to 6.3. TASK-1 has a pKa (acid dissociation constant) ~ 7.3 whereas TASK-3 has a pKa ~ 6.8 (Kang et al., 2004a, Berg et al., 2004b). The activity of these two channels can be influenced by several regulatory factors in the same direction, such as G-protein receptors, oxygen and partner proteins located in C-terminus (e.g. 14-3-3, β-COP and p11). For instance,

stimulation of $G_q$-coupled receptors leads to an inhibition of TASK-1 and TASK-3 currents. The effect is mediated by liberation of $G_q\alpha$, which binds directly to and inhibits the channels (Enyedi and Czirjak, 2010, Feliciangeli et al., 2015). In addition, TASK-1 and TASK-3 can form a functional heteromeric channels exhibiting properties distinct from TASK-1 and TASK-3 alone (Czirjak and Enyedi, 2002, Berg et al., 2004a), however TASK-5 is unable to form functional channels with other $K_{2P}$ channels (Enyedi and Czirjak, 2010). TASK-1 has been reported widely expressed in pancreas, placenta, brain, lung and less so in heart. TASK-3 abundantly distributed in brain with lower expression levels in a variety of peripheral organs (Lotshaw, 2007).

Similarly to TREK subfamily, TASK channels are insensitive to classic $K^+$ blockers, TEA, $Ba^{2+}$ and 4-AP, as well as arachidonic acid (Maingret et al., 2000b, Maingret et al., 2001). The endocannabinoid anandamide and its more stable analog, methanandamide, exhibit high selectively for TASK-1 and TASK-3, as it does not inhibit other $K_{2P}$ channels (Maingret et al., 2001). The polyvalent catonic dye ruthenium red is a selective blocker for TASK-3 channel, and can be used to distinguish TASK-3 currents from other $K_{2P}$ channel currents (Czirjak and Enyedi, 2002, Aller et al., 2005). Volatile anaesthetic agents such as isoflurane and halothane, activate TASK-1 and TASK-3 and this requires the proximal cytoplasmic C-terminal domain (Patel et al., 1999, Sirois et al., 2000).

### 1.5.4 Alkaline-activated TALK subfamily

The TWIK-related alkaline pH-activated $K^+$ channel (TALK) subfamily is comprised of three members: TASK-2 (KCNK5), TALK-1 (KCNK16) and TALK-2 (KCNK17). All three members are

sensitive to extracellular pH levels in the alkaline range and are either completely or almost completely inhibited at the physiological pH of 7.4, exhibiting robust currents by alkalinisation at a pH range from 7.5 to 10 (Girard et al., 2001, Reyes et al., 1998). TASK-2 channels are broadly distributed in epithelial tissues in kidney and pancreas and to lesser extents in liver, placenta and small intestine, and are also expressed in nervous tissue in brain (Reyes et al., 1998). TALK-2 channels are localised to pancreas, liver, heart, lung and placenta. In contrast, TALK-1 channels have to date only been shown to be expressed in exocrine pancreas (Duprat et al., 2005, Girard et al., 2001).

All TALK channel currents are voltage-independent and sensitive to $Ba^{2+}$ and volatile anesthetics (*e.g.* halothane), but not to other traditional $K^+$ channel blockers, such as TEA, 4-AP and $Cs^+$. Quinine has been reported to inhibit the basal activity of TALK-1 channels, whereas activate TALK-2 channels (Girard et al., 2001). An interesting pharmacological feature of TALK-2 channels is their stimulation by nitric oxide , eliciting robust TALK-2 channel currents, a mechanism notably absent in TALK-1 channels (Duprat et al., 2005). Clofilium know as a blocker of the hERG channel which also inhibits TASK-2 with an $IC_{50}$ of 20 μM (Niemeyer et al., 2001).

### 1.5.5 Halothane-inhibited THIK subfamily

The halothane-inhibited THIK subfamily comprises three members, THIK-1 (KCNK13) and the non-functional THIK-2 (KCNK12), and THIK-1 exhibits leak currents displaying weak inward rectification in symmetrical $K^+$ (Rajan et al., 2001). In rat, THIK-1 mRNA was widely expressed through the body (e.g. muscle, heart, testis, lung, brain, kidney, liver and

stomach) and THIK-2 mRNA was similarly wide distributed except in skeletal muscle, heart and testis (Rajan et al., 2001) . Unfortunately, the expression of THIK-1 and THIK-2 have not been investigated in human yet. THIK-1 is insensitive to extracellular pH levels, temperature and lysophospholipids. However, THIK-1 is activated by arachidonic acid and inhibited by halothane, giving the name to this subfamily (Rajan et al., 2001).

### 1.5.6 Calcium-activated TRESK subfamily

The calcium-activated TRESK subfamily is the last $K_{2P}$ subfamily to be identified, consisting of only one subunit TRESK (KCNK18) (Enyedi and Czirjak, 2010). The predicted topology of TRESK followed the generalisations established for all $K_{2P}$ channels presenting 4 transmembrane domains and 2 pore domains. However, TRESK is differed in possessing an exceptionally long (91 amino acids) intracellular TM2-TM3 linker and a short intracellular C-terminus (~13 residues) (Kew and Davies, 2010). Interestingly, the human and mouse homolog of TRESK exhibited an unexpectedly low (68%) sequence identity, and thus mouse homolog of TRESK was reported and presented as TRESK-2 (Kang et al., 2004b). TRESK mRNA expression was initially found only in spinal cord (Sano et al., 2003), but has since been detected in brain (Liu et al., 2004).

The TRESK channel is regulated by the calcium/calmodulin-dependent protein phosphatase, calcineurin, meaning that increasing intracellular $Ca^{2+}$ levels activate the channel. TRESK channels are also sensitive to volatile anesthetics, including isoflurane, halothane, sevoflurane, desflurane and chloroform (Czirjak et al., 2004, Enyedi and Czirjak, 2010) and both human and mouse homologues are sensitive to intracellular pH levels.

Human TRESK is weakly sensitive to extracellular pH while the mouse TRESK was strongly regulated within the physiological to pathophysiological range of extracellular pH (Keshavaprasad et al., 2005, Kang et al., 2004b). Zinc and mercuric ions distinguish TRESK from other $K_{2P}$ channels, inducing a significant and potent inhibitory effect (Czirjak and Enyedi, 2006).

### 1.5.7 Heterodimerization between $K_{2P}$ subunit genes

Heterodimerization of subunits is a widespread mechanism for increasing diversity in $K^+$ channel subfamilies. The resulting heterodimers are typically characterized by different biophysical and regulatory properties from the homodimers of the parent subunits. Certain $K_v$, $K_{ir}$ or $K_{2P}$ (e.g. $K_v$8.1, $K_{ir}$5.1 or $K_{2P}$1.1) subunits cannot form functional homodimers on their own, however, via heterodimerization they can also gain important physiological function. There are several heteromeric $K_{2P}$ channels (see Table) have been described in recent studies. For example, TASK-1 and TASK-3 can form functional heterodimers detecting in several cell type (Berg et al., 2004a, Kang et al., 2004a, Kim et al., 2009), and exhibiting properties distinct from TASK-1 and TASK-3 alone, which showed intermediate pH sensitivity and ruthenium red insensitivity (Czirjak and Enyedi, 2002). TWIK-1 was also reported that can form heterodimeric channels with TASK channel subunits (TASK-1 or TASK-3) and TREK-1 channel, and these heterodimeric channels exhibit biophysical and pharmacological properties different from their parental channels (Plant et al., 2012, Hwang et al., 2014, Choi et al., 2018).

**Table 1.2:** Heterodimers of $K_{2P}$ channels.

| **$K_{2P}$ Heterodimers** | **Biophysical/Pharmacological Activity** |
|---|---|
| TWIK-1/TREK-1 | The heterodimer generate passive conductance and was reported in hippocampal astrocytes (Hwang et al., 2014). |
| TWIK-1/TASK-1 (or TASK-3) | The heterodimer exhibit acid-sensitive and halothane-sensitive outwardly rectifying $K^+$ currents in cerebellar granule neurons (Plant et al., 2012, Choi et al., 2018). |
| TREK-1/TREK-2 | The heterodimer was inhibited by extracellular acidification and by spadin similarly to TREK-1 (Lengyel et al., 2016). |
| TRAAK/TREK-1 (or TREK-2) | The heterodimer exhibit different electrophysiological, regulatory and pharmacological properties different from those of homodimeric channels (Blin et al., 2016). |
| TASK-1/TASK-3 | The heterodimer mediate the pH and isoflurane-sensitive $K^+$ currents (Berg et al., 2004a, Czirjak and Enyedi, 2002). |
| TASK-1/TALK-2 | The heterodimer display unique hybrid to extracellular pH sensitivity and halothane compared to their parental channel (Suzuki et al., 2017). |
| THIK-1/THIK-2 | THIK1 was able to counteract the endoplasmic retention of THIK-2 (Blin et al., 2014). |

## 1.6 Aims

Gastrointestinal tract motility relies on highly coordinated contractions of its longitudinal and circular smooth muscles. Disruption to this physiological process can result in long term motility disorders such as IBS. Although much is known about the ionic conductances responsible for GI smooth muscle contraction, comparably little is known about the underlying $K^+$ channels responsible for suppressing smooth muscle contractility and promoting GI tract relaxation. The hypothesis underpinning this thesis is that $K_{2P}$ channels

have expressed and play a function role in regulating intestinal contractility. The overall aims of my PhD are; 1) to characterise the expression profiles of potassium channel subtypes along the mouse ileum and colon using quantitative RT-PCR methodology, 2) to describe the localisation of various $K_{2P}$ potassium channel subtypes along the mouse ileum and colon using immunohistochemical techniques, 3) to determine the functional role of potassium channel subtypes in regulating intestinal smooth muscle contractility, and 4) to further characterise the biophysical and pharmacological properties of mechano-gated TREK channels cloned from mouse.

# Chapter 2 - Materials and Method

## 2.1 Animals

Adult (2-4 months old) C57BL/6 mice (Charles River, Margate, UK) of either sex (weighing ~20-30 g) were used through whole project study. SOX10-lox-GFP-4xPolyA-lox-DTA transgenic mice were also used in immunohistochemistry studies, which express the enhanced green fluorescent protein (EGFP) under transcriptional control of the SOX10 gene (Kessaris et al., 2006). The SOX10-EGFP transgenic line was from Professor Arthur Butt (University of Portsmouth, U.K.), and was originally a gift from Professor Bill Richardson (University College London, U.K.). All procedures involving l animals were approved by the Ethics Committee of the University of Portsmouth and were performed by a personal licence holder, in accordance with the regulations issued by the Home Office of the United Kingdom under the Animals (Scientific Procedures) Act, 1986. All animals were housed in standard plastic cages, on sawdust bedding in an air-conditioned room at 22 ± 1°C under lighting controls with 12 hrs light and dark cycles. Standard mouse chow and tap water were provided *ad libitum*.

## 2.2 Quantitative RT-PCR

### 2.2.1 Total RNA Extraction

Adult C57BL/6 mice (N = 3) were killed by cervical dislocation and approximately 100 mg of distal ileum and distal colon were dissected and stored in RNA Later (Qiagen, Manchester, UK) with ice. Extraction of total RNA was performed using the RNeasy Midi kit (Qiagen, Manchester, UK) following the manufacturer's instructions. Briefly, tissue was disrupted and homogenized using the TissueRuptor with sterile plastic pestle (Fisher) in round

bottomed collection tubes containing 2 ml guanidine thiocyanate (GITC) lysis buffer (RLT) and then centrifuged at 5000 x g for 10 minutes at 20°C. GITC is a chaotropic salt, i.e. a potent protein denaturant which inactivates RNases thus allowing for the RNA to be isolated intact. The supernatant was carefully removed and transferred to new collection tubes by pipetting before adding 70 % molecular grade ethanol at 1:1 ratio. Samples were then transferred onto an RNeasy Midi tube containing a silica-gel membrane upon which the RNA would bind during subsequent centrifugation at 5000 x g for 5 minutes. A wash with 4 ml of a chaotropic salt containing buffer RW1 were added onto tube and performed at 5000 x g for 5 minutes in order to wash away any remaining contaminating impurities such as degraded proteins. A further wash with 2.5 ml ethanol RPE buffer was applied at 5000 x g for 2 minutes, then this step was repeated at 5000 x g for 5 minutes in order to wash away any remaining salts. Finally, high quality total RNA was eluted in 150 µl RNA-free water by centrifugation for 3 minutes at 5000 x g.

The purity and concentration of isolated total RNA was evaluated using a ND-1000 Spectrophotometer (NanoDrop Technologies, Wilmington, DE, USA) to measure the UV absorption of each of the samples. The absorption at 260 nm ($A_{260}$) was used to identify the concentration of single stranded RNA in undiluted samples. The ratio of absorbance at 260 nm and 280 nm ($A_{260}/A_{280}$) was used to quantify the purity of samples. A ratio of ~1.8 indicates an acceptable purity for DNA, and a ratio of ~2.0 for RNA. RNA optimally absorbs light at a wavelength of 260 nm due to its high content of nucleotides, while proteins and other impurities that might be contaminating the isolated RNA absorb best at 280 nm, thus the $A_{260}/A_{280}$ ratio is the preferred method to evaluate sample purity.

mRNA was reverse transcribed into complementary DNA (cDNA) using the $RT^2$ first Strand Kit (Qiagen, Manchester, UK), following the manufacturer's instructions. Briefly, 500 ng total RNA was incubated in a two-step process with genomic DNA elimination mix and Reverse-transcription enzyme mix. Random hexamers and oligo-dT prime reverse transcription in an unbiased manner and generates full length cDNA.

### 2.2.2 Quantitative real-time PCR (qRT-PCR)

qRT-PCR was used to define the expression profiles of 96 potassium channel gene transcripts from ileum and colon tissue sections. Primers were designed to target the 15 identified mouse $K_{ir}$ genes, 40 $K_v$ genes, 8 $K_{ca}$ genes, 14 $K_{2P}$ genes (mice lack the KCNK17 gene encoding for TALK-2), 16 β subunit genes and 3 housekeeping genes including GAPDH, RPLP0 and HPRT. All qRT-PCR plate arrays were bought from Primerdesign (Southampton, UK). 1350 µl of 2x SYBR Green qRT-PCR Mastermix (Qiagen) was mixed with 102 µl cDNA and 1248 µl RNA-free water. Then, 25 µl of cDNA mixture was pipetted in each well of the 96-well-plate, and along with the 5 µl of primer already contained in each well, gave a total reaction volume of 30µl. The reactions were thermo cycled on a Roche Lightcyclcer 96 instrument (Roche) using the following protocol; pre-incubation, 95°C for 60 seconds (1 cycle), followed by 2 step amplification, 95°C for 15 seconds and 60°C for 1 minutes (45 cycles), finally melting step, 60°C for 15 seconds and 95°C for 1 seconds. Results were analyzed in the LightCycler 96 initially, using relative quantitative method in order to analyze changes in gene expression in given samples relative to the reference samples. Data normalization was performed using the best housekeeping genes for each

experiment. Optimal housekeeping gene were chosen using the NormFinder logarithm (Andersen et al., 2004) and the standard deviation (SD) method (Mane et al., 2008), which is a way to establish which housekeeping gene or combination of genes was the most stable and therefore appropriate to use for normalisation. Then, data were analyzed by using ΔCt method for studying the expression level of each potassium channel transcript with following formula:

**Ct sample – Ct Calibrator (mean of best housekeeping genes) = ΔCt**

**Relative quantity = Average ($2^{-\Delta Ct}$)**

The Ct (cycle threshold) is defined as the number of cycles required for the fluorescent signal to across the threshold (i.e. exceeds background level). Ct levels are inversely proportional to the amount of target nucleic acid in the sample. All graphs were constructed using GraphPad Prism7 software (GraphPad Software, San Diego, CA, USA).

## 2.3 Reverse transcription-polymerase chain reaction (RT-PCR)

mRNA from mouse ileum, colon and whole brain were extracted (2.2.1) and reverse transcribed into complementary DNA (cDNA) using SuperScript™ First-Strand Synthesis System for RT-PCR kit (Invitrogen, California, USA). In some cases plasmid DNA constructs expressing mTREK-1, mTREK-2 and mTRAAK genes were used as positive controls and were a kind gift from G. Sandoz (Université de Nice Sophia Antipolis, Nice, France). The total PCR reaction volume was 50 µl, containing 32.5 µl dd$H_2O$, 1 µl dNTP mix, 1 µl DMSO, 10 µl x5 reaction buffer, 1 µl cDNA (10 ng), 2 µl Forward Primer (10 µM), 2 µl Reverse Primer (10 µM), 0.5 µl Iproof Taq (2 units/µl). The primers used in this study (**Table 2.1**) were designed

using the National Center for Biotechnology information (NCBI) Primer-BLAST tool (http://www.ncbi.nlm.nih.gov/tools/primer-blast/) and synthesised by Sigma-Aldrich (Gillingham, UK). The PCR reaction were cycled in C1000 Touch Thermal Cycler (Biorad, Hercules, CA) as following protocol: a single step at 98 °C for 2 minutes, followed by 35 cycles of 98 °C for 10 seconds, 55 °C for 30 seconds and 72 °C for 30 seconds, and a final single step at 72 °C for 10 minutes. 25 µl of the RT-PCR reaction products were seperated on a 2 % (w/v) agarose gel at 10 V/cm for 30-40 minutes. The agarose gel was made by dissolving 1 g of agarose in 50 ml of 1 x TAE buffer (containing 40 mM tris-base, 20 mM acetic acid, 1 mM EDTA, pH was adjusted to 8.0) and adding 5 µl of SYBR safe DNA Gel Stain (Invitrogen) to allow visualisation of DNA. Gel images were captured under UV light using a BioRad Gel Doc EZ System (BioRad).

**Table 2.1: Details of RT-PCR primer sequences.**

| Mouse Gene | Accession number | Primer sequence | RT-PCR Product length (bp) |
|---|---|---|---|
| **TREK-1** | XM_006497121.3 | **F:** GTTTGGCTTTCTACTGGCTG<br>**R:** GACCGTTCAGATAGATGCTC | 676 |
| **TREK-2** | NM_001316665.1 | **F:** GGCTAATGTCACTGCTGAGTTCC<br>**R:** ACAAGACAACACATAGTCCAATTCC | 624 |
| **TRAAK** | NM_008431.3 | **F:** GTGACCCAGCGAACTGGGCC<br>**R:** GCCACGCTCACTCTGCGTGT | 219 |
| **β actin** | NM_007393.5 | **F:** TGCCGCATCCTCTTCCTC<br>**R:** CGCCTTCACCGTTCCAGT | 647 |

## 2.4 Immunohistochemistry

### 2.4.1 Tissue preparation for immunohistochemistry

Adult C57BL/6J mice and SOX10 transgenic mice of either sex were anesthetised with isoflurane and pentobarbitone (1.25 mg/kg bodyweight, i.p.). Animals were transcardially perfused using a fixative containing 1 % paraformaldehyde and 15 % v/v saturated picric acid in 0.1 M phosphate buffer (pH 7.4), as previously described (Seifi et al., 2014). After perfusion, ileum and colon tissues were surgically removed and post-fixed in the same fixative overnight at 4 °C, before washing in 0.1 M phosphate buffer to clear residual fixative. Whole-mount preparations of the longitudinal muscle-myenteric plexus and circular muscle-submucosal plexus were obtained by removing the mucosa and submucosa layer and cut open along its longitudinal axis using a dissecting microscope and fine forceps, and stored in 0.1 M phosphate buffer containing 0.05% sodium azide at 4 °C until use.

### 2.4.2 Smooth muscle cell preparation for immunocytochemistry

Adult C57BL/6J mice were killed by cervical dissociation and the ileum/colon was quickly removed and placed in a Sylgard-lined dish containing $Ca^{2+}$-free Hanks' solution (containing 125 mM NaCl, 5.36 mM KCl, 15.5 mM $NaHCO_3$, 0.336 mM $Na_2HPO_4$, 0.44 mM $KH_2PO_4$, 10 mM glucose, 2.9 mM sucrose, 11 mM HEPES, adjusted pH to 7.4 with tris). The ileum/colon was cut open along its longitudinal axis and secured to a Sylgard-lined dish by micropins, with the serosal side uppermost. The mucosa and submucosa layer were removed by using a dissecting microscope and fine forceps to leave a layer of smooth muscle. The muscle layer was then cut into small pieces (~ 0.5 cm) and incubated in Hank's solution containing 1.6 mg/ml collagenase type I , 4 mg/ml fatty acid-free bovine serum albumin, 1 mg/ml

papain and 1 mM dithiothreitol (all purchased from Sigma-Aldrich, Gillingham, UK) at 37 °C for 10-12 minutes. After enzymatic digestion the muscles were washed with $Ca^{2+}$-free Hanks' solution 5-6 times. Muscle tissues were then gently triturated to create a cell suspension, and visualised under a microscope. 1 µl of 100 mM $CaCl_2$ (final concentration 100 µM) and 0.5 µl of 1M $MgCl_2$ (final concentration 500 µM) were added into 1 ml smooth muscle cell suspension, and then stored at 4 °C for 1 hour before use.

### 2.4.3 Immunohistochemistry

The native $K_{2P}$ subunits (mechano-gated TREK subfamily, TWIK subfamily and TASK subfamily) immunoreactivity patterns within the ENS and smooth muscle cells of the mouse ileum and colon were confirmed in at least 3 animals. Nonspecific binding of secondary antibodies was blocked by incubating the tissue with 20 % normal horse serum, diluted in Tris buffer saline containing 0.3 % Triton X-100 (TBS-Tx) for 2h at room temperature. Tissue sections were then incubated with cocktails of primary antibodies (**Table 2.2**), diluted in TBS-Tx and 20 % normal horse serum (Sigma-Aldrich) overnight at 4 °C on a rotating platform. Tissues were then washed with TBS-Tx 3 times and incubated in a mixture of appropriate secondary antibodies (all acquired from Jackson ImmunoResearch, Ely, UK) conjugated with either AlexaFluor 488 (1:1000), indocarbocyanine (Cy3 1:1000) or indodicarbocyanine (Cy5 1:500) for 2 h at room temperature. The tissue was then washed in TBS-Tx again 3 times and mounted on glass slides in Mowiol mounting medium (Polysciences) under a cover slip. Secondary antibody specificity was assessed by omitting the primary antibodies in the incubation sequence. To confirm the absence of cross reactivity between IgGs in double and triple immunolabeling experiments, some sections

were processed using only a single primary antibody with the full complement of secondary antibodies. Immunohistochemical labelling was determined by confocal microscopy (see 2.4.5), based on 3-4 sections for each antibody from *n* = 3 ileums and colons.

### 2.4.4 Immunocytochemistry

Smooth muscle cells were transferred into cover slip by pipette and left for 45 minutes in order to settle and adhere to the cover slip. Cell solution was then removed and fixed with 4 % paraformaldehyde/PBS (Alfa Aesar, Heysham, UK) for 20 minutes. After washing cells 3 x 5 minutes in PBS (Sigma-Aldrich), cells were blocked for 45 minutes at room temperature using 10 % normal horse serum/PBS containing 0.1 % Triton X-100 in order to prevent non-specific binding of both the primary and secondary antibodies to other antigens in the cells. Smooth muscle cells were then incubated for 1 h with primary antibodies (**Table 2.2**), diluted in PBS/0.1 % Triton X-100 (PBST) and 10 % normal horse serum, then washed 3 x 5 minutes with PBST. The secondary antibody cocktails were made in (PBST) and 10 % normal horse serum and added to the cells for 1 hour at room temperature. After completion of immune-staining, the cells were once again washed 3 x 5 minutes with PBST. Finally, cover slips were washed once in milliQ water and then mounted on clean slides, using mounting medium (PolySciences, Warrington, PA, USA).

**Table 2.2: Details of antibodies used for immunohistochemistry and immunocytochemistry.**

| Primary antibody | Host | Source | Dilution | Secondary antibody |
|---|---|---|---|---|
| **NOS** | Sheep polyclonal | Millipore (AB1529) | 1:1000 | Donkey anti-sheep Alexa 488 |
| **ChAT** | Goat polyclonal | Millipore (AB144P) | 1:500 | Donkey anti-goat Alexa 488 |
| **CR** | Goat polyclonal | Swant (CG1) | 1:500 | Donkey anti-goat Alexa 488 |
| **α-actinin** | Mouse monoclonal | Sigma-Aldrich (A5044) | 1:500 | Donkey anti-mouse cy5 |
| **TWIK-1** | Rabbit polyclonal | Alomone Labs (APC-110) | 1:2000 | Donkey anti-rabbit cy3 |
| **TWIK-2** | Rabbit polyclonal | Alomone Labs (APC-040) | 1:1000 | Donkey anti-rabbit cy3 |
| **TASK-1** | Rabbit polyclonal | Alomone Labs (APC-024) | 1:1000 | Donkey anti-rabbit cy3 |
| **TASK-2** | Rabbit polyclonal | Alomone Labs (APC-037) | 1:1000 | Donkey anti-rabbit cy3 |
| **TASK-3** | Rabbit polyclonal | Alomone Labs (APC-044) | 1:2000 | Donkey anti-rabbit cy3 |
| **TREK-1** | Rabbit polyclonal | Alomone Labs (APC-047) | 1:1000 | Donkey anti-rabbit cy3 |
| **TREK-2** | Rabbit polyclonal | Alomone Labs (APC-055) | 1:1000 | Donkey anti-rabbit cy3 |
| **TRAAK** | Rabbit polyclonal | Alomone Labs (APC-108) | 1:1000 | Donkey anti-rabbit cy3 |

### 2.4.5 Image capture and analysis

Sections were examined with a confocal laser-scanning microscope (LSM710; Zeiss) using either a Plan Apochromatic 40x DIC oil objective (NA 1.3; pixel size 0.29 µm) or a Plan Apochromatic 63x oil objective (NA 1.4; pixel size 0.13 µm). Z-stacks were used for routine evaluation of labelling. All images shown represent a single optical section. Images were acquired using sequential acquisition of different channels to avoid crossover between fluorophores, with the pinholes adjusted to one airy unit for all channels. Identical settings were used to image negative controls. Images were processed using Zen2009 Light Edition software (Zeiss, Cambridge, UK) and exported into Adobe Photoshop CC 2015.5. Only brightness and contrast were adjusted for the whole frame, and no part of a frame was enhanced or modified in any way.

## 2.5 Organ bath

### 2.5.1 Equipment setup

Adult WT C57BL/6 mice of either sex (weighing~20-30 g) were used in this study. Mice were euthanised by carbon dioxide asphyxiation and cervical dislocation. Both distal ileum and distal colon were isolated and cut into segments of about 2-3 cm in length. The faecal matter was gently removed by flushing with 1 ml Kreb's solution consisting of (in mM); NaCl (118), $KH_2PO_4$ (1.2), $NaHCO_3$ (25), $D^+$ glucose (11), $MgSO_4$ (1.2), KCl (4.7) and $CaCl_2$ (2.5), pH 7.4. Tissues were mounted longitudinally on an aerator and suspended from a force transducer (Harvard, UK) in a 10 ml chambered Harvard Apparatus 230 V heated tissue organ bath containing Krebs solution at either 32°C (CCh pre-contracted experiments) or 37°C (spontaneous contraction experiments). Gas containing 95 % oxygen and 5 % carbon

dioxide continually aerated the organ bath solution (**Figure 2.1**). changes in isometric tension was monitored and recorded by use of a fore displacement transducer (range 0-50g) coupled with a bridge amplifier(Harvard, UK) (set to a range of 5 mV) connected to a desktop PC running the data acquisition software Lab Chart 7 (AD instrument, Oxford, UK); with a further noise filter on the program set to 20 Hz. For calibration of the apparatus, a one gram weight was placed on the force transducer to display the changes in amplitude recorded by the force transducer in grams, the tissue segment was then subjected to one gram of resting tension and then left to equilibrate for at least 30 minutes.

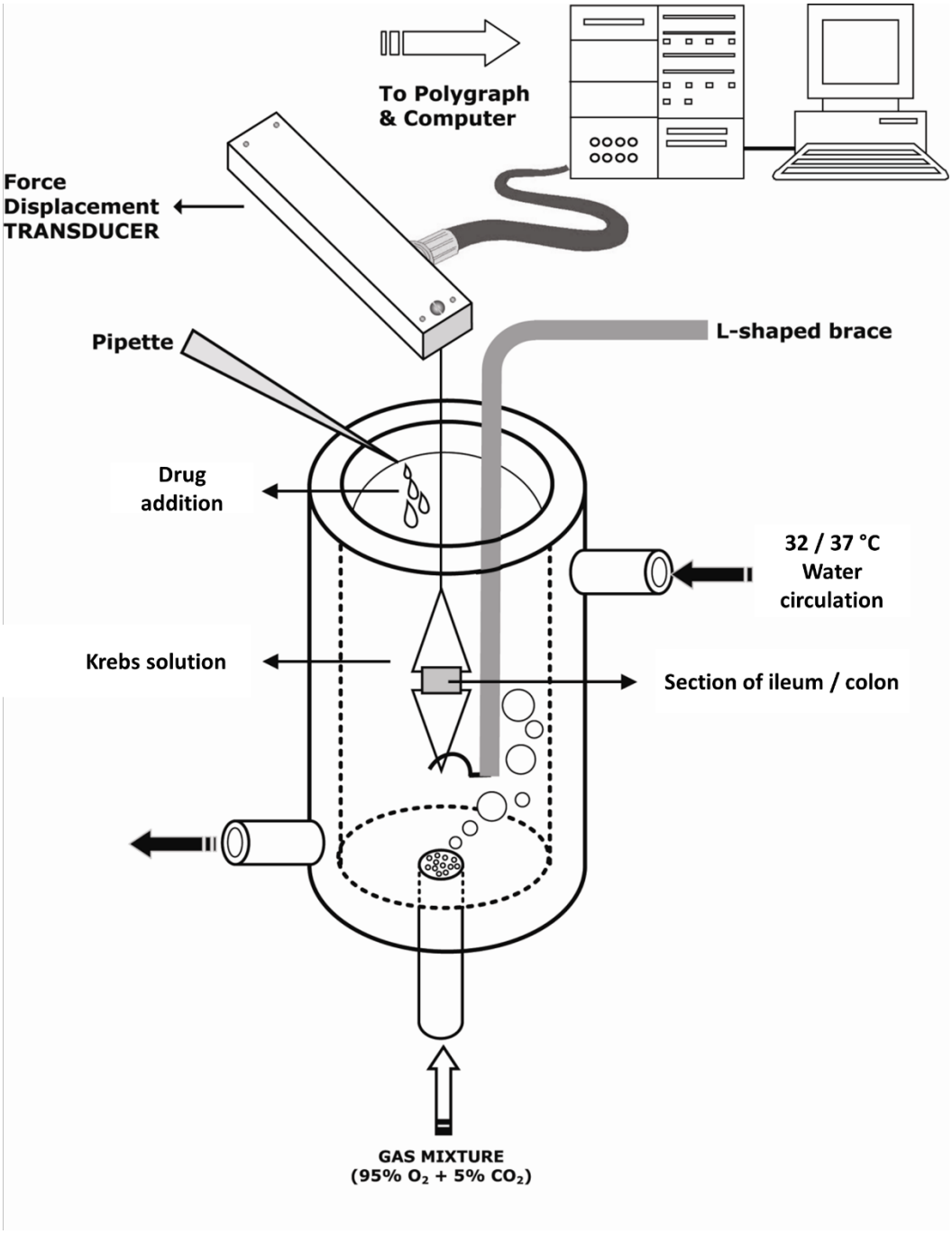


**Figure 2.1:** A schematic diagram of a mouse gut preparation in an organ bath (Yildiz et al., 2013).

### 2.5.2 Organ bath pharmacology

Viability of ileum and colon tissues was assessed in parallel by exposure to the parasympathomimetic carbachol (CCh) at concentrations ranging from $10^{-9}$ to $10^{-4}$ M. Each concentration was applied for approximately 2 minutes, followed by a rinse cycle (30 seconds per cycle) repeated 3-4 times with fresh Kreb's solution before the application of the next concentration. Responses to classical potassium channel blockers were performed directly into bath when spontaneous contraction was stable, changes in the force were measured. Like CCh, blockers were applied for approximately 2 minutes before the wash. Responses to potassium channel activators were performed after exposure to submaximal concentrations of CCh or 60mM KCl and quantified by assessing maximum changes in steady state tension. Drugs were applied for approximately 3-4 minutes, followed by a repeated wash cycle (4-8 times) to return tension to baseline. Moreover, 10 µl drugs were applied if the vehicle DMSO was used, in order to control the DMSO concentration within 0.1 %. Furthermore, the inhibition effects of $K^+$ channel blocker in activation of BL-1249 (10 µM) were also investigated. $Ba^{2+}$, sapdin or tetrodotoxin (TTX) were individually added to the bath for 5 or 10 (TTX) minutes before which the relaxation effects was induced by BL-1249.

In separate experiments, spontaneous contractile activity was quantified. Tissues were prepared as described above. After stable baselines were established, changes in the force and frequency induced by $K_{2P}$ modulators were recorded and quantified over 5 minutes periods pre- and post-drug application.

### 2.5.3 Data analysis for organ bath

In CCh or KCl pre-contracted experiments, changes in tension were measured from baseline to the highest steady state contraction. The relaxation percentage was determined by following formula (**Figure 2.2**); % relaxation = ((C1 – C2)/ C1) X 100, where C1 represents the contraction size before the drug and C2 represents the contraction size after the drug. All organ bath experiment results were collected from LabChart 7 reader (ADInstruments, Oxford, UK) and analyzed in GraphPad Prism software (GraphPad Software, San Diego, CA, USA). All data are presented as the arithmetic mean ± SEM unless stated otherwise. Sigmoidal curve fitting for determination of $IC_{50}$ / $EC_{50}$ values were performed using the non-liner regression normalized response function. Statistical analysis were performed using either the Student's *t*-test (paired or unpaired where appropriate) or two-way ANOVA, and deemed significant at $p < 0.05$.

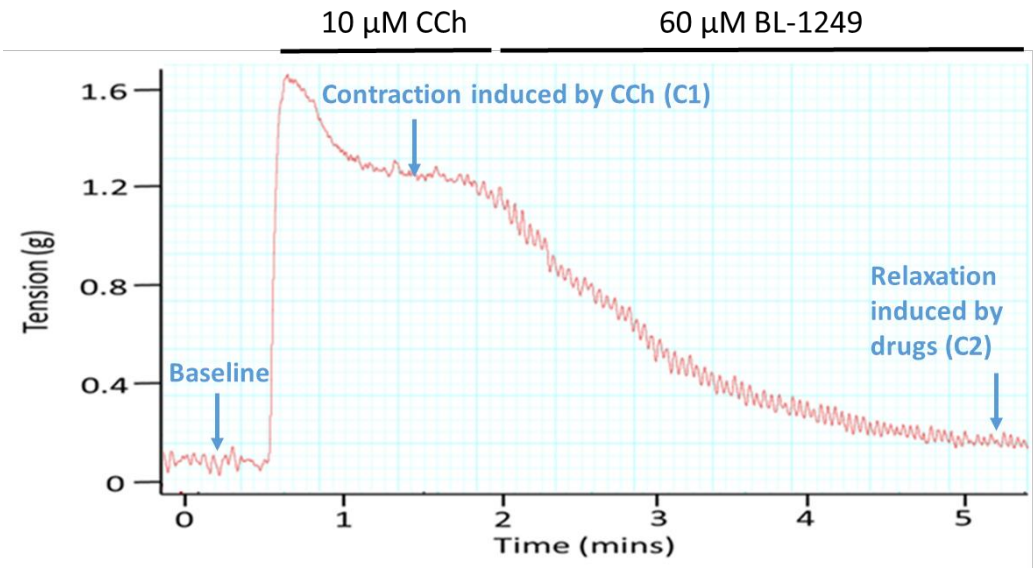


**Figure 2.2:** Exemplar trace identifying the measurement of tissue contraction.

## 2.6 LB medium and LB agar plates

Lysogeny broth (LB) medium were made by adding 10 g Bacto-tryptone, 5 g yeast extract and 10 g NaCl (Sigma-Aldrich, UK) to 1 litre of deionised water, and the pH adjusted to 7.5 using NaOH. LB agar plates (1.5 %) were made by adding 15 g agar into 1 litre LB medium to make solid media. Both were autoclaved at 121°C for 20 minutes and allowed to cool to 50 °C before adding 1 ml of stock ampicillin (100 mg/ml) in case of LB agar media to make a final concentration of 100 µg/ml. Plates were poured into petri dishes under a Bunsen flame in a designated sterile area washed with virkon (500 mg/ml) and 70 % ethanol prior to use. Plates were then left to set under a constant flame before being stored inverted at 4 °C. Both LB agar plates and LB media stored for up to 3 months with antibiotic present.

## 2.7 Sub-cloning

### 2.7.1 Transformation

Each TREK gene has been cloned into pEXO vector and shipped dried on filter paper. To recover the plasmids, a clean razor blade was used to cut out the marked area containing the DNA, which were then place in a micro-centrifuge tube with 10 µl of dH2O. Tubes were briefly vortexed and let stand for 10 minutes, following by quick centrifuge using microcentrifuge minister (VWR, Lutterworth, UK) to elute DNA samples. To a Falcon polypropylene snap top tube 5 µl of the plasmid DNA samples and 50 µl of DH10B competent cells (bacteria cell, gift from Dr R. Draheim, University of Portsmouth, UK) were added and mixed gently using a pipette before being incubated on ice for 30 minutes. The snap top tubes were then transferred to a water bath pre-heated to 42 °C and heat shocked

for 45 seconds, then returned to ice for a further 2 minutes. 300 µl of LB medium was added to each tube and incubated for 1 hr in a MaxQ 8000 incubator (Thermo Scientific, UK) at 220 rpm and 37 °C. Under a constant Bunsen flame the contents of the tube was spread over an LB agar plate using a sterile spreader and left to dry under the flame. The plates were then left inverted in a stationary incubator overnight at 37 °C (16-24 hrs). Selected colonies were lifted from the plate using a sterile pipette tip and placed in a tube with 4 ml of LB medium containing 100 µg/ml ampicillin before being transferred to a shaking incubator to be incubated overnight at 200 rpm and 37°C (maximum 16 hrs).

### 2.7.2 Plasmid purification

Plasmid DNA was isolated using the QIAquick Mini Prep Kit (Qiagen, Manchester, UK) as per manufacturer's instructions. Inoculated LB media was pelleted at 5,000 rpm for 3 mins at 20 °C in a table top Heraeus Megafuge (Thermo scientific, UK). The supernatant liquid media was removed and the pellet re-suspended in 250 µl buffer P1 and pipetted gently up and down to mix it until no clumps were visible. The re-suspension was transferred into a 1.5 ml micro-centrifuge tube before 250 µl of buffer P2 was added and the tube gently inverted 4-6 times before 350 µl of buffer N3 was added and the tube inverted again for another 4-6 times. The solution was centrifuged at 13,000 rpm for 10 mins at 20 °C. The supernatant was transferred to a supplied spin column and centrifuged for 1 minute at 13, 000 rpm and the flow-through discarded. The column was then washed with 750 µl of buffer PE (containing ethanol) and centrifuged again for 1 minute at 13,000 rpm, the flow-through discarded and the centrifugation step repeated to remove any residual PE buffer. The column was transferred to a clean Eppendorf tube and the DNA eluted with 50 µl of

dd$H_2O$ for 1 min and then centrifuged for 1 minute at 13,000 rpm. Recombinant plasmid purity and concentration was assessed by using ND-1000 Spectrophotometer as previously described (section ***2.2.1***).

### 2.7.3 Restriction Digests

Recombinant plasmids were digested in a reaction volume of 30 µl (5 µl Recombinant plasmid; 3 µl Cutsmart buffer; 1 µl EcoRI; 1 µl XbaI; 20 µl ddH2O) and incubated for 2 hrs at 37 °C using C1000 Touch Thermal Cycler (Biorad, Hercules, CA). The digested recombinant plasmids products were then mixed with 6 µl 6 x DNA loading dye (Thermo Scientific, UK) and separated on a 1 % agarose gel as previously described (section ***2.3***) .

### 2.7.4 DNA purification from agarose gel

The agarose gel was visualized under UV light by using UVP Visi-Blue™ Transilluminators (Fisher Scientific, UK), and gel slice containing the DNA fragments were excised using clean scalpel blade and placed into a 1.5ml microtube. The mass of agarose gel was determined by comparing the weight of the tube with that on an empty microtube using a sartorious scale. Plasmids were purified from the gel using the QIAquick Gel Extraction Kit (Qiagen, Manchester, UK) as per manufacturer's instructions. The gel section was dissolved in 3 x volumes of OG buffer (e.g. 300 µl for 100 mg of gel) and then incubated in heatblock at 50 °C for 10 minutes until the gel had completely dissolved. 1 volumes of 100 % isopropanol was added to the solubilized gel solution, and transferred to a supplied QIAquick spin column and centrifuged for a 1 minute at 13,000 rpm and the flow-through discarded. 750

µl of buffer PE were applied to the column and centrifuged for a further 1 minute at 13,000 rpm. The flow-through was discarded and the column centrifuged to remove any residual PE buffer. The spin column was then transferred to a clean 1.5 ml micro-centrifuge tube and the DNA eluted with 30 µl of dd$H_2O$ for 1 min and before centrifugation at 13,000 rpm for 1 minute. The concentration of DNA was assessed using a nanodrop ND-1000 Spectrophotometer, as previously described (section ***2.2.1***).

## 2.7.5 Ligation

Ligation is a process joining of DNA sticky ends using a specialised enzyme, T4 DNA ligase. Reactions contained 1 µl ligase buffer, 1 µl T4 ligase enzyme (New England Biosciences), 2 µl pMAX vector and 6 µl DNA insert. The reaction was incubated at room temperature (between 20 and 22 °C) for 1 hour. Ligations were then transformed into bacteria as described in section ***2.7.1***, colonies selected and grown (section 2***.7.1***.) and plasmid DNA extracted (Section ***2.7.2***). Successful ligations were verified by performing a diagnostic digest as described in section ***2.7.3***. The New England Biosciences (NEB) enzymes EcoRI (5'-GAATTC-3') and XhoI (5'-CTCGAG-3') were identified two single cut restriction sites which flanked the gene in the site of pMAX vector.

## 2.7.6 Sequencing

Recombinant plasmids were sent for Mix2Seq sequencing by using a pre-paid service (Eurofins, Ebersberg, Germany). Plasmids were diluted in 15 µl of deionised water to a concentration of 100 ng/µl and mixed with 2 ul of a single primer (10 uM), either a forward

primer (T7 short) or a reverse primer (XBG) making the final volume of each tube 17 µl. Read lengths were sufficient to enable coverage of the entire gene using plasmid specific, gene flanking sequencing primers. DNA sequencing were then compared to the templet sequencing by using software DNASTAR (DNASTAR, Inc, Madison, WI, USA).

## 2.8 Site directed mutagenesis

Mutagenesis primers were designed using online freeware PrimerX (http://www.bioinformatics.org/primerx/index.htm). Primer parameters were set for a primer melt temperature between 75 – 85°C, GC content between 40 % - 60 %, and a length between 25 – 45 base pairs, and primers were also designed to terminate with a G or C, and have the mutation site at the centre of the primer were possible. All primers were synthesised by Sigma-Aldrich oligo (details see **Table 2.3**). Primers were reconstituted to 100 µM stock concentrations with deionised water according to manufactures guidelines and diluted to give 10 µM working solutions.

**Table 2.3: Details of mutagenesis primer sequences**

| Mutagenesis gene | Primer sequence |
|---|---|
| **mTREK-2-V188A** | **F:** CTTTTGTATTTTATATGCCATCTTTGGGATCCCGC<br>**R:** GCGGGATCCCAAAGATGGCATATAAAATACAAAAG |
| **mTRAAK-K38Q** | **F:** GCAGGCTCAGAAGCAAATGGATCATGGC<br>**R:** GCCATGATCCATTTGCTTCTGAGCCTGC |
| **mTRAAK-K330Q** | **F:** GCACCCGCAGAGCAGGTTGAGACTC<br>**R:** GAGTCTCAACCTGCTCTGCGGGTGC |

50 µl PCR reaction samples were prepared as above (section ***2.3***). Samples were cycled in C1000 Touch Thermal Cycler (Biorad, Hercules, CA) as following protocol; 98 °C for 2 minutes (1 cycle), followed by 18 cycles of 98 °C for 10 seconds, 56 °C for 30 seconds and 72 °C for 2 minutes 30 seconds, and a final single elongation step of 72 °C for 10 minutes. After cycling had completed, 1 µl DpnI (20,000 units/ml) (New England Biosciences, Hitchin, UK) enzyme was added into PCR sample and incubated for a further 1 hr at 37 °C in order to digest the parental/template DNA. PCR products were separated by 1% agarose gel electrophoresis and visualised to verify successful amplification (section ***2.3***). 10 µl of successful amplifications were transformed (section ***2.7.1***), colonies selected, cultured (section ***2.7.1***) and plasmid DNA purified by miniprep (section ***2.7.2***). To remove the influence of any spurious mutations generated during the process, mutated genes were subcloned into fresh wild type backbone pMAX plasmid following previously described protocols (digestion with restriction enzymes (section ***2.7.3***), separation on agarose gel and subsequent extraction(section ***2.7.4***), ligation into fresh pMAX vector (section ***2.7.5***), transformation of new construct (section ***2.7.1***), purification by mini prep (section ***2.7.2***), diagnostic digest (section ***2.7.5***) and sequencing to check for the correct mutation and position (section ***2.7.6***).

## 2.9 Chimera constructs

Chimera of mTREK-2 channel were C-terminus was replaced with the C-terminus of mTREK-1 were constructed using PCR methodology using a two-step process. TREK-1 C-terminus cloned by PCR using forward primers (5’-GTGTGGTTCTGGATCCTCGTTGG-3’) and reverse primer (5’-GGGTGTTCTTGAGGCTGGTTTAGTGG-3’) and TREK-1 as template using protocol

in section ***2.3***. The cloning product was a 434 bp amplicon. Then the processes it goes though 1 % agarose gel running (section ***2.3***) and subsequent extraction (section ***2.7.4***) and is then PCR amplicon used as a reverse primer in PCR reaction containing TREK-2 as template and forward primer (5'-TAATACGACTCACTATAGGG-3'). The final amplified product was a 1336 bp amplicon. Again PCR amplicons treated as before (section ***2.3***) and purified (section ***2.7.4***). Since the clone contains ORF and 5' and 3' MCS digest performed to allow subcloning into prepared pMAX wild type backbone, following noted procedures digestion with restriction enzymes (section ***2.7.3***), separation on agarose gel and subsequent extraction(section ***2.7.4***), ligation into fresh pMAX vector (section ***2.7.5***), transformation of new construct (section ***2.7.1***), purification by mini prep (section ***2.7.2***), diagnostic digest (section ***2.7.5***) and sequencing to check for the correct mutation and position (section ***2.7.6***).

## 2.10 cRNA generation

### 2.10.1 Linearisation

Successful recombinant plasmids were linearised by cutting the plasmid construct 3' downstream of the gene and poly A tail so that subsequent in *virto* transcription only transcribes the gene and not the whole plasmid. 30 µl reaction sample was prepared (containing 10 µg Recombinant plasmid; 4 µl Cutsmart buffer; 1 µl PacI; made to volume with dd$H_2O$) and incubated for 2 hrs at 37°C (section ***2.7.3***). Successful linearisation was assessed on a 1% agarose gel (section ***2.3***). Reactions were PCR purified using the QIAquick Gel Purification Kit (Qiagen, Manchester, UK) as per manufacturer's instructions. The total reaction volume (29 µl) is mixed with 5 volumes of PB (1 volume = 29 µl) for a total of

volume of 174 µl. The total reaction is placed onto a spin column and centrifuged at 20 °C at 13,000 rpm for 1 min and the flow-through discarded. The spin column is then loaded with 750 µl of wash buffer PE and spun again at 20 °C for 1 min and the flow-through discarded. The spin column is then spun a subsequent time at 20 °C for 1 min to remove any excess wash solution. The spin column is then placed into a fresh Eppendorf tube and 30 µl dd$H_2O$ added directly onto the column membrane, the column is then left for 1 min before being spun at 20 °C for 1 min to collect and the flow-through is collected at the end ready to check purity and concentration using a ND-1000 spectrophotometer (section ***2.1.2***).

### 2.10.2 *In-vitro* transcription

cRNA was prepared from linearised constructs using the T7 m-Message Machine Kit (Ambion, Austin, TX). The cRNA reaction volume was 20 µl (10 µl 2 x NTP/CAP; 2 µl 10 x Reaction Buffer; linearised TREK-1 pMAX construct (1 µg); ddH2O; 2 µl enzyme mix). Reactions were gently vortexed before being incubated for 2 hrs at 37°C using a C1000 Touch Thermal Cycler (Biorad, Hercules, CA. USA). The reaction was then transferred into 1.5 ml Eppendorf containing 30 µl lithium chloride (7.5 M) and 30 µl ddH2O, mixed and then incubated at -20°C for overnight to allow cRNA precipitation. The precipitate was then pelleted at 13,000 rpm 15 min at 4°C and the supernatant removed using a pipette. The pellet was then washed with 1 ml of ice cold (- 20°C) 70 % ethanol and re-centrifuged at 13,000 rpm for 15 mins at 4°C. The ethanol was then removed using a pipette, and the pellet was left to air dry for no more than 5 mins. The pellet was reconstituted in RNase and DNase free molecular grade water to a volume of 20 µl. cRNA was qualitatively

assessed by separation by electrophoresis on a 1 % agarose gel (section ***2.3***) and quantified spectrophotometrically using a ND-1000 spectrophotometer (section ***2.2.1***.). All cRNA samples were stored at -80°C.

## 2.11 Electrophysiology

### 2.11.1 Preparation of oocytes

*Xenopus laevis* ovaries were provided by European Xenopus Resource Centre (University of Portsmouth, Portsmouth, UK) and oocytes subsequently prepared and isolated as detailed. In brief, frogs were anesthetized and sacrificed using a Schedule 1 method (MS222) followed by pithing and ovariectomy, in accordance with the Animals (Scientific Procedures) Act 1986 (UK) by a licence holder. Ovaries were stored in 50 ml falcon tubes containing $Ca^{2+}$-free OR-2 solution (in mM): NaCl (82.5), KCl (2.5), $MgCl_2$ (1), HEPES (10), pH 7.4 tris-base. Oocytes were manually separated using forceps into clumps of 10-15 oocytes and rinsed 3-4 times with OR-2 solution. Oocytes were suspended in 40 ml of OR-2 solutions containing 80 mg (2 mg/ml) of type II collagenase (Worthington, US) for 1 hour – 1 hour 30 minutes at room temperature on tube rotator (Stuart, UK) with speed 10 rpm. Oocytes were spot checked under a binocular compound microscope to visually assess the loss of the follicular layer, classified by the absence of the vascular network covering the oocytes (**Figure 2.3**). The enzymatic reaction was halted and collagenase removed by rinsing oocytes3-4 times in calcium containing ND-96 solution (in mM): NaCl (96), KCl (2), $MgCl_2$ (1), $CaCl_2$ (1.8), HEPES (10), pH 7.6 tris-base, containing 50 µg/ml gentamycin and 1% penicillin/streptomycin remove. Suspended oocytes were then transferred to a petri dish. Stage IV-V oocytes were selected using a pasture pipette, modified to possess an enlarged

polished outlet to provide safe transports of oocytes, and distributed into small petri-dishes containing fresh ND-96 solution and incubated at 16°C.

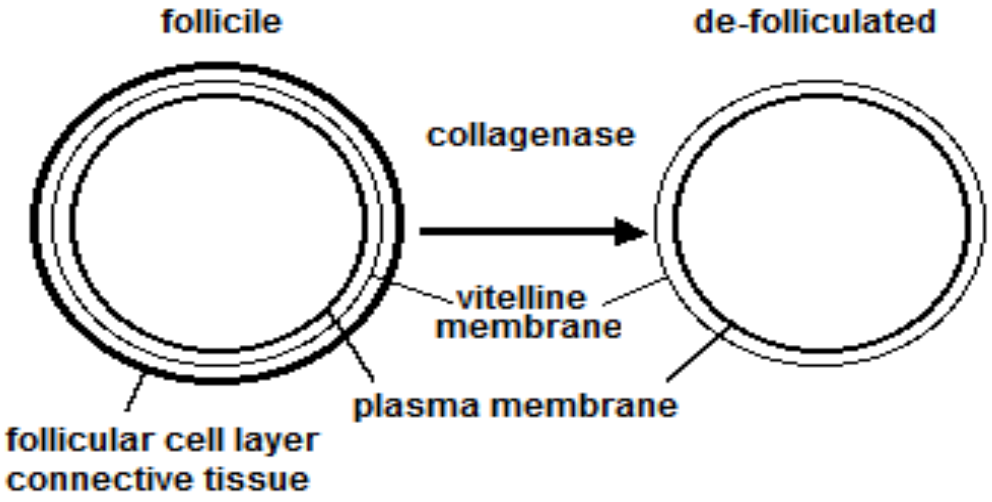


**Figure 2.3:** Schematic demonstrating the removal of the follicular cell layer and connective tissue via the use of collagenase enzymes. Post-treatment the oocyte only has the inner plasma membrane and its vitelline membrane intact, ready for injection.

### 2.11.2 Pipette fabrication

Glass micropipettes were fabricated via a two-stage process using a Narishige PP-83 pipette puller (Narishige Scientific Instrument Laboratory, Japan). For TEVC pipette fabrication, the glass used for injection and recording electrodes were manufactured from microinjection capillaries borosilicate glass with 3.5 inch length bores for Drummond Nanoject (alphalavoratores, Eastleigh, UK), and thin-walled borosilicate glass capillaries with 1.0mm OD, 0.78mm ID, 75 mm L (Harvard Apparatus, UK), respectively.

### 2.11.3 Oocyte injection

Glass pipettes were back filled with mineral oil (Sigma-Aldrich) and inserted onto the Nanoinject Microinjector. Pipettes were then broken under microscope by carefully crushing the tip against the petri dish until a break was made which resembled the end of a hyper dermic needle (an opening between 2-3 µm in diameter). Injections were performed in a sterile injection-chamber constructed to provide a wall to serve as mechanical resistance to the oocytes during insertion of the microinjection pipette (**Fig 2.4**). The chamber was filled with ND96 throughout the procedure to ensure oocytes were covered in solution at all times.

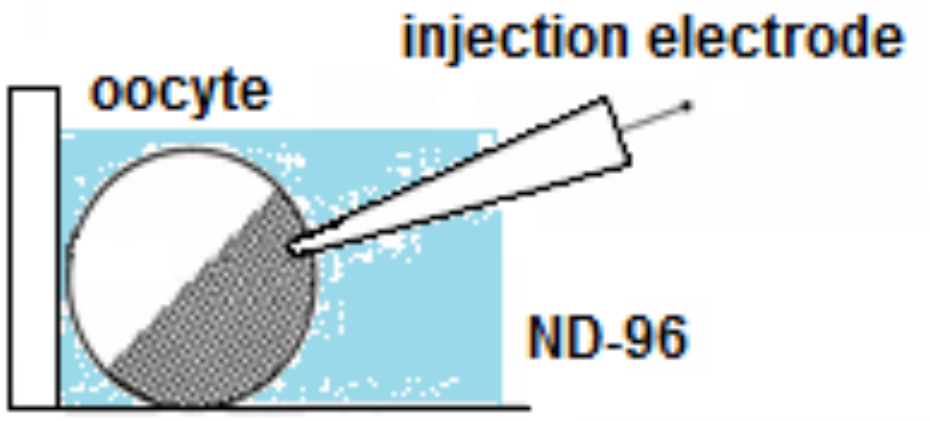


**Figure 2.4**: Schematic of the injection procedure. Oocytes are placed into a dish filled with a raised wall. Oocytes are placed alongside this wall, which serves as mechanical resistance during injection. The dish is filled with ND-96 storage buffer throughout the procedure.

All cRNA samples were diluted to a final concentration of 10 ng/ 23 nl which equates to 43.47 ng/nl, except mTRAAK, which diluted to a final concentration of 20 ng/ 23 nl. For example, concentration of RNA for mTREK-1 500 ng/µl, so 500/43.47 = factor of 11.5, which give us concentration 11.5 ng / 23 nl. Hence using equation $C_1V_1 = C_2V_2$ to calculate that dilute 8.3 µl of RNA with 1.7 µl of RNase-free water to get a concentration of 10 ng/ 23 nl.

So when 23 nl is injected it will in fact be 10 ng of mTREK-1 RNA. Selected oocytes were injected one-by-one with cRNA (2-10 ng per oocyte; 23 nl injection volume) and transferred to fresh ND-96 daily and infected, damaged oocytes removed to prevent cross contamination, and stored at 16 °C.

### 2.11.4 Two-electrode voltage clamp (TEVC)

Whole-cell currents of injected oocytes were assessed using TEVC, a technique was used to measure ionic currents in response to precisely controlled changes in the transmembrane potential of an isolated cell. TEVC Oocyte currents were recorded using an OC-725C oocyte clamp amplifier (Warner Instruments, Harvard Apparatus, UK) and Axon Digidata 1440A (Molecular Devices, UK) and visualised using pCLAMP 10.4 software (Molecular Devices, LLC, Sunnyvale, CA) installed on a computer with a Windows 7 operating system. All experiments were performed at room temperature (between 20 – 22°C) with constant, gravity fed solution flow at 1-2 ml/min with a bathing solution containing (in mM): 96 NaCl, 4 KCl, 1 MgCl2, 0.3 CaCl2, 10 HEPES (pH 7.6, tris-base). Two microelectrodes were backfilled half way with 3 M KCl using a MicroFil syringe needle (VWR, Lutterworth, UK) and one electrode secured into each of the two electrode holders, making sure that Ag/AgCl wire makes contact and therefore electrical connection with KCl solution in the pipette. Pipette tip resistances were measured by placing the electrodes into the bath solution and adjusting the offset. A resistance of 0.2 - 1 MΩ is desirable. Electrodes were advanced into the oocyte one at a time using manually controlled micromanipulators attached to the base of the TEVC platform. Electrodes touching the oocytes form a slight indent on the oocyte membrane, at this point the electrodes were advanced further and successful penetration

is seen when the LCD display for each electrode on the amplifier reads the membrane potential of the cell (**Fig. 2.5A**). The clamp was adjusted to fast and the gain turned to maximum before the voltage protocol was applied. Oocyte membrane potential was held at -80 mV and step depolarised to potentials ranging from -120 mV to +60 mV in 10 mV steps for a duration of 1 s (**Figure 2.5B**). Recorded currents were not adjusted for leak or capacitance.

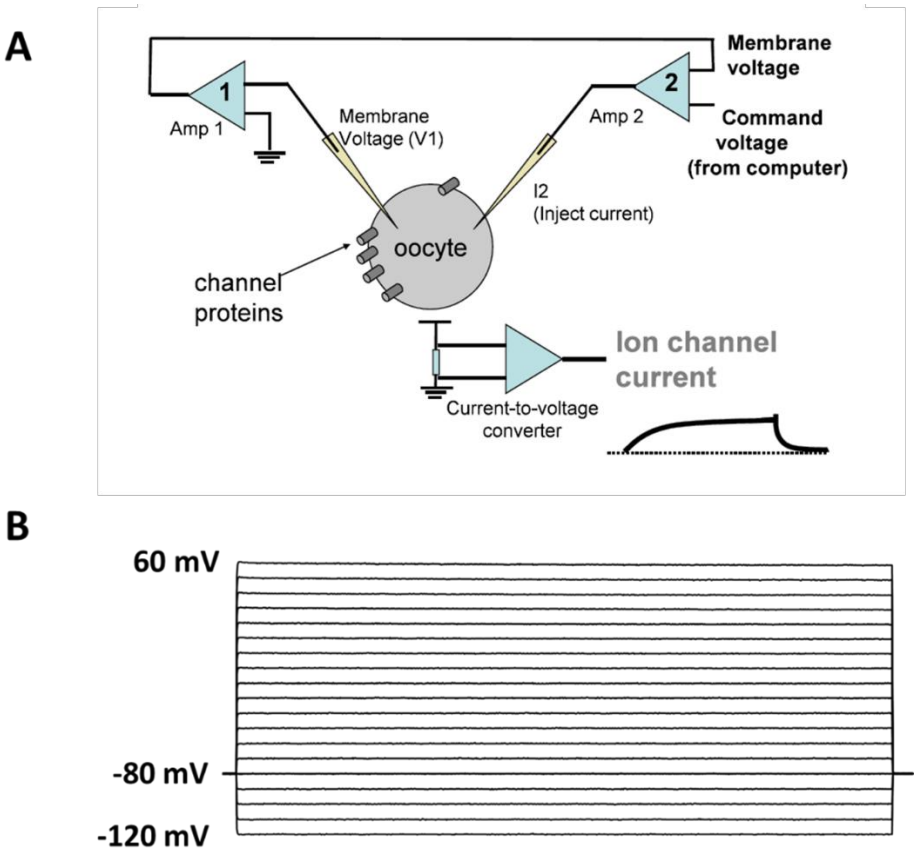


**Figure 2.5**: Schematic summarising the oocyte set-up in as part of a TEVC recording. **A)** The oocyte is impaled by two glass microelectrodes, one for voltage sensing and one for current injection. The transmembrane potential is measured by the voltage-sensing electrode (V1) connected to a high input impedance amplifier (Amp 1). This signal is compared to a command voltage generated by a computer at the input of Amp 2. The output of the high gain feedback Amp 2 is a current delivered to the cell interior by the second micropipette. This current is sufficient to force the transmembrane potential to equal the command voltage. The current delivered by micropipette 2 is monitored as "I2" via a current-to-voltage converter. **B)** Diagram of a typical voltage protocol for recording voltage families. -80 mV denotes the command potential, -120 to -60 mV are the highest and lowest voltages of the step protocol.

### 2.11.5 Potassium selectivity experiments

For selectivity measurements, oocytes were exposed to different levels of extracellular $K^+$; $[K^+]_o$ of 4, 20, 100 and 140 mM (**Table 2.4**). Briefly, ionic currents were initially recorded using the voltage family protocol in bath solution containing 4 mM $K^+$. The solution was then be switched to one containing 20 mM $K^+$ and allowed to equilibrate for 1-2 minutes before applying the voltage protocol again. This procedure was repeated after exchange of the bath solution again to one containing 100 mM $K^+$ and 140 mM $K^+$. Current-voltage (IV) curves were plotted using Clampfit 10.7 software (Axon Instruments, Inc.), and the data transferred into an excel spreadsheet to calculate the mean IV relationship for all cells in that experiment. Traces were modified with the x-axis cut off at 1200ms with the y-axis value dependent on maximum current amplitude of that experiment. Channel reversal potential was calculated from IVs (between -120 to 60 mV) taken from whole cell recordings. IVs were analysed for the point at which the line of the graph crossed the x-axis. In the case of $K^+$ selectivity experiments the average reversal potential was plotted against the $[K^+]_o$ to produce a Nernstian slope. This slope could be directly compared to the theoretical slope of a perfectly selective channel derived using the Nernst equation in differing potassium conditions;

$$E_K = \frac{RT}{zF} \ln \frac{[K]i}{[K]o}$$

Where ***R*** is the universal gas constant (8.3145 J $mol^{-1}$ $K^{-1}$), ***T*** is the temperature in kelvin, ***F*** is the Faraday constant ($9.6485 \times 10^4$ C $mol^{-1}$), ***z*** is the valance and $[K]_i$ / $[K]_o$ are the concentrations of $K^+$ ions inside and outside the cell respectively. The Nerstian slope of a

channel which only passes potassium is theorised to have a Nerstian slope of 58.2 mV, such that a 10 fold increase in extracellular $K^+$ ion concentration should shift reversal potential 58.2 mV positive.

**Table 2.4: The composition of different concentration of $K^+$ solution.**

| Compound | 4 mM $K^+$ | 20 mM $K^+$ | 100 mM $K^+$ | 140 mM $K^+$ |
|---|---|---|---|---|
| **NaCl** | 96 mM | 80 mM | X | X |
| **KCl** | 4 mM | 20 mM | 100 mM | 140 mM |
| **$MgCl_2$** | 1 mM | 1 mM | 1 mM | 1 mM |
| **$CaCl_2$** | 0.3 mM | 0.3 mM | 0.3 mM | 0.3 mM |
| **HEPES, pH 7.6 (Tris)** | 5 mM | 5 mM | 5 mM | 5 mM |

## 2.11.6 Application of drugs

TREK family channel pharmacology were conducted by diluting the stock concentration of the compound of interest in 30 ml of 4 mM $K^+$ solution to the desired working concentration. Pharmacological compounds were applied by gravity perfusion at a rate of 1 ml per minute. Oocytes expressing mTREK-1, hTREK-1, mTREK-2 and mTRAAK channels were recorded in 4 mM $K^+$ solution as a control to establish baseline current levels, using protocol showing **Figure 2.5B**. To ascertain the successful exchange of bath solutions between 4 mM $K^+$ and drugs, a single-pulse protocol was used where oocytes were clamped at -80 mV and subjected to a 1 s pulse of 50 mV at 0.1Hz until equilibrium had been reached,

and then the relevant protocol applied. After the experiment had been conducted the same protocol was applied to observe the wash out of the compound, with equilibrium once again dictating when this was successfully achieved.

### 2.11.7 Data Analysis for TEVC

All TEVC data were analysed using Clampfit 10.7 (Axon Instruments, Inc.), and tabulated in Excel (Microsoft Office 2013). Current-voltage (I-V) relationships were generated from steady-state currents at potentials between -120 mV and +60 mV. Statistical analyses and graphical evaluations were performed with GraphPad Prism 7.0 (GraphPad Software, San Diego, CA, USA). For all analysis, n values represent the number of oocytes. All data are presented as the arithmetic mean ± SEM unless stated otherwise. Statistical comparisons were made using either Student's paired *t*-test or two-way ANOVA. A $p < 0.05$ was considered statistically significant.

## 2.12 Drugs

All pharmacological compounds were reconstituted/diluted where applicable and in accordance with manufacturer's instructions (**Table 2.5**).

**Table 2.5: Details of drugs used in organ bath (OB) and TEVC studies.**

| Drug | Company | Stock conc. (mM) | Dissolved in | Used for |
|---|---|---|---|---|
| **CCh** | Sigma-Aldrich | 10 | Kreb's solution | OB |
| **KCl** | Sigma-Aldrich | 30 | $ddH_2O$ | OB |
| **$Ba^{2+}$** | Sigma-Aldrich | 1000 | $ddH_2O$ | OB & TEVC |
| **TEA** | Sigma-Aldrich | 1000 | $ddH_2O$ | OB |
| **4-AP** | Tocris Bioscience | 1000 | $ddH_2O$ | OB |
| **XE-991** | Tocris Bioscience | 100 | DMSO | OB |
| **Chromanol 293B** | Tocris Bioscience | 100 | DMSO | OB |
| **Riluzole** | Sigma-Aldrich | 100 | DMSO | OB |
| **Retigabine** | Tocris Bioscience | 100 | DMSO | OB |
| **Arachidonic acid** | Sigma-Aldrich | 100 | DMSO | OB & TEVC |
| **Flufenamic acid** | Sigma-Aldrich | 100 | DMSO | OB |
| **BL-1249** | Sigma-Aldrich | 30 | DMSO | OB & TEVC |
| **CDC** | Sigma-Aldrich | 100 | DMSO | OB & TEVC |
| **ML-365** | Tocris Bioscience | 10 | DMSO | OB |
| **melittin** | Tocris Bioscience | 100 | $ddH_2O$ | OB |
| **zileuton** | Tocris Bioscience | 100 | DMSO | OB |
| **aspirin** | Sigma-Aldrich | 100 | DMSO | OB |
| **diazoxide** | Tocris Bioscience | 100 | DMSO | OB |
| **cromakalim** | Tocris Bioscience | 20 | DMSO | OB |
| **NS5806** | Tocris Bioscience | 50 | DMSO | OB |
| **NS19504** | Tocris Bioscience | 100 | DMSO | OB |
| **NS11021** | Tocris Bioscience | 100 | DMSO | OB |
| **NS309** | Tocris Bioscience | 100 | DMSO | OB |
| **SKA-31** | Tocris Bioscience | 100 | DMSO | OB |
| **TTX** | Tocris Bioscience | 0.1 | $ddH_2O$ | OB |
| **DHA** | Sigma-Aldrich | 100 | DMSO | TEVC |
| **spadin** | Tocris Bioscience | 1 | $ddH_2O$ | OB & TEVC |

# Chapter 3 – Expression of potassium channel transcripts in the mouse ileum and colon

## 3.1 Introduction and Aims

Potassium channels form the largest family of ion channel proteins, and can be structurally and functionally divided into three distinct sub families: voltage-gated ($K_v$), inward-rectifier ($K_{ir}$) and leak ($K_{2P}$). Opening of potassium channels allows $K^+$ ion efflux down its electrochemical gradient resulting in membrane potential repolarization, and therefore is central to controlling cellular excitability and signal transduction. Given this key physiological role, potassium channels are important therapeutic targets for a multitude of pathologies in neuronal, cardiovascular and muscular tissues. Recently, potassium channels encoded by KCNQ genes ($K_v7$) have been identified in smooth muscle and revealed as important regulators of vascular contractility (Greenwood and Ohya, 2009). However, little is currently known about the expression profiles of KCNQ/$K_v7$ channels in other smooth muscle tissues, including that of the GI tract. Similarly, $K_{2P}$ channels are a large subfamily of potassium channels whose functional characteristics make them ideal for setting and regulating membrane potential. However, very little is currently known about the expression, distribution or functional contribution of $K_{2P}$ channels to GI smooth muscle contractility. Thus, the initial goal of this study was to establish the expression profile of potassium channel transcripts in GI tract, with a view to identifying specific potassium channels that could be functionally targeted to modulate GI motility. This was achieved utilising quantitative RT-PCR analysis of mRNA transcripts of potassium channel genes in mouse ileum and colon whole tissue preparations. To determine relative transcript expression levels of the 93 known potassium channels in the mouse, mRNA was quantified by real-time PCR (qPCR) analysis from 3 animals, and normalised against the combined housekeeping genes GAPDH + HPRT by the comparative $2^{-\Delta Ct}$ method. This was followed by

qualitative RT-PCR to specifically highlight mRNA expression of the mechano-gated $K_{2P}$ channels TREK-1, TREK-2 and TRAAK in GI tissue.

## 3.2 Results

### 3.2.1 Determination of most stable reference genes

The Mouse Intestinal Ion Channels RT$^2$ Profiler$^{TM}$ qPCR Array contained multiple reference genes, and the NormFinder algorithm (Andersen et al., 2004) was used to establish which single gene or combination of genes was the most stable and therefore appropriate to use for normalisation. The three reference gene options GAPDH, RPLP0 and HPRT are presented in **Figure 3.1** and with a stability value of 0.04, 0.143 and 0.036 respectively in ileum, and 0.60, 1.74 and 0.14 respectively in colon. GAPDH and HPRT presented the lowest stability value in both ileum and colon, and therefore were determined to be the best combination references for normalisation.

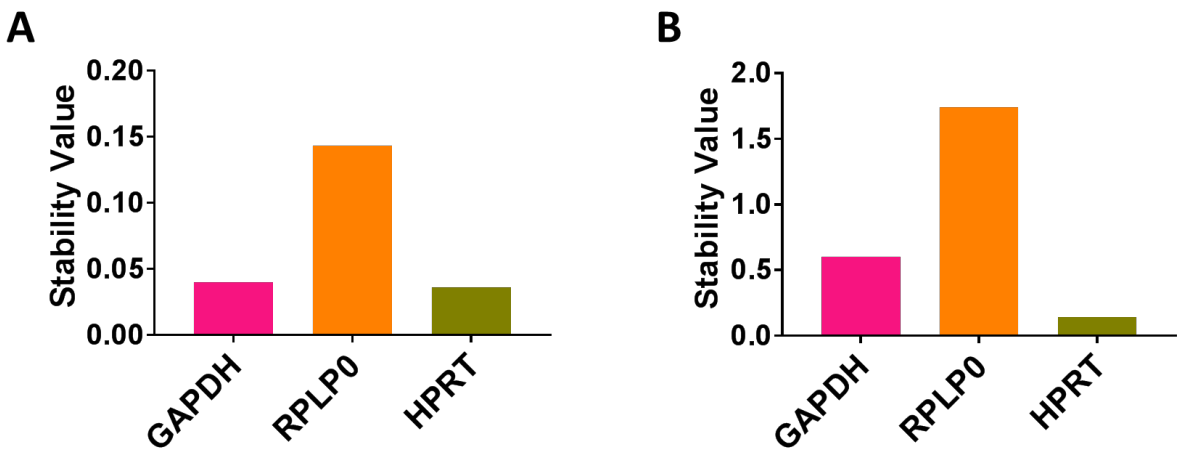


**Figure 3.1:** Estimation of stability of candidate reference genes using NormFinder. Genes are ranked according to their expression stability across all samples in ileum **(A)** and colon **(B)**.

Mane et al, (2008) suggested that ideal reference genes should have a normal distribution across samples and a low standard deviation. In the customised plate for potassium channels, statistical analysis was performed to identify reference genes with the lowest standard deviation of the Ct values across all ileum and colon samples, and confirmed GAPDH to be a suitable stable gene for normalisation in the customised array (**Figure 3.2**).

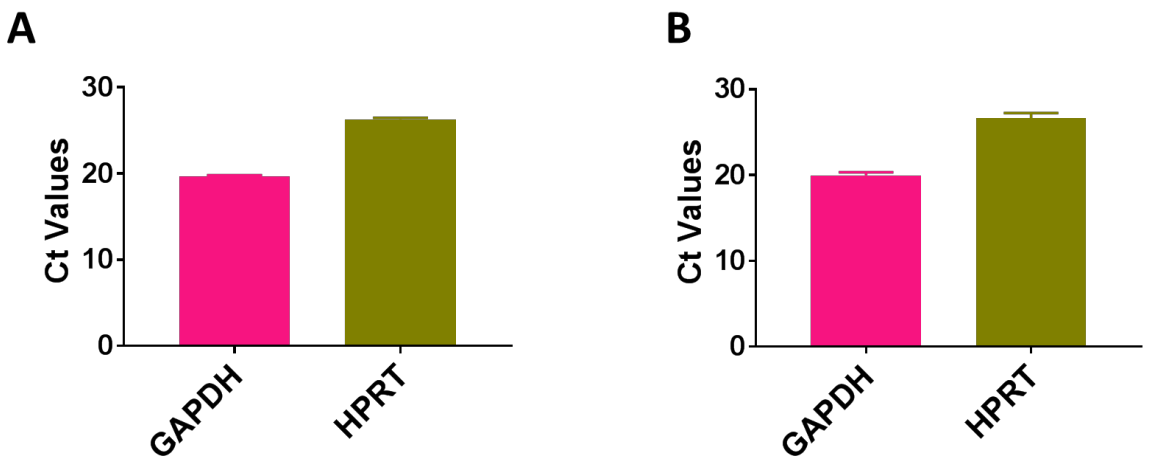


**Figure 3.2:** Calculation of stability of candidate reference genes based on Ct stability. Genes are ranked according to their expression stability across all samples in ileum **(A)** and colon **(B)**. Data are expressed as Ct values of housekeeping gene GAPDH and HPRT (mean ± SD, *n* = 3).

### 3.2.2 Voltage-gated $K^+$ channels ($K_v$)

The $K_v$ family consist of 40 α subunits in 12 subfamilies. These channels include three major groups of the following proteins: 1) members of $K_v1$-$K_v6$ subfamilies and $K_v8$-$K_v9$ subfamilies; 2) proteins of $K_v7$ subfamily (often called KCNQ family); 3) the $K_v10$-$K_v12$ subfamilies (Kew and Davies, 2010). **Table 3.1** lists both the gene and protein names of all $K_v$ channels studied.

**Table 3.1:** Voltage-gated $K^+$ channel alpha subunits, providing both the gene and protein names and details of their accessory subunits.

| Classification | Family | Gene Name (Protein Name) | Main accessory subunits |
|---|---|---|---|
| **$K_v$1.x** | Shaker | KCNA1 ($K_v$1.1), KCNA2 ($K_v$1.2), KCNA3 ($K_v$1.3), KCNA4 ($K_v$1.4), KCNA5 ($K_v$1.5), KCNA6 ($K_v$1.6), KCNA7 ($K_v$1.7), KCNA8 ($K_v$1.8) | $K_v$ β1- β2 |
| **$K_v$2.x** | Shab | KCNB1 ($K_v$2.1), KCNB2 ($K_v$2.2) | |
| **$K_v$3.x** | Shaw | KCNC1 ($K_v$3.1), KCNC2 ($K_v$3.2), KCNC3 ($K_v$3.3), KCNC4 ($K_v$3.4) | KCNE3 ($K_v$ 3.4) |
| **$K_v$4.x** | Shal | KCND1 ($K_v$4.a), KCND2 ($K_v$4.2), KCND3 ($K_v$4.3) | KCNIP1-4 |
| **$K_v$5.1** | Modifier | KCNF1 ($K_v$5.1) | - |
| **$K_v$6.x** | Modifiers | KCNG1 ($K_v$6.1), KCNG2 ($K_v$6.2), KCNG3 ($K_v$6.3), KCNG4 ($K_v$6.4) | - |
| **$K_v$7.x** | - | KCNQ1 ($K_v$7.1), KCNQ2 ($K_v$7.2), KCNQ3 ($K_v$7.3), KCNQ4 ($K_v$7.4), KCNQ5 ($K_v$7.5) | KCNE1-4 |
| **$K_v$8.x** | Modifiers | KCNV1 ($K_v$8.1), KCNV2 ($K_v$8.2) | - |
| **$K_v$9.x** | Modifiers | KCNS1 ($K_v$9.1), KCNS2 ($K_v$9.2), KCNS3 ($K_v$9.3) | - |
| **$K_v$10.x** | EAG | KCNH1 ($K_v$10.1), KCNH5 ($K_v$10.2) | - |
| **$K_v$11.x** | ERG | KCNH2 ($K_v$11.1), KCNH6 ($K_v$11.2), KCNH7 ($K_v$11.3) | KCNE1 |
| **$K_v$12.x** | ELK | KCNH8 ($K_v$12.1), KCNH3 ($K_v$12.2), KCNH4 ($K_v$12.3) | KCNE1 |

**Figure 3.3** displays the mRNA transcript levels of $K_v$ channels investigated in the mouse ileum and colon. Results from qRT-PCR array signified that the most abundant $K_v$ channel subunit mRNA in the mouse ileum was $K_v7.1$, almost 13-times greater than the next most abundant gene encoding $K_v1.3$ ($n$ = 3, $p$ < 0.0001, Student's paired $t$-test) (**Figure 3.3A**). Next, in rank order in ileum were the transcript levels for genes encoding $K_v4.3$, $K_v2.1$ and $K_v5.1$, followed by $K_v1.2$, $K_v1.1$, $K_v11.1$, $K_v6.3$, $K_v6.4$, $K_v12.2$, $K_v1.5$, $K_v3.3$ and $K_v1.6$. Several genes were also detected in ileum but at very low levels; $K_v2.2$, $K_v2.1$, $K_v3.4$, $K_v4.1$, $K_v4.2$, $K_v6.1$, $K_v6.2$, $K_v7.2$, $K_v7.3$, $K_v7.4$, $K_v7.5$, $K_v8.2$, $K_v9.3$, $K_v10.1$, $K_v11.2$ and $K_v12.1$. The rest, including $K_v1.4$, $K_v1.7$, $K_v1.8$, $K_v3.2$, $K_v8.1$, $K_v9.1$, $K_v9.2$, $K_v10.2$, $K_v11.3$ and $K_v12.3$ were not or barely detectable in ileum. In colon (**Figure 3.3B**), the $K_v7.1$ gene also presented the highest relative expression level of the 40 subunits, 7-times greater than the next two abundant transcripts for subunits $K_v5.1$ and $K_v4.3$. This was followed in rank order in colon by $K_v1.1 > K_v2.1 > K_v6.4 > K_v1.3 > K_v11.1 > K_v1.2 > K_v12.2 > K_v9.3 > K_v1.6$. In addition, $K_v3.3$, $K_v4.1$, $K_v6.2$, $K_v6.3$, $K_v7.2$, $K_v7.4$, and $K_v12.1$ were also above the detectable level. Gene transcripts encoding for $K_v2.2$, $K_v3.1$, $K_v3.4$, $K_v4.2$, $K_v6.1$, $K_v7.3$, $K_v7.5$, $K_v10.1$, and $K_v11.2$ were barely detectable when normalized to housekeeping gene, whereas transcripts encoding for $K_v1.4$, $K_v1.7$, $K_v1.8$, $K_v3.2$, $K_v8.1$, $K_v8.2$, $K_v9.1$, $K_v9.2$, $K_v10.2$, $K_v11.3$ and $K_v12.3$ were not detected in mouse colon at all as concluded from a lack of measureable Ct value after 40 cycles of PCR.

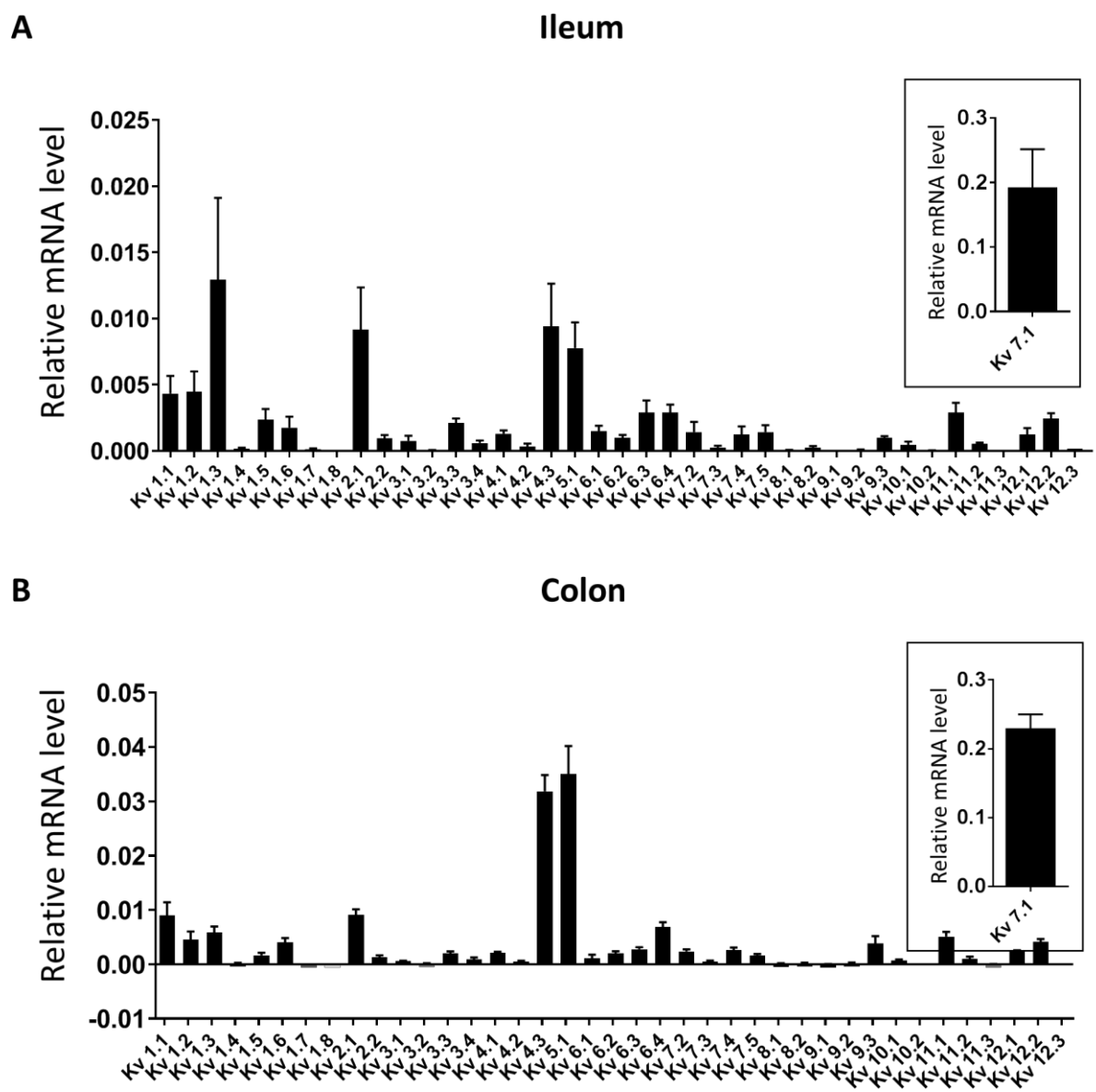


**Figure 3.3:** Differential expression of $K_v$ subtype transcripts in the mouse ileum and colon. Quantitative, real-time PCR performed on lysates of acutely isolated ileum **(A)** and colon **(B)** from wild type mice. Data are expressed as relative mRNA levels ($2^{-\Delta Ct}$) compared to the housekeeping gene GAPDH (mean ± SEM, *n* = 3). $K_v$7.1 (KCNQ1) displayed the highest relative expression levels in both ileum and colon and is shown in the inset for clarity. Channel protein names have been used instead of the gene names for simplicity as the protein names are more commonly known.

### 3.2.3 Calcium-activated $K^+$ channels ($K_{Ca}$)

$K_{Ca}$ channels contains 8 members and classified into five classes: small conductance (SK) channels, intermediate conductance (IK) channels, big conductance (BK) channels, $K_{Ca}4$ subfamilies and $K_{Ca}5$ channels as shown in **Table 3.2**.

**Table 3.2:** Calcium-activated $K^+$ channel subunits, providing both the gene and protein names and details of their accessory subunits.

| Classification | Family | Gene Name (Protein Name) | Main accessory subunits |
|---|---|---|---|
| **$K_{Ca}1.1$** | BK | KCNMA1($K_{Ca}1.1$) | β1- β4 |
| **$K_{Ca}2.x$** | SK | KCNN1 ($K_{Ca}2.1$), KCNN2 ($K_{Ca}2.2$), KCNN3 ($K_{Ca}2.3$) | - |
| **$K_{Ca}3.1$** | IK | KCNN4 ($K_{Ca}3.1$) | - |
| **$K_{Ca}4.x$** | - | KCNT1 ($K_{Ca}4.1$), KCNT2 ($K_{Ca}4.2$) | - |
| **$K_{Ca}5.1$** | - | KCNU1 ($K_{Ca}5.1$) | - |

All $K_{ca}$ channel gene transcripts showed lower expression levels in both ileum and colon compared with other types of potassium channel genes. KCNN4, encoding the IK channel was the most abundantly expressed transcript throughout the ileum and colon. KCNMB, encoding the BK channel alpha subunit was the second greatest expressed channel transcript, the relative expression level was almost 4-times greater in colon than in ileum. The SK3 ($K_{Ca}2.3$) channel gene was the highest expressed channel gene from SK family in both ileum and colon. Transcripts for $K_{Ca}4.2$ and SK1 were detected in both ileum and colon but at low levels, whilst transcripts for $K_{Ca}4.1$, $K_{Ca}5.1$ and SK2 were barely detectable (**Figure 3.4**).

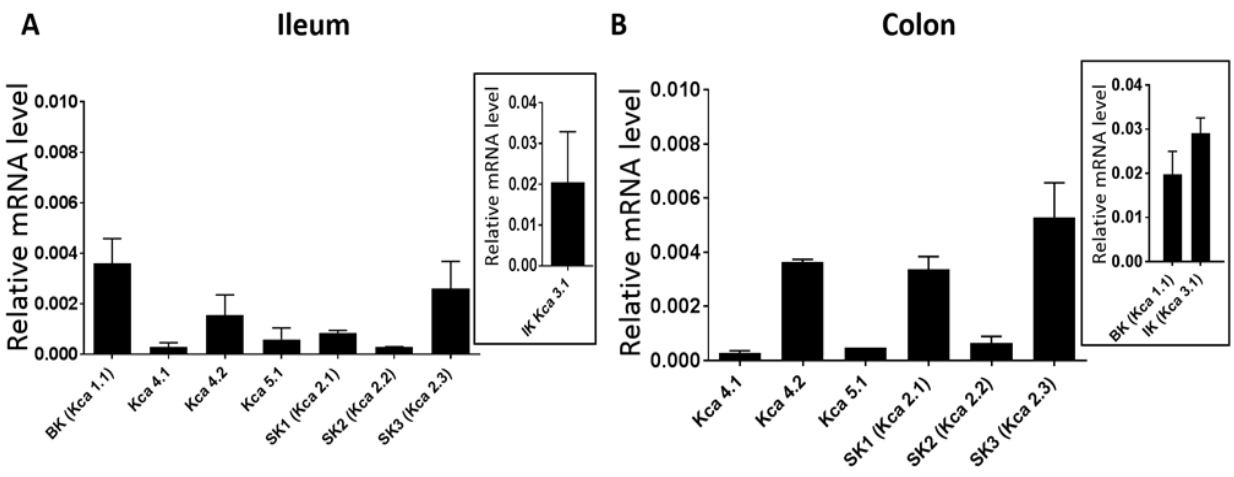


**Figure 3.4:** Differential expression of $K_{Ca}$ subtype transcripts in the mouse ileum and colon. Quantitative, real-time PCR performed on lysates of acutely isolated ileum **(A)** and colon **(B)** from wild type mice. Data are expressed as relative mRNA levels ($2^{-\Delta Ct}$) compared to the housekeeping gene GAPDH (mean ± SEM, *n* = 3). IK (KCNN4) displayed the highest relative expression levels in both ileum and colon and is shown in the inset for clarity. Channel protein names have been used instead of the gene names for simplicity as the protein names are more commonly known.

### 3.2.4 Voltage-gated $K^+$ channel accessory subunits

$K_v$ channels are comprised of α and β subunits, the $K_v$ α subunits form the channel conducting pore and β subunits are modulatory subunits. These $K_v$ modulatory subunits (e.g. $K_v$β, KCNE, KCNIP) are auxiliary proteins that do not have the ability to form functional channels in their own right, but associate with α subunits to modulate channel function (Pongs and Schwarz, 2010).

**Table 3.3:** β accessory $K^+$ channel subunits, displaying the details of accessory β subunits, providing both the gene and protein names and details of their associated α subunits

| Classification | Gene Name (Protein Name) | Associated α subunits |
|---|---|---|
| **β subunits** | KCNMB1(β1), KCNMB2(β2), KCNMB3(β3), KCNMB4(β4) | BK channel |
| **KCNE** | KCNE1, KCNE2, KCNE3, KCNE4, KCNE1L (KCNE5) | $K_v$7 channels |
| **KCNIP** | KCNIP1 (KChIP1), KCNIP2 (KChIP2), KCNIP3 (KChIP3), KCNIP4 (KChIP4) | $K_v$4 channels |
| **$K_v$β subunits** | KCNAB1 ($K_v$β1), KCNAB2 ($K_v$β2), | $K_v$1 channels |

KCNE3 gene transcripts, encoding the MiRP2 protein, were the most abundantly expressed of all transcripts tested relative to housekeeping genes, and had almost 4-times higher expression in colon than in ileum. KCNAB2 (encoding $K_v$β2 subunits) was the second highest accessory subunit transcript in ileum, followed by KCNMB1 and KCNIP2. KCNMB4, KCNE4, KCNAB1 & 3, KCNIP1 & 3 were detected at very low levels in ileum. KCNMB2 & 3, KCNE1, 2 & 4 and KCNIP4 were negative (not detected) or barely detectable in mouse ileum. In colon, KCNMB1 was showed the second highest relative expression level, and the only accessory subunit gene detected in the $K_{Ca}$β subunits group. Moreover, KCNMB1 subunit gene levels were 2-times greater in colon than in ileum. Next in rank order were the transcript levels of the KCNAB2, KCNIP4, KCNIP1, KCNE4 and KCNAB1. KCNE2, KCNAB3, KCNIP2 and KCNIP3 were detected at very low levels, and KCNMB2-4, KCNE1 & 5 were negative or barely overserved in mouse colon (**Figure 3.5**).

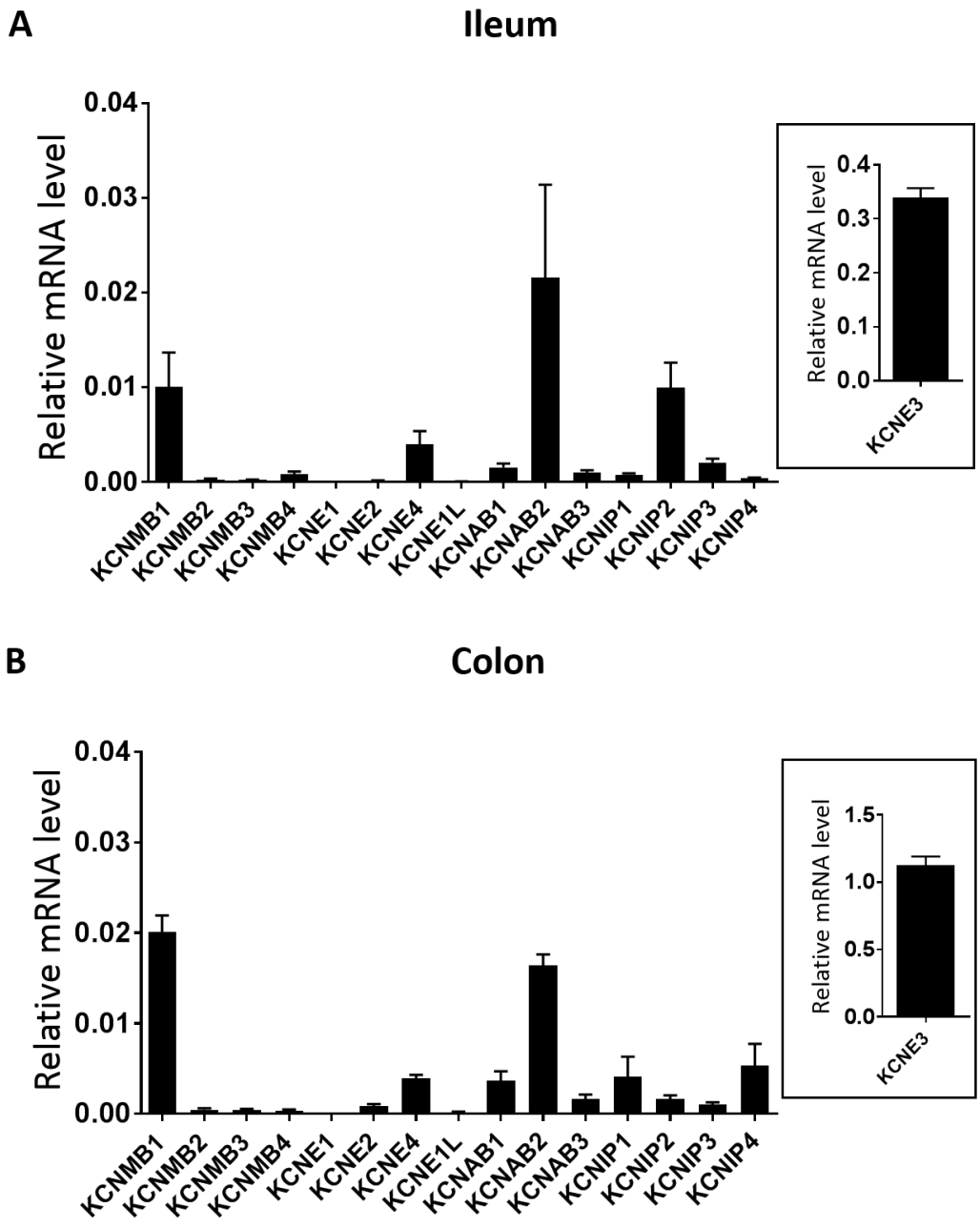


**Figure 3.5:** Differential expression of accessory subunits subtype transcripts in the mouse ileum and colon. Quantitative, real-time PCR performed on lysates of acutely isolated ileum **(A)** and colon **(B)** from wild type mice. Data are expressed as relative mRNA levels ($2^{-\Delta Ct}$) compared to the housekeeping gene GAPDH (mean ± SEM, $n = 3$). Regulatory subunits KCNE3 displayed the highest relative expression levels in both ileum and colon and were shown as insets for clarity. Channel protein names have been used instead of the gene names for simplicity as the protein names are more commonly known.

### 3.2.5 Inwardly rectifying $K^+$ channels ($K_{ir}$)

$K_{ir}$ family consist of 15 subunit genes, which can be classified into four following subfamilies: 1) classical $K_{ir}$ channels ($K_{ir}2.x$), 2) G-protein gated subfamilies ($K_{ir}3.x$), 3) $K^+$-transport channels ($K_{ir}1.x$, $K_{ir}4.x$, $K_{ir}5.x$, and $K_{ir}7.x$), 4) ATP-sensitive $K^+$ channels ($K_{ir}6.x$) as shown in **Table 3.4**.

**Table 3.4:** Inwardly Rectifying $K^+$ channels ($K_{ir}$), providing both the gene and protein names.

| Family | Classification | Gene Name (Protein Name) |
|---|---|---|
| **Classical $K_{ir}$** | $K_{ir}2.x$ | KCNJ2($K_{ir}2.1$), KCNJ12($K_{ir}2.2$), KCNJ4($K_{ir}2.3$), KCNJ14($K_{ir}2.4$) |
| **G-Protein Coupled $K_{ir}$** | $K_{ir}3.x$ | KCNJ3($K_{ir}3.1$), KCNJ6($K_{ir}3.2$), KCNJ9($K_{ir}3.3$), KCNJ5($K_{ir}3.4$) |
| **$K_{ATP}$ channels** | $K_{ir}6.x$ | KCNJ8($K_{ir}6.1$), KCNJ11($K_{ir}6.2$) |
| **$K^+$ Transport $K_{ir}$** | $K_{ir}1.1$ | KCNJ1 ($K_{ir}1.1$) |
| | $K_{ir}4.x$ | KCNJ10 ($K_{ir}4.1$), KCNJ15 ($K_{ir}4.2$) |
| | $K_{ir}5.1$ | KCNJ16 ($K_{ir}5.1$) |
| | $K_{ir}7.1$ | KCNJ13 ($K_{ir}7.1$) |

$K_{ir}6.1$ transcript was the highest expressed subunits with similar expression level in both ileum and colon, with the following rank order; $K_{ir}6.1 > K_{ir}7.1 > K_{ir}4.1 > K_{ir}2.1 > K_{ir}3.1$ in ileum (**Figure 3.6A**) and $K_{ir}6.1 > K_{ir}2.1 > K_{ir}7.1 > K_{ir}4.1 > K_{ir}2.2$ in colon (**Figure 3.6B**). $K_{ir}2.1$ showed nearly 3-times higher relative expression in colon than in ileum, whereas $K_{ir}7.1$ showed similar expression levels across both tissues. Other members of the $K_{ir}$ subfamily displayed low or no detectable transcript levels (**Figure 3.6**).

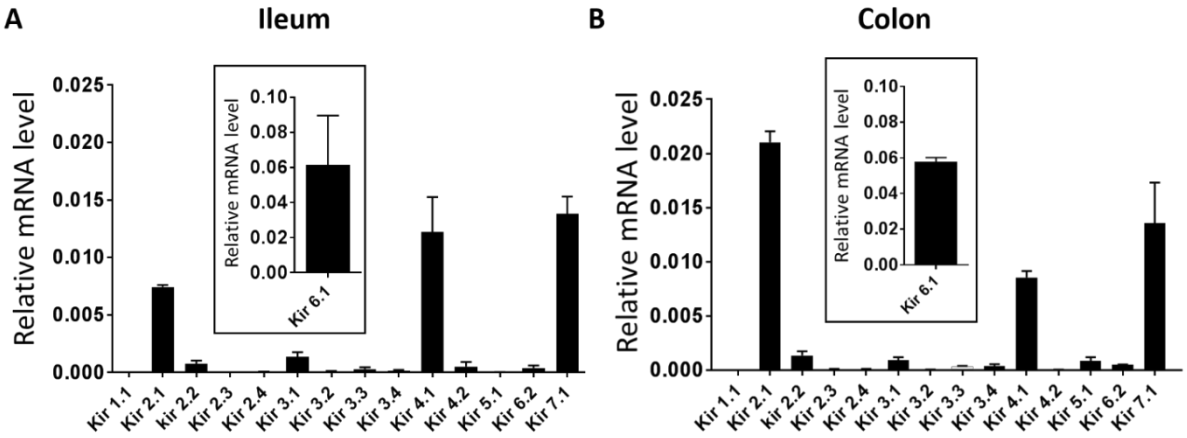


**Figure 3.6:** Differential expression of $K_{ir}$ subtype transcripts in the mouse ileum and colon. Quantitative, real-time PCR performed on lysates of acutely isolated ileum **(A)** and colon **(B)** from wild type mice. Data are expressed as relative mRNA levels ($2^{-\Delta Ct}$) compared to the housekeeping gene GAPDH (mean ± SEM, *n* = 3). $K_{ir}$6.1 (KCNJ8) displayed the highest relative expression levels in both ileum and colon and is shown in an inset for clarity. Channel protein names have been used instead of the gene names for simplicity as the protein names are more commonly known.

## 3.2.6 Two-Pore $K^+$ channels ($K_{2P}$)

The sub-family of $K_{2P}$ channels includes 14 members in the mouse genome, which can be divided into 6 functional subfamilies (TWIK, TASK, TREK, THIK, TALK and TRESK) on the basis of sequence and function similarities, as shown in **Table 3.5.**

**Table 3.5:** Two-Pore $K^+$ channels ($K_{2P}$), providing both the gene and protein names.

| Classification | Gene Name (Protein Name) |
|---|---|
| **TWIK** | KCNK1 ($K_{2P}$1.1; TWIK-1), KCNK6 ($K_{2P}$6.1; TWIK-2), KCNK7 ($K_{2P}$ 7.1) |
| **TASK** | KCNK3 ($K_{2P}$3.1; TASK-1), KCNK9 ($K_{2P}$9.1; TASK-3), KCNK15 ($K_{2P}$15.1; TASK-5) |
| **TREK** | KCNK2 ($K_{2P}$2.1; TREK-1), KCNK4 ($K_{2P}$4.1; TRAAK), KCNK10 ($K_{2P}$10.1; TREK-2) |
| **THIK** | KCNK13 ($K_{2P}$13.1; THIK-1), KCNK12 ($K_{2P}$12.1; THIK-2) |
| **TALK** | KCNK16 ($K_{2P}$16.1; TALK-1), KCNK17 ($K_{2P}$17.1; TALK-2), KCNK5 ($K_{2P}$5.1; TASK-2) |
| **TRESK** | KCNK18 ($K_{2P}$18.1; TRESK) |

The most abundant $K_{2P}$ channel transcripts through mouse gut was KCNK1 (encoding TWIK-1, $K_{2P}$1.1), and showed twice the relative expression levels in colon than in ileum. KCNK5, encoding TASK-2 channels, was ranked second highest but showed similar expression levels across ileum and colon. The rank order was as follows; TWIK-1 > TASK-2 > TREK-1 > TASK-1> TWIK-2 > THIK-1 > $K_{2P}$ 7.1 in ileum and TWIK-1 > TASK-2 > TWIK-2 > TASK-1 > TREK-1 > THIK-1 > $K_{2P}$ 7.1 in colon (**Figure 3.7**). In both tissues, genes encoding TRAAK, TASK-3, TREK-2, THIK-2, TASK-5, TALK-1 appeared barely detectable when normalised to housekeeping gene GAPDH, whereas transcript encoding for TRESK was not detected in either ileum or colon.

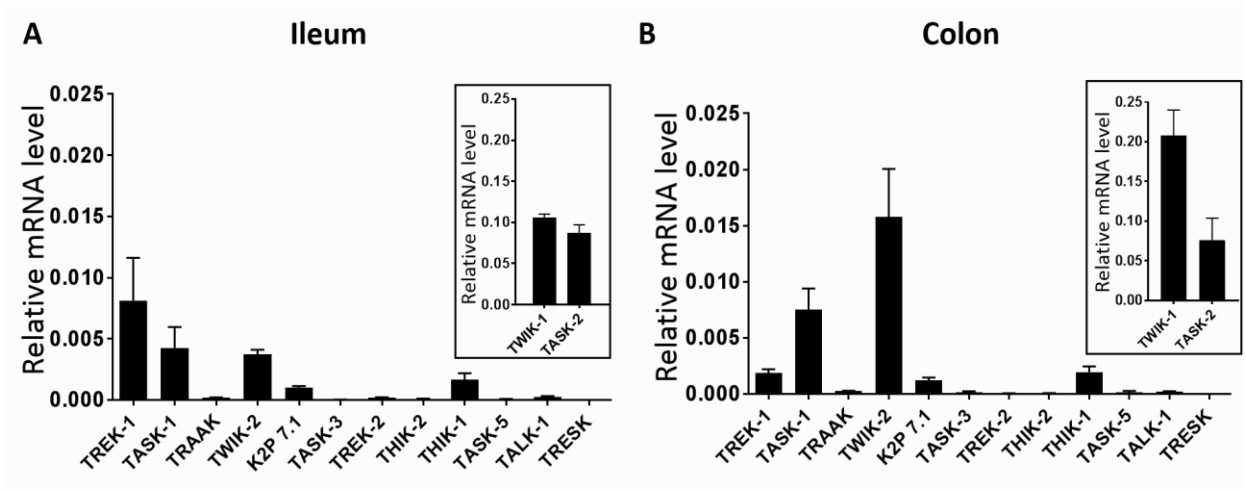


**Figure 3.7:** Differential expression of $K_{2P}$ subtype transcripts in the mouse ileum and colon. Quantitative, real-time PCR performed on lysates of acutely isolated ileum **(A)** and colon **(B)** from wild type mice. Data are expressed as relative mRNA levels ($2^{-\Delta Ct}$) compared to the housekeeping gene GAPDH (mean ± SEM, *n* = 3). TWIK-1 (KCNK1) and TASK-2 (KCNK5) displayed the highest relative expression levels in both ileum and colon and are shown in insets for clarity. Channel protein names have been used instead of the gene names for simplicity as the protein names are more commonly known.

### 3.2.7 TREK family subunits mRNA expression in the mouse ileum and colon

Evidence of an important stretch-dependent potassium (SDK) channel has been cited in mouse colonic smooth muscle cells(Koh and Sanders, 2001). The molecular identity of the channel is unknown, but has the biophysical hallmarks of a mechano-gated TREK-like channel. Given that all three TREK subfamily channels were shown to be expressed in ileum and colon, albeit at different levels I performed complimentary expression profiling of the three TREK subfamily genes to conclusively determine their expression in ileum and colon. Non-quantitative RT-PCR revealed mRNA expression for genes encoding TREK-1, TREK-2 and TRAAK (*n* = 3) (**Figure 3.8**). Plasmids containing the three genes served as a positive control for the primers, and β actin was also served as positive control transcript for the PCR reaction in ileum and colon. The negative control consisted of a no-template reaction, where nuclease-free water replaced cDNA, and served to indicate the presence of

unwanted contaminating DNA. The results demonstrate all three mechano-gated TREK channel genes were expressed in both ileum and colon with band sizes equating to those amplicons derived from the positive control reactions, and no band was detected in the absence of cDNA in the negative control (**Figure 3.8**).

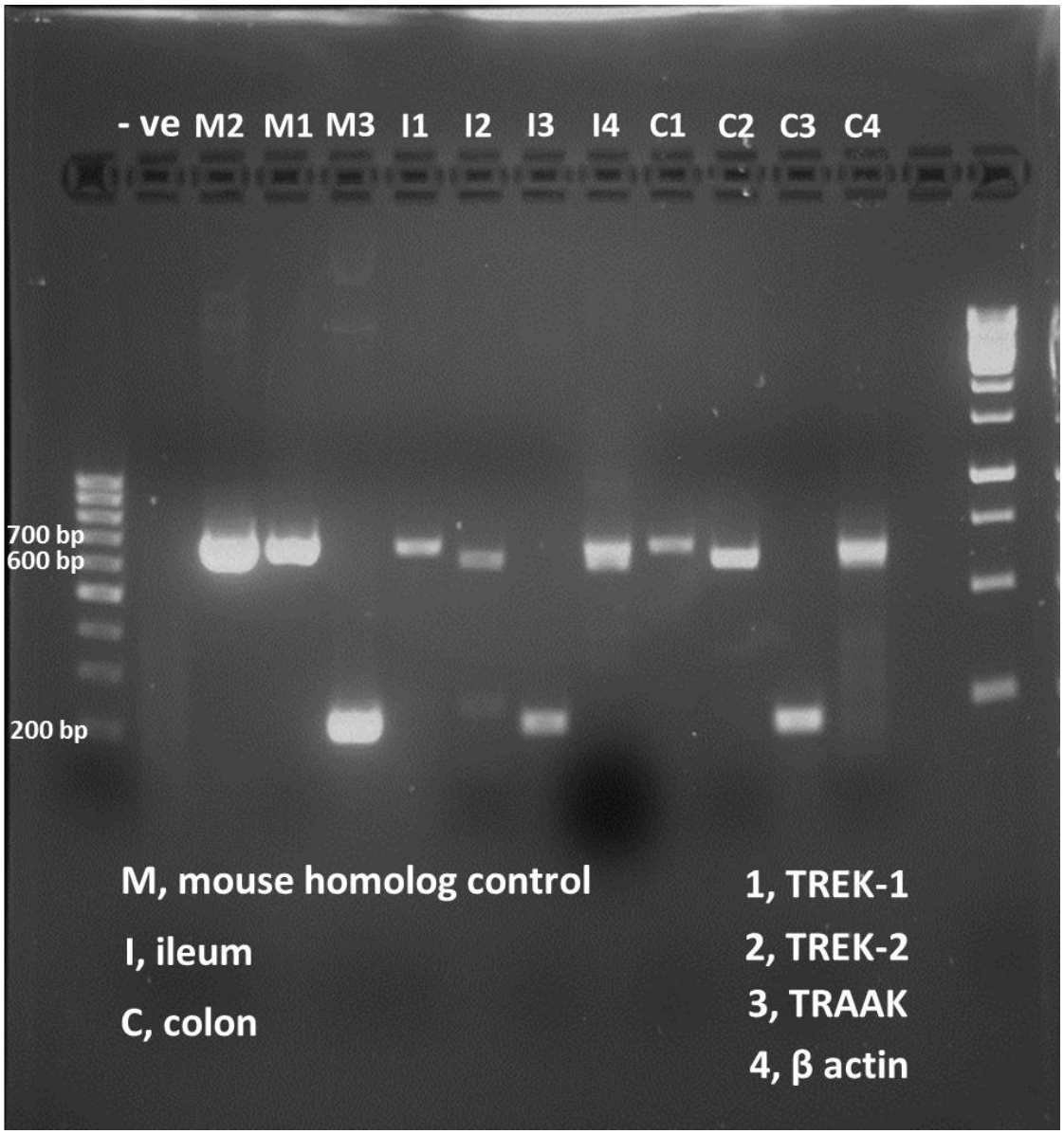


**Figure 3.8:** Qualitative mRNA expression of TREK family channel genes in the mouse ileum and colon. Representative gel electrophoresis images of cDNA amplicons for all three TREK family subunits using RT-PCR from homogenates from whole mouse ileum (I) and colon (C) (*n* = 3). Plasmids containing mouse homologues of TREK-1, TREK-2 and TRAAK were used as a positive control (M). A negative control (-ve), containing is shown. The expected amplicon sizes were 676 bp (TREK-1), 624 bp (TREK-2), 219 bp (TRAAK), 647 bp (β actin).

## 3.3 Discussion

Gastrointestinal motility disorders, such as irritable bowel syndrome (IBS), can occur when coordinated smooth muscle contractility is disrupted. Muscle contraction is a calcium dependent process and in smooth muscle requires transmembrane influx of calcium ions through voltage-gated calcium channels (VGCC). Aside from the calcium channels, potassium ion channels also play an important role in regulating the intracellular concentration of $Ca^{2+}$ by controlling membrane potential, and thus the open probability of VGCC, and so in turn regulate GI smooth muscle tone(Vogalis, 2000). However, our understanding of the expression profiles and functional roles of $K^+$ channels, particularly in smooth muscle tissue of the GI tract, is rather limited. The results within this chapter revealed the transcript profiles of the whole family of $K^+$ channels (93 transcripts) in the two main anatomical sections of GI tract concerned with GI motility disorders, namely the distal section of the small intestine (ileum) and the large intestine (colon). My data showed robust transcript expression for many different types of $K^+$ channels in both ileum and colon. Regarding $K_v$ family genes, more than 50 % of the genes displayed detectable expression in the mouse GI tract. In particular, $K_v7.1$ and its modulatory subunit MiRP2 (KCNE3) were the most highly expressed transcripts across the whole $K^+$ channel family. From the $K_{ir}$ subfamily, $K_{ir}6.1$ showed the highest relative expression in the mouse GI tract, echoing a previous RT-PCR study in colonic muscle tissue (Jin et al., 2004). However, the most novel findings came from the profiling of $K_{2P}$ channel transcripts across small and large intestine, as there is a distinct lack of research knowledge regarding these channels in the GI system. Therefore the finding of high relative levels of mRNA expression for TWIK-1 and TASK-2 revealed these channels may have important functions roles in the GI system, which

have not previously been noted. Together these data characterising the expression levels of $K^+$ channel subtype genes along the mouse ileum and colon, forms the foundation for further investigations in this study.

### 3.3.1 Limitations of the qRT-PCR analysis

Before I critically discuss the outcomes of the transcript profiling using quantitative PCR technology, there needs to be a clear discussion of the limitations of the conducted experiments to contextualise the resulting data. qRT-PCR is a powerful and sensitive technology for the quantification and validation of gene expression. Despite the power of qRT-PCR, however, a number of key considerations need to be addressed in order to get the quantification of mRNA right, from sample preparation through data analysis.

Firstly, my qPCR experiments utilised mRNA extracted from whole tissue sections. Hence, it was not possible to unequivocally differentiate the expression profiles of the channel genes across different types of cells. Ideally, the expression of channel genes in smooth muscle tissue alone versus other cell types, including epithelia, neuronal and glia, would have been desirable. However, a qPCR study on purified smooth muscle tissues was not feasible in the ileum and colon, due to the difficulty of accurate tissue dissection. This could have been overcome through the profiling of cell specific gene markers to help compare relative gene expression of channel genes versus cell specific genes, however I was limited by the number of genes I could assess on my array, and was unable to include cell specific genes to assess proportions of different cell types in the whole sample. Together, this means that low level expression levels of some $K^+$ channels transcripts (e.g. $K_v7.4$, TREK-2,

and TRAAK etc.) could likely represent either general low expression across the whole tissue or perhaps high expression levels in discrete, specific populations of cells that were ultimately diluted across the whole tissue. Future studies should include cell specific genes to help quantify gene expression profiles in specific cell populations.

A further limitation is that some channel transcripts were actually expressed in tissue, but could not be determined in my data after analysis. The relative quantification analysis of $2^{-\Delta Ct}$ method used here are the simplest and most commonly used method for accurately determining relative expression levels and changes in expression transcripts. This analysis method assumes almost 100% efficient target and standard gene PCR reactions given that results conform to certain criteria (Livak and Schmittgen, 2001), and this was confirmed in my experiments using three positive reference genes in each running. Since PCR efficiencies may change between runs or between target and standard genes, other numerous methods called "DART method" have emerged that calculate template concentrations using amplification simulations or PCR efficiencies derived from CT values or fluorescence data (Pfaffl, 2001, Peirson et al., 2003). However, a lack of consensus existed on how to best perform and evaluate qPCR experiments. In addition, previous studies analysed results from a salmon lice starvation experiment by using both $2^{-\Delta Ct}$ method and the DART method adjusting for PCR efficiency differences, they found these 2 methods showed different results (Skern et al., 2005). Moreover, they would not have more confidence in one method than the other unless they had data from their microarray experiments. Therefore, despite the fact that both methods are theoretically sound given a number of assumptions, we may be misled when these assumptions are not fulfilled. Indeed, in my qRT-PCR experiment, I

clearly show several gene transcripts show high expression level, but my RT-PCR findings also confirms those low expression levels or absent expression of some $K^+$ transcripts (e.g. TREK-2 and TRAAK) were actually expressed in the tissue and also display strong mRNA signal band compared TREK-1 channel. Moreover, previous studies confirmed the high expression level of BK (Zhu and Huizinga, 2008) or $K_v$7.4/7.5 channels (Jepps et al., 2009) in mouse intestine, but both genes display low expression level in my studies. All analysis methods of qRT-PCR data are based on a number of assumptions, and due to experimental errors none or few of these assumptions will be completed entirely. Unfortunately, it is not always obvious when assumptions are broken to a degree that invalidates the conclusions. Since the sources of potential problems are diverse, there is no simple solution, universal analytical approach and direct guidelines available for qRT-PCR analysis, and ensure a correct conclusion. Therefore, we should urge caution when analysing results, and further experiments should be performed with qRT-PCR experiment together, such as RT-PCR and microarray, in order to confirm and support your conclusions.

### 3.3.2 Voltage-gated potassium channels ($K_v$)

Evidence for the expression of $K_v$ channels in the GI system is poor, with transcript profiles restricted to the $K_v$4 and $K_v$7 subfamilies. In this study, we performed the first, whole family profiling of $K_v$ channel mRNA in the mouse GI tract. Our data showed robust transcript expression for multiple $K_v$ channels including $K_v$4.3, $K_v$7.1, $K_v$5.1 and $K_v$2.1.

$K_v$ channels can be classified as delayed rectifiers or inactivating A-type channels (Vogalis, 2000). Inhibition of A-type currents has been reported to increase smooth muscle

excitability and contractility in different region of GI tract (e.g. fundus, antrum, jejunum and colon). A-type currents have been suggested to be formed through association of $K_v4$ channels, which can be assembled as homo- or heterotetramers of $K_v4.1$, $K_v4.2$ and $K_v4.3$ subunits (Amberg et al., 2003), and through association with KChIP auxiliary subunits. Previous studies revealed all three $K_v4$ channel transcripts were expressed in murine proximal colon circular smooth muscle cells, and dampen excitability and may participate in maintaining the phasic pattern of electrical activity (Koh et al., 1999). My data showed that transcripts encoding $K_v4.3$ exhibited highest expression level among $K_v4$ subfamily genes in the whole tissue of both ileum and colon, which echoed previous qPCR studies in colonic and jejunal smooth muscle (Amberg et al., 2002). Furthermore, protein for all three $K_v4$ subfamily subunits has been confirmed in murine muscular antrum by immunohistochemistry (Amberg et al., 2002). The authors also confirmed the contribution of $K_v4$ channels to colonic A-type currents by using flecainide, which is a blocker displaying higher sensitivity to $K_v4$ channels ($IC_{50} \leq 20$ μM) than $K_v1$ channels ($IC_{50} \geq 50$ μM) (Amberg et al., 2002). Moreover, $K_v4.3$ protein expression recently was detected in the smooth muscle regions of small intestine, but the immunoreactivities in mucosa layer was not found (Liu et al., 2014). KChIPs, which belongs to the neuronal calcium sensor (NCS) family of proteins, binds to the N-terminal region and the T1 domain of $K_v4$ proteins (An et al., 2000, Rosati et al., 2001). This protein act as positive modulators improving $K_v4$ current density by increasing expression of the channels in the plasma membrane (Bahring et al., 2001, An et al., 2000), and also modify the kinetic behaviour of $K_v4$ channels (Beck et al., 2002). There are four known KChIP genes (KChIP1-KChIP4), which all exert similar effects on $K_v4$ channels (Kew and Davies, 2010). Amberg et al, (2002) identified KCNIP1, encoding the KChIP1 accessory protein, as the highest expressed KChIP subunit in isolated colonic

smooth muscle cells. My data shows the KChIP2 transcript as the highest expressed KChIP transcript in ileum and KChIP4 transcript in colon. A-type current in ventricular myocytes were underlied by $K_v4$ channels (Xu et al., 1999, Nerbonne, 2000), and the transcript expression of KChIP2 has been shown to account the transmural gradient of A-type currents in canine and human ventricles (Rosati et al., 2001). The KChIP2 knock-out mice exhibited normal cardiac structure and function, but ventricular A-type currents were reduced by approximately half compared to wild-type myocytes. Moreover, KChIP2 knock-out mice did not express functional A-type currents, and a marked increase in action potential duration (Kuo et al., 2001), thereby similar regulation of functional $K_v4$ channels by KChIP2 may occur in GI smooth muscles as cardiac myocytes. Interestingly, the KCNE3 β-subunit gene, encoding the MiRP2 protein has been reported as a strong inhibitory effect on current conducted by heterologously expressed $K_v4.3$ channels, and this inhibitory effect to be specific for $K_v4.3$ within the $K_v4$ channel family. MiRP2 reduces the $K_v4.3$ current amplitude, and it slows down the channel activation and inactivation as well as the recovery from inactivation. MiRP2 also inhibits A-type currents generated by $K_v4.3$ in complex with the KChIP2 accessory subunit (Lundby and Olesen, 2006). Given the different methodologies between the previous studies and the one here, it is difficult to compare the results directly. However, high relative expression of $K_v4.3$ channel genes and their accessory subunits KChIP2 and MiRP2 indicate a possible important role for these channels in GI tract physiology.

The $K_v7$ subfamily, encoded by the KCNQ genes, are slow delayed rectifier channels and have been identified to play an important role in regulating smooth muscle contractility in

different body systems, including the vasculature, bladder, GI tract and airway (Jepps et al., 2009, Brueggemann et al., 2012, Anderson et al., 2013, Jepps et al., 2013, Greenwood and Ohya, 2009). KCNQ4 and 5 have been showed as the most abundantly expressed KCNQ transcripts in isolated smooth muscle of murine GI tract (Jepps et al., 2009). Conversely, our qPCR analysis revealed the prominent expression of the KCNQ1 gene (encoding $K_v7.1$) among KCNQ genes in the whole tissue of both ileum and colon, which indicate KCNQ1 may be expressed in other cell types, such as neurons and epithelial. Moreover we showed that the accessory β-subunit gene KCNE3, encoding the MiRP2 protein, displays the highest relative expression level among all $K^+$ channels genes. KCNE genes have single transmembrane domain and can significantly affect the activation of threshold KCNQ channels (Dedek and Waldegger, 2001). For example, the interaction between $K_v7.1$ and MinK (encoded by the KCNE1 gene) was the first characterised of any $K_v7$/KCNE complex, and underlies the slowly activating $K^+$ ($I_{ks}$) current in the heart (Ramakers et al., 2003). The protein expression of KCNQ1 and KCNE1 have been shown in epithelial cells of gut and exocrine pancreas (Warth et al., 2002). However, we were unable to detect significant transcript levels of the KCNE1 in either ileum or colon. Importantly, MiRP2 (KCNE3) also forms functional complexes with $K_v7.1$. Co-assembly forms a voltage-independent leak channel which is constitutively open at resting potentials (Schroeder et al., 2000). Moreover, this channel complex has been shown to be important in $K^+$ transport in a number of epithelial tissues including pancreas, airways and intestine (Bleich and Warth, 2000, Preston et al., 2010, Abbott, 2016, Al-Hazza et al., 2016). For instance, KCNE3 co-complexes with KCNQ1 has been shown to be a pivotal conductance in intestinal and tracheal chloride transport as demonstrated through KCNE3 disruption (Preston et al., 2010). In addition, KCNQ1 and KCNE3 proteins have been demonstrated to be located to

the basolateral membranes of crypt cells of the colon and small intestinal (Dedek and Waldegger, 2001). In the GI tract, basolateral potassium channels play an important part in the process of transcellular cAMP-stimulated chloride secretion (Schroeder et al., 2000). Taken together, the absence of KCNQ1 transcripts in isolated intestinal smooth muscle cells (Jepps et al., 2009), and my study showing high levels of KCNQ1 and KCNE3 in whole gut tissue, suggests that KCNQ1 and KCNE3 may both be significantly expressed in epithelial layers of the GI tract, and form the basolateral potassium conductance to regulate the cAMP-mediated $Cl^-$ secretion. However, further functional studies are required.

$K_v5$, $K_v6$, $K_v8$ and $K_v9$ were collectively identified as electrically silent $K^+$ channels, and do not form functional homotetrameric channels when expressed alone, but are able to co-assemble with $K_v2$ family to form heterotetrameric complexes and increasing $K_v$ channel functional diversity (Bocksteins, 2016). Both KCNB1 ($K_v2.1$) and KCNF1 ($K_v5.1$) had the highest expression levels of the KCNB and silent subunit gene families in our qPCR analysis. $K_v2.1$ is a prominent neuronal potassium channel, and is widely expressed across brain tissue, but has also been shown to play roles in non-neuronal tissues including vascular smooth muscle where its modulation is associated with hypertension (Joseph et al., 2013, Kew and Davies, 2010). $K_v2.1$ has also been recently reported in guinea pig detrusor smooth muscle, and through its association with silent $K_v$ channel subunits has been proposed to control smooth muscle excitability and contractility (Hristov et al., 2012). Given the prominent expression of KCNB1 and KCNF1 transcripts across ileum and colon shown here, it is possible that $K_v2.1$ may have a similar functional role in GI smooth muscle tissues, either alone or in complex with silent subunits including $K_v5.1$. However, direct protein

localisation in smooth muscle and neuronal tissue and conclusive pharmacological evidence is currently lacking.

With regards to other voltage-gated delayed rectifier channels, members of the $K_v1$ family, particularly $K_v1.1$-1.3, encoded by KCNA1-3 genes showed relatively high levels of mRNA expression in the ileum and colon, and along with expression of KCNAB2, encoding the associated β subunit $K_v\beta2$ which was the second most abundant accessory subunit in ileum and colon, suggests a role for these channel complexes in GI tissues. Like $K_v2$ family channels, $K_v1$ channels are prominently expressed in neuronal tissues of the central and peripheral nervous systems, and they regulate action potential firing and neurochemical signalling (Kew and Davies, 2010). However, the expression of KCNA2 ($K_v1.2$) transcripts has been previously reported in canine GI smooth muscle cells, but KCNA1 ($K_V1.1$) and KCNA3 ($K_V1.3$) transcripts were not detected (Epperson et al., 1999), while KCNA1 ($K_v1.1$) transcripts have also been reported in interstitial cells of Cajal (ICC) (Hatton et al., 2001). Although it is not clear which cell types $K_v1$ channels are expressed in, their prominent expression is suggestive of a functional role. It is likely that these channels are expressed in the enteric nervous system, although further experimental evidence is required. However, what is clear is a role for $K_v1.3$ channels in gut lymphocytes and the gut mucosal immune system, linked to inflammatory bowel diseases including IBD and Crohn's (Kazama, 2015). Therefore, the notable expression of $K_v1.3$ transcripts in both ileum and colon shown by our study likely represent specific immune cell expression patterns in the GI system. Furthermore, $K_v6.3$ and $K_v10.1$ have been previous reported expressed in both human small

intestine and colon tissue (Ottschytsch et al., 2002). Our results were consistent with the literature that $K_v6.3$ and $K_v10.1$ also expressed in mouse ileum and colon.

### 3.3.3 Calcium-gated potassium channels ($K_{Ca}$)

The $K_{Ca}3.1$ channel (IK) gene, KCNN4, was strongly expressed in both ileum and colon, together with the BK ($K_{Ca}1.1$) gene, KCNMA1, and their β1 subunit gene, KCNMB1. Interestingly, both the BK channel and β1 subunit genes displayed higher expression levels in the colon than in ileum, and the β1 subunit gene was the only expressed subunit gene from the $K_{Ca}$ accessary β subunit subfamily. This suggests that any intestinal BK channel complexes are likely formed through association with the β1 subunit. The BK channel has been well-studied in GI tract, with previous studies reporting both mRNA and protein expression of BK channel in colonic myocytes and involved in stretch activation of the tissue and mechanoelectric transduction (Wang et al., 2010), and their protein expression has been also shown in ICCs in mouse jejunum (Zhu and Huizinga, 2008). Patch clamp recording in either longitudinal or circular of canine proximal colon muscle strips did not implicate BK channels in regulating resting membrane potential, but their blockade by inhibitors such as TEA and charybdotxin (ChTX) were able to induce depolarization and subsequent contraction of colonic longitudinal smooth muscle cells (Carl et al., 1995). In addition, inhibitors (TTX) of BK channels have been shown to increase spontaneous contractile activity of ileum longitudinal muscle (Hong et al., 1997) with activators (LDD175) reduce the spontaneous contractions (Dela Pena et al., 2009). Thus, the expression and functional contribution of BK channels to GI tract smooth muscle contractility suggests that modulators of BK channels could provide potential treatments of GI motility disorders. A

further identified role for BK channels is in colonic $K^+$ excretion in crypt cells. BK channels serve as the luminal (apical) exit pathway according to the pump-leak model of $K^+$ secretion. $K_{Ca}\beta2$ subunits have been shown to be co-expressed in crypt cells but molecular ablation leaves BK channel activity intact (Sorensen et al., 2008, Larsen et al., 2017). $K_{Ca}$ channel β1 subunit has been reported in airway (Semenov et al., 2011) and bladder smooth muscle (Petkov et al., 2001) and it is known to interact with BK α subunit in order to regulating smooth muscle contraction (Li et al., 2013). We revealed that transcript for the $K_{Ca}\beta1$ subunits was the highest expressed $K_{Ca}\beta$ subunit in mouse GI tract, and therefore may associate with BK to form a physiologically important channel complex. Given the important role in determining aspects of BK channel pharmacology, for example modulation by alcohol (Kuntamallappanavar and Dopico, 2016), it will be important to establish subunit composition profiles of BK channel complexes when designing drugs targeting BK channels in GI smooth muscle tissues.

All $K_{Ca}2$ (SK) subfamily subunit genes were detected in the ileum and colon, with a rank order of SK3 > SK1 > SK2. Both SK1 and SK3 positive immunolabelling have been established in the human colon muscular layers (Chen et al., 2004). The SK1 channel has also been localised in enteric neurons (Chen et al., 2004), whereas SK3 channel is mainly found in ICCs (Fujita et al., 2001). In previous functional studies, blockers of SK channels depolarize the resting membrane potential of circular muscle cells in the ileum (Niel et al., 1983) and contracts colonic smooth muscle (Okuno et al., 2011). Activators also induce concentration-dependent relaxation effects of the pre-contracted proximal stomach (Curro, 2016),

indicating that SK channels, like BK channels, may play important roles in the regulation of GI smooth muscle contractility.

The strong expression of the $K_{Ca}3.1$ (IK) channel subunit gene in our qPCR analysis agreed with previous reports indicating a widespread expression in GI tract, including enteric neurons, where they mediate the slow afterhyperpolarization potential (Chen et al., 2004, Neylon et al., 2004), smooth muscle cells of canine colon (Koh et al., 1996) and epithelial cells of murine colon (Thompson-Vest et al., 2006).

### 3.3.4 Inward rectifying potassium channels ($K_{ir}$)

High mRNA levels for the ATP-sensitive $K^+$ channel ($K_{ATP}$) $K_{ir}6.1$ gene (KCNJ8) were detected in both ileum and colon, which agrees with findings from a previous RT-PCR study revealing expression in colonic smooth muscle cells (Jin et al., 2004). $K_{ATP}$ channels consist of a hetero-octameric complex of pore forming subunits, $K_{ir}6.1$, $K_{ir}6.2$, and sulfonylurea receptor subunits (SUR1 and SUR2) (Koh et al., 2012). They couple the metabolic state of a cell to its electrical activity. Although $K_{ir}6.2$ and SUR2B gene expression has been previous detected in colonic smooth muscle cells (Koh et al., 1998, Jin et al., 2004), qPCR in mouse GI tissues indicates a very low expression level of the $K_{ir}6.2$ gene in our analysis. Moreover, both $K_{ir}6.2$ and SUR1 positive immunolabelling were detected on cholinergic neurons in the guinea pig ileum, many of which were identified as sensory by their co-storage of substance P and/or calbindin (Liu et al., 1999). Recently, cultured ICC have also been reported to express $K_{ATP}$ channels that are encoded by $K_{ir}6.1$ and SUR2B genes in colon cells and $K_{ir}6.2$ and SUR2B genes in small intestine cells (Na et al., 2017). Also, both gene and protein

expression of $K_{ir}$6.1 and $K_{ir}$6.2, and two regulatory subunits (SUR1 and SUR2B) were identified by RT-PCR and immunohistochemistry which found they are present in the basolateral membrane of the colonic epithelium (Pouokam et al., 2013). Therefore, there are different cell types expressing $K_{ATP}$ channel transcripts in gut which likely explains their prominent expression profile in my qPCR analysis of whole tissue.

qPCR indicated strong expression of the $K_{ir}$2.1 gene (KCNJ2) mRNA, being the second most abundant $K_{ir}$ gene in the colon, and displaying twice the level of expression than in ileum. $K_{ir}$2.1 transcript have previously been reported in circular muscle layer of canine ileum and colon, and it also be expressed in ICC which contribute to the generation and maintenance of negative membrane potentials between slow waves (Flynn et al., 1999).

A novel finding of the qPCR study was the high relative expression levels of the $K_{ir}$7.1 gene (KCNJ13) and $K_{ir}$4.1 gene (KCNJ10) in mouse ileum and colon, which have not previously been reported in GI tract. $K_{ir}$7.1 expression has been demonstrated in uterine myocytes, and a functional role in regulating the transition from quiescence to contractions in the pregnant uterus (McCloskey et al., 2014). It is also known that $K_{ir}$7.1 channels play a significant role in $K^+$ transport in the retinal pigment epithelium (Yang et al., 2008). Given its notable expression in ileum and colon, it is likely the channel may have roles in both epithelia and smooth muscle tissues. $K_{ir}$4.1 channels on the other hand are known for their prominent expression in glial cells supporting neuronal tissue in the central nervous system and are critical in setting the glial resting membrane potential and in $K^+$ spatial buffering (Butt and Kalsi, 2006). Glial cells are present in GI tract tissue, supporting cells of the enteric

nervous system and are notably required for regulation of intestinal motility (Rao et al., 2017). $K_{ir}$4.1 channels have not been shown in GI tract smooth muscle cells specifically, and it is likely that their expression is highest in the supporting glia cells. Therefore high expression of $K_{ir}$4.1 transcript in the GI tract may reflect a high expression levels and/or high numbers of glia cells in the GI system.

### 3.3.5 Two-pore domain potassium channels ($K_{2P}$)

Our understanding of the expression profiles and functional roles of $K_{2P}$ channels, particularly in smooth muscle tissue of the GI tract, is poor, with transcript profiles restricted to the TASK and TREK subfamilies. However, of the $K_{2P}$ channels described to date, the mechano-gated TREK subfamily of $K_{2P}$ channels are appearing as potential regulators of smooth muscle contractility (Parelkar et al., 2010, Lembrechts et al., 2011, Monaghan et al., 2011, Lei et al., 2014).

In this study we performed the first, whole family profiling of $K_{2P}$ channel mRNA in the GI tract. Our data showed robust transcript expression for multiple $K_{2P}$ channel genes including those encoding TWIK-1 (KCNK1), TASK-2 (KCNK5), TASK-1 (KCNK3) and TREK-1 (KCNK2), and TWIK-2 (KCNK6) The profiles of $K_{2P}$ channel mRNA was comparable across ileum and colon, at least at the whole tissue level. The caveat to our transcript profiling, that mRNA levels were assessed in whole tissues and could not differentiate between the proportions within different cell types present in the GI tract (smooth muscle, neuron, glia, epithelia), meant the low level expression of some $K_{2P}$ channel transcripts including TREK-2 (KCNK10) and TRAAK (KCNK4) may represent discrete, cell specific expression profiles.

Given the potential that TREK subfamily channels could be involved in GI smooth muscle cells as stretch-activated channels, we conducted further qualitative RT-PCR profiling of the three family members, confirming TREK-1, TREK-2 and TRAAK positive expression in ileum and colon. A novel finding from our qPCR was the high expression of TWIK-1 and TASK-2 mRNA in both ileum and colon, indicating these two channels may play a prominent role in GI tract physiology. Indeed Cho *et al*., (2005) previously highlighted TASK-2 expression in murine colon and a TASK-2-like conductance as a potential contributor to resting membrane potential, although the pharmacological tools used to assess this (lidocaine) were used at concentrations too high to be TASK-2 specific. Interestingly, TWIK-1 has been recently reported that form functional heterodimers with TREK-1 channel (Hwang et al., 2014). Since both TWIK-1 and TREK-1 display high expression level in our qPCR analysis, this may indicate that the two channel subunits may form the heterodimers in the GI tract. However, along with a current lack of pharmacological tools for TWIK-1, the physiological importance of TASK-2 and TWIK-1 channels in the GI system remains to be conclusively determined.

The detection of TREK-1, TASK-1, TASK-2 and TASK-3 genes also agrees with finding from past RT-PCR studies in colonic muscle tissue (Koh et al., 2001, Cho et al., 2005, Kubota et al., 2015). However, beyond the transcript profiling, specific localisation and functional contributions of $K_{2P}$ channels to GI physiology is severely lacking.

## 3.4 Summary and Conclusions

The overall aim of this chapter was to provide an insight into the mRNA expression profiles of the family of $K^+$ channel genes across mouse ileum and colon, using qPCR and RT-PCR analysis. It is evident from the results that $K^+$ channels are abundantly and widely expressed in mouse GI tract. Key novel findings are the demonstration of high expression of mRNA encoding for $K_v7.1$ and its accessory KCNE3 subunit gene, and $K_{ir}7.1$, $K_{ir}4.1$, TWIK-1 and TASK-2 channel genes in ileum and colon. However, it is likely that the expression level of some $K^+$ channel transcripts is a product of cell-specific expression patterns. Therefore, direct protein localisation studies were required to characterize the distribution of specific $K^+$ channel subtypes in muscle and nervous tissue of the mouse GI tract. Given the prominent roles of $K_{2P}$ channels in neuronal and cardiac physiology and the opposing underwhelming knowledge of $K_{2P}$ channels in GI physiology, I decided to focus my future studies on the specific localisation and functional roles of $K_{2P}$ channels in the GI system.

# Chapter 4 – Localisation of $K_{2P}$ channels in the mouse ileum and colon

## 4.1 Introduction and Aims

$K^+$ channels are formed from multimers of subunits containing either a single ($K_{1P}$) or tandem ($K_{2P}$) pore domain structure. A multitude of voltage-dependent and voltage-independent $K_{1P}$ channels have been shown to be expressed in smooth muscles of the GI tract (for review see Koh *et al*., 2012). In contrast, our understanding of the expression of the voltage-independent $K_{2P}$ channel subfamily in GI tissues is limited. An assessment of K2P transcript expression by qRT-PCR as detailed in Chapter 3 provided an insight into the gene expression profile of the entire family of $K_{2P}$ channels in both mouse ileum and colon, and in particular the high expression of TWIK-1 and TASK-2 channel genes. Previous studies have indicated that TREK-like channels may underlie a stretch-dependant conductance in colonic smooth muscle cells, based on its biophysical phenotype and similarity to cloned murine TREK-1 channels including mechano-sensitivity, insensitivity to classical potassium channel blockers, and regulation by nitrenergic stimulation (Koh and Sanders, 2001, Koh et al., 2001, Park et al., 2005). However, the specific localisation of $K_{2P}$ channel proteins in mouse ileum and colon is still unclear. In this chapter, I will examine the precise cellular locations of different $K_{2P}$ channel subtypes including members of the mechano-gated TREK subfamily and those channels that displayed high relative expression levels (TWIK-1 and TASK-2). I am particularly interested in profiling their expression in neurons and smooth muscle cells, and will utilise immunolabelling in whole mouse gut tissue sections of the ileum and colon and more specifically in isolated single smooth muscle cells.

## 4.2 Results

### 4.2.1 TWIK-1 and TASK-2 expression in ileum and colon

Our qPCR data indicated that the genes encoding TWIK-1 and TASK-2 were the two most abundantly expressed transcripts within the mouse intestine. Immunohistochemical studies were therefore performed with channel specific and cell-type specific antibodies to identify the precise cellular location of TWIK-1 and TASK-2 proteins in different tissue layers of mouse ileum and colon. Expression of TWIK-1 protein was detected on plasma membranes and in cytoplasmic compartments of NOS-immunopositive myenteric plexus (MP) neurons of both mouse ileum and colon (**Figures 4.1 A1, B1**). Immunoreactivity for TWIK- 1 was also observed in the longitudinal smooth muscle (LM) cells in both ileum and colon, as demonstrated by co-localisation with the smooth muscle cell marker α-actinin (**Figures 4.1 A2, B2**). Immunoreactivity for the TASK-2 channel protein was significantly enriched in the cell membranes of NOS-immunopositive MP neurons (**Figures 4.1 C1, D1**), but was not detectable in LM cells of either mouse ileum or colon (**Figures 4.1 C2, D2**). These data indicate that TWIK-1 and TASK-2 channels are widely distributed across neuronal and smooth muscle tissues and correlates with the abundant transcript expression observed in both ileum and colon.

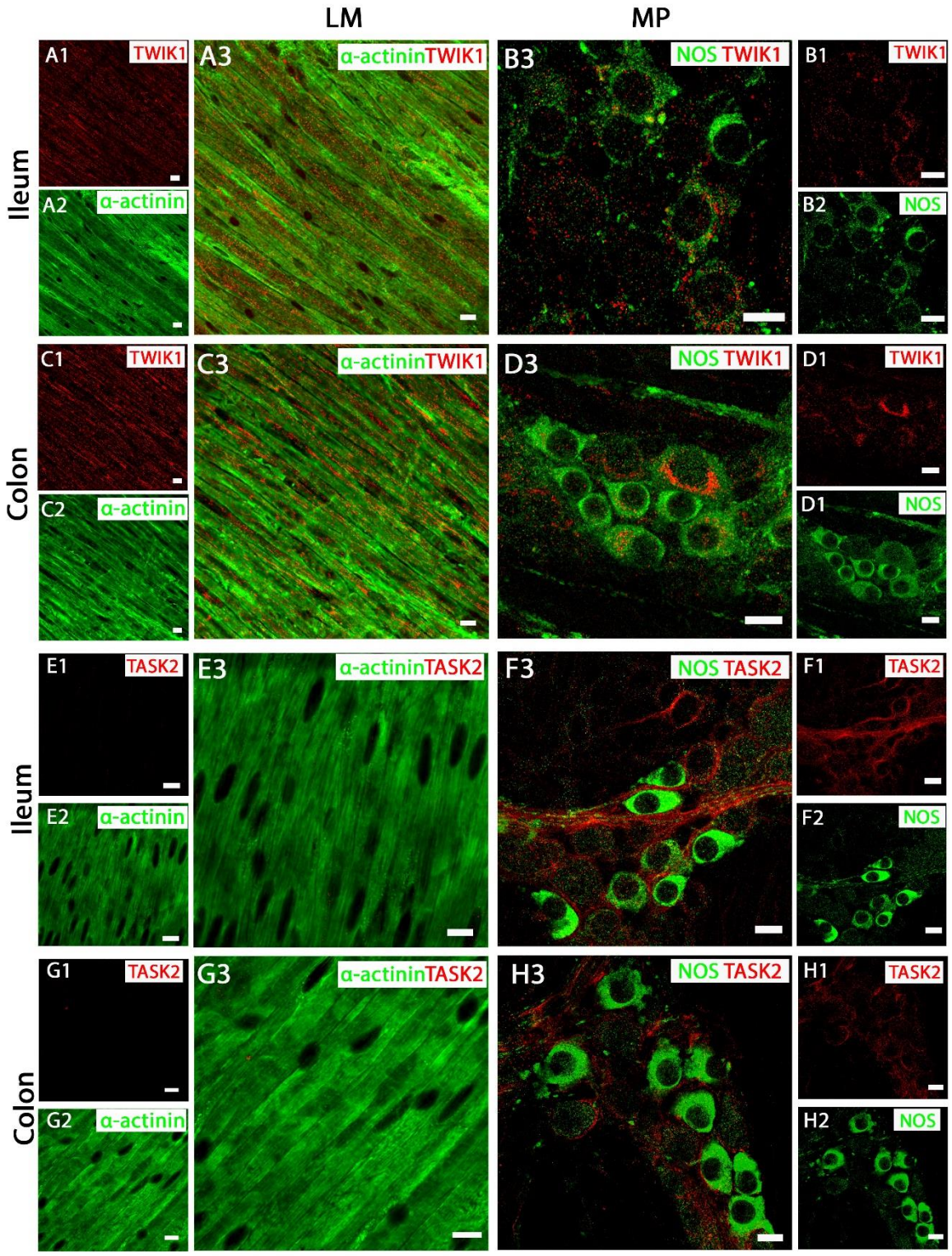


**Figure 4.1:** TWIK-1 and TASK-2 channels are distributed in myenteric plexus inhibitory neurons and longitudinal smooth muscle layers of the mouse ileum and colon. Panels show overlays of cell specific markers (green) and individual $K_{2P}$ channel markers (red) throughout. For clarity, panels **A1, A2, B1, B2, E1, E2, F1** and **F2** (ileum) and **C1, C2, D1, D2, G1, G2, H1** and **H2** (colon) show the individual images from corresponding merges in **A3, B3, C3, D3, E3, F3, G3** and **H3**. Scale bars represent 10 µm.

### 4.2.2 TREK-1 expression in ileum and colon

Our qPCR and RT-PCR indicated that the TREK subfamily channel gene transcripts (TREK-1, TREK-2 and TRAAK) are present in both mouse ileum and colon, but their levels were relatively low and may be suggestive of cell specific expression patterns. Given the proposal that a TREK-like conductance may underlie an important stretch-activated current in the GI smooth muscle, we therefore utilised TREK family channel specific antibody immunolabeling to characterise the specific distribution of TREK channels in muscle and nervous tissue of the mouse GI tract. For consistency with planned organ bath pharmacology studies, we firstly focused on their expression profiles in LM layers and MP neurons. Immunoreactivity for the TREK-1 channel protein indicated it was widely distributed across LM cells in both ileum and colon (**Figure 4.2 A, B**), as visualised by overlapping immunoreactivity with the smooth muscle cell marker α-actinin. In contrast, TREK-1 immunoreactivity was not detected in NOS-immunopositive MP neurons and submucosal plexus neurons (**Figure 4.2 C, D**). I also performed duplicate experiments to look at the expression in circular smooth muscle layers and neighbouring submucosal plexus (SP) neurons in both ileum and colon. TREK-1 channel protein was also detected throughout circular smooth muscle (CM) layers, as demonstrated by co-localisation with the smooth muscle cell marker α-actinin, but TREK-1 immunoreactivity was again not detected in NOS-immunopositive SP neurons (**Figure 4.3 A, B**).

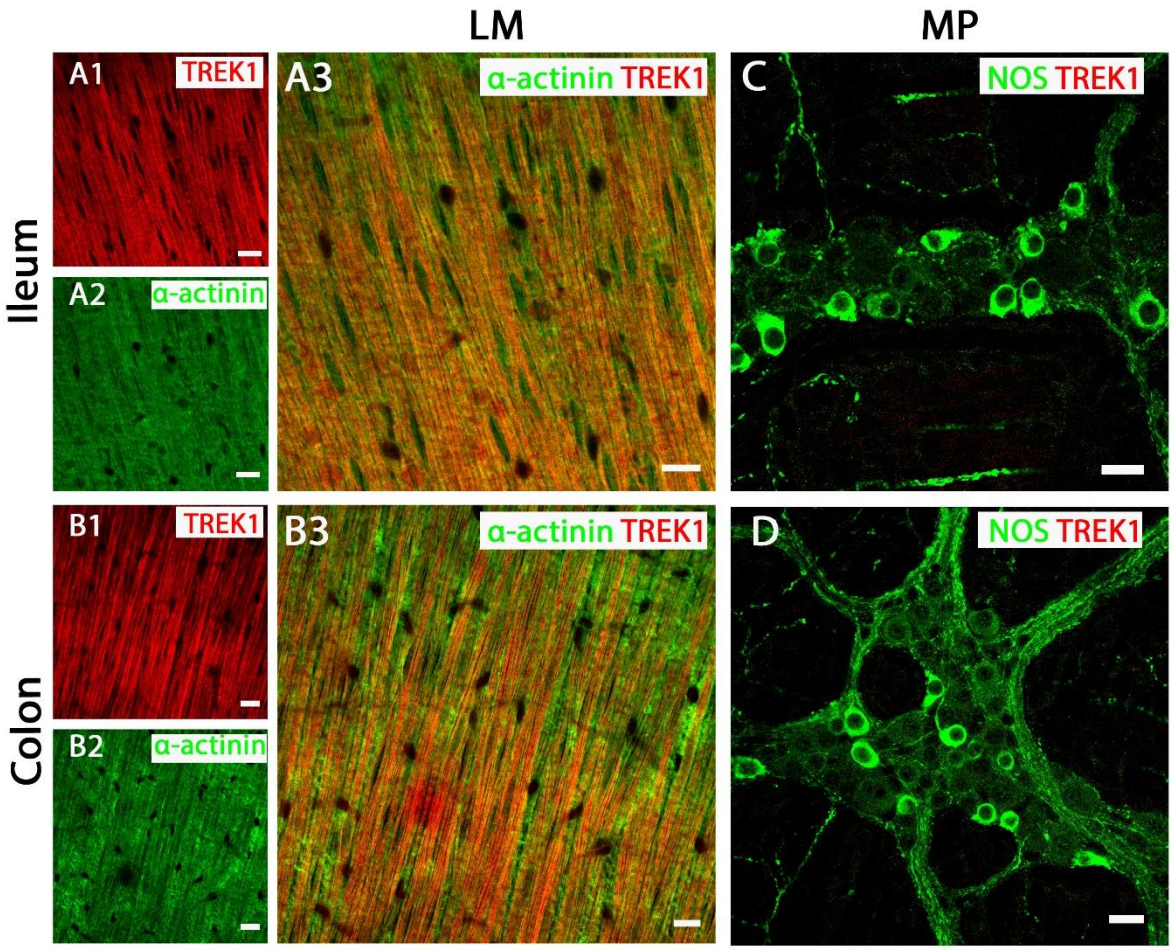


**Figure 4.2:** TREK-1 channel are expressed in longitudinal smooth muscle tissue of both mouse ileum and colon. Panels **A3**, and **C** (ileum) and **B3** and **D** (colon) show overlays of cell specific markers (*green*) and the TREK-1 channel marker (*red*). For clarity, panels **A1** and **A2** (ileum) and **B1** and **B2** (colon) show individual images from corresponding positive merges in smooth muscle. Panels **(C)** and **(D)** show overlays for NOS immunoreactive myenteric plexus neurons and the TREK-1 channel in ileum and colon, respectively. Scale bars represent 10 µm.

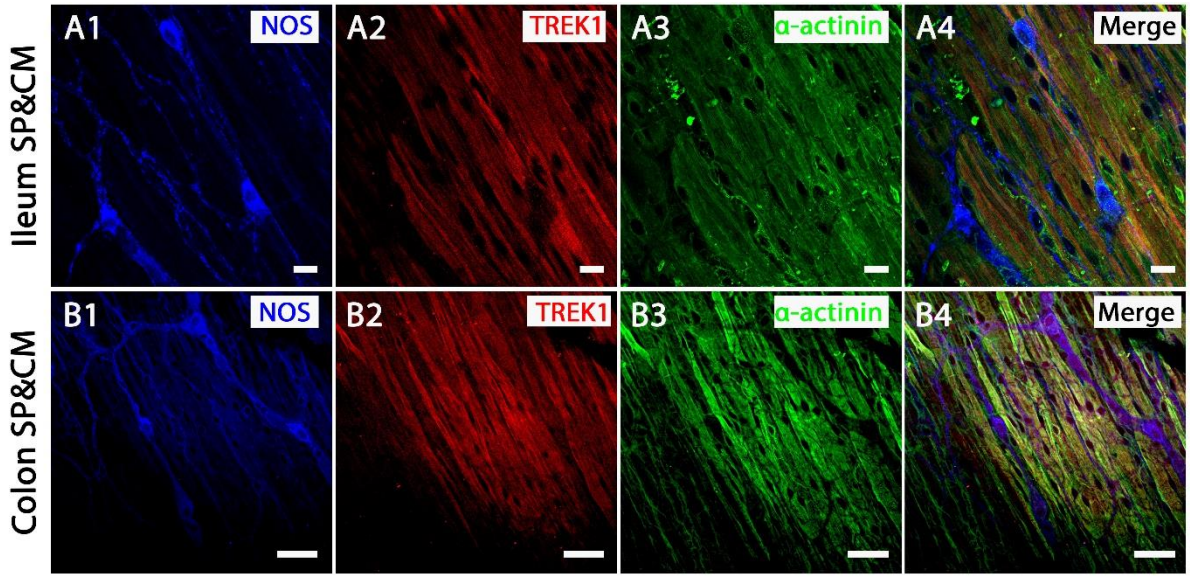


**Figure 4.3:** TREK-1 channels are expressed in circular smooth muscle of both mouse ileum and colon. Images show the expression of NOS immunoreactive submucosal plexus neurons (*blue*, **A1** and **B1**), TREK-1 channel (*red*, **A2** and **B2**) and α-actinin immunoreactive smooth muscle cells (*green*, **A3** and **B3**) in mouse ileum and colon as indicated. **(A4)** and **(B4)** are overlays of **(A1-3) and (B1-B3)** respectively. Scale bar represents 20 µm **(A1-A4)** and 50 µm **(B1-B4)**.

### 4.2.3 TREK-2 expression in ileum and colon

In both mouse ileum and colon, I was unable to detect immunoreactivity for the TREK-2 channel protein in LM cell layers (**Figure 4.4 A, B**) and CM cell layers (**Figure 4.5 A, B**). Conversely, strong TREK-2 labelling was observed within NOS-immunopositive MP neurons (**Figure 4.4 C, D**) and SP neurons (**Figure 4.5 A, B**). Moreover, TREK-2 was also detected in a number of NOS-negative enteric neurons, and thus I also investigated TREK-2 expression in other types of neurons including cholinergic neurons and interneurons. TREK-2 was detected in interneurons (**Figure 4.6 A, B**) and excitatory neurons (**Figure 4.6 C, D**), as visualised by co-labelling with the calcium binding protein, calretinin and ACh synthesizing enzyme, choline acetyltransferase (ChAT) respectively.

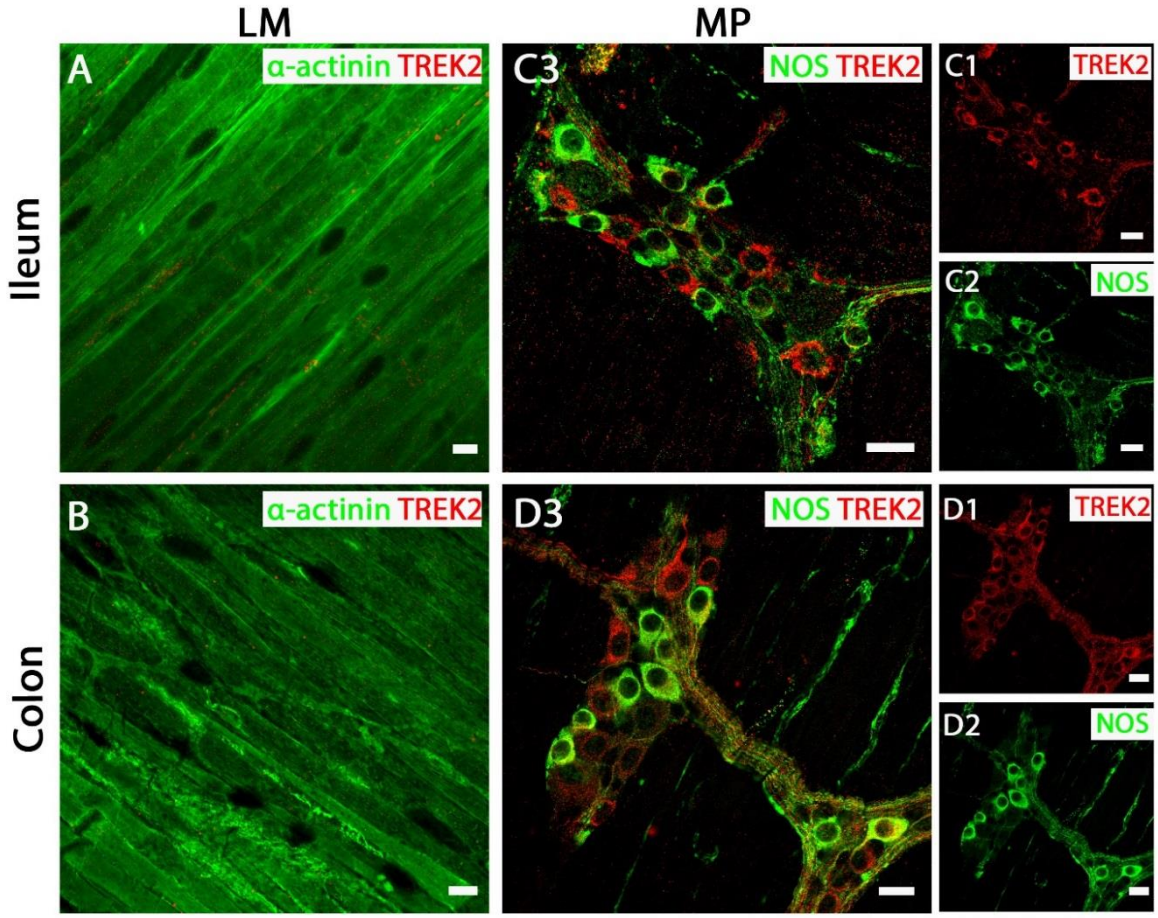


**Figure 4.4:** TREK-2 channels are expressed in myenteric plexus neurons of both mouse ileum and colon. Panels **A**, and **C3** (ileum) and **B** and **D3** (colon) show overlays of cell specific markers (*green*) and the TREK-2 channel marker (*red*). For clarity, panels **C1** and **C2** (ileum) and **D1** and **D2** (colon) show individual images from corresponding positive merges in enteric neurons. Panels **(C3)** and **(D3)** show overlays for NOS immunoreactive myenteric plexus neurons and the TREK-2 channel in ileum and colon respectively. Scale bars represent 10 µm **(A, B)** and 20 µm **(C1-C3, D1-D3)**.

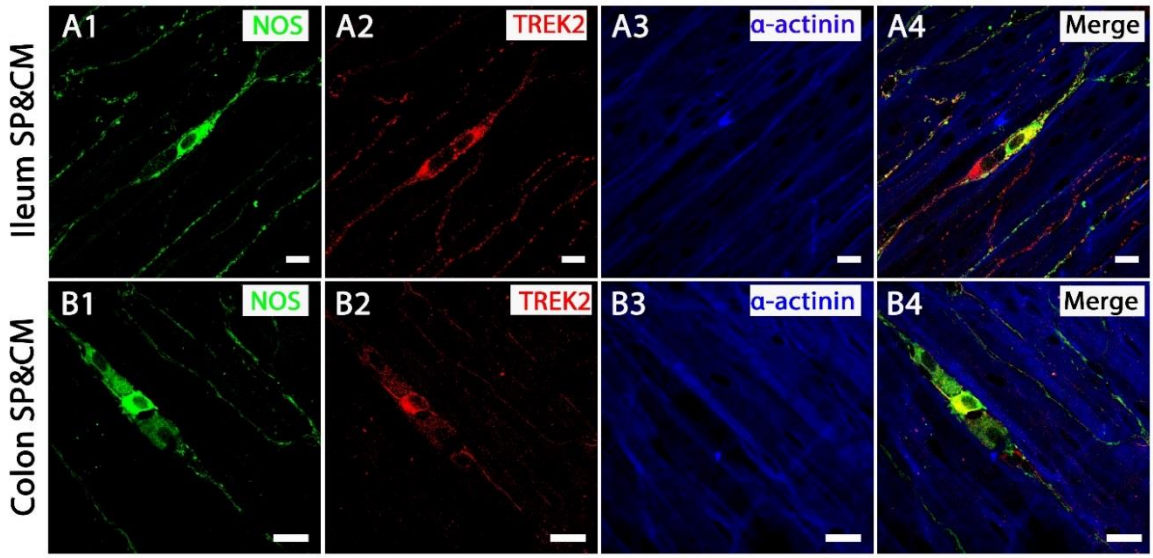


**Figure 4.5:** TREK-2 channels are expressed in submucosal plexus of both mouse ileum and colon. Images show the expression of NOS immunoreactive submucosal plexus neurons (*green*, **A1** and **B1**), TREK-2 channel (*red*, **A2** and **B2**) and α-actinin immunoreactive smooth muscle cells (*blue*, **A3** and **B3**) in mouse ileum and colon as indicated. **(A4)** and **(B4)** are overlays of **(A1-3) and (B1-B3)** respectively. Scale bar represents 20 µm **(A1-A4)** and 20 µm **(B1-B4)**.

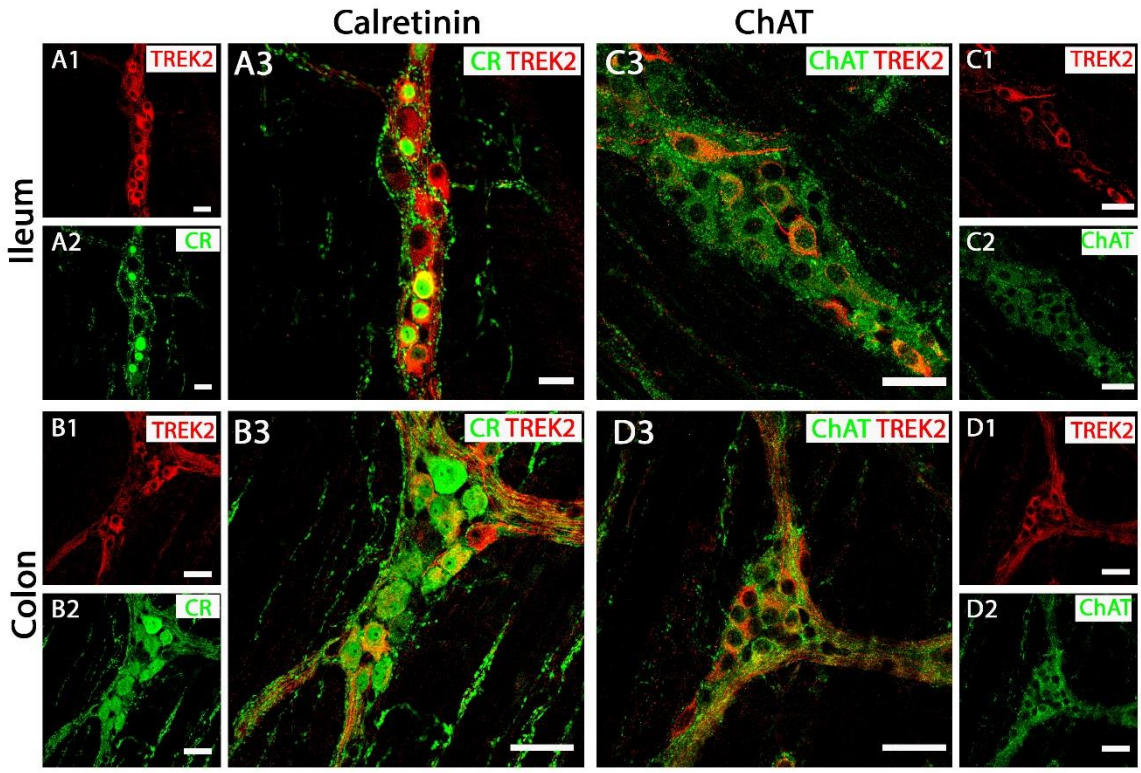


**Figure 4.6:** TREK-2 channels are expressed in ChAT-positive and calretinin-positive myenteric plexus neurons in mouse ileum and colon. Panels **A3** and **C3** (ileum) and **B3** and **D3** (colon) show overlays of cell specific markers (green) and the TREK-2 channel marker (red). For clarity, panels **A1** and **A2** (ileum) and **B1** and **B2** (colon) show the individual images from corresponding merges in **A3** and **B3**, panels **C1** and **C2** (ileum) and **D1** and **D2** (colon) show the individual images from corresponding merges in **C3** and **D3**. Overlays shown in **A3** and **B3**. Scale bars represent 20 µm **(A1-A3)**, 40 µm **(B1-B3),** 30 µm **(C1-C3)** and 40 µm **(D1-D4)**.

### 4.2.4 TRAAK expression in ileum and colon

TRAAK channel specific antibody immunolabeling was utilised to characterise the distribution of the TRAAK channel protein in muscle and nervous tissue of the mouse GI tract. Similar to TREK-2, I could find no evidence for TRAAK expression in LM cells (**Figure 4.7 A, B**) and CM cells (**Figure 4.8 A, B**) in either mouse ileum or colon. The pattern of TRAAK protein labelling observed in the MP neurons (**Figure 4.7 C, D**) and SP neurons (**Figure 4.8 C, D**) of ileum and colon were analogous to that observed for TREK-2, displaying a wide

distribution across both NOS-immunopositive and NOS-immunonegative cell types of enteric neurons. Furthermore, TRAAK protein was also detected in interneurons (**Figure 4.9 A, B**) and cholinergic neurons (**Figure 4.9 C, D**), as visualised by co-labelling with the calretinin and ChAT respectively.

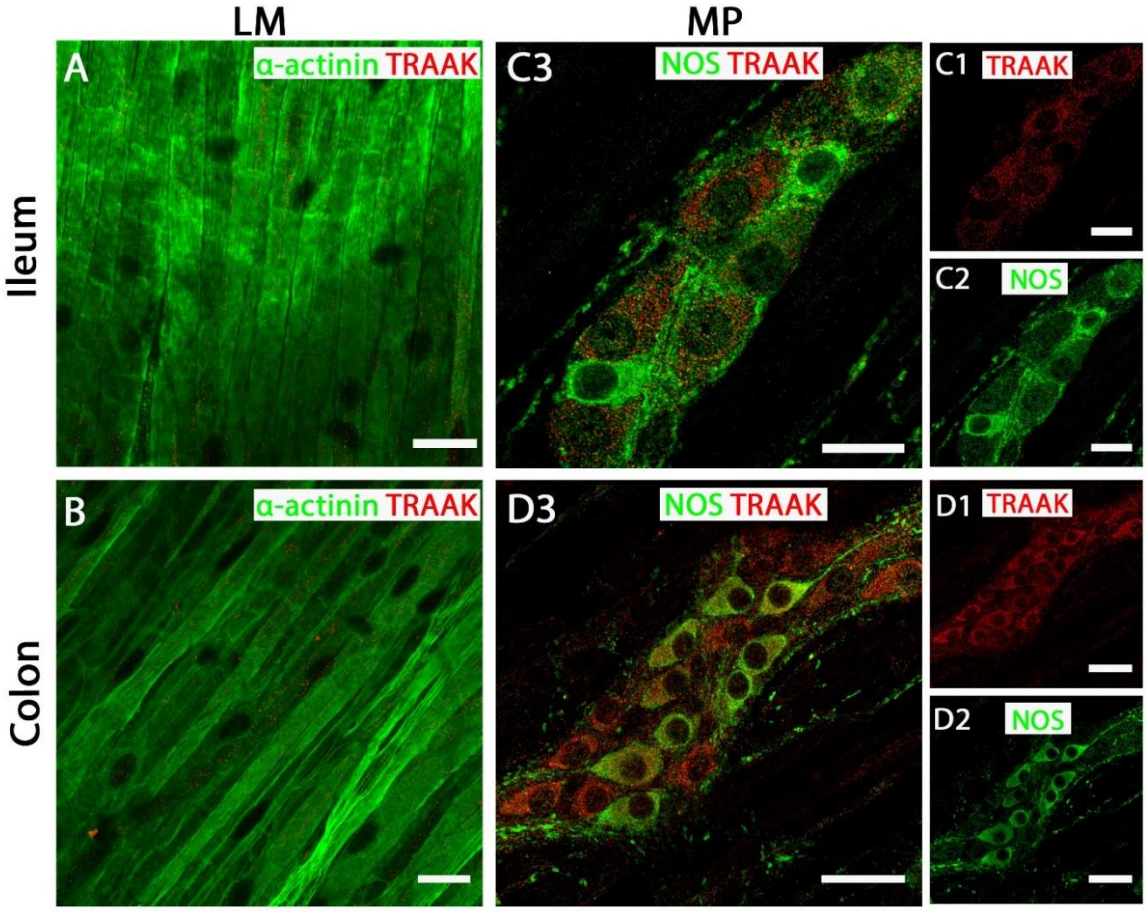


**Figure 4.7.** TRAAK channels are expressed in myenteric plexus neurons of both mouse ileum and colon. Panels **A**, and **C3** (ileum) and **B** and **D3** (colon) show overlays of cell specific markers (*green*) and the TRAAK channel marker (*red*). For clarity, panels **C1** and **C2** (ileum) and **D1** and **D2** (colon) show individual images from corresponding positive merges in enteric neurons. Panels **(C3)** and **(D3)** show overlays for NOS immunoreactive myenteric plexus neurons and the TRAAK channel in ileum and colon respectively. Scale bars represent 20 µm **(A, B, C1-C3)** and 40 µm **(D1-D3)**.

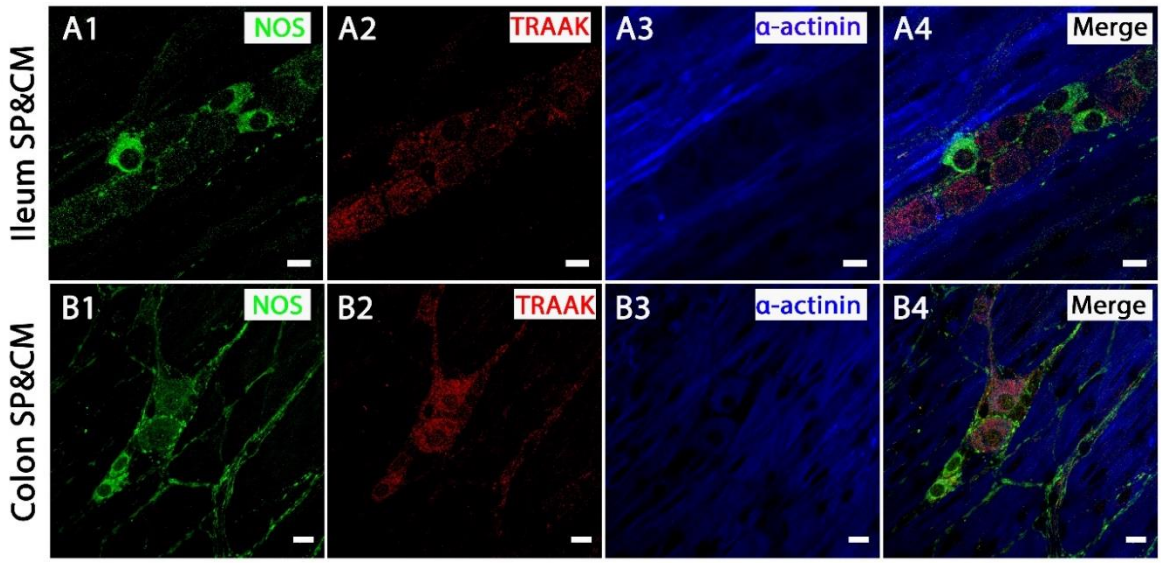


**Figure 4.8:** TRAAK channels are expressed in submucosal plexus of both mouse ileum and colon. Images show the expression of NOS immunoreactive submucosal plexus neurons (*green*, **A1** and **B1**), TRAAK channel (*red*, **A2** and **B2**) and α-actinin immunoreactive smooth muscle cells (*blue*, **A3** and **B3**) in mouse ileum and colon as indicated. **(A4)** and **(B4)** are overlays of **(A1-3)** and **(B1-B3)** respectively. Scale bar represents 10 µm **(A1-A4)** and 20 µm **(B1-B4)**.

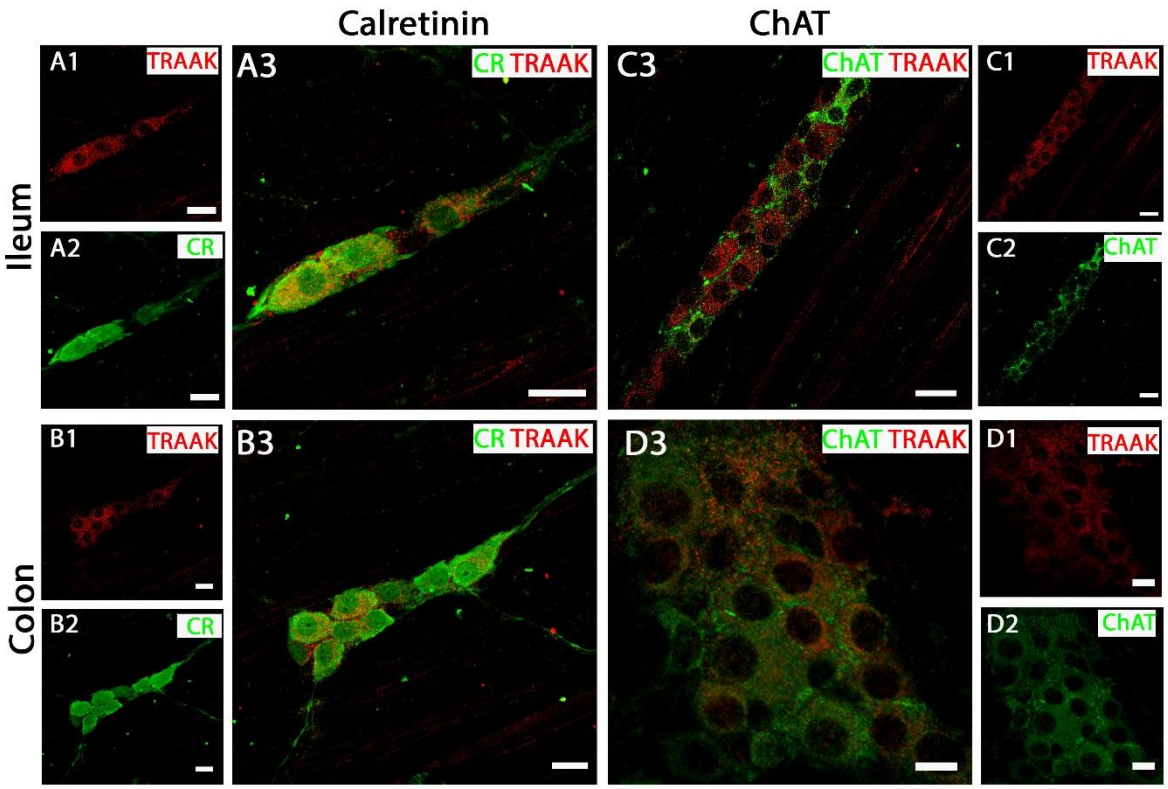


**Figure 4.9:** TRAAK channels are expressed in ChAT-positive and calretinin-positive submucosal/ myenteric plexus neurons in mouse ileum and colon. Panels **A3** and **C3** (ileum) and **B3** and **D3** (colon) show overlays of cell specific markers (green) and the TRAAK channel marker (red). For clarity, panels **A1** and **A2** (ileum) and **B1** and **B2** (colon) show the individual images from corresponding merges in **A3** and **B3**, panels **C1** and **C2** (ileum) and **D1** and **D2** (colon) show the individual images from corresponding merges in **C3** and **D3**. Scale bars represent 20 µm **(A1-A3)**, 20 µm **(B1-B3),** 20 µm **(C1-C3)** and 10 µm **(D1-D4)**.

### 4.2.5 Expression of other $K_{2P}$ subtypes in ileum and colon

Our qPCR data indicated that TASK-1 and TWIK-2 genes also displayed high relative expression levels in both ileum and colon. TASK-3 genes had been previously reported in rat colon (Kim et al., 2000), although they were barely detectable in my qPCR studies. Taken together, I thought it pertinent to classify the precise cellular locations of these three $K_{2P}$ channel subtypes in the mouse intestine, as determined by immunohistochemistry and confocal microscopy. Expression of TASK-1 protein was detected on plasma membranes and in NOS-immunopositive MP neurons of both mouse ileum and colon (**Figures 4.10 A1,**

**B1**). Immunoreactivity for TASK-1 was also observed in the cytoplasmic compartments of LM cells in both ileum and colon, as demonstrated by co-localisation with the smooth muscle cell marker α-actinin (**Figures 4.10 A2, B2**). Immunoreactivity for TASK-3 channel subunits was located on MP neurons. Clustered immunoreactivity for the TASK-3 protein was evident on NOS-immunopositive MP neurons (**Figures 4.10 C1, D1**), but was not detectable in LM cells of either mouse ileum or colon (**Figures 4.10 C2, D2**). Similar to TREK-2 and TRAAK, we could find no evidence for TWIK-2 expression in LM cells in either mouse ileum or colon (**Figure 4.10 E2, F2**). The expression pattern of TWIK-2 channel labelling displays an evident in the NOS-immunopositive MP neurons of both ileum and colon (**Figure 4.10 E1, F1**).

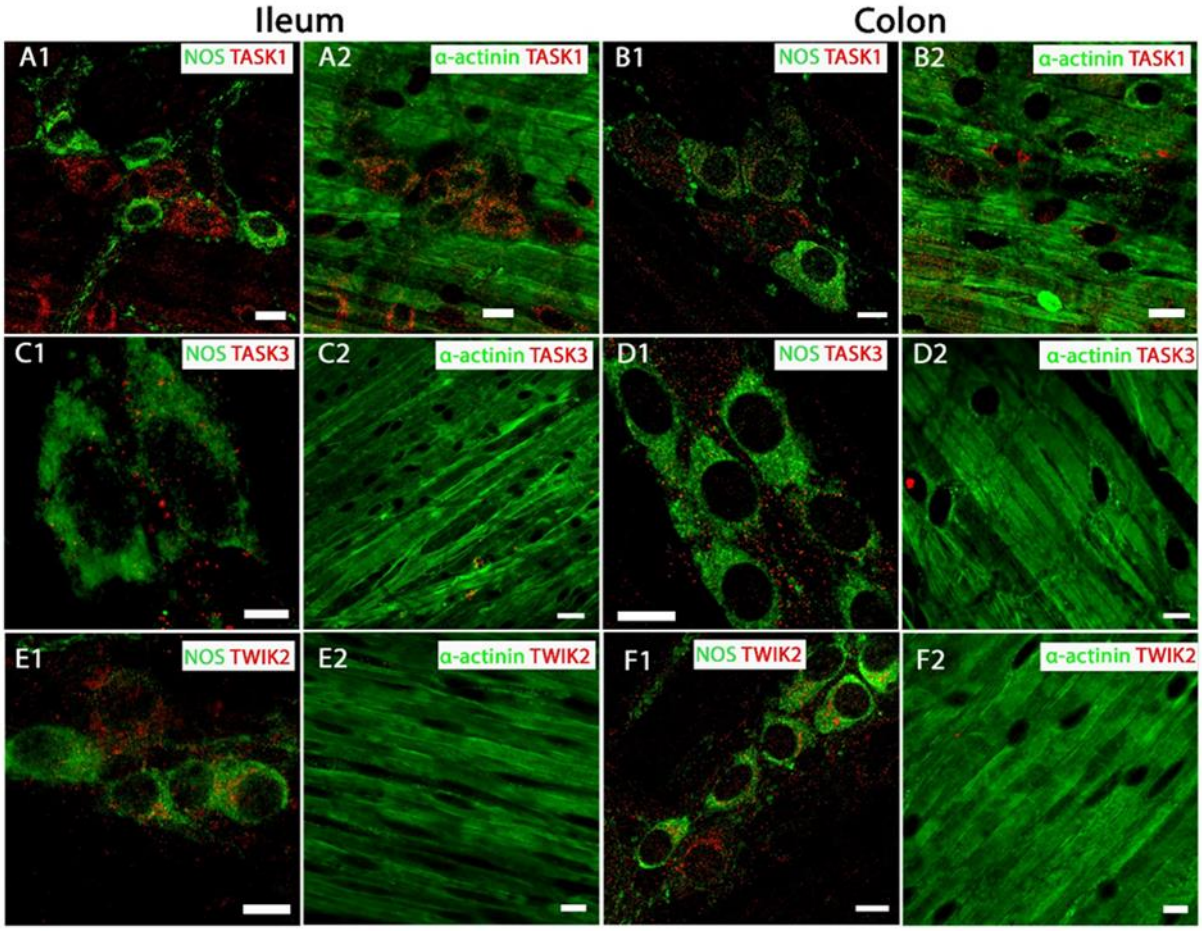


**Figure 4.10:** TASK-1, TASK-3 and TWIK-2 channels are distributed in enteric plexus inhibitory neurons and smooth muscle layers of the mouse ileum and colon. Panels show overlays of cell specific markers (green) and individual $K_{2P}$ channel markers (red) throughout. **(A1)** and **(B1)** show overlays for NOS immunoreactive submucosal plexus neurons and the TASK-1 channel in ileum and colon respectively. Panels **(C1)** and **(D1)** show overlays for NOS immunoreactive myenteric plexus neurons and the TASK-3 channel in ileum and colon respectively. Bottom panels **(E1)** and **(F1)** show overlays for NOS immunoreactive myenteric plexus neurons and the TWIK-2 channel in ileum and colon respectively. Scale bars represent 5 µm **(C1)**, 10 µm **(A1; A2; B1; B2; D1; D2; E1; E2; F1; F2)**, 20 µm **(C2)**.

Since TWIK-1 and TASK-2 exhibit protein expression pattern in both enteric neurons and smooth muscle, we also investigate whether these two channels also expressed in other cell types such as glia cell. The glia cell also play an essential role in GI function which providing structural and metabolic support for neurons, although there is no previous research which indicated that these channels might be expressed in glial. We could find no

evidence for both TWIK-1 and TASK-1 expression in SOX-10-immunopositive enteric glial cells in either mouse ileum or colon, only observed their expression pattern in NOS-immunopositive MP neurons (**Figure4.11**).

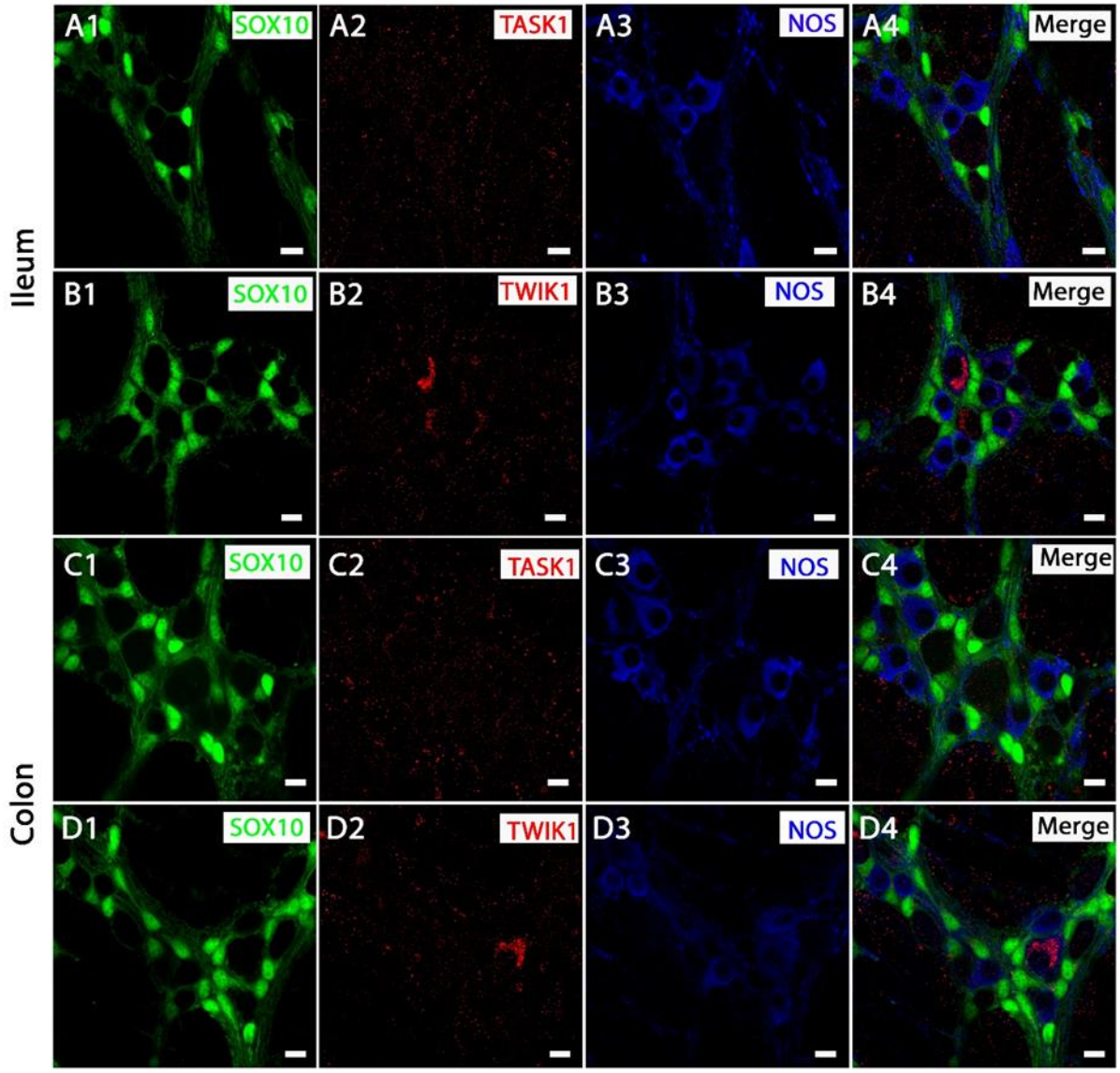


**Figure 4.11:** TASK-1 and TWIK-1 channels are not expressed in enteric glia in both mouse ileum and colon. Images show the expression of SOX10 immunoreactive enteric glia neurons (*green*, **A1**, **B1, C1, D1**), TASK-1 channel (*red*, **A2** and **C2**), TWIK-1 (*red*, **B2** and **D2**) and NOS immunoreactive myenteric plexus neurons (*blue*, **A3**, **B3, C3, D3**) in mouse ileum and colon as indicated. **(A4, B4, C4, D4)** are overlays of **(A1-3), (B1-B3), (C1-C3)** and **(D1-D3)** respectively. All scale bar represents 10 µm.

### 4.2.6 $K_{2P}$ subtypes expression in isolated smooth muscle cells

From the whole tissue mounts it was evident that TREK-1, TWIK-1 and TASK-1 proteins were present in smooth muscle layers, and the $K_{2P}$ channel subtypes TREK-2 and TRAAK were not. To reinforce these K2P channel protein expression profiles, I also determined the expression of the $K_{2P}$ channel proteins in isolated colonic smooth muscle cells by using immunocytochemistry and confocal microscopy. Immunoreactivity for TREK-1, TWIK-1 and TASK-1 proteins was detected in the isolated intestinal smooth muscle cell preparations, as demonstrated by overlapping fluorescence with the smooth muscle cell marker α-actinin (**Figure 4.12 A, D, E**). In contrast, I could find no evidence for TREK-2 and TRAAK expression in isolated single smooth muscle cells (**Figure 4.12 B, C**). Collectively, these data confirmed the smooth muscle specific distribution of TREK-1, TWIK-1 and TASK-1 in mouse ileum and colon.

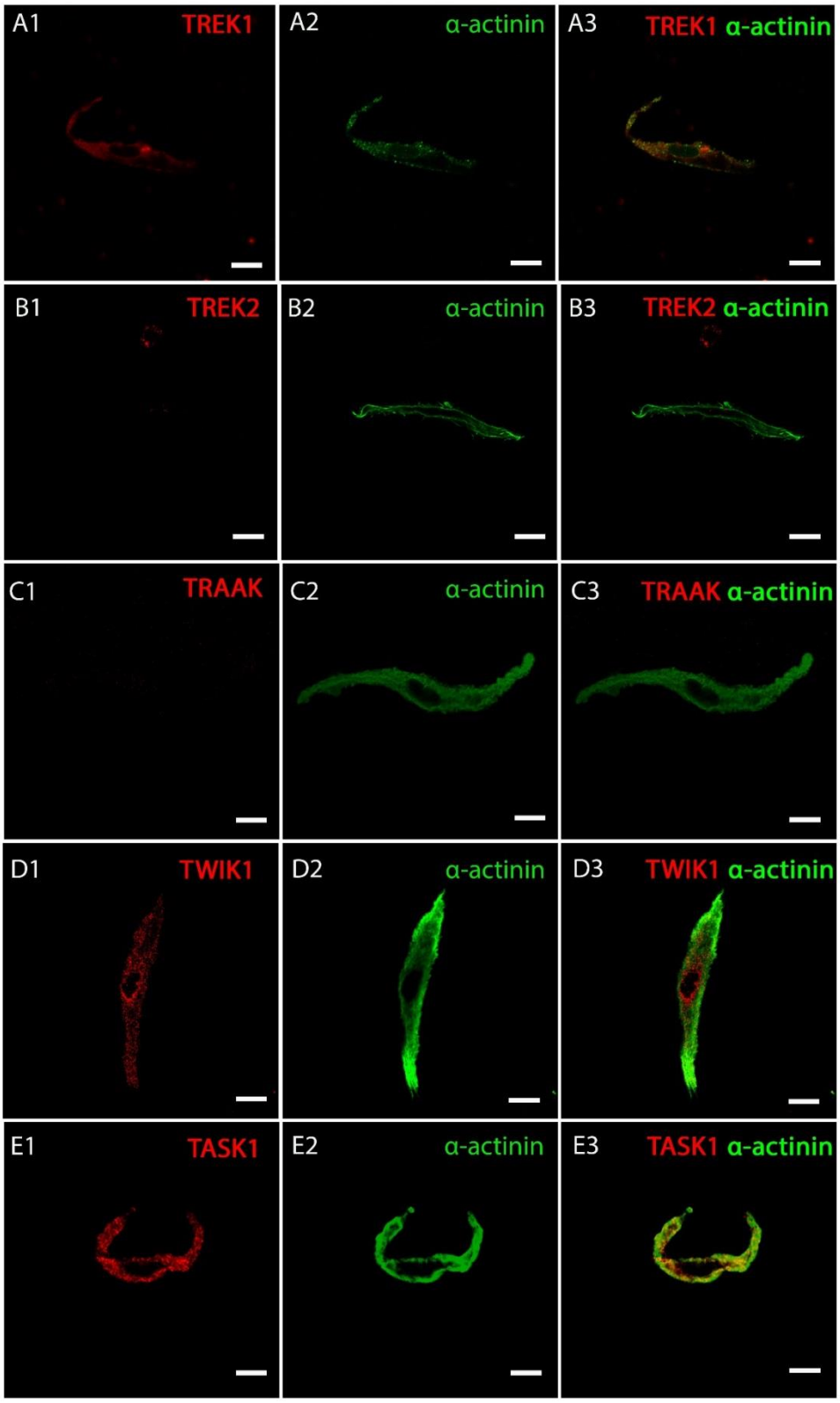


**Figure 4.12:** $K_{2P}$ channel expression in isolated colonic smooth muscle cells. Double immunofluorescence labelling for TREK-1, TREK-2, TRAAK, TWIK-1 and TASK-1 (*red*, **A1, B1, C1, D1 and E1**) and the smooth muscle marker α-actinin (*green*, **A2, B2, C2, D2 and E2**) The co-expression appears yellow in the overlays (**A3, B3, C3, D3 and E3)**. All scale bar represents 10 µm.

## 4.3 Discussion

The cell specific expression and localisation of $K_{2P}$ channel subtypes in the GI tract is poorly understood. A physiological role for a mechano-gated $K_{2P}$ channel has been proposed. Previous functional characterisation along with transcript expression profiles point toward TREK-1 as the molecular correlate of the stretch-dependent potassium (SDK) conductance in colonic myocytes (Koh and Sanders, 2001), although direct protein localisation and conclusive pharmacological evidence is lacking. The immunohistochemical results shown in this chapter reveal that $K_{2P}$ channel subtypes are expressed throughout the mouse intestine and distributed across different cell types. TREK-1 channels displayed a primarily smooth muscle cell expression, with TREK-2, TRAAK, TASK-2 and TASK-3 channels being limited to the circuitry of the enteric nervous system, whereas TWIK-1 and TASK-1 channels were shown to be widely distributed across neuronal and smooth muscle tissues. These novel findings provide a new perspective on the distinctive expression of $K_{2P}$ channel subtypes in enteric neurons and intestinal smooth muscle cells, and implies an important yet uncharacterised functional role for these different channels in specific populations of cells.

### 4.3.1 Antibody Validation

Antibodies raised against proteins are among the most frequently used research tools for studying the expression of ion channels and receptors. To validate an antibody, it must be shown to be specific, selective, and reproducible in the context for which it is to be used. Although there are no universally accepted guidelines or standardized methods for determining the validity of these reagents, there have been a number of previous

publications on the subject, and an assortment of recommendations is available in the literature and online resources. Ideally, a negative control could be a cell line or tissue that is known not to express the protein of interest, such as the knock-out mice. Similarly, non-expressing cells, transfected with the protein of interest, provide the best positive controls. Although I did not provide either negative or positive control for the antibodies used in this chapter due to lack-of $K_{2P}$ knock-out mice, the specific protein labelling and distinct expression within neuron cells and smooth muscle cells in mouse intestine confirm the specificity of the Alomone Lab $K_{2P}$ antibodies I have used in my immunohistochemistry studies.

It has been previously shown by immunohistochemistry that TWIK-1, TREK-1 and TASK-1 are expressed in hippocampal astrocytes (Zhou et al., 2009). Moreover, pre-incubation in the blocking peptide completely abolished $K_{2P}$ channel immunolabelling in hippocampal tissue sections (Zhou et al., 2009), indicating the specificity of these antibodies from Alomone Lab. In later studies, Immunohistochemical staining of TREK-1 have been shown in both cultured astrocytes (Banerjee et al., 2016) and mouse brain sections (Woo et al., 2018). In addition, lack of TREK-1 staining in TREK-1 knock-out mice confirms antibody specificity (Woo et al., 2018). Previous Immunohistochemical studies show TREK-2 expression in DRG neurons from rat brain, antibody recognizes heterologously expressed TREK2 but not the structurally closely related TREK1 or any of the other $K_{2P}$ channels tested (TWIK1, TASK3, THIK2, THIK1), indicating very high selectivity for TREK2 (Acosta et al., 2014). Moreover, the specificity of TREK-2 antibody was also confirmed by western blot of DRG tissue (Acosta et al., 2014). The specificity of the TRAAK channel antibody had been

confirmed in a previous immunocytochemical studies in mouse oocytes (Hur et al., 2012), and western-boot studies in mouse hippocampal tissue (de la Pena et al., 2012). TASK-2 channel has been previously shown by immunohistochemistry in HEK 293 cells, and blocking peptide was added to the primer reaction as the negative control, demonstrating the specificity of TASK-2 antibody (Gonczi et al., 2006). Thus, previous studies provide strong evidence for the specificity of $K_{2P}$ channel antibodies that I have used in this chapter.

### 4.3.2 Distinctive GI expression of TREK family

Previous studies have indicated that TREK-like channels underlie a SDK in colonic smooth muscle cells, based on the biophysical phenotype and similarity to cloned murine TREK-1 channels, including mechano-sensitivity, insensitivity to classical potassium channel blockers, and regulation by nitrergic stimulation (Koh and Sanders, 2001, Koh et al., 2001, Park et al., 2005). Immunohistochemical analysis of all three mechano-gated $K_{2P}$ channel proteins in the murine GI tract revealed a distinct expression pattern of these channels. I found evidence for TREK-1 channel expression in longitudinal and circular smooth muscle tissues, but not in nitrenergic enteric neurons of the myenteric and submucosal plexuses, whereas TREK-2 and TRAAK channel proteins were only observed in enteric neurons and were not detected in smooth muscle layers. This distinctive expression pattern is analogous to previous observations in airway, where TREK-1 channels show expression in smooth muscle cells of mouse lung tissue, while TRAAK channels show expression in nerve endings located in different layers of intrapulmonary airways (Lembrechts et al., 2011), and in bladder where TREK-1 displays labelling in single freshly dispersed human bladder smooth muscle cells (Lei et al., 2014). Furthermore, my protein localisation findings contrast TREK-

1 and TRAAK expression in the central nervous system, where they show overlapping expression in a variety of neurons, and are thought to form functional heterodimers (Blin et al., 2016). Furthermore, there is no evidence to date for TREK-2 protein localisation in smooth muscle cells of any other organs, with TREK-2 being largely confined to expression in neurons of the CNS and PNS (Viatchenko-Karpinski et al., 2018, Talley et al., 2001a), which again is analogous to the specific expression of TREK-2 channels in enteric neurons of the gut.

In addition, I found TREK-1 channel protein expression in isolated intestinal smooth muscle cells by using immunocyctochemical studies, whereas TREK-2 and TRAAK channels protein were absent from these smooth muscle cells, which further confirmed their distinct cellular localization in intestine tissue. However, I have only looked their protein expression in single cell, further studies in quantification of proportion of cells showing signal could be investigated in the future.

Given that my project is ultimately concerned with the functional role of $K_{2P}$ channels in GI motility, the pacemaker cells of the gut, the Interstitial Cells of Cajal (ICC) are an import subset of cells that should be investigated. ICC are important regulators of GI function, communicating with enteric neurons and smooth muscle cells, inducing propagating electrical slow wave potentials and thus helping to regulate phasic contractile activity of GI smooth muscle (Al-Shboul, 2013). However, in preliminary experiments, the low specificity of the ICC antibody I used restricted further investigation. Given the importance of the ICC

in regulating motility, further experiments are required to detail the expression of $K_{2P}$ channels in these pacemaker cells of the gut.

### 4.3.3 Distinctive GI expression of TWIK family

The novel finding from our qPCR was the high expression of TWIK-1 and TWIK-2 mRNA in both murine ileum and colon. Detailed immunohistochemical analysis for these proteins demonstrated a wide distribution pattern across smooth muscle and neuronal cell types in ileum and colon and may be suggestive of important roles in GI physiology. Although TWIK-1 and TWIK-2 genes are widely expressed in many region of the CNS and in a number of peripheral tissues such as stomach, pancreas, spleen and uterus (Medhurst et al., 2001, Kew and Davies, 2010), their role as background $K^+$ channels is still speculative. This is because there is no TWIK-1 or TWIK-2 channels have yet been recorded from any native tissues. Previous studies in TWIK-1 knock-out mice suggest that TWIK-1 may contribute to $K^+$/water transport in proximal tubule and medullary collecting duct of kidney (Nie et al., 2005). In the human heart, TWIK-1 gene is strongly expressed in the atria, the Purkinje fibers and the ventricles (Ordog et al., 2006, Ellinghaus et al., 2005, Gaborit et al., 2007, Lesage et al., 1996), but whether TWIK-1 plays a functional role in heart has not yet been reported. In addition, recent studies found TWIK-1 deficiency caused a depolarizing shift in the resting membrane potential of dentate gyrus granule cells (DGGCs) and enhanced their firing rate in response to depolarising current injections, suggesting TWIK-1 channel is involved in the intrinsic excitability of DGGCs in mouse hippocampus (Yarishkin et al., 2014). There is currently a distinct lack of available evidence for expression of TWIK-1 and TWIK-2 channels in GI tract, and so my findings that the TWIK-1 channel protein not only localised

in enteric neurons but also in smooth muscle layers, and TWIK-2 channel proteins are only observed in enteric neurons greatly enhances the knowledge within this field of research. Although TWIK-1 channels are widely expressed, the physiological significance of TWIK-1 channels has been questioned due to the difficulties encountered in demonstrating functional currents in heterologous systems. It has been proposed that TWIK-1 channels are present at the cell membrane but it is normally silent and requires modulation by SUMO (Rajan et al., 2005). However, a later study failed to show sumolyation of TWIK-1 and suggest that TWIK-1 is lack functional due to it is present in the cytosolic which do not trafficked to the membrane (Feliciangeli et al., 2007).

TWIK-1 were reported to form heterodimeric channels with TASK channel subunits (TASK-1 or TASK-3), and these heterodimeric channels exhibit acid-sensitive and halothane-sensitive outwardly rectifying $K^+$ currents in cerebellar granule neurons (Plant et al., 2012, Ma et al., 2012). Also, recent studies showed that TWIK-1 were associate with TASK-3 in DGGCs of mouse hippocampus when both genes were overexpressed in the cells, and this complex displayed outwardly rectifying currents and involves in the intrinsic excitability of DGGCs (Choi et al., 2018). My immunohistochemical staining data showed that TASK-3 proteins were localised in the MP neurons, and TASK-1 proteins were detected in both smooth muscle cells and neurons, and this localization is similar to the expression pattern of TWIK-1 where localised in both smooth muscle cells and MP neurons, although whether those two channels were expressed in the same cells stills remains unknown. Furthermore, TWIK-1 was also reported to form a functional channel with TREK-1, which contribute to mediate astrocytic passive conductance and cannabinoid-induced glutamate release from

astrocytes proteins (Hwang et al., 2014). TREK-1 was exhibited predominately pattern in both circular and longitudinal smooth muscle cells in my data. Therefore, all these co-expression pattern indicates TWIK-1 may form functional heterodimers with other $K_{2P}$ channels (TASK-1, TASK-3 and TREK-1 channels) and contribute to the GI physiology such as regulating intestinal smooth muscle contractility. However, along with a current lack of pharmacological tools for TWIK family, the physiological importance of these two channels in the GI system remains to be conclusively determined.

### 4.3.4 Distinctive GI expression of other $K_{2P}$ subunits

TASK-1 and TASK-2 were previously identified to be expressed in smooth muscle cells of murine small and large intestine by analysis of mRNA distribution (Cho et al., 2005). In addition TASK-2 channel proteins have also been shown in both smooth muscle layers and enteric neurons. Furthermore a TASK-2-like conductance has been proposed as a potential contributor to resting membrane potential in smooth muscle cells, although the pharmacological tools used to assess this, including lidocaine, were used at concentrations too high to be TASK-2 specific (Cho et al., 2005). This report is in contrast to my findings here where I show expression of TASK-2 in enteric neurons of the GI tract, but no detectable expression in smooth muscle cell layers of either the ileum or colon. Due to the lack of double staining with a smooth muscle cell marker and good control experiments it is not possible to decipher from their data whether the channel protein staining was due to non-specific binding. Functional corroboration of these current data will depend on the identification of specific pharmacological tools for TASK-2 channels. Previous studies have not only indicated the positive immunohistochemical expression of TASK-2 channel in

uterine circular muscle of mouse, but also showed that TASK-2 inhibitors such as quinidine, lidocaine, and extracellular acidosis produced smooth muscle contraction in uterine (Hong et al., 2013). Moreover, both gene and protein expression of TASK-1 channel have been detected in pulmonary artery smooth muscle cells (Gurney et al., 2003). The arterial conductance (Gurney et al., 2003) showed similar pH-sensitivity as the conductance observed in intestinal muscles (Cho et al., 2005), suggesting that TASK family channels may be generally important in visceral smooth muscles as regulators of membrane potential. My studies identified that TASK-1 protein is located in longitudinal muscle and a small portion of neuronal cells in MP, and TASK-3 protein was only expressed in enteric neurons. These findings are in good accordance with previous immunohistochemical studies in rat proximal colon, which TASK-1 was localized in the LM layer and MP and TASK-3 was localised in MP (Kubota et al., 2015). In the same studies, authors also detected TASK-3 protein expression in ICC cells in the MP layer. Although both TASK-1 and TASK-3 exhibit NOS-immunopositive in MP neurons, it is hard to distinguish whether they were expressed in the same cells. Notably, TASK-1 and TASK-3 can form functional heterodimers exhibiting properties distinct from TASK-1 and TASK-3 alone, which showed intermediate pH sensitivity and ruthenium red insensitivity (Czirjak and Enyedi, 2002). Moreover, recent studies reported that TASK-3 was localized at the plasma membrane of isolated cardiomyocytes, but single channel recording observed a TASK-1/TASK-3 complex channel conductance, suggesting TASK-1/TASK-3 may form heteromeric complexes in human atrial cardiomyocytes (Rinne et al., 2015). Therefore, TASK-1 and TASK-3 may also form functional heterodimers in enteric neurons to play an important role in GI physiology, but further experiments are required to identify the co-expression details of TASK-1 and TASK-3 channels in MP neurons.

## 4.4 Summary and Conclusions

The key finding of this chapter is that both enteric neurons and smooth muscle cells differentially express $K_{2P}$ channels. Whole-mount preparations, rather than cross-sections of the tissue preparations were used. This therefore technically restricted the inspection of the epithelial layers of the GI microscopically, precluding the verification of $K_{2P}$ subunits localisation in mucosal elements. Thus, this could be an interesting set of experiments in the future to further characterise the localisation of $K_{2P}$ channels in epithelial layers of the intestine, since the pathophysiological mechanisms of IBS also include the alterations in the epithelial barrier and secretory properties of the gut (Camilleri and Ford, 2017).

In summary, these data provide new information on the cell type specific expression of mechano-gated TREK family channels in GI tract, with the novel finding that TREK-1 expression is limited specifically to smooth muscle layers were as expression of TREK-2 and TRAAK channels was confined to enteric neurons. The high expression of TWIK-1 mRNA in the GI tract correlated with combined protein expression observed across both smooth muscle and enteric neurons and is suggestive of important roles in GI physiology. The physiological function of TREK family channels in GI smooth muscle and neurons is unknown, but given their pattern of cellular localisation in the various layers of the GI tract in both ileum and colon supports a hypothesis for a potential role in regulating enteric neuronal excitability and neurochemical signalling and intestinal smooth muscle contractility. Therefore, the next step was to directly assess the functional contribution of TREK channels to smooth muscle contractility using organ bath pharmacology methodologies.

# Chapter 5 – Functional role of Potassium Channels in GI smooth muscle contractility

## 5.1 Introduction and Aims

There is a great deal of molecular and functional evidence describing the various ionic conductance's responsible for GI smooth muscle contraction, including transient receptor potential channels and voltage-dependent calcium channels. However, comparably little is known about the underlying $K^+$ channels responsible for suppressing smooth muscle contractility and promoting GI tract relaxation, a mechanism that could be exploited therapeutically to treat hypermotility disorders, such as IBS. In chapter 3, I demonstrated that several different $K^+$ transcripts (e.g. $K_v4.3$, $K_v7.1$, $K_{ir}6.1$, & mechano-gated $K_{2P}$ channels) are prominently expressed throughout the murine intestine. In this chapter, I utilised pharmacological techniques to dissect the distribution and contribution of various subtypes of $K^+$ channels in regulating intestinal motility in the mouse. Moreover, in chapter 4 I revealed the precise cellular location of $K_{2P}$ channel subtypes within both ileum and colon, and suggested a potential role for the mechano-gated TREK channel family in ENS/smooth muscle medicated GI function. Historically, specific pharmacological tools targeting $K_{2P}$ channels have been rather limited, therefore direct pharmacological validation of TREK channel activity in GI smooth muscle has been difficult to confirm. Recent reports have begun to highlight multiple chemical modulators of TREK family channels, in order to to support our immunohistochemical findings I sought further pharmacological evidence for mechano-gated $K_{2P}$ functional expression in murine ileum and colon using an organ bath preparation.

## 5.2 Results

### 5.2.1 Potassium channel blockers alter muscle tension

To broadly assess the expression and contribution of potassium channels to gut contractile activity, the broad spectrum $K^+$ channel inhibitors TEA, $Ba^{2+}$ and 4-AP were exposed to both mouse ileum and colon segments under basal conditions at 32 °C and changes in muscle tension monitored (**Figure 5.1**). The cholinergic agonist carbachol (CCh) and potassium chloride (KCl) were firstly applied to tissues to confirm the functionality of the tissues. As expected, both CCh and KCl induced significant increases in the basal tension of the ileum and colon (*n* = 6 each condition). TEA at a bath concentration of 10 mM induced a significant increase in the tension of ileum and colon tissues (**Figure 5.1**). The induced contraction was non-significantly different between ileum and colon (0.52 ± 0.1 g *vs* 0.52 ± 0.4 g respectively; *n* = 6; *p* = 0.9872, un-paired Student's *t*-test). $Ba^{2+}$ at a bath concentration of 10 mM also promoted a significant increase in tension in both ileum and colon (1.13 ± 0.3 g *vs* 0.45 ± 0.3 g respectively; *n* = 6). However, the amplitude of $Ba^{2+}$ induced contractions were significantly less in colon versus ileum (*p* = 0.0035, un-paired Student's *t*-test). Conversely, exposure to 4-AP (5 mM) did not markedly effect tension in either ileum or colon (*n* = 6 each condition). Together, these results suggest that potassium channels, especially the $K_{2P}$ channels are expressed and play a direct functional contribution to the contractile physiology of longitudinal muscle in both mouse ileum and colon, since $K_{2P}$ channel is the only $K^+$ channels stay opening when cells at rest. The $K^+$ channel blockers, which inhibit $K_{2P}$ channels, caused contraction of smooth muscle cells result in inhibition of currents around the resting membrane potential and depolarized membrane potential.

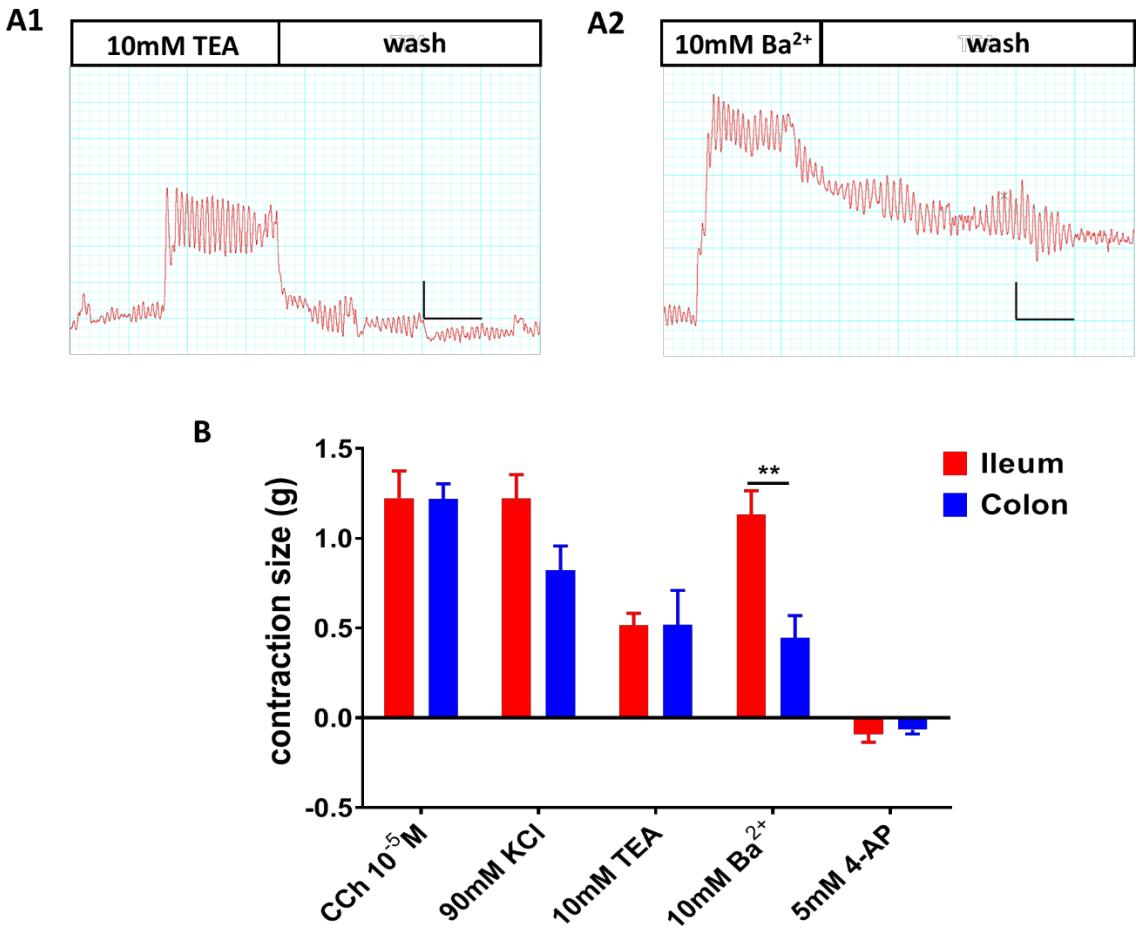


**Figure 5.1.** *Top panels*, representative traces showing the time course of the addition of classical $K^+$ channel blockers 10mM tetraethylammonium (TEA) **(A1)** and 10mM barium ($Ba^{2+}$) **(A2)** to mouse ileum. Scale bars represent 0.2g (vertical) and 30 seconds (horizontal). **(B)** Bar graph showing mean change in tension induced by carbachol (CCh), potassium chloride (KCl) and broad spectrum $K^+$ channel inhibitors TEA, 4-amino pyridine (4-AP) and $Ba^{2+}$ and in both mouse ileum and colon ($n$ = 6 each condition). **indicates $p$ = 0.0035, unpaired $t$-test.

## 5.2.2 Activation of $K_v$ channels induces relaxation in ileum and colon

Due to the high relative expression levels of $K_v$7.1 and $K_v$4.3 transcripts observed in my qPCR data and the significant contraction effects caused by the classic $K^+$ channel blockers TEA and $Ba^{2+}$, the functional role of $K_v$ channels in smooth muscle tone were investigated using more selective $K_v$ channel modulators. Application of increasing concentrations of CCh where first utilised to measure ascertain concentration-responses of longitudinal

smooth muscle in both ileum and colon to determine the functional viability of the tissues and to gauge contraction amplitudes of each tissue. Sub-maximal concentrations of CCh could then be chosen to assess the impact of $K_v$ channel activation in CCh pre-contracted tissues. **Figure 5.2** shows mean data collated from experiments were ascending concentrations of the parasympathomimetic drug CCh (from $10^{-9}$ to $10^{-5}$ M) were applied to both ileum and colon resulting in concentration-dependent contractions, which when approximated with a non-linear curve revealed an $EC_{50}$ of 1.83 ± 0.22 µM in ileum and 5.76 ± 0.73 µM in colon (*n* = 9) .

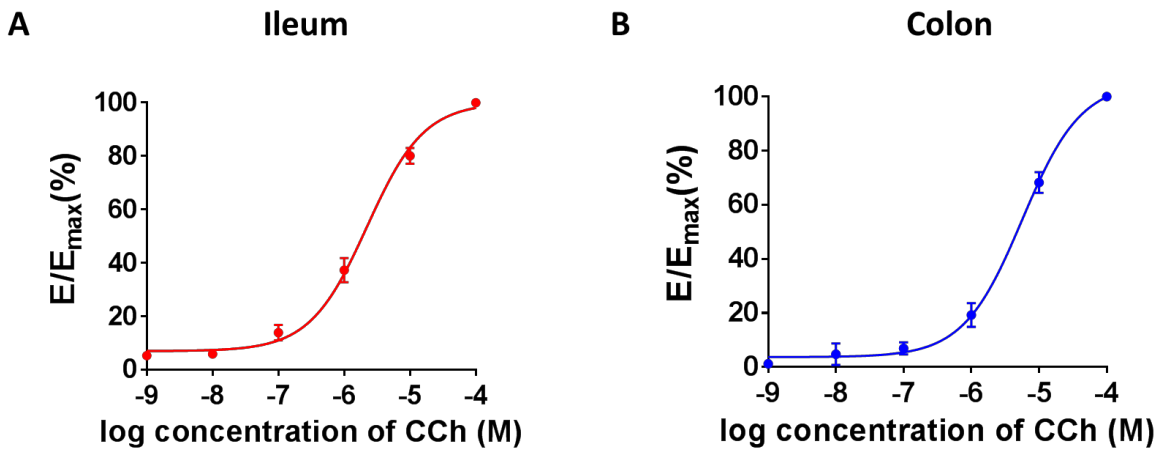


**Figure 5.2:** Carbachol induced concentration-response curve of the mouse ileum **(A)** and colon **(B)**, *n* = 9 each. Data is displaced as mean percentage (%) contraction ± SD and approximated with a non-linear curve. $EC_{50}$ = 1.83 ± 0.22 µM (ileum); 5.76 ± 0.73 µM (colon). HillSlope is 0.77 ± 0.04 (ileum); 0.95 ± 0.10 (colon).

Submaximal concentrations of CCh were applied to tissues and tonic contractions allowed to stabilise. To assess the contribution of potassium channels to GI tract smooth muscle contractility, various $K_v$ channel activators were applied to the CCh pre-contracted tissues and smooth muscle relaxation was monitored. Firstly, isolated ileum and colon segments were pre-contracted with CCh (10 µM) and the generated tension allowed to reach steady

state before the addition of the $K_v7$ activator, retigabine (**Figure 5.3 A1, A2**). Changes in tension induced by addition of activators were normalised to steady-state pre-contracted tension in each individual experiment and are reported as percentage. On average 10 µM CCh generated a tension of 1.2 ± 0.03 g in ileum and 1.3 ± 0.05 g in colon (both *n* = 100). Retigabine (1-100 µM) induced a concentration-dependent decrease in muscle tension in both ileum and colon. Relaxation induced by 100 µM retigabine was not maximal but differed significantly between ileum and colon (54.3 ± 1.9 % *vs* 35.4 ± 3.1 %, *p* =0.0004; see **Figure 5.3 B1, B2**). To further clarify the functional presence of $K_v7$ channels, the broad spectrum Kv7 inhibitor, XE991, was applied at baseline tension at a bath concentration of 100 µM. XE991 induced a small contractile response and generated a tension of 0.33 ± 0.1 g in ileum and 0.17 ± 0.2 g in colon (both *n* = 6, Figure 5.3 C). However, addition of the $K_v7.1$ specific blocker, Chromanol 293B, which does not modulate $K_v7.2$-7.5 channels, at a bath concentration of 100 µM did not significantly affect tension in either ileum or colon (*n* = 6; *p* = > 0.05, see **Figure 5.3 C**).

To assess the functional expression of $K_v4.3$ channels in ileum and colon, a single concentration of the selective $K_v4.3$ channel activator NS5806 (50 µM) was used (Lundby et al., 2010). NS5806 induced a marked but limited relaxatory effect in CCh pre-contracted ileum and colon tissues [**Figure 5.3 D**; 27.5 ± 3.7 % (ileum) and 14.4 ± 3.5 (colon); both *n* = 6]. Comparatively, relaxation induced by NS5806 in ileum was significantly greater than effect in colon (*p* =0.0393, un-paired Student's *t*-test).

Taken together, these results suggest that $K_v$7.2-7.5 and $K_v$4.3 channels have a functional role in regulating the GI contractility. In contrast, $K_v$7.1 channel does not appear to functionally contribute to contractility of GI longitudinal smooth muscle.

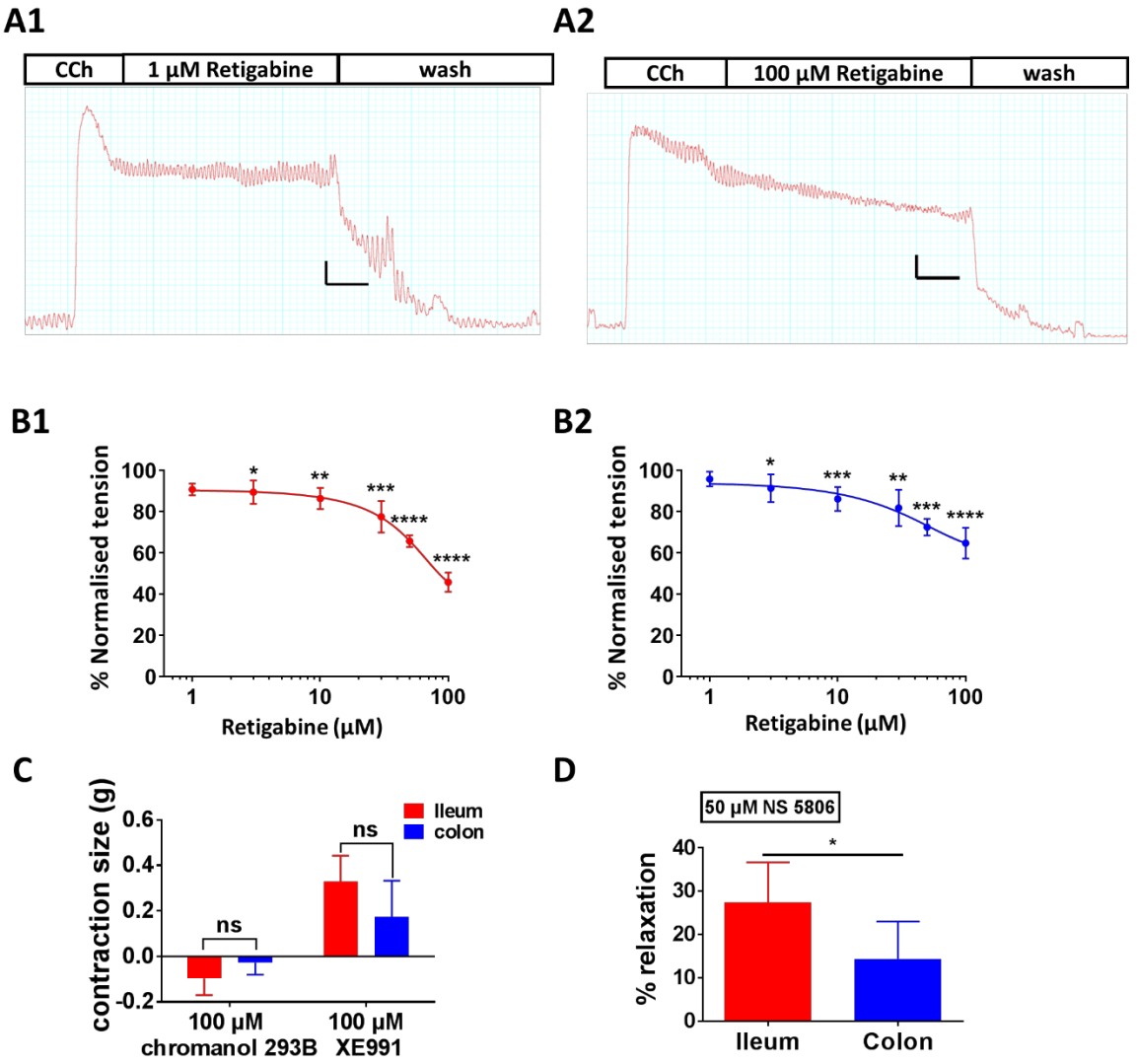


**Figure 5.3:** *Top panels*, exemplar traces showing relaxation induced by the $K_v$7 channel agonist retigabine (1 µM) **(A1)** and retigabine (100 µM) **(A2)** in mouse ileum. Scale bars represent 0.2g (vertical) and 30 seconds (horizontal). Mean concentration-response relationships for retigabine in mouse ileum **(B1)** and colon **(B2)** are shown below the corresponding traces, *n* = 6 each. Both plots were fitted with non-linear regression. **(C)** Bar graph showing mean change in tension induced by $K_v$7 channel inhibitors XE991 and chromanol 293B (*n* = 6 each). **(D)** Mean normalised relaxation in CCh pre-contracted ileum and colon in response to $K_v$4.3 activator NS5806 (*n* = 6). Error bars represent standard deviation (SD), * $p < 0.05$, ** $p < 0.01$, *** $p < 0.001$ **** $p < 0.0001$, student's paired *t*-test (B1 & B2), student's un-paired *t*-test (C & D).

### 5.2.3 Activation of $K_{Ca}$ channels induced relaxation in ileum and colon

Of 8 $K_{Ca}$ genes analysed, IK and BK transcripts showed the largest relative expression within mouse ileum and colon. Therefore, the impact of $K_{Ca}$ channel activation in CCh pre-contracted tissues was probed by directly measuring changes in both ileum and colon muscle tension during application of a range of specific $K_{Ca}$ activators including SKA-31 and NS 309 (activators of IK / SK channels) (Sankaranarayanan et al., 2009, Strobaek et al., 2004, Morimura et al., 2006), and specific activator of BK channels, NS 19504 (Nausch et al., 2014). Single concentration additions of the SKA-31 (100 μM) and NS 309 (50 μM) both induced marked relaxations of CCh pre-contracted ileum and colon tissues [**Figure 5.4 A, B**; SKA-31, 68.9 ± 8.9% (ileum) and 48.6 ± 12.6% (colon); NS 309, 41.6 ± 14.9% (ileum) and 33.5 ± 8.1% (colon)]. SKA-31 produced a significantly greater magnitude of relaxation in ileum compared to colon ($n$ = 6, $p$ = 0.0093, Student's unpaired $t$-test), whereas NS 309 effects were not significantly different between ileum and colon ($n$ = 6, $p$ = 0.4373, Student's unpaired $t$-test).

Tissue exposure to the selective BK channel agonist NS19504 produced a concentration dependent relaxation in CCh pre-contracted ileum ($IC_{50}$ = 57.5 ± 2.4 μM, $n$ = 6, **Figure 5.4, C1**). Relaxation to NS 19504 in colon was also concentration dependent ($IC_{50}$ = 25.85 ± 3.1 μM, $n$ = 6, **Figure 5.4 C2**), however the relaxations at all effective concentrations were significantly larger than those observed in ileum ($n$ = 6, $p$ = 0.0182, Student's unpaired t-test). The relaxation induced by NS 19504 was also investigated in 60 mM KCl pre-contracted ileum and colon segments. 100 μM NS 19504 produced a significantly greater relaxation when the ileum was pre-contracted with KCl compared to CCh (**Figure 5.4 D;**

106.5 ± 17.0% vs. 73.8 ± 12.4%, *n* = 6, *p* = 0.0021, Student's unpaired t-test). A robust relaxation effect was similarly observed in KCl pre-contracted colon with NS 19504, but was not significantly different from the relaxation observed during CCh pre-contraction (**Figure 5.4 D;** 100.8 ± 15.8% vs. 87.3 ± 5.2%, *n* = 6, *p* = 0.0748, Student's unpaired t-test). The classic $K^+$ channel blocker TEA has been shown to effectively inhibit BK channels at a concentration of 10 mM (Sun et al., 1999). We therefore tested the ability of the BK activator NS 19504 to relax CCh pre-contracted ileum and colon in the presence of 10 mM TEA. As would be predicted, addition of 10 mM TEA significantly attenuated the relaxatory response to NS 19504 in colon, but interestingly, not in ileum (**Figure 5.4 E**). In ileum, 10 µM NS 19504 induced a mean normalised relaxation of 24.0 ± 5.6% which was only slightly reduced to 19.2 ± 13.0% in the presence of TEA (*n* = 5 each, p = 0.5176, Student's paired t-test). However in colon, 10 µM NS 19504 induced a mean normalized relaxation of 31.1 ± 6.7% compared to 7.3 ± 10.6% in the presence of TEA (*n* = 5 each, *p* = 0.0091, Student's paired t-test).

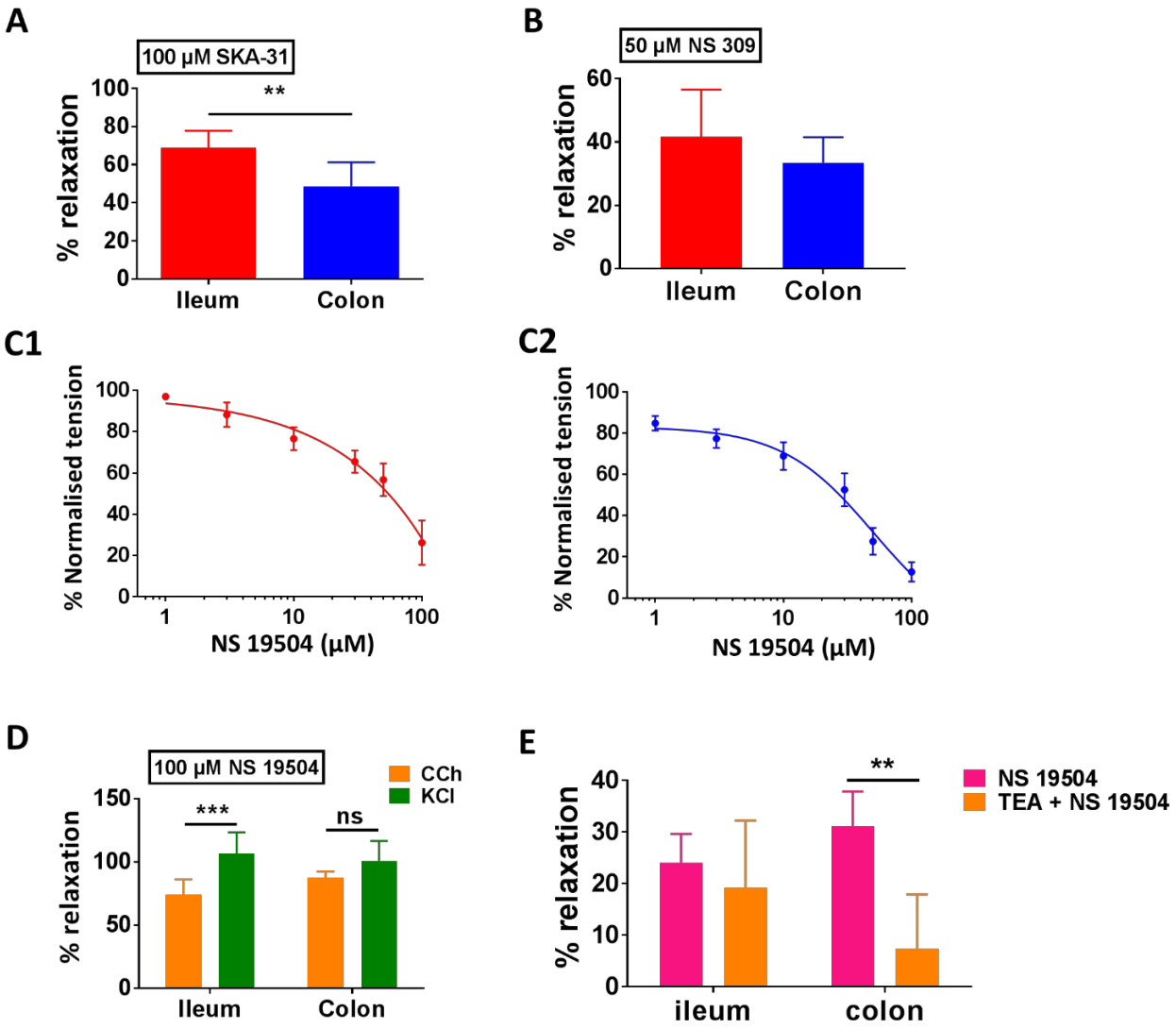


**Figure 5.4:** Bar graph showing the relaxatory effects induced by the IK channel agonists SKA-31 **(A)** and NS 309 **(B)** in CCh pre-contracted mouse ileum and colon (*n* = 6 each), ** indicates *p* = 0.0093, student's un-paired *t*-test. Mean concentration-response relationships for NS19504 in CCh pre-contracted mouse ileum **(C1)** and colon **(C2),** *n* = 6 each. Both plots were fitted with non-linear regression. **(D)** Bar graph illustrating the BK channel agonists NS 19504 induced a differential relaxation in CCh (yellow bar) and KCl (green bar) pre-contracted ileum and colon (*n* = 6 each condition), **indicates *p* = 0.0005, two-way ANOVA. **(E)** Bar graph showing relaxation (%) in ileum and colon to 10 µM NS 19504 in the absence (pink bar) and presence (yellow bar) of 10 mM TEA (*n* = 5 each condition), **indicates *p* = 0.008, student's un-paired *t*-test

### 5.2.4 Activation of $K_{ir}$6.1 channels induced a modest relaxation in ileum and colon

$K_{ir}$6.1 had the highest relative expression of the 15 $K_{Ir}$ genes examined. To clarify any potential functional role of $K_{ir}$6.1 in GI motility, I exposed CCh pre-contracted tissues to the known $K_{ir}$6.1 activators, diazoxide (Cui et al., 2001) and cromakalim (Gopalakrishnan et al., 1999). 100 µM diazoxide caused a small but significant relaxation of both CCh pre-contracted ileum (14.8 ± 6.9 %, *n* = 6, *p* = 0.0034, Student's paired *t*-test) and colon (15.2 ± 2.5 %, *n* = 6, *p* = 0.0002, Student's paired *t*-test) (**Figure 5.5 A**). 20 µM cromakalim also induced a significant relaxation of CCh pre-contracted ileum (43.9 ± 8.5 %, *n* = 6, *p* = 0.0002, Student's paired *t*-test) and colon (17.4 ± 4.8 %, *p* = 0.0002, Student's paired *t*-test), and the observed relaxations to cromnakalim were significantly greater in ileum than in colon (**Figure 5.5 B**, *n* = 6, *p* < 0.0001, Student's unpaired *t*-test).

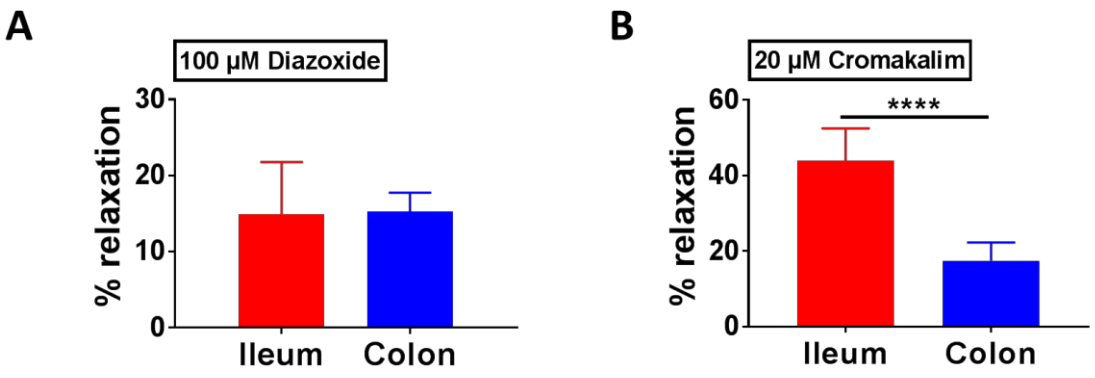


**Figure 5.5:** Bar graph showing that mean normalised relaxation in CCh pre-contracted ileum and colon in response to $K_{ir}$6.1 activators diazoxide in 100 µM **(A)** and cromakalim in 20 µM **(B)**. *n = 6* each condition, error bars represent standard deviation (SD), ****indicates *P* < 0.0001, student's un-paired *t*-test.

### 5.2.5 Activation of mechano-gated TREK channels induces relaxation in ileum and colon

Across 14 mouse $K_{2P}$ genes, TWIK-1 and TASK-2 transcripts showed the greatest relative expression in ileum and colon, with the TREK-1 transcript prominent in ileum but not colon. My immunohistochemical analysis showed wide distribution of TWIK-1 and TASK-2 across gut tissues, but revealed the unique expression of TREK-1 in smooth muscle only, whilst other members of the TREK subfamily, TREK-2 and TRAAK, were confined to neurons of the enteric nervous system. Given a paucity of specific pharmacological modulators for TWIK-1 and TASK-2, I focussed on characterising the functional contribution of mechano-gated K2P channels in CCh pre-contracted tissues, employing the organ bath system to directly monitor changes in both ileum and colon muscle tension during application of a range of specific mechano-gated $K_{2P}$ activators including the cyclooxygenase (COX) inhibitor BL-1249 and the lipoxygenase inhibitor cinnamyl 1-3,4-dihydroxy-alpha-cyanocinnamate (CDC) (Veale et al., 2014, Danthi et al., 2004).

Isolated ileum and colon segments were pre-contracted with CCh (10 µM) and the generated tension allowed to reach steady state before the addition of $K_{2P}$ activators (**Figure 5.6 A1, B1**). Bath exposure to the caffeic acid derivative and lipoxygenase inhibitor CDC produced a relaxation in ileum, the magnitude of which was concentration dependent ($IC_{50}$ = 8.5 ± 1.0 µM, *n* = 6, **Figure 5.6 A2**), resulting in a 88.5 ± 1.2 % relaxation at 30 µM (illustrated in the exemplar trace in **Figure 5.6 A1**). Relaxation to CDC in colon was also concentration dependent ($IC_{50}$ = 18.6 ± 3.5 µM, *n* = 6, **Figure 5.6 A2**), however the relaxations at all effective concentrations were significantly smaller than those observed in

ileum, only reaching a maximally observed relaxation of 57.1 ± 3.4 % at 60 µM CDC (**Figure 5.6 A2**). I propose that the relaxation induced by CDC did not occur through inhibition of lipoxygenase, as application of an alternative lipoxygenase inhibitor, Zileuton (10 µM), did not induce a significant change in tension in either CCh pre-contracted ileum (4.8 ± 1.3 %, $n$ = 6, $p$ = 0.70, Student's paired $t$-test) or colon (6.2 ± 1.4 %, $n$ = 6, $p$ = 0.058, Student's paired $t$-test) as shown in **Figure 5.6 C1, C2**.

Similar to CDC, the TREK subfamily activator and COX inhibitor BL-1249 induced a concentration dependent decrease in muscle tension in both CCh pre-contracted ileum and colon (**Figure 5.6 B2**), with a predicted $IC_{50}$ of 13.7 ± 1.4 µM (ileum, $n$ = 6) and 60.8 ± 4.2 µM (colon, $n$ = 6). Although relaxation induced by the highest concentration of BL-1249 used (60 µM) was not maximal, it differed significantly between ileum and colon tissues (93.1 ± 1.2 % versus 56.1 ± 4.2 % respectively, $n$ = 6, $p$ <0.0001, two-way ANOVA followed by a Bonferroni multiple comparisons test).

As BL-1249 induced a strong and significant relaxation effect in both ileum and colon, the mechanism of this drug became of interest. BL-1249 has been reported as a COX inhibitor, leading to enhanced intracellular arachidonic acid (AA) accumulation, and AA is a potent activator of TREK/TRAAK channels (Patel et al., 1998). To confirm whether the BL-1249 activation of TREK subfamily channels and subsequent muscle relaxation was direct or due to enhancement of intracellular AA levels, I applied the broad spectrum COX-inhibitor aspirin (100 µM). Aspirin did not cause a significant change in tension in either CCh pre-contracted ileum (5.3 ± 1.6 %, $n$ = 6, $p$ = 0.88, Student's paired t test) or colon (2.0 ± 2.3 %,

*n* = 6, *p* = 0.95, Student's paired t test) as shown in **Figure 5.6 C1, C2**, indicating that BL-1249 activity was direct to reinforce this argument, I also assessed the effects of melittin, a $PLA_2$ activator. Phospholipase A2 catalyses the hydrolysis of glycerophospholipids to liberate AA (Gijon and Leslie, 1999). Application of 10 µM melittin did induce a small and significant relaxation in ileum (21.4 ± 9.0 %, *n* = 6, *p* = 0.0054, Student's paired t test, **Figure 5.6 C1**), but not in colon (6.6 ± 5.4 %, *n* = 5, *p* = 0.38, Student's paired t test, **Figure 5.6 C2**). Finally, I assess the effects of directly applying AA to CCh pre-contracted ileum and colon. Unexpectedly, application of 100 µM AA did not induce a significant relaxation in either ileum (0.85 ± 0.2 %, *n* = 6, *p* = 0.95, Student's paired t test, **Figure 5.6 C1**) or colon (1.25 ± 0.2 %, *n* = 6, *p* = 0.33, Student's paired t test, **Figure 5.6 C2**).

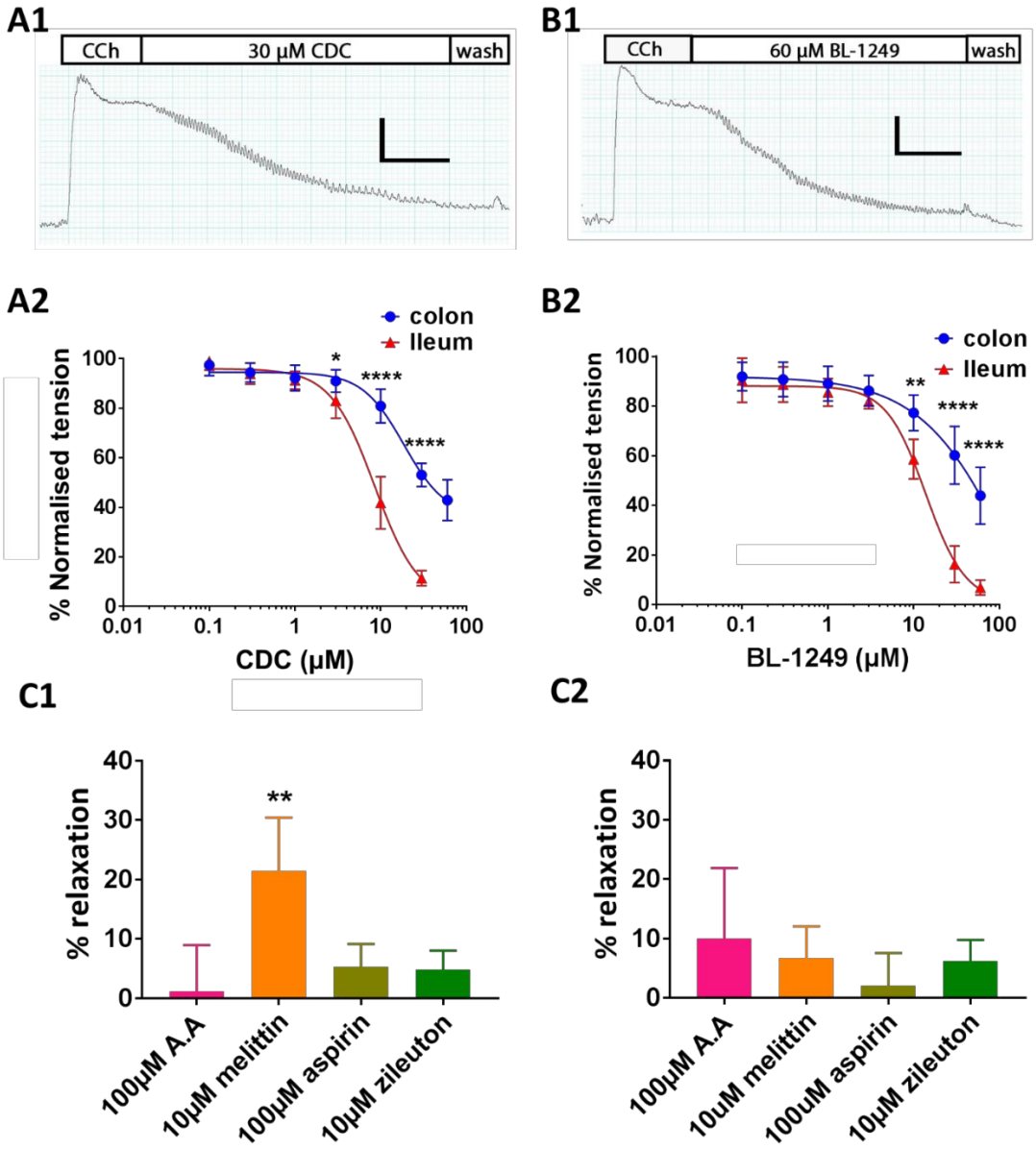


**Figure 5.6:** *Top panels*, representative traces showing the time course of the addition of mechano-gated $K_{2P}$ channel activators 30 µM CDC **(A1)** and 60 µM BL-1249 **(B1)** to mouse ileum, pre-contracted with 10 µM carbachol (CCh). Scale bars represent 0.4g (vertical) and 1 min (horizontal). Mean concentration-response relationships in CCh pre-contracted ileum (red triangles) and colon (blue circles) for Cinnamyl 1-3,4-dihydroxy-alpha-cyanocinnamate (CDC) **(A2)** and the fenamate BL-1249 **(B2)** are shown below the corresponding traces. All data was fitted with non-linear regression giving predicted $IC_{50}$ of CDC (8.516 ± 0.97 µM in ileum versus 18.67 ± 3.539 µM in colon); BL-1249 (13.68 ± 1.372 µM in ileum versus 60.82 ± 4.18 µM in colon). *Lower panels*, Bar graph illustrating the relaxatory effects of mechano-gated $K_{2P}$ channel activator arachidonic acid (AA), the phospholipase A2 activator melittin, COX inhibitors aspirin, and zileuton in both ileum **(C1)** and colon **(C2)**, All data represents $n$ = 6 animals, error bars represent standard deviation (SD), * $p < 0.05$, ** $p < 0.01$, **** $p < 0.0001$, two-way ANOVA followed by the Bonferroni post hoc test (A2 and B2), student's paired $t$ test (C1 and C2).

### 5.2.6 Relaxation induced by TREK activator BL-1249 can be attenuated by barium

There is currently a lack of well characterised, specific TREK-1 inhibitors. However the non-selective potassium channel pore blocker, barium chloride ($Ba^{2+}$), has been shown to effectively inhibit TREK-1 channels with an $IC_{50}$ of ~1 mM (Ma et al., 2011). I therefore tested the ability of the TREK-1 activator BL-1249 to relax CCh pre-contracted ileum and colon in the presence of 1 mM $Ba^{2+}$. As might be predicted, addition of 1 mM $Ba^{2+}$ significantly attenuated the relaxatory response to BL-1249 in both ileum (**Fig. 5.7 A1**) and colon (**Fig. 5.7 A2**). In ileum, 10 µM BL-1249 induced a mean normalised relaxation of 63.2 ± 12.3 % which was reduced almost by half to 32.1 ± 7.7 % in the presence of $Ba^{2+}$ ($p$ = 0.0003, Student's paired $t$-test). A similar effect was observed in colon were 30 µM BL-1249 induced a mean normalised relaxation of 42.8 ± 5.3 % compared to 29.9 ± 5.0 % in the presence of 1 mM $Ba^{2+}$ ($p$ = 0.0143, Student's paired $t$-test). To further reinforce the notion that TREK-1 currents formed a significant component of the smooth muscle conductance in ileum and colon, I investigated the ability of BL-1249 to relax CCh pre-contracted tissue in the presence of spadin, a proposed blocker of TREK-1 channels. Spadin has been recently described to exhibit high selectively to TREK-1 channels with an $IC_{50}$ of ~100 nM (Mazella et al., 2010). Interestingly, the relaxation of CCh pre-contracted tissues induced by BL-1249 (10 µM) persisted in the presence of 1 µM spadin; in ileum (**Figure 5.7 B1**), 59.8 ± 11.1 % (without spadin) vs. 54.8 ± 21.5 % (with spadin), $n$ = 6, $p$ = 0.3689, Student's paired $t$-test. In colon (**Figure 5.7 B2**), 40.8 ± 2.0 % (without spadin) vs. 33.2 ± 8.5 % (with spadin), $n$ = 6, $p$ = 0.1259, Student's paired $t$-test.

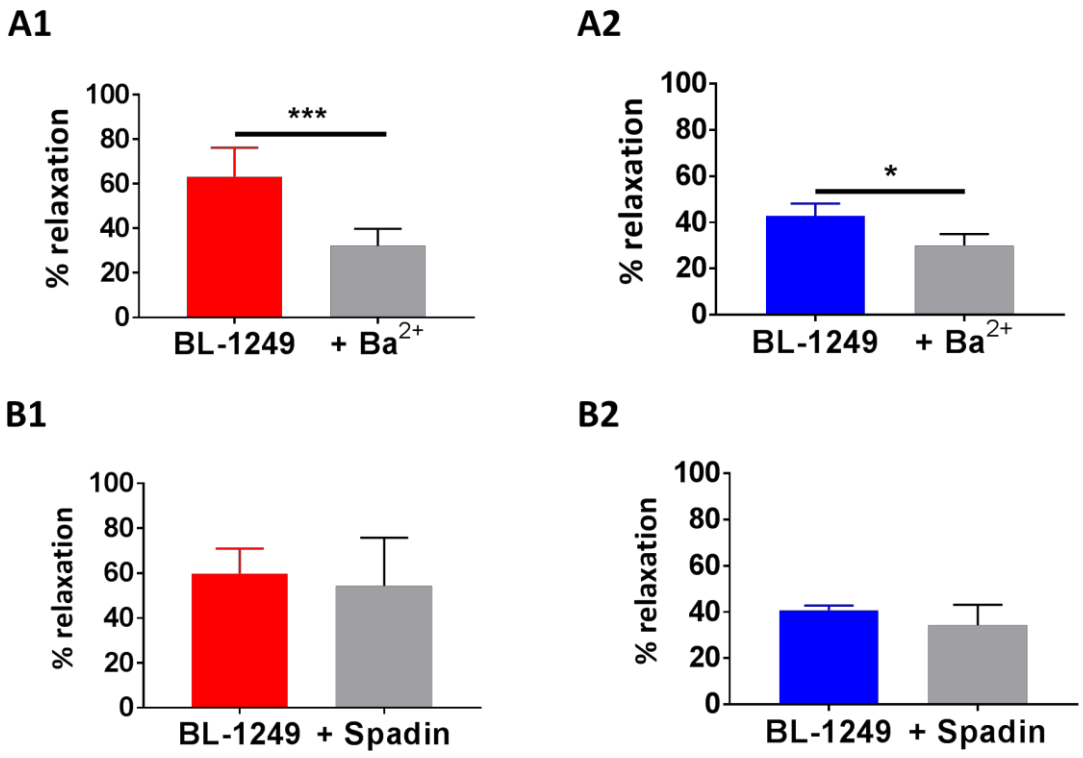


**Figure 5.7: (A1)** mean normalised relaxation in ileum to 10 µM BL-1249 in the absence (red bar) and presence (grey bar) of 1 mM barium chloride ($Ba^{2+}$). **(A2)** mean normalised relaxation in colon to 30 µM BL-1249 in the absence (Blue bar) and presence (grey bar) of 1 mM barium chloride ($Ba^{2+}$). **(B1)** mean normalised relaxation in ileum to 10 µM BL-1249 in the absence (red bar) and presence (grey bar) of 1 µM Spadin. **(B2)** mean normalised relaxation in colon to 30 µM BL-1249 in the absence (Blue bar) and presence (grey bar) of 1 µM Spadin. All data represents *n* = 6 animals. Error bars represent standard deviation (SD), * indicates *p* = 0.0143, *** indicates *p* = 0.0003, student's paired *t* test.

### 5.2.7 Relaxation induced by mechano-gated $K_{2P}$ activators occurs via smooth muscle mechanisms

To investigate further whether the activation of mechano-gated $K_{2P}$ channels influences intestinal contractions, we also applied the antidepressant drug riluzole and fenamate flufenamic acid (FFA) to CCh pre-contracted tissues. Both these compounds have been reported previously as activators of TREK channels (Duprat et al., 2000, Veale et al., 2014). Single concentration additions of the FFA (100 µM) and the riluzole (100 µM) induced

marked relaxations in CCh pre-contracted ileum and colon tissues, although to a lesser degree than those observed with BL-1249 and CDC (**Figure 5.8 A**; FFA, 63.3 ± 6.2% (ileum) and 41.1 ± 3.4 % (colon); riluzole, 37.1 ± 4.7 % (ileum) and 18.9 ± 4.0 % (colon). Consistent with our data obtained with CDC and BL-1249, the observed relaxations to FFA and Riluzole were significantly greater in ileum versus colon (**Figure 5.8 A**, $n$ = 6, $p$ <0.05, Student's unpaired $t$-test).

On the whole, data from all these functional pharmacological studies demonstrated a clear contribution of TREK-like channels to GI tract smooth muscle contractility. However, it was unclear whether the observed relaxations induced by $K_{2P}$ activators occurred at the level of the smooth muscle (via TREK-1) or potentially through modulation of neuronal input to smooth muscles, thus involving TREK-2/TRAAK. To clarify this, I performed drug additions in two separate experiments; (1) in tissues pre-contracted with potassium chloride (60 mM KCl) and (2) in tissues pre-contracted with CCh in the presence of tetrodotoxin (TTX).

Isolated ileum and colon segments were pre-contracted with 60 mM KCl and the generated tension allowed to reach steady state before the addition of $K_{2P}$ activators. Changes in tension induced by addition of TREK-1 activators were normalised to steady-state pre-contracted tension in each individual experiment and are reported as percent. On average 60 mM KCl generated a tension of 0.6 ± 0.04 g in ileum and 0.8 ± 0.05 g in colon (both $n$ = 50). All mechano-gated $K_{2P}$ channel activators applied (riluzole, BL-1249, FFA and CDC) induced robust relaxations of KCl pre-contracted ileum and colon tissues (**Figure 5.8 B**) with BL-1249 and FFA producing significantly greater magnitudes of relaxation in ileum

compared to colon ($n$ = 6, $p$ = <0.05, Student's unpaired $t$-test). In ileum, the extent of the relaxation induced by BL-1249, FFA and CDC was independent of the manner of pre-contraction, however riluzole produced a significantly greater relaxation when the ileum was pre-contracted with KCl compared to CCh (72.1 ± 3.6 % versus 37.1 ± 3.9 %, $n$ = 6, $p$ < 0.0001, Student's unpaired $t$-test). This phenomenon was similarly observed in colon with riluzole (78.3 ± 5.2 %, KCl versus 18.9 ± 4.4 %, CCh, $n$ = 6, $p$ < 0.0001, Student's unpaired $t$-test) and CDC (76.2 ± 6.9 % in KCl versus 57.1 ± 3.3 % in CCh, $n$ = 6, $p$ = <0.01, Student's unpaired $t$-test).

These data are consistent with a direct smooth muscle effect. To reinforce this hypothesis I assessed the effects of a $K_{2P}$ activator in the presence of tetrodotoxin (TTX). TTX is a voltage-gated sodium channel blocker, which in this preparation has been previously shown to block neuronal action potentials and prevent ENS activity (Seifi et al., 2014). The relaxation of CCh pre-contracted tissues induced by BL-1249 (60 µM) persisted in the presence of TTX (1 µM); in ileum (**Figure 5.8 C1**), 91.1 ± 2.0 % (without TTX) versus 98.2 ± 3.7 % (with TTX), $n$ = 6, $p$ = 0.038, Student's paired $t$-test; in colon (**Figure 5.8 C2**), 63.6 ± 2.9 % (without TTX) versus 64.8 ± 5.0 % (with TTX), $n$ = 6, $p$ = 0.74, Student's paired $t$-test.

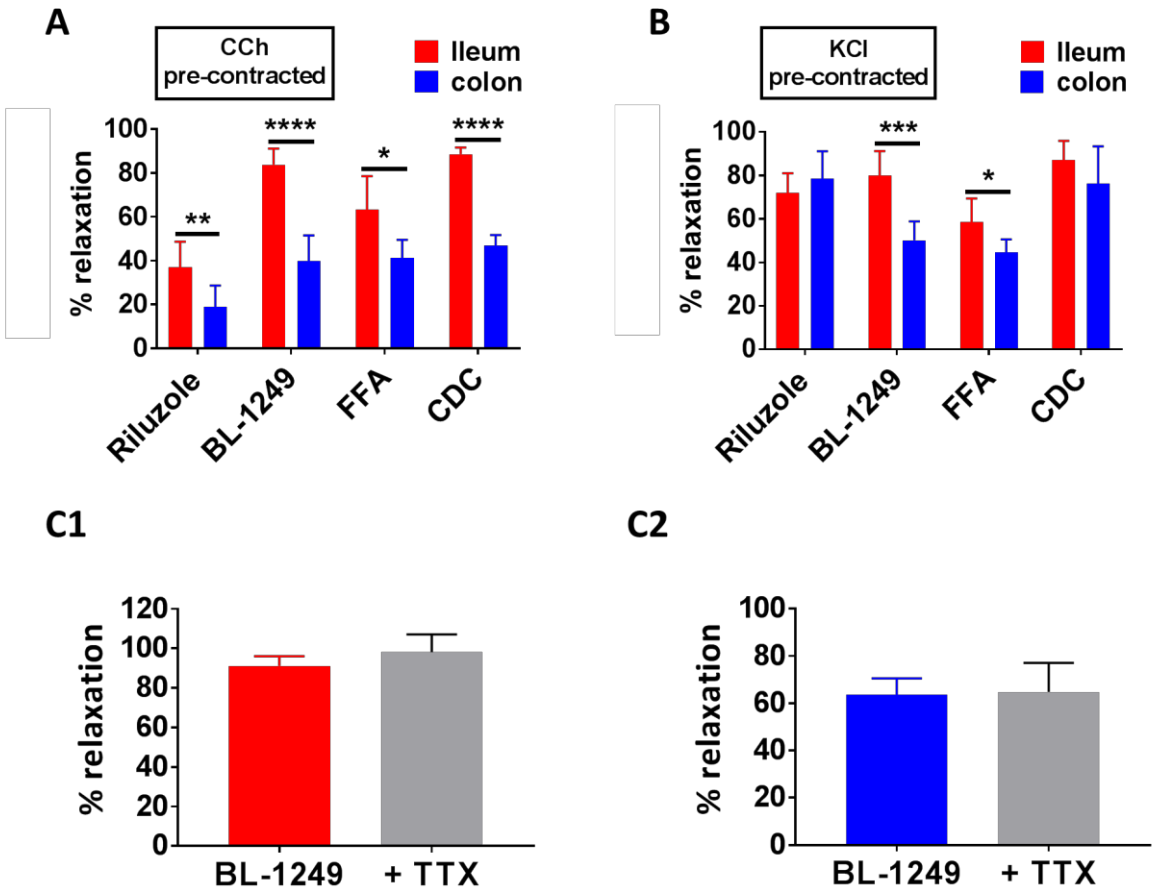


**Figure 5.8:** Bar graph showing mean normalised relaxation of CCh **(A)** and KCl **(B)** pre-contracted ileum (red bars) and colon (blue bars) by Riluzole (100 µM), BL-1249 (30 µM), fluflenamic acid (FFA) (100 µM) and CDC (30 µM). **(C1)** mean normalised relaxation in ileum to 30 µM BL-1249 in the absence (red bar) and presence (grey bar) of 1 µM tetrodotoxin (TTX). **(C2)** mean normalised relaxation in colon to 60 µM BL-1249 in the absence (Blue bar) and presence (grey bar) of 1 µM tetrodotoxin (TTX). Error bars represent standard deviation (SD). All data represents $n$ = 6 animals. * $p$< 0.05, ** $p$ < 0.01, *** $p$ < 0.001, **** $p$< 0.0001, student's unpaired $t$-test.

### 5.2.8 Potassium channel modulators regulate the force but not frequency of spontaneous contractions

Finally, in order to understand whether the activation or inhibition of potassium channels is able to directly influence physiological intestinal contractions, I applied the classical $K^+$ channel blocker (TEA, $Ba^{2+}$), KCNQ channel blocker/activator (XE991/retigabine), TASK

channel blocker (ML-365), and mechano-gated $K_{2P}$ channel activators (riluzole, BL-1249) to isolated mouse ileum and colon segments using the organ bath system and measured changes in the force and frequency of spontaneous contractions. **Table 5.1** summarises the effects of the modulators used in regulating both frequency and force of spontaneous contractions. None of the compounds displayed a significant effect on the frequency of spontaneous contractions in ileum or colon. Furthermore, the TASK-1 channel blocker ML365 (Zou et al., 2010), only induced a significant increase in the force of spontaneous contractions in colon (0.04 ± 0.02 g versus 0.07± 0.01 g, n = 5, p = 0.0082, Student's paired t-test) but not in ileum (0.13 ± 0.07 g versus 0.24± 0.13 g, n = 5, p = 0.07, Student's paired t-test).

**Table 5.1:** Summary table showing the effects of different $K^+$ channel blockers and activators on both ileum and colon spontaneous contraction (*n* = 6 each condition). Key: ↓=currents inhibited. ↑=currents increased. **X** =no effect

| | Ileum | | colon | |
|---|---|---|---|---|
| | Force (g) | Frequency | Force(g) | Frequency |
| 10mM TEA | ↑ | X | ↑ | X |
| 10mM BaCl | ↑ | X | ↑ | X |
| 100µM XE991 | ↑ | X | ↑ | X |
| 10µM ML365 | X | X | ↑ | X |
| 100µM Riluzole | ↓ | X | ↓ | X |
| 100µM Retigabine | ↓ | X | ↓ | X |
| 30µM BL-1249 | ↓ | X | X | X |

Riluzole (100 μM), significantly decreased the force of spontaneous contractions in ileum (0.19 ± 0.04 g versus 0.07 ± 0.01 g, *n* = 6, *p* = 0.0216, Student's paired *t*-test, **Figure 5.9, A2**) and in colon (0.07 ± 0.01 g versus 0.03 ± 0.01 g, n = 6, p = 0.0074, Student's paired t test, **Figure 5.9 B2**) and produced a noticeable reduction in basal tone as illustrated in the exemplar traces shown in **Figure 5.9 A1, B1**. Likewise, addition of BL-1249 (30 μM) significantly reduced the force of spontaneous contractions in ileum (0.14 ± 0.02 g versus 0.06 ± 0.01 g, *n* = 7, *p* = 0.0030, Student's paired *t*-test) but not colon (0.06 ± 0.02 g versus 0.05± 0.02 g, *n* = 7, *p* = 0.0917, Student's paired *t*-test) as shown in **Figure 5.9 C2, D2** respectively. Neither Riluzole nor BL-1249 had any significant effect of the frequency of spontaneous contractions in ileum or colon (**Figure 5.9 A3, B3, C3 and D3**).

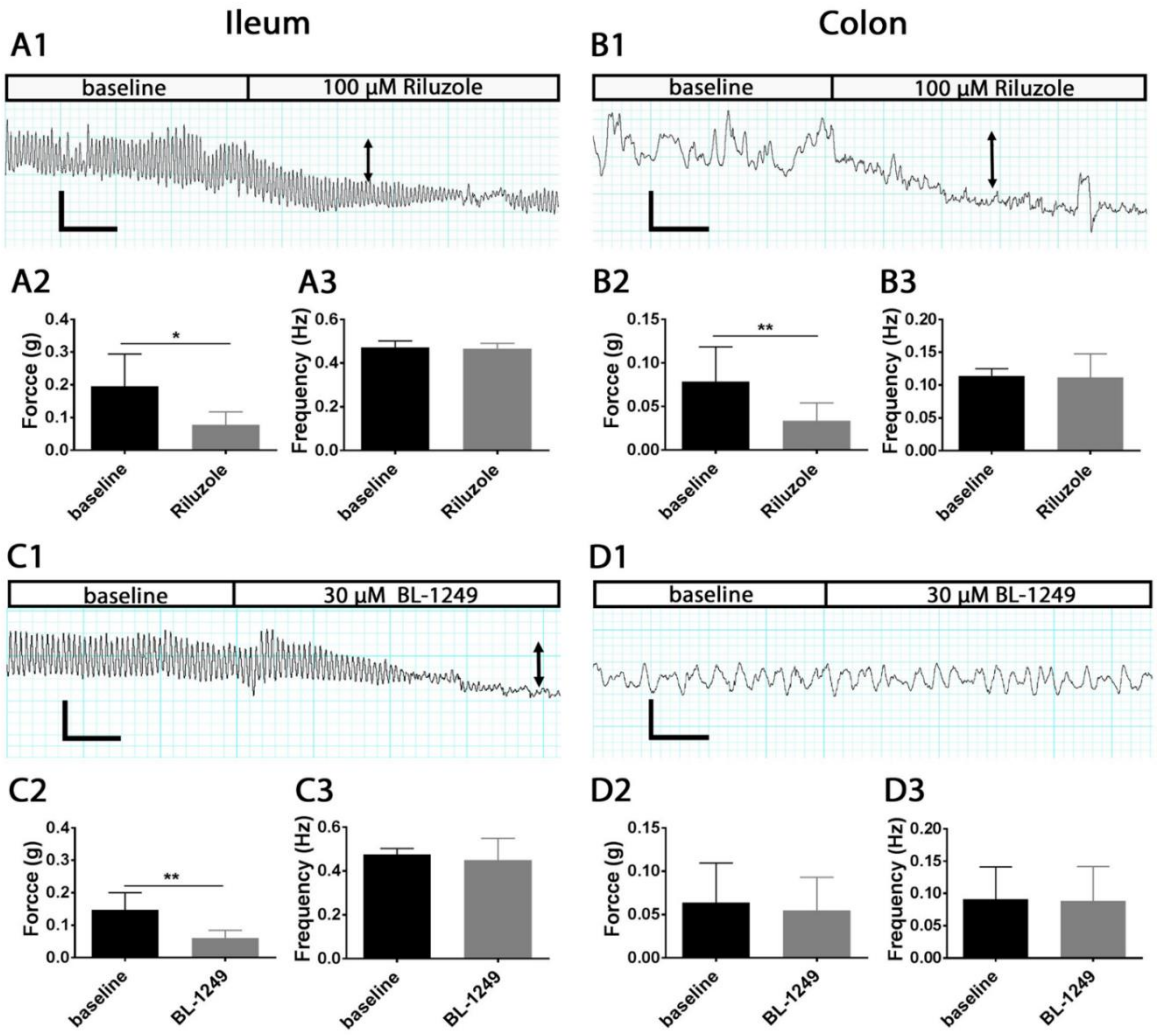


**Figure 5.9:** Spontaneous contractions were recorded in the presence and absence of 100 µM Riluzole (**A** and **B** panels) and 30 µM BL-1249 (**C** and **D** panels) in ileum (*left*) and colon (*right*) as indicated. *Upper panels*, representative traces show the effects of 100 µM Riluzole on the spontaneous contractile responses obtained from mouse ileum **(A1)** and colon **(B1)**. Arrows signify reduction in basal tone. Mean data for force of contraction and frequency is displayed in chart form below the corresponding traces for ileum (**A2** and **A3**) and for colon (**B2** and **B3**). *Lower panels*, representative traces show the effects of 30 µM BL-1249 on the spontaneous contractile responses obtained from mouse ileum **(C1)** and colon **(D1)**. Arrows signify reduction in basal tone. Mean data for force of contraction and frequency is displayed in chart form below the corresponding traces for ileum (**C2** and **C3**) and for colon (**D2** and **D3**). For traces, scale bars represent 0.2 g (vertical) and 30 s (horizontal) for panels **A1** and **C1**, and 0.1 g (vertical) and 30 s (horizontal) for panels **B1** and **D1**. For bar charts, error bars represent standard deviation (SD); $n$ = 6 animals. * $p$ < 0.05, ** $p$ < 0.01, student's paired $t$-test.

## 5.3 Discussion

The expression of specific potassium channel subunits, especially the mechano-gated $K_{2P}$ channels, on distinct cell types (smooth muscles and enteric neurons) of the mouse ileum and colon suggested a role for distinct potassium channel subtypes in modulating intestinal motility (Chapter 3 & 4). Functional and pharmacological evidence presented in this chapter reinforces this notion. The application of variety of specific potassium channel modulators induced contrasting effects on both force and frequency of spontaneous contraction and in pre-contracted tissues of the ileum and colon in organ bath experiments. Results showed that potassium channel activation was sufficient to induce significant relaxatory effects, whereas inhibition of potassium channel activity induced significant increases in tension in both ileum and colon. The implications are that multiple potassium channel subtypes play functional role in determining GI contractility.

### 5.3.1 $K_v$ channel subtypes have contrasting effects on the intestinal contractility

$K_v7$ channels are appearing as major regulators of muscle contractility, particularly in cardiac muscle and vascular smooth muscle (Greenwood and Ohya, 2009). To date, research on the expression profile of $K_v7$ channels in smooth muscle has revealed that $K_v7.4$ and $K_v7.5$ transcripts show abundant expression and functionally are key regulators of smooth muscle contractility in the vasculature of the stomach and intestine (Jepps et al., 2009, Ipavec et al., 2011, Yeung et al., 2007). Since $K_v7.1$ channel transcripts displayed the highest relative expression of all $K_v7$ subfamily members in both ileum and colon, I focused my attention on the potential functional roles for these channels by using pharmacological

tools in organ bath preparation. Previously, retigabine has been reported as a potent agonist of $K_v7$ channels, specifically activating $K_v7.2$-7.5 but not $K_v7.1$ channels (Stott et al., 2014, Schenzer et al., 2005). In contrast, Chromanol 293B blocks only $K_v7.1$ channels and not $K_v$ 7.2-7.5 (Lerche et al., 2007), while XE991 blocks all heterologously expressed $K_v7$ channels (Yeung et al., 2007). The combined influence of these three compounds on GI contractility suggests that $K_v7.1$ does not play a major functional role in mouse intestinal contractility. Indeed, Schroeder et al. (2000) previously highlighted $K_v7.1$ expression in the epithelium, and expression in murine colonic epithelium has been noted (Jepps et al., 2009). In this same study, the authors utilised retigabine and XE991, demonstrating direct regulation of spontaneous contraction of the circular smooth muscle in mouse distal colon, and combined with immunohistochemical characterisation suggested $K_v7.4$ and $K_v7.5$ are important in regulating contractile activity in the GI tract. This correlates directly with my data revealing $K_v7$ channels, but not $K_v7.1$, also play an essential role in regulating the contraction of longitudinal smooth muscle in both mouse ileum and colon. Given that the accessory subunit transcript for KCNE3, encoding MiRP2, shows high expression in gut tissue, and when in complex with $K_v7.1$ forms a leak conductance, it is likely that the physiological role of $K_v7.1$ channels in GI tissue is in intestinal and tracheal chloride transport.

It has been suggested that the A-type currents in the GI smooth muscle are generated by $K_v4$ channels, and their inhibition increases smooth muscle excitability and contractility (Amberg et al., 2003). Consequently, the activation of A-type currents should have opposite effects, inducing smooth muscle relaxation. Recently, NS5806 has been reported as an

activator of $K_v4$ channels, and modulate channel gating depending on the presence of KChIP2 accessory subunit (Calloe et al., 2010, Lundby et al., 2010). NS5806 had little effects on current density and current decay of $K_v4.2$ and $K_v4.3$ in the absence of KChIP2, whereas it significantly increased current density and slowed the current decay for channel co-expressed with KChIP2 (Lundby et al., 2010, Calloe et al., 2010). Moreover, co-expression of $K_v4.3$ with and without KChIP2 with DPP6, DPP10, KCNE2 or KCNE3 β-subunits corroborated that NS5806 only slowed current decay of channel complexes containing KChIP2 (Lundby et al., 2010). In contrast, for $K_v4.1$, the slowing of current decay by NS5806 was independent of the KChIP2 subunit (Lundby et al., 2010, Witzel et al., 2012). The $EC_{50}$ of NS5806 in $K_v4.3$/KChIP2 was 25.4 ± 1.1 μM (Lundby et al., 2010), but at concentration over 100 μM an inhibition effect of current amplitude was observed in HEK293 cells (Witzel et al., 2012). Therefore, 50 μM NS5805 was selected for my organ bath preparation, and induced significant relaxation in both ileum and colon, although the relaxatory effect was smaller than that previously observed with $K_v7$ activator retigabine. The smaller effect could be due to a lower potency or efficacy of the $K_v4$ compound or a lower functional expression of $K_v4$ channels and therefore contribution to contractility. NS5806 has also been shown to inhibit $K_v1.4$ channel currents, and to a lesser extent, $K_v1.5$ channel currents (Lundby et al., 2010). Blockade of these $K_v$ channels would promote contraction and counterbalance the relaxatory effect of $K_v4$ channel activation, thus partially masking the full impact of $K_v4$ channel currents to GI tract contractility. Moreover, both $K_v1.4$ and $K_v1.5$ transcripts were shown to be expressed in ileum and colon as shown by my qPCR data. However, the combination of high transcript expression for $K_v4.3$, and ability for $K_v4$ activator, NS5806, to induce relaxation in both ileum and colon, and previous studies in colonic myocytes by Amberg et al, 2002, strongly infer that $K_v4.3$ channels form a

physiologically important current in GI smooth muscle cells. However, given their lesser impact on relaxation compared to other channel subtypes, argues they are not first choice potential therapeutic targets for GI tract motility disorders.

### 5.3.2 Both BK and SK channels play a role in the regulation of GI smooth muscle

Previous studies have revealed that SK protein are expressed in the GI muscular layer (Chen et al., 2004), whereas IK protein are mainly expressed in enteric neurons, in which they mediate the slow afterhyperpolarization (Neylon et al., 2004). To investigate the functional role of calcium-activated potassium channels in GI tract I studied the effects of the SK/IK channel openers [SKA-31 (Sankaranarayanan et al., 2009) and NS306 (Strobaek et al., 2004)] on murine intestinal contractility using the organ bath technique. The results presented in this chapter revealed that both SKA-31 and NS309 caused a significant reduction in CCh-induced contraction amplitude and muscle tone, suggesting that activation of the SK/IK channels is able to repolarise smooth muscle potential preventing further $Ca^{2+}$ influx and therefore contraction. Both drugs were higher selectivity for IK over SK, and show no effect on BK channel activity (Strobaek et al., 2004, Sankaranarayanan et al., 2009), but the concentration I used was in the range to activate both IK and SK channels. Given the inability to distinguish the functional contributions of SK and IK channels here, it is difficult to identify how each channel contributes to smooth muscle relaxation. However a previous report by Ipavec & Curro (2015) reported that NS309 produced relaxatory effects in the pre-contracted proximal stomach smooth muscle which were not affected by the selective IK channel blocker TRAM-34, but were greatly inhibited by the selective SK

channel blocker UCL-1684. A similar phenomena was exhibited in human bladder smooth muscle were the selective SK channel blocker apamin readily reversed the relaxatory effect induced by SKA-31, suggesting that SKA-31 inhibits bladder smooth muscle contractions mainly by its action on the SK channels (Soder et al., 2013). Thus, the role of IK/SK in intestinal smooth muscle may be similar to other types of smooth muscle in that IK/SK activators likely relaxes the GI contractility via SK activation. However, further studies using a similar pharmacological approach would have to be conducted in ileum and colon to conclusively determine the contribution of SK and IK channels individually to GI tract motility.

Previous studies have revealed that activation of large conductance, calcium activated $K^+$ channels (BK) channels reduced the spontaneous motor activity of the mouse ileum (Dela Pena et al., 2009), while inhibition of this channel increased the spontaneous contractile activity of ileum longitudinal muscle (Hong et al., 1997). Therefore, BK channels are proposed to have an important physiological role in regulating the smooth muscle contractility in the GI tract. My data presented here demonstrates that BK channel activator NS19504 could induce an almost complete relaxation of pre-contracted colon, and less so in ileum. This strong impact of BK channels in controlling contractile responses in smooth muscle tissues have also been recognised previously in bladder smooth muscle contraction (Nausch et al., 2014). The observed differences in relaxation effects of BK activation between ileum and colon could be explained by the differential transcript expression level along the GI tract, since I revealed the levels of BK transcript was higher in colon than in ileum (Chapter 3).

In order to provide evidence that the relaxatory effect of BK channel activation originated at the level of the smooth muscle I pre-contracted the tissue with potassium chloride (KCl). Increasing external KCl concentration shifts the reversal potential of potassium channel currents, as predicted by the Nernst equation to more depolarise potentials, thereby adjusting the resting membrane potential to amore depolarised potential. The depolarisation of the cell membrane directly activates plasma membrane L-type voltage-gated $Ca^{2+}$ channels, causing an influx of calcium to induce smooth muscle contraction. This mechanism is receptor independent, and therefore by passes neuronal input and any G protein coupled signalling pathways that normally determine cell contractile state. NS19504 caused a significant relaxation of ileum and colon tissues pre-contracted with KCl, suggesting that BK channel activation likely occurred at the level of the smooth muscle. To further reinforce the suggestion that the observed relaxation occurred via activation of BK channels, I investigated the impact of the known, but not specific, BK channel inhibitor TEA on the ability of the BK activator NS19504 to induce relaxation in both ileum and colon. TEA was chosen due to a lack of suitable alternative BK blockers. Charybdotoxin is a potent blocker of BK channels (Gribkoff et al., 1996), however it also inhibits the IK channel (Anderson et al., 1988). Iberiotoxin is another potent BK blocker, but it has been shown that it does not affect the resting membrane potential of colonic circular smooth muscle cells and does not induce contraction of the basally quiescent gastric fundus smooth muscle (Carl et al., 1995). Although TEA is not specific for BK, it does not inhibit SK and IK channels (Kew and Davies, 2010). Pre-exposure of TEA significantly attenuated the relaxatory response to the BK channel activator, NS 19504 in colon, providing further support for the suggestion that NS19504 likely relaxes the GI smooth muscle via BK activation. However,

that this response was not observed in ileum may suggest that NS19504 has modulatory effects on other channels other than BK.

### 5.3.3 $K_{ATP}$ channels may play a functional role in intestinal contractility

In smooth muscle cells, intracellular ATP can directly regulate the activity of $K_{ir}6$ ($K_{ATP}$) channels (Vogalis, 2000). Therefore, the open probability of these $K_{ATP}$ channels is directly linked to the metabolic activity of the smooth muscle cells. A number of studies have confirmed the presence of $K_{ATP}$ channels in GI smooth muscle. Koh *et al*. (1998) reported that the $K_{ATP}$ channel agonist, cromakalim hyperpolarized membrane potential and reduced spontaneous contractility of mouse intestine. Together with the RT-PCR analysis the authors suggests that $K_{ATP}$ channels are functionally expressed in mouse intestine and are formed by $K_{ir}6.2$ and SUR2B subunits. Another study in muscle strips of mouse gastric fundus suggested that the relaxation induced by opening of $K_{ATP}$ channels occurred mainly via smooth muscle cells and did not involve ENS input, since $K_{ATP}$ channel agonists caused relaxation in KCl pre-contracted tissue (Sun and Benishin, 1994, Richardson et al., 1992, McPherson and Angus, 1990). In my study here using mouse ileum and colon, I found that $K_{ATP}$ agonists (diazoxide & cromakalim) caused a small but significant relaxation in both pre-contracted ileum and colon tissues and is consistent with these previous observations. It also parallels a previous study in rat, where another $K_{ATP}$ opener, $H_2S$ was shown to cause a modest relaxation of small intestine and colonic smooth muscle (Lu et al., 2014). In the same study, the authors also provided immunohistochemical analysis revealing that both $K_{ir}6.1$ and $K_{ir}6.2$ were localised in smooth muscle layers.

The $K_{ATP}$ agonist, cromakalim, has been shown to directly and reversibly activate $K_{ATP}$ channels but has also been reported to activate $K_v$ channels (McHugh and Beech, 1995) and inhibit L-type $Ca^{2+}$ channels (Post et al., 1991), and would provide an explanation for the stronger relaxation to cromakalim compared to diazoxide in both ileum and colon. In addition, although not specific, $Ba^{2+}$ is a potent blocker of $K_{ATP}$ channel (Quayle et al., 1988). Application of $Ba^{2+}$ in this study not only induced significant contraction, but also increased the force of smooth muscle spontaneous contraction. Together, this and previous data provide further support for the suggestion that $K_{ATP}$ channels may play a functional role in intestinal contractility. However, the lack of selectivity makes the currently available $K_{ATP}$ channel modulators unsuitable for the treatment of GI disorders.

### 5.3.4 Pharmacological modulators of TREK family channels regulate intestinal contraction

In chapters 3 and 4, I revealed the transcripts for all three mechano-gated TREK family channels, TREK-1, TREK-2 and TRAAK are expressed in the ileum and colon and that their channel proteins are localised in distinct cell types within the different layers of the wall of the GI tract. In support of my findings, I sought further pharmacological evidence for mechano-gated $K_{2P}$ function in intestinal contractility. I therefore assessed the repolarising power of documented mechano-gated $K_{2P}$ channel activators in pre-contracted tissues and during spontaneous contractile activity. This approach yielded strong evidence for a functional role of smooth muscle TREK-1 in murine GI tract, both under basal conditions and during smooth muscle relaxation.

Available data suggests all utilised compounds are potent activators of mechano-gated $K_{2P}$ channels. Riluzole has been shown to directly activate TREK-1, TREK-2 and TRAAK channels (Duprat et al., 2000), and CDC to activate TREK-1 (Danthi et al., 2004) at micromolar concentrations. Fenamates, non-steroid anti-inflammatory drugs, including BL-1249 and flufenamic acid (FFA) have been revealed to directly and reversibly activate TREK-1, TREK-2 and TRAAK channels (Takahira et al., 2005, Veale et al., 2014). All four compounds produced comparable effects on pre-contracted ileum and colon tissues and have previously been used to describe functions of mechano-gated $K_{2P}$ channels in native tissues including sympathetic neurons (Cadaveira-Mosquera et al., 2011), dorsal root ganglion cells (Han et al., 2016), the blood brain barrier (Bittner et al., 2013), bladder (Tertyshnikova et al., 2005), and adrenocortex (Enyeart et al., 2002, Danthi et al., 2004).

The relaxatory effect of BL-1249 after pre-contraction was stronger than that observed from exposure to FFA in both tissues, and is consistent with data from Veale *et al*. (2014) who revealed that BL-1249 is the most potent of the fenamates compounds for activating TREK-1 channel. However, fenamates are not ion channel specific compounds. Guinamard *et al*. (2013) provided an overview of different ion channels targeted by FFA to aid in interpreting its effects, including inhibition of L-type $Ca^{2+}$ channels, chloride channels, transient receptor potential (TRPC) channels and activation of several types of potassium channels including $K_v7.1$ and BK, all of which are known to be expressed in GI tissues (Guinamard et al., 2013). For example, FFA has been shown to activate TRPC6 (Foster et al., 2009) and TRPA1 channels (Hu et al., 2010). TRPC channels are $Ca^{2+}$-permeable non-selective cation channels implicated in diverse physiological functions, including smooth

muscle contractility and synaptic transmission (Montell et al., 2002). Deletion of TRPC6 channels in mice impairs smooth muscle contraction and intestinal motility *in vivo* (Tsvilovskyy et al., 2009). Therefore, the differential relaxatory effect between BL-1249 and FFA could also be potentially explained by FFA activation of TRPC6 channels which would resist the relaxatory response induced by activation of TREK channels. However, given that BL-1249 is a structurally-related drug to FFA, it may also affect other channels including TRP channels. Furthermore, the mechano-gated $K_{2P}$ activator AA was largely without impact, confounding the functional role of TREK channels in modulating GI contractility. However, AA is also not a selective compound and although a highly potent activator of TREK family channels, it also modulates a number of other ion channels and cellular targets including members of the $K_v4$ family. AA has been demonstrated to inhibit the A-type $K^+$ currents formed by $K_v4.2$ when expressed in oocytes, and also native hippocampal A-type currents (Villarroel, 1993, Meves, 2008). Given the prominent function of A-type currents in GI tissues, thought to be carried by $K_v4$ channels, it is plausible that the depolarising effect of AA inhibition of $K_v4$ channels would counterbalance the repolarising effects of activating TREK family channels, resulting in a minimal functional effect on GI tract contractility.

Although the specificity of Riluzole, FFA, BL-1249 and CDC can be debated, it is clear that all four compounds have qualitatively similar effects on GI tract contractility that likely arise from modulation of a common target. In order to further reinforce the suggestion that the observed relaxations occur via activation of TREK channels, I took the further step of investigating the impact of the known TREK channel inhibitor barium and the proposed TREK-1 channel blocker, spadin, on the ability of the TREK activator BL-1249 to induce

relaxation in both ileum and colon. These blockers were chosen based on previously highlighted flaws with other characterised TREK channel blockers. For example, the proposed TREK-1 inhibitor, L-methionine, was used to demonstrate the functional presence of TREK channels in colonic myocytes (Park et al., 2005). However, it has since been argued that the effects of L-methionine in native tissue do not involve TREK-1 (Gil et al., 2012). Fluoxetine is another potent blocker of TREK-1 (Kennard et al., 2005), however its activity as a serotonin (5-hyroxytryptamine) reuptake inhibitor would modulate contractile activity in the GI tract through mechanisms independent of TREK-1 and therefore precluded its use. So even though barium is not a specific blocker of TREK channels, its mechanism of action is well characterised, its potency for TREK channels is reasonable ($IC_{50}$ for TREK-1 block is ~ 1 mM (Ma et al., 2011) and given its mechanism is likely to only affect potassium channel activity, thus minimising the likelihood of off target effects. Pre-exposure of ileum and colon tissues to 1 mM barium attenuated the relaxatory response to the TREK activator, BL-1249, by 50 and 30% respectively, in line with what might be predicted, and provides further support for the suggestion that BL-1249 likely relaxes the GI smooth muscle via TREK channel activation. Interestingly, the relaxation induced by BL-1249 persisted in the presence spadin, which is a proposed TREK-1 blocker (Mazella et al., 2010). However, Gil *et al*. (2012) utilised spadin and observed no effect on colonic membrane potential or spontaneous motility. Mechanistically, it has currently only been shown to block AA-activated TREK-1 currents, and the specific molecular mechanism of action has not been described. Therefore its ability to prevent TREK-1 activation by riluzole, FFA, CDC and BL-1249 has not been established or confirmed.

### 5.3.5 Relaxation by mechano-gated TREK activators occurs via smooth muscle

In spontaneous contraction studies, I found BL-1249 and riluzole both reduced the force of spontaneous contractions, without affecting their frequency. The frequency of spontaneous contraction in GI tract is mainly controlled by ICC (Yoneda et al., 2001) and I have no evidence that TREK channels are expressed here, but the ineffectiveness of TREK channel activators on frequency suggests they are not likely expressed in ICC. However, TREK compounds affect the force of contraction suggests it may take place to modulate the intestinal contractions via multiple and distinct mechanism. For example, it may either be acting directly on enteric neurons or regulating the amount of calcium allowed to enter the cell to change the amplitude of the contractions. Since, I demonstrated in previous chapter that TREK channel subtypes localised in different cell types, it would be beneficial to understand which particular cellular pathway of TREK channels modulates the contractile process.

In order to investigate whether the relaxatory effect of the activators originated at the level of the smooth muscle we pre-contracted with potassium chloride. In the case of Riluzole, the relaxatory effect was stronger than that previously observed with CCh pre-contraction. This differential effect could be explained by activation of nitrenergic neurons as I revealed TREK-2 and TRAAK expression in enteric neurons in Chapter 4, which would counteract the relaxatory response at the smooth muscle. This would also provide an explanation for the enhanced relaxation to BL-1249 observed during neuronal action potentials blockade via TTX. Alternatively, the mechanism of pre-contraction could also be influential. Carbachol,

a parasympathomimetic, activates metabotropic muscarinic receptors inducing contraction via: (1) transmembrane calcium influx through TRPC channels, (2) subsequent transmembrane calcium influx via voltage-dependent calcium channels (VDCC) and (3) SR calcium release (Ambudkar, 2009). When using KCl as the contractile stimulus, only transmembrane calcium influx via VDCC occurs and calcium influx through TRPC channels and SR calcium release would not occur. Thus the use of TREK activators would be expected to modulate the membrane potential driven calcium influx through VDCC (receptor independent) and therefore might appear less efficacious in CCh pre-contracted tissues.

## 5.4 Summary and Conclusions

Overall, these data suggest that the relaxation induced by activation of mechano-gated $K_{2P}$ channels is independent of enteric neuron input and therefore likely occurs at the level of the smooth muscle. Given that the localisation studies I presented in Chapter 4 clearly highlight that TREK-1 was the only TREK family channel member expressed in smooth muscle layers, strongly suggests that pharmacological modulators of mechano-gated TREK channels likely act on TREK-1 to regulate the GI smooth muscle contractility. Therefore TREK-1 channels represent a favourable pharmacological/therapeutic target for treating hypermotility disorders.

# Chapter 6 – Biophysical and pharmacological characterisation of TREK channels

## 6.1 Introduction and Aims

In Chapter 5, I provided evidence that TREK-1 channels may play an important functional role in mouse intestine, with their pharmacological activation resulting in smooth muscle relaxation. However, verification was constrained by a lack of well-defined $K_{2P}$ modulators and species specific pharmacology. I utilised a number of defined TREK family activators, however a number of these have been shown to modulate other ion channels, some of which may be expressed in GI tissues. Likewise, demonstrating the specificity of the activators in the GI tract was hampered by a lack of specific TREK family channel blockers. For example, BL-1249 induced a potent GI tract relaxation in pre-contracted ileum and colon, and has been shown previously to activate all mechano-gated TREK channels (including TREK-1, TREK-2 and TRAAK), although BL-1249 external application exhibit different selectively with different $EC_{50}$ to members of the TREK subfamily (Pope et al., 2018). Spadin has been proposed to be a specific TREK-1 blocker (Mazella et al., 2010), but I observed no effect on either spontaneous contractility or in inhibiting relaxation induced by BL-1249 in my organ bath studies. This brought into question whether spadin is indeed a blocker of TREK-1 and whether its mechanism of block would be expected to prevent the activity of BL-1249. Further to this, the inhibitory effects of spadin have only been studied in AA-activated TREK-1 currents, and its impact on TREK channel currents activated by other chemical compounds are currently lacking. Therefore, the aim of this chapter was to investigate the pharmacological specificity and the inhibition activity of spadin in the presence of different chemical activators of the mechano-gated $K_{2P}$ channels TREK-1, TREK-2 and TRAAK. Channels were overexpressed in *Xenopus* oocytes and ion channel mediated potassium currents measured using the two-electrode voltage clamp technique.

Furthermore, given that mouse tissue had been used through my whole project, for consistency the mouse homologues of the three TREK channels were used to allow direct comparison to other data in my thesis. However, the cloned mouse channels have not been described previously and so in the first instance, their biophysical phenotypes were sought.

## 6.2 Results

### 6.2.1 Biophysical characterisation of mouse TREK-1, TREK-2 and TRAAK channels

*Xenopus laevis* oocytes were injected with 2-10 ng of cRNA encoding the mTREK-1 and mTREK-2 channels and 20 ng of cRNA encoding the mTRAAK and assessed using TEVC. To obtain a comprehensive picture of mTREK-1, mTREK-2 and mTRAAK channels, I measured currents in response to 1-s voltage steps (from -120 to +60 mV). Robust ionic currents were recorded in standard bath solution containing 4 mM $K^+$ from both mTREK-1 (**Figure 6.1, A1**) and mTREK-2 (**Figure 6.1, B1**) expressing oocytes, but were very small in mTRAAK (**Figure 6.1, C1**) expressing oocytes. In addition, significant currents were not observed in un-injected oocytes. The phenotype of all three channel currents resembled that of characterised human $K_{2P}$ channels, displaying no time-dependent activation, strong outwardly rectifying currents in physiological solutions, with minimal inward currents observed in 4 mM $K^+$. However, when the external $K^+$ concentration ($[K^+]_{out}$) was increased to 20 mM, 100 mM and 140 mM $K^+$ respectively, the I-V curves were shifted rightwards, and prominent inward currents were revealed upon hyperpolarization below $E_K$ for all three channels (**Figure 6.1, A2, B2 & C2**). The experimental data aligns with that predicted by the Goldman Hodgkin-Katz current equation at different $[K^+]_{out}$ concentrations, a

phenomenon described previously in other cloned $K_{2P}$ channels. Increasing extracellular $K^+$ concentration from 4 mM to the highest concentration of 140 mM induced a shift in the voltage threshold at which outward ionic currents could be observed. A plot of the reversal potential as a function of $[K^+]_{out}$ is shown for each channel in Figure 6.1 (A3, B3 and C3). showed that the slope was 47.3 ± 2.2 mV (mTREK-1; *n* = 7), 49.4 ± 0.4 mV (mTREK-2; *n* = 8) and 45.3 ± 3.5 mV (mTRAAK; *n* = 8), which all close to the calculated Nernst value of 58 mV at 20°C, indicating these three channels continue to permit the passage of $K^+$ ions as expected for a highly selective $K^+$ channel.

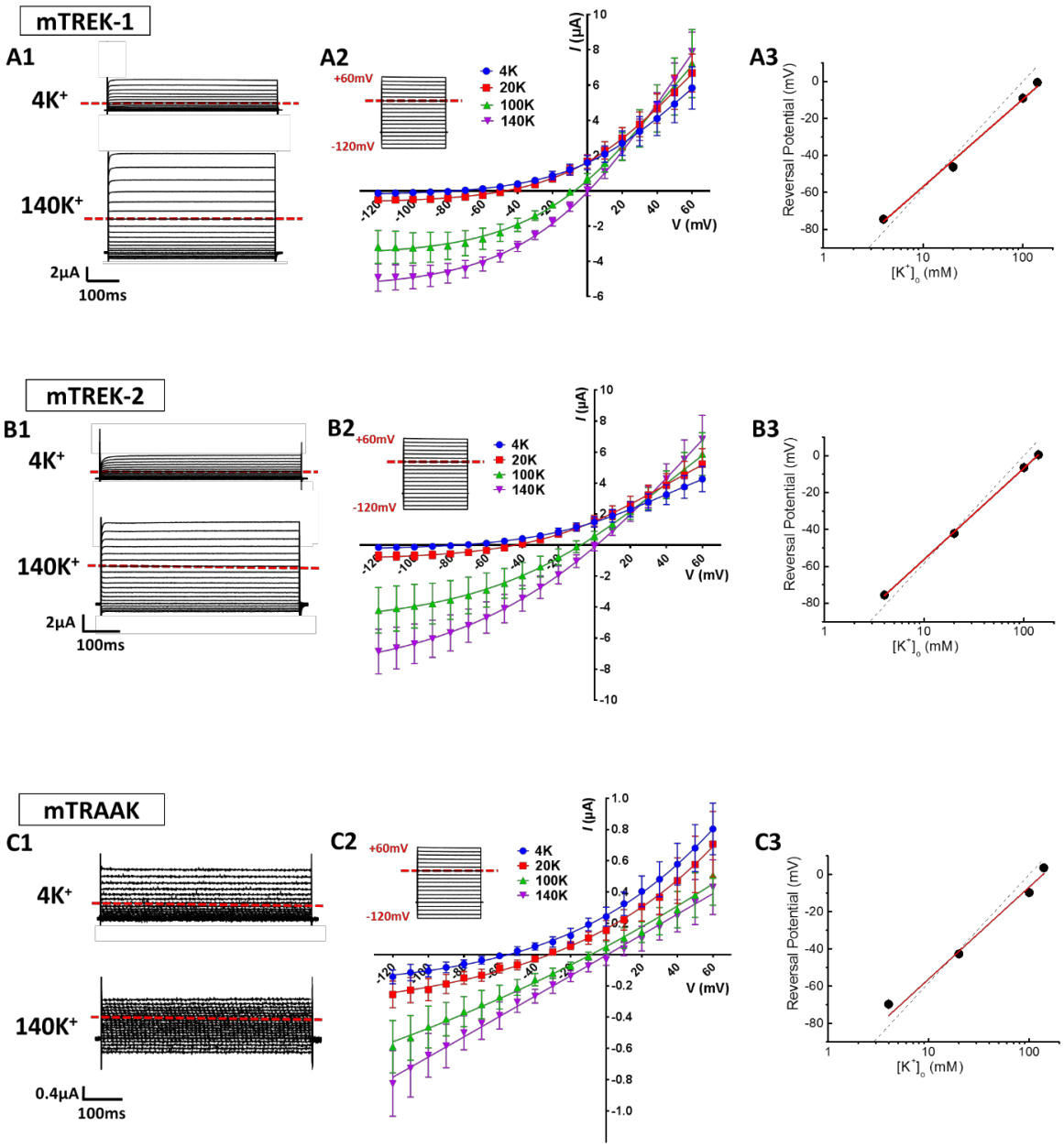


**Figure 6.1.** Biophysical characterisation of mTREK-1 **(A1-A3)**, mTREK-2 **(B1-B3)** and mTRAAK **(C1-C3)**. Currents of mTREK-1 **(A1)**, mTREK-2 **(B1)** and mTRAAK **(C1)** elicited by voltage pulses from -120 to +60 mV in 10 mV steps, 1 s in duration, from a holding potential of -80 mV, in low $K^+$ solutions (4 mM) or high $K^+$ solutions (140 mM). In each panel, scale bars represent 2 $\mu$A and 100 ms. The 0 mV current level is indicated by red dashed line. Mean current-voltage (I-V) relationships taken from steady-state currents in the presence of differing concentrations of extracellular $K^+$; 4 mM (blue), 20 mM (red), 100 mM (green) and 140 mM (purple) for mTREK-1 (**A2**, $n$ = 7), mTREK-2 (**B2**, $n$ = 8) and mTRAAK (**C2**, $n$ = 8). Reversal potentials of mTREK-1 currents **(A3)**, mTREK-2 currents **(B3)** and mTRAAK currents **(C3)** were plotted as a function of $[K^+]_{out}$ (mean ± SD). Data points are fitted with a linear relationship (red line). Dashed line represents Nerstian theoretical linear relationship of $E_K$ with changing $[K^+]_o$ as calculated using the Nernst equation assuming $[K^+]_i$ is 140 mM (slope = -58.2 mV).

### 6.2.2 Mutation of predicted SUMOylation sites in mTRAAK channel did not increase channel activity

mTRAAK generated only very small ionic currents at the voltages test, at cRNA concentrations of 20 ng/23 nl and incubation duration of up to 72 hours. Low activity of human TRAAK when expressed heterologously has been described previously (Soussia et al., 2018). The related $K_{2P}$ channel, TWIK-1, has also been shown to be problematic when overexpressed in *Xenopus* oocytes or mammalian cells and its activity at the plasma membrane has been proposed to be influenced by sumoylation of a critical lysine residue in its C-terminus. Mutation of K274 to either an arginine, glutamine, tyrosine or cysteine, prevents sumoylation by SUMO protease (Rajan et al., 2005) and generates robust, functional currents. Thus, I hypothesised whether mTRAAK activity was also similarly controlled by sumoylation in *Xenopus* oocytes. Analysis of the mTRAAK sequence using sumolyation prediction software (GPS-SUMO) highlighted positions K38 ($p$ = 0.072) and K330 ($p$ = 0.047) respectively as highly probably sumoylation sites. Both sites were independently mutated to glutamine (Q) and expressed in oocytes. However, neither K38Q (0.80 ± 0.17 µA versus 0.97 ± 0.40 µA, $p$ = 0.2314, Student's paired *t*-test, **Figure 6.2 A2**) or K330Q (0.80 ± 0.17 µA versus 0.79 ± 0.38 µA, $p$ = 0.9512, Student's paired *t*-test, **Figure 6.2 B2**) mutation produced a significant increase in channel currents, even after prolonged expression durations (up to 72 hours) and injection of high cRNA concentrations (up to 20 ng/23 nl). Given the low functional activity of mTRAAK channels and the inability to increase activity through mutations, it was decided that mTRAAK channel currents would not be used further in this study. However, given time it would be useful in the future to address the low functional expression of this channel. I would be particularly interested to label

mTRAAK channel proteins and to assess their expression levels at the surface of the cell membrane using biotinylation and Western blot techniques.

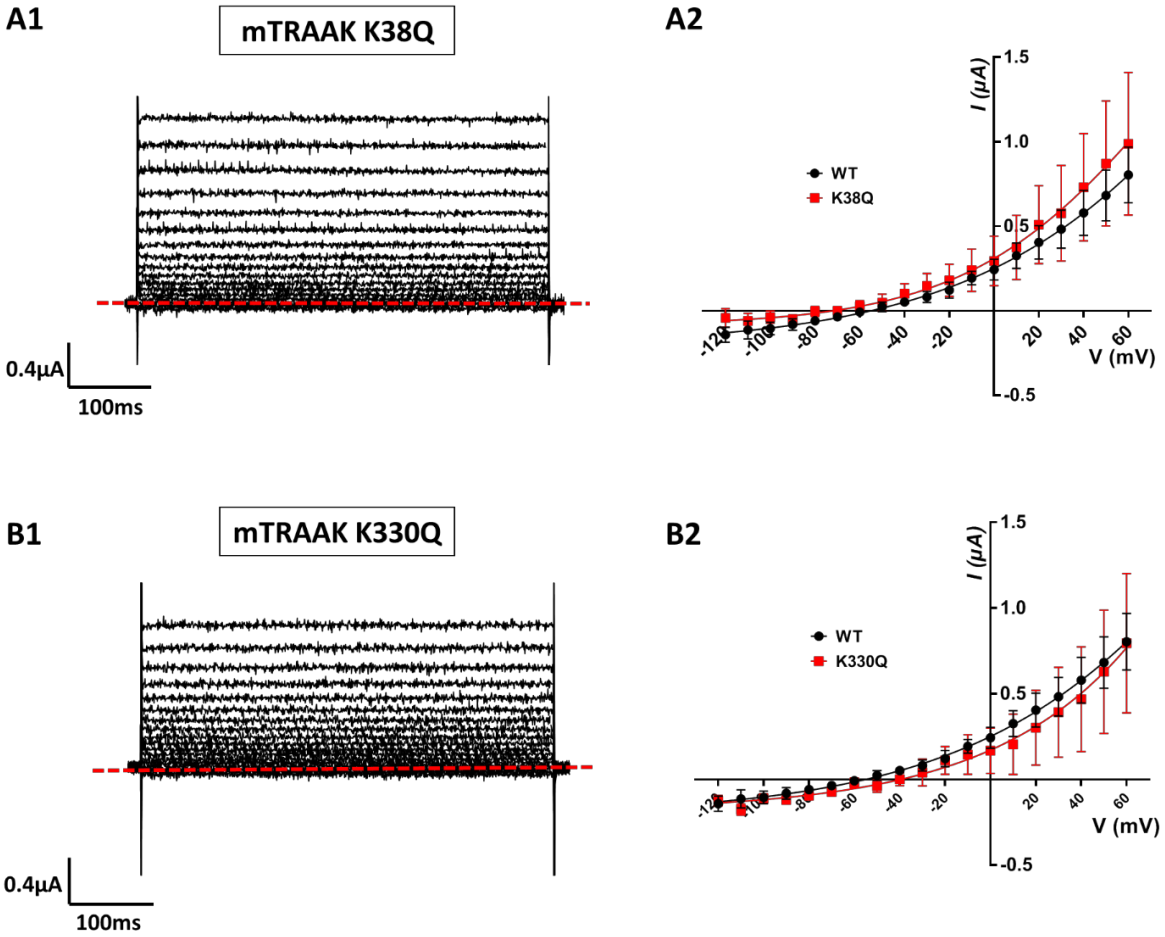


**Figure 6.2.** Exemplar currents of sumoylation mutations of mTRAAK channel; in the N-terminus K38Q **(A1)** and the c-terminus K330Q **(B1)**. Currents were elicited by voltage pulses from -120 to +60 mV in 10 mV steps, 1 s in duration, from a holding potential of -80 mV, in recording solution with concentration 4 mM $K^+$. In each panel, scale bars represent 0.4 $\mu$A of current and 100 ms time. The red dashes line indicated the current at -80 mV to point zero current. **A2** and **B2** indicate mean steady-state current-voltage (I-V) relationship for WT mTRAAK (black) and K38Q mutation and K330Q mutation (red) respectively.

### 6.2.3 Pharmacological characterisation of mTREK-1 and mTREK-2 channels

Given the pharmacological results from my previous organ bath investigations, I felt it pertinent to establish a clear pharmacology profile of mTREK-1 and mTREK-2 channels, and therefore decided to expose mTREK-1 and mTREK-2 channels heterologously expressed in *Xenopus* oocytes to previously characterised human TREK family pharmacological agents (e.g. activators AA, BL-1249, CDC, and the blocker $Ba^{2+}$). AA is a well-established activator of mammalian $K_{2P}$ channels, having been shown to activate currents in all TREK family subtypes (Fink et al., 1996, Bang et al., 2000, Lesage et al., 2000). BL-1249 has been shown to greatly increase hTREK-1 currents at 1 µM (Veale et al., 2014), whereas CDC has been shown to be a potent activator of bTREK-1 channels at a concentration of 10 µM (Danthi et al., 2004). It was important to establish whether extracellular application of these regulators would elicit a response in mouse homologues of TREK channels. **Figure 6.3** shows representative whole-cell current traces and I-V relationship curve of mTREK-1 in both control ($4K^+$ solution) alone and in the presence of 10 µM AA (**Figure 6.3 A**), 1 µM BL-1249 (**Figure 6.3 B**), 10 µM CDC (**Figure 6.3 C**) and 1mM $Ba^{2+}$ (**Figure 6.3 D**). mTREK-1 currents at 0 mV were significant increased by application of AA (256.8 ± 6.7 %, $n$ = 8, $p$ = 0.0005, Student's paired $t$-test), BL-1249 (392.9 ± 29.5 %, $n$ = 9, $p$ = 0.0003, Student's paired $t$-test) and CDC (307.8 ± 10.1 %, $n$ = 8, $p$ < 0.0001, Student's paired $t$-test) respectively (**Figure 6.5 A**). Application of 1 mM $Ba^{2+}$ exhibited a significant reduction of mTREK-1 currents, with an inhibition of 56.1 ± 1.4 % at 0 mV compared to control ($n$ = 7, $p$ < 0.0001, Student's paired $t$-test; **Figure 6.5 A**).

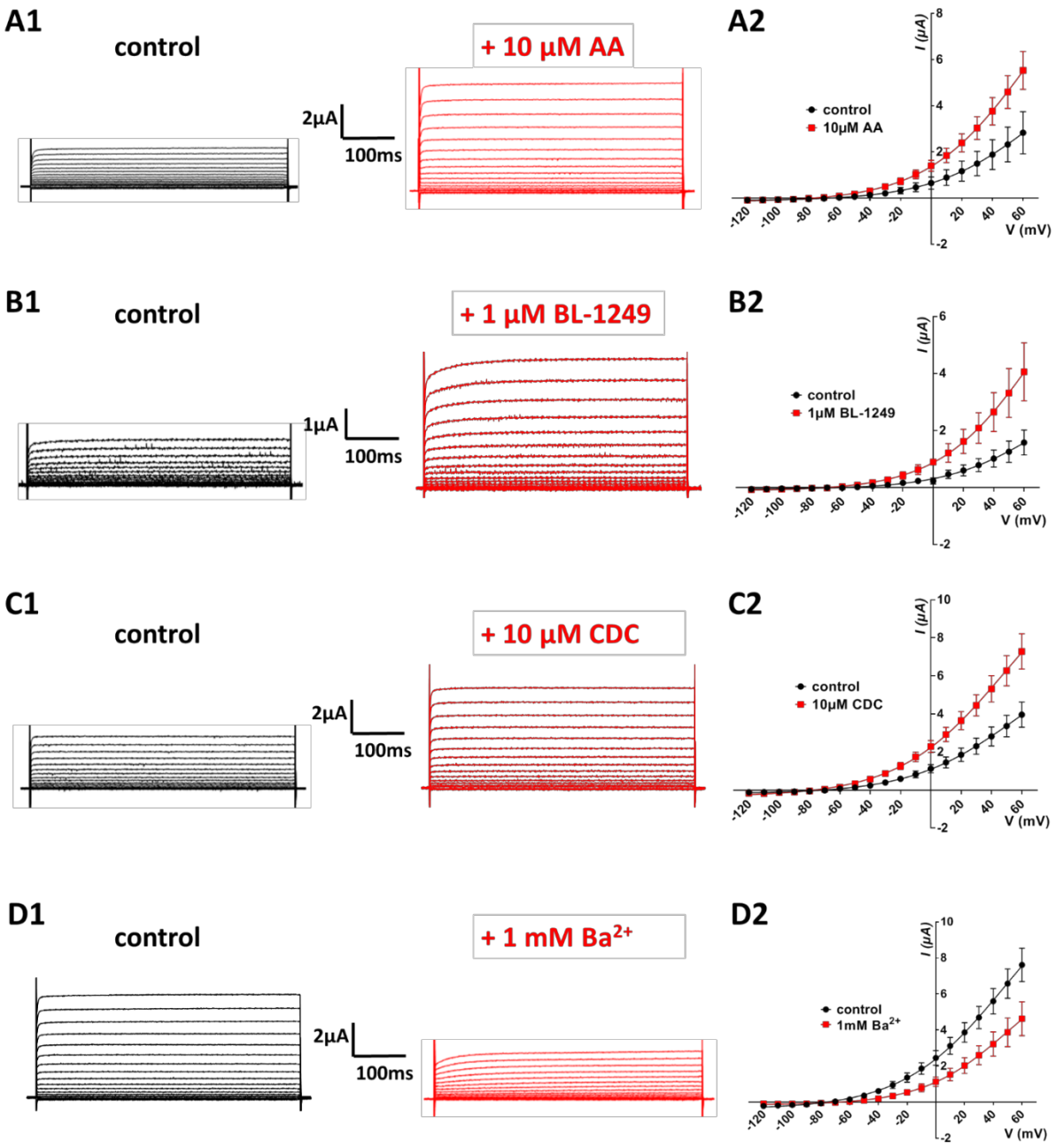


**Figure 6.3:** TEVC measurements of mTREK-1 in different TREK pharmacological modulators. **(A1-D1)** Whole-cell current measurements taken from *Xenopus laevis* oocytes in 4 mM KCl (Control) and AA (10 µM), BL-1249 (1 µM), CDC (10 µM) and $Ba^{2+}$ (1 mM). **(A2-D2)** Mean steady-state current-voltage (I-V) relationship for mTREK-1 control (Black) and drug (Red).

Similar activation and inhibition effects were observed in mTREK-2 channel. **Figure 6.4** shows representative whole-cell current traces and I-V relationship curve of mTREK-2 in both control ($4K^+$ solution) alone and in the presence of 10 µM AA (**Figure 6.4 A**), 3 µM BL-

1249 (**Figure 6.4 B**), 10 μM CDC (**Figure 6.4 C**) and 1mM $Ba^{2+}$ (**Figure 6.4 D**) respectively. Application of 10 μM AA induced a significant augmentation of mTREK-2 currents compared to control at 0 mV, with an increase of 265.77 ± 6.5 % ($n$ = 6, $p$ < 0.0001, Student's paired t-test; **Figure 6.5 B**). Application of 3 μM BL-1249 exhibited a significant activation in mTREK-2 currents, with an increase of 378.2 ± 42.5% ($n$ = 9, $p$ = 0.005, Student's paired $t$-test; **Figure 6.5 B**). Measurement of the concentration-response curves for BL-1249 activation of mTREK-1 and mTREK-2 channels is displayed in **Figure 6.6 A**. Concentration-response curves did not saturate and therefore $EC_{50}$ was not estimated. The data suggest that extracellular application of BL-1249 activates both mechano-gated TREK-1 and TREK-2 channels, having a more potent effect on TREK-1. Application of 10 μM CDC exhibited a significant enhancement of mTREK-2 currents, with an increase of 333.7 ± 19.3 % at 0 mV compared to control ($n$ = 6, $p$ = 0.0006, Student's paired $t$-test; **Figure 6.5 B**). Construction of concentration-response curves for mTREK-1 and mTREK-2 to extracellular application of CDC (**Figure 6.6 B**) revealed similar effects with currents size augmentation at the highest concentration of CDC (30 μM) being 3.3 ± 0.4 μA and 3.7 ± 0.5 μA for mTREK-1 and mTREK-2, respectively. Similar to mTREK-1, mTREK-2 currents recorded at 0 mV exhibited significant decrease in the presence of 1 mM $Ba^{2+}$ (55.5 ± 3.4 % of inhibition, $n$ = 7, $p$ = 0.0004, Student's paired $t$-test; **Figure 6.5 B**). These results demonstrated that mTREK-1 and mTREK-2 possess a similar pharmacological phenotype as their human counterparts, and can be activated by AA, BL-1249 and CDC, and inhibited by barium.

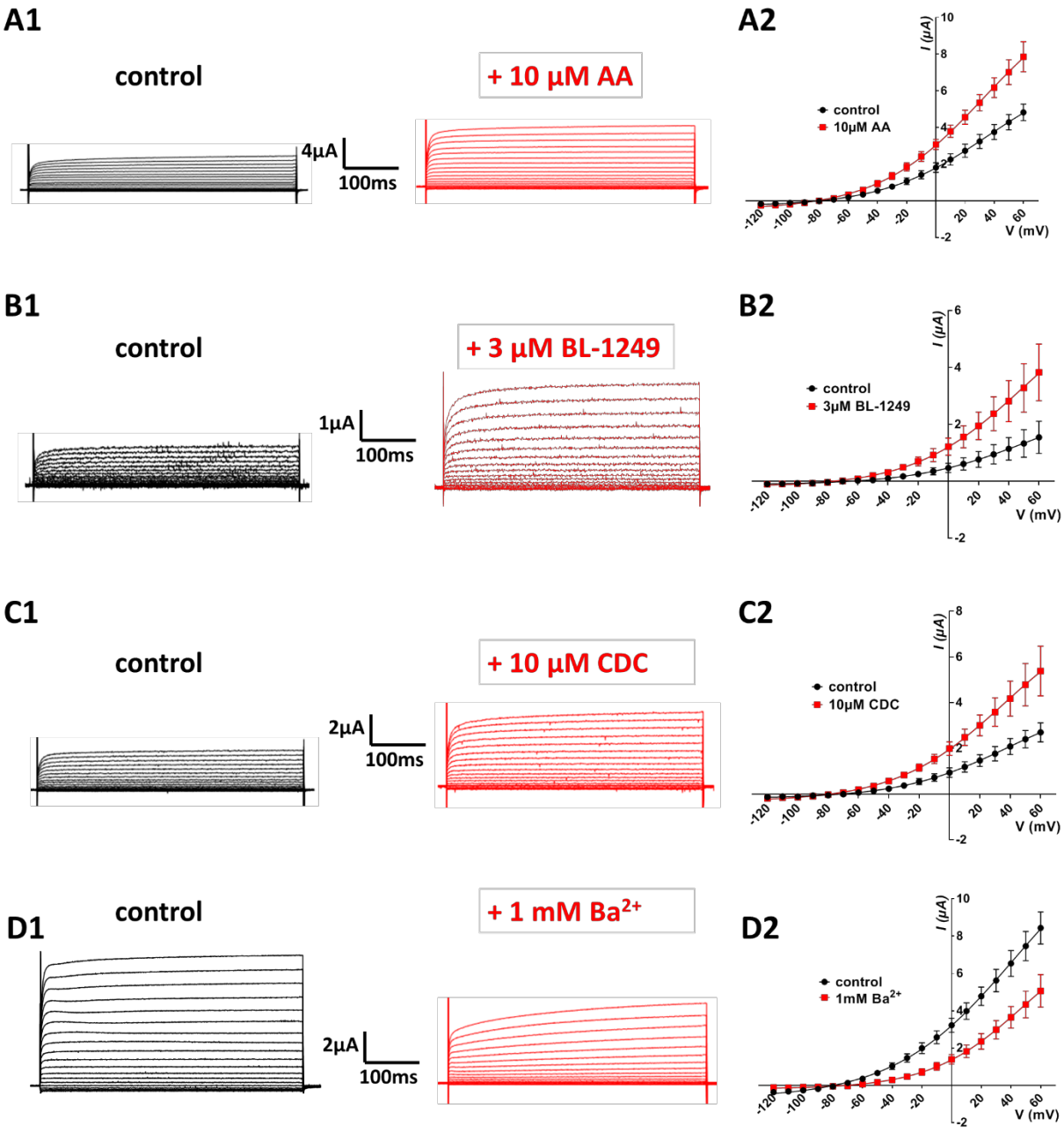


**Figure 6.4:** TEVC measurements of mTREK-2 in different TREK pharmacological modulators. **(A1-D1)** Whole-cell current measurements taken from *Xenopus laevis* oocytes in 4 mM KCl (Control) and AA (10 µM), BL-1249 (1 µM), CDC (10 µM) and $Ba^{2+}$ (1 mM). **(A2-D2)** Mean steady-state current-voltage (I-V) relationship for mTREK-2 control (Black) and drug (Red).

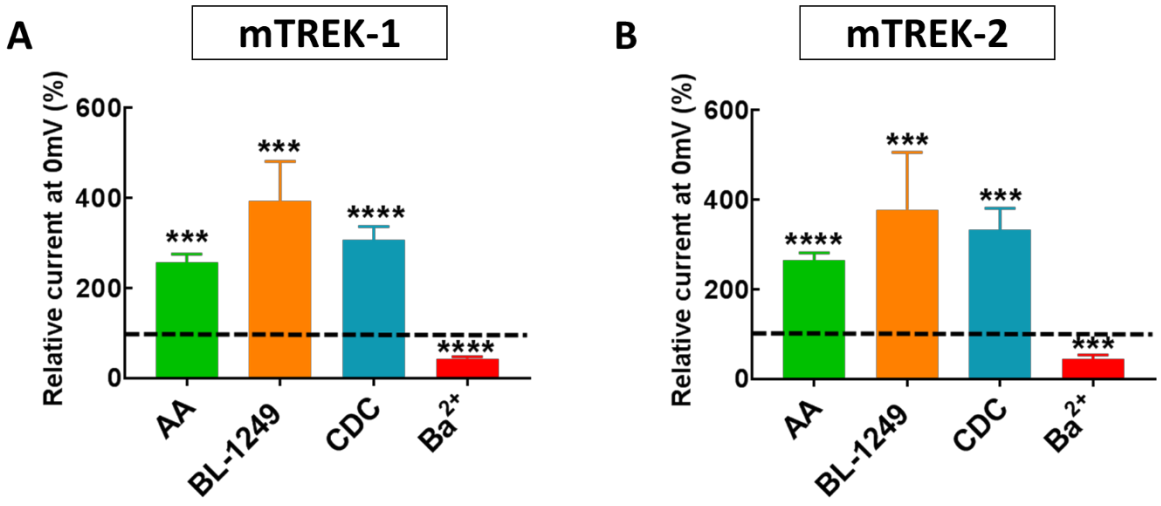


**Figure 6.5:** Mean normalized activation (%) of AA, BL-1249, CDC and $Ba^{2+}$ in mTREK-1 **(A)** and mTREK-2 **(B)** currents measured at 0 mV. Dashes line indicated the basal line, data below the line means the inhibition effects. Error bars represent SD. All data represents *n* > 6 oocytes. ****P* < 0.001, *****P* < 0.0001, Student's paired *t*-test.

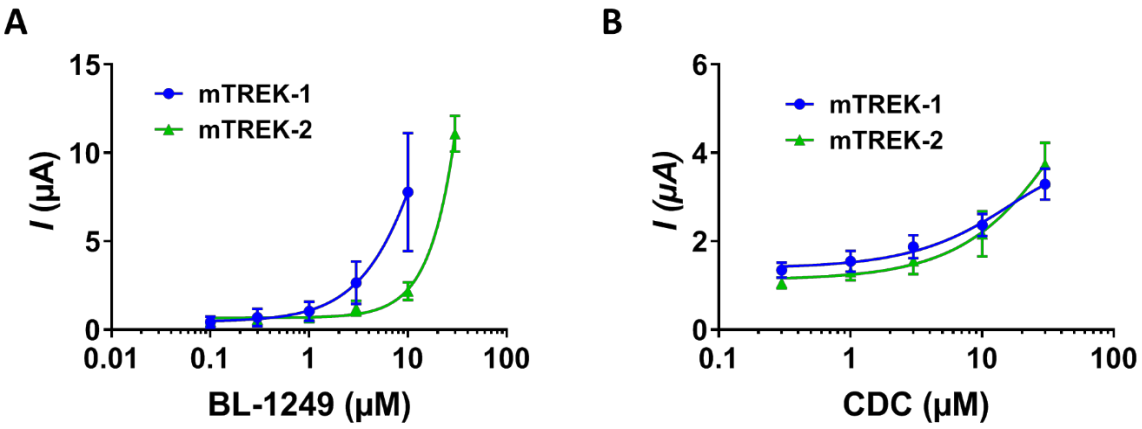


**Figure 6.6:** External application of BL-1249 and CDC selectively activates mechano-gated TREK channels. **(A)** BL-1249 dose-response curves for mTREK-1 (blue circles), mTREK-2 (green triangles), (*n*=9 in both). **(B)** CDC dose-response curves for mTREK-1 (blue circles), mTREK-2 (green triangles). (*n*=8 and 6 respectively).

### 6.2.4 Spadin does not block baseline or AA-activated mTREK-1 channels

Spadin has been proposed to be a blocker of TREK-1 channels, with 100 nM spadin apparently blocking 63 ± 12 % of the hTREK-1 current after stimulation by AA (Mazella et al., 2010). However, application of 1 µM spadin exhibited no effects in my previous organ bath study and led me to speculate whether the published effects were possibly species specific or channel specific and what the mechanism of action of this compound might be. Therefore, the effects of spadin were studied on the mTREK-1 channel expressed in *Xenopus* oocytes using TEVC. Firstly, I wanted to see if I could recapitulate previous findings using the mouse homologue, so mTREK-1 channels were activated with 10 µM AA and when the current amplitude stabilised I measured the ability of 1 µM spadin to inhibit the mTREK-1 channel activity (time scale of this effect shown in **Figure 6.7 A1**). Spadin did not significantly affect the amplitude of AA-activated mTREK-1 measured at 0 mV (**Figure 6.7 A2**). Values of current density were 1.9 ± 0.1 µA (AA activated current, *n* = 8) and 2.1 ± 0.1 µA (AA activated current + spadin, *n* = 8). Furthermore, mTREK-1 basal channel activity was also insensitive to spadin, with channel currents at 0 mV measured as 1.4 ± 0.1 µA (control mTREK-1 current, *n* = 12) versus 1.5 ± 0.1 µA (in the presence of 1 µM spadin, *n* = 12) (**Figure 6.7 B2**).

### 6.2.5 Spadin specifically antagonises AA-activation of mTREK-1 channels

Given that spadin was not a blocker of mTREK-1, I decided to investigate whether spadin could antagonise AA-activation of mTREK-1 channels. Oocytes were incubated for 5-10 mins in bath solution containing 1 µM spadin before subsequent addition of 10 µM AA (time scale of this experiment shows in **Figure 6.7 B1**). Pre-application of 1 µM spadin

significantly perturbed the activation of mTREK-1 channels by AA by 52.2 ± 14.7% ($n$ = 12, $p$ < 0.0001, one-way ANOVA) (**Figure 6.7 B2**). Full activation of mTREK-1 channels was observed after removal of spadin. These data suggest that spadin does not block mTREK-1 channels, but rather antagonises its activation by AA.

In order to further investigate the action of spadin on mTREK-1 channels, I wanted to assess the effects of spadin in the presence of another PUFA to assess the specificity of spadin activity. DHA is a related PUFA and has been reported activated TREK-1 channels (Patel et al., 2001). Application of 10 µM DHA exhibited a significant enhancement of mTREK-1 currents, with an increase of 2.3 ± 0.2-fold at 0 mV compared to control ($n$ = 6, $p$ = 0.0003, one-way ANOVA; **Figure 6.7 C**). However, 1 µM spadin did not affect the current amplitude measured at 0 mV of the DHA-activated mTREK-1 currents (**Figure 6.7 C** 2.6 ± 0.2 µA (DHA activated current, $n$ = 6) versus 2.9 ± 0.3 µA (DHA activated current + spadin, $n$ = 6, $p$ = 0.53, one-way ANOVA). Moreover, spadin did not prevent the DHA stimulation of mTREK-1 currents (**Figure 6.7 D**). At membrane potential of 0 mV, currents were 3.0 ± 0.3 µA versus 3.3 ± 0.2 µA in the presence ($n$ = 7) and absence respectively of spadin ($n$ = 7, $p$ = 0.88, one-way ANOVA).

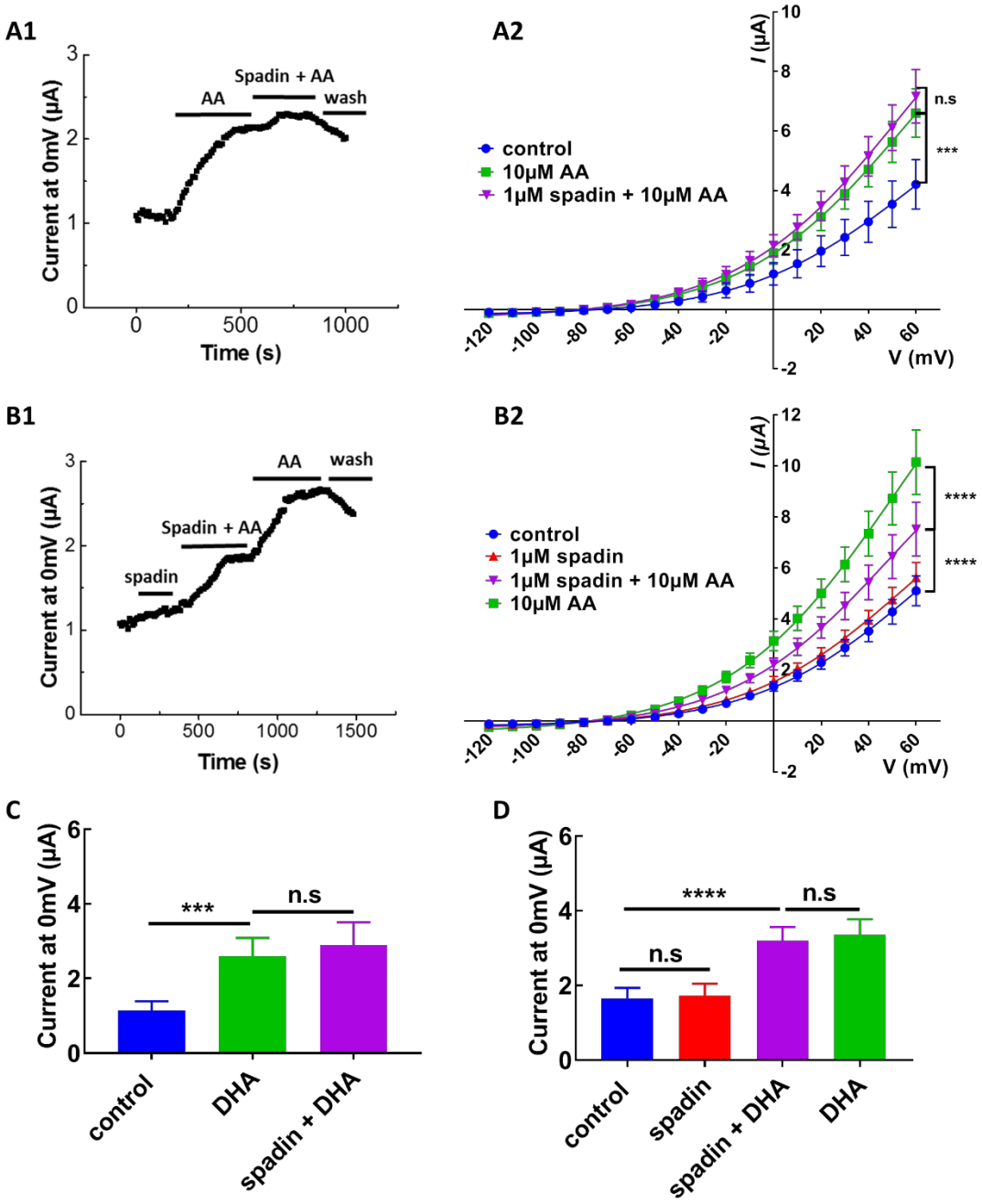


**Figure 6.7:** Effects of spadin on the mTREK-1 channel activity. **(A1, B1)** show time series plot of currents at 0 mV evoked from oocytes by adding spadin (1 μM) before the AA-activation and after the AA-activation. **(A2, B2)** I-V plots for effects of spadin in mTREK-1 currents. **A2,** currents were recorded after mTREK-1 AA-activation by 10 μM arachidonic acid (AA) and AA + spadin (1 μM) (*n* = 8). **B2,** currents were recorded in absence (control) and in presence of spadin (1 μM), followed by AA (10 μM) + spadin (1 μM) and then AA (10 μM) (*n* = 12). **(C-D)** Mean current amplitudes recorded at 0 mV with bath conditions (control; 4 $K^+$) and following treatment with the agents spadin (1 μM), DHA (10 μM) and DHA + spadin (1 μM). The effects of spadin after DHA-activation shows in (**C**, *n* = 6), before shows in (**D**, *n* = 7). Error bars represent SD, ****P* < 0.001, *****P* < 0.0001, one-way ANOVA followed by Tukey's multiple comparisons test.

Given the clear results and the conflict with previous findings I decided to investigate whether spadin shows same activity in human TREK-1 channels under the same conditions. Similar effects were observed in hTREK-1 channel (**Figure 6.8**), application of 1 µM spadin did not inhibit AA-activated currents at 0 mV; 3.6 ± 0.3 µA (AA-activated current, *n* = 8) and 3.9 ± 0.5 µA (AA-activated current + spadin, *n* = 8, *p* = 0.16, one-way ANOVA; **Figure 6.8 A**). Nor did 1 uM spadin block the hTREK-1 channel basal current at 0 mV, which were measured as 2.4 ± 0.3 µA (without spadin, n = 10) and 2.4 ± 0.4 µA (with spadin, *n* = 10, *p* = 0.99, one-way ANOVA; Figure 6.6, B).Furthermore, pre-application of 1 uM spadin significantly antagonised AA-activation of hTREK-1 at 0 mV by 67.9 ± 18.6% (*n* = 10, *p* < 0.0001, one-way ANOVA; **Figure 6.8 B**). Therefore, I conclude that the mechanism of action of spadin involves antagonism of AA-activation of TREK-1 channels, a mechanism that appears to be lipid specific.

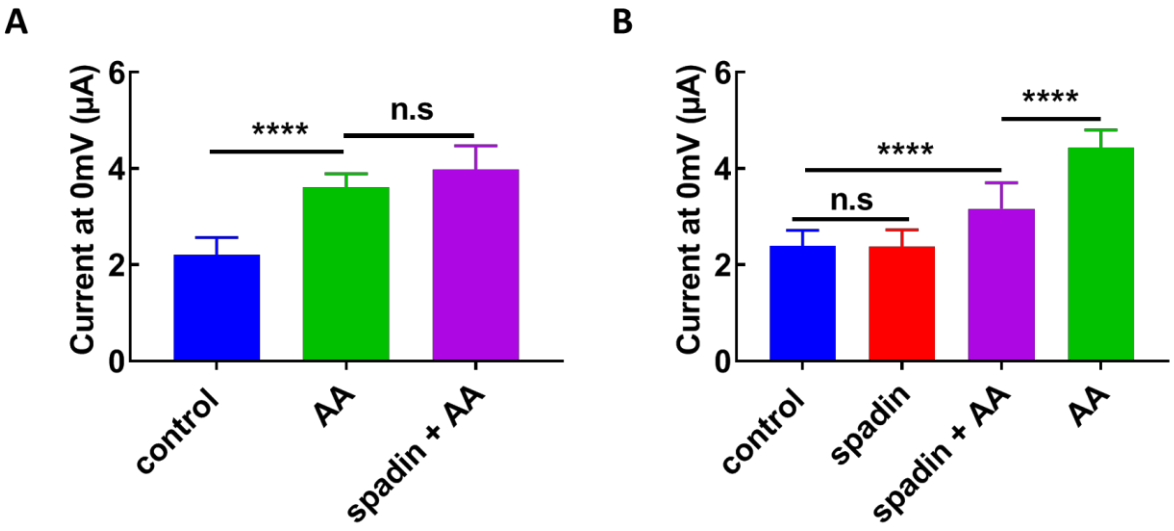


**Figure 6.8:** Effects of spadin on hTREK-1 channel activity. Mean currents were recorded at 0 mV. **(A)** shows the effect of 1 µM spadin applied after AA-activation of hTREK-1 currents (*n* = 8). **(B)** displays the effect of 1 µM spadin applied before AA-activation of hTREK-1 currents (*n* = 10). Error bars represent SD, *****P* < 0.0001, one-way ANOVA followed by Tukey's multiple comparisons test.

### 6.2.6 Spadin does not affect AA-activation of mTREK-2 channels

Given the effects of spadin on human and mouse TREK-1 channels, and the close biophysical phenotypes of TREK-1 and TREK-2, the effects of spadin were tested on mTREK-2 channels**. Figure 6.9** shows that 1 µM spadin was unable to block mTREK-2 channel activated by AA (**Figure 6.9 A2**); currents measured at 0 mV were 3.1 ± 0.1 µA and 3.3 ± 0.1 µA in the absence (*n* = 7) or presence of spadin (*n* = 7) respectively. Again, spadin alone failed to inhibit mTREK-2 currents under standard bath conditions. The current densities measured at 0 mV were 2.2 ± 0.1 µA (control mTREK-2 current, *n* = 10) and 2.3 ± 0.1 µA (in the presence of spadin, *n* = 9, *p* = 0.99, one-way ANOVA; **Figure 6.9 B2**). Furthermore, it was observed that the antagonistic effect of spadin on AA-activation in mTREK-1 channels was absent in mTREK-2 channels (**Figure 6.9 B1, B2**). Pre-application of 1 µM spadin showed a small antagonization of the AA activation of mTREK-2 at 0 mV by 25.8 ± 23.11 %, but this is not statistically significant (*n* = 9, *p* = 0.99, one-way ANOVA; **Figure 6.9 B2**).

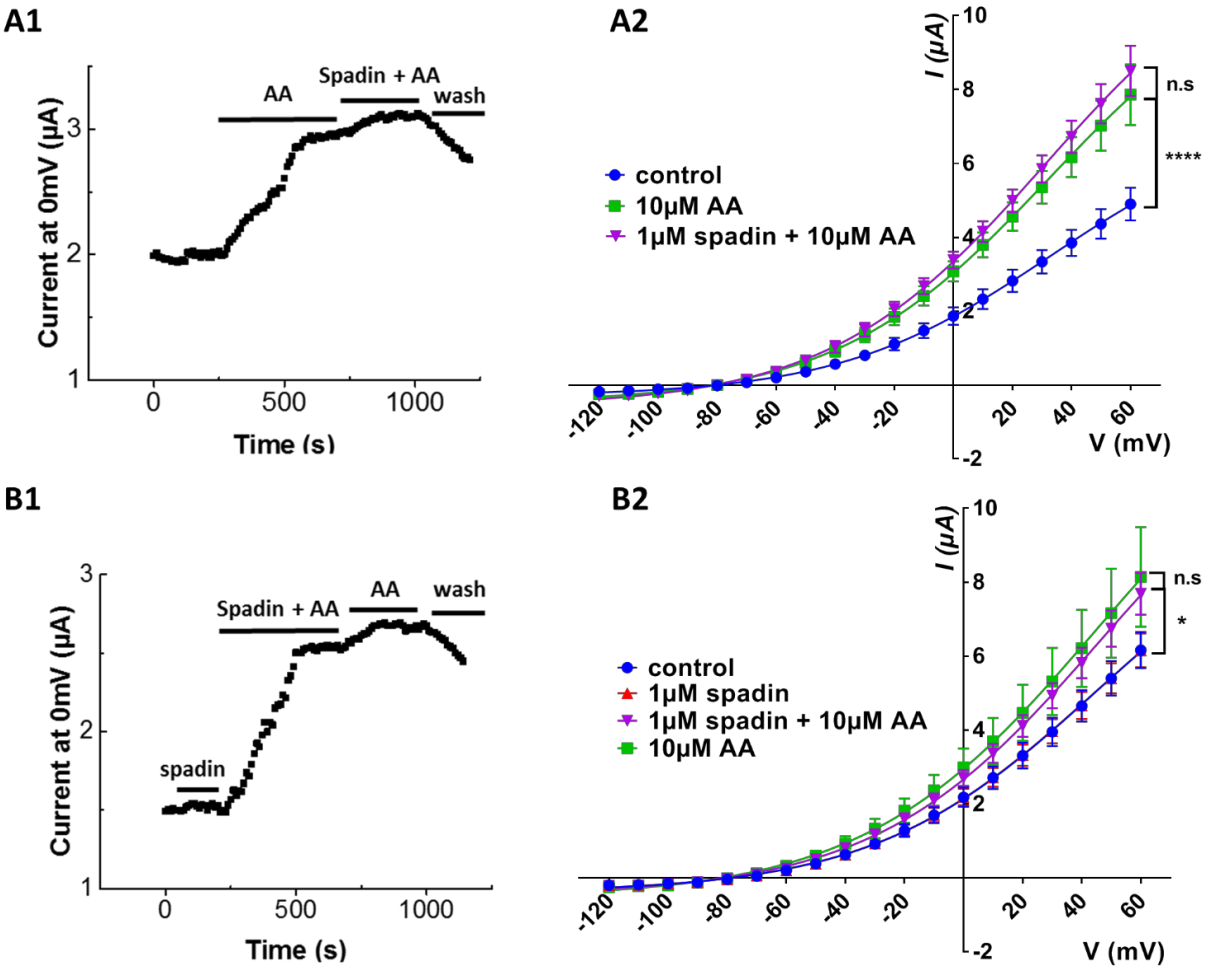


**Figure 6.9.** Effects of spadin on the mTREK-2 channel activity. **(A1, B1)** show time series plot of currents at 0 mV evoked from oocytes by adding spadin (1 μM) before the AA-activation and after the AA-activation. **(A2, B2)** I-V plots for effects of spadin in mTREK-2 currents. **A2**, currents were recorded after mTREK-2 AA-activation by 10 μM arachidonic acid (AA) and AA + spadin (1 μM) (*n* = 7). **B2**, currents were recorded in absence (control; 4 $K^+$) and in presence of spadin (1 μM), followed by AA (10 μM) + spadin (1 μM) and then AA (10 μM) (*n* = 9). Error bars represent SD, **P* < 0.05, *****P* < 0.0001, one-way ANOVA, followed by Tukey's multiple comparisons test.

### 6.2.7 Spadin does not antagonise other known activators of TREK channels

To investigate whether spadin also influences the activation of mTREK-1 and mTREK-2 channels induced by other TREK family agonists, I applied spadin to mTREK-1 and mTREK-2 before the addition of the cyclooxygenase (COX) inhibitor BL-1249 or CDC. Neither activation of mTREK-1 nor mTREK-2 currents by BL-1249 were significantly antagonised by

pre-exposure to 1 μM spadin. Values of current density recorded at 0 mV were [**Figure 6.10 A**; mTREK-1, 3.3 ± 0.2 μA (1 μM BL-1249 with spadin) and 3.5 ± 0.2 μA (1 μM BL-1249 without spadin), $n$ = 10, $p$ = 0.74, one-way ANOVA; **Figure 6.10 B**; mTREK-2, 2.8 ± 0.1 μA (3 μM BL-1249 with spadin) and 2.9 ± 0.2 μA (3 μM BL-1249 without spadin), $n$ = 10, $p$ = 0.93, one-way ANOVA]. Consistent with our data obtained with BL-1249, the observed activation of CDC (10 μM) recorded at 0 mV was not antagonised by spadin in either mTREK-1 currents (**Figure 6.10 C**) or mTREK-2 currents (**Figure 6.10 D**). The mean values of currents in mTREK-1 channel were measured as 3.4 ± 0.1 μA (10 μM CDC with spadin, $n$ = 10) and 3.7 ± 0.2 μA (10 μM CDC without spadin, $n$ = 10, $p$ = 0.35, one-way ANOVA). The mean values of currents in mTREK-2 channel were measured as 2.8 ± 0.2 μA 10 μM CDC with spadin, $n$ = 8) and 3.1 ± 0.3 μA (10 μM CDC without spadin, $n$ = 8, $p$ = 0.56, one-way ANOVA). Therefore, I conclude that neither BL-1249 nor CDC activation of mTREK-1 and mTREK-2 channels was antagonised by spadin.

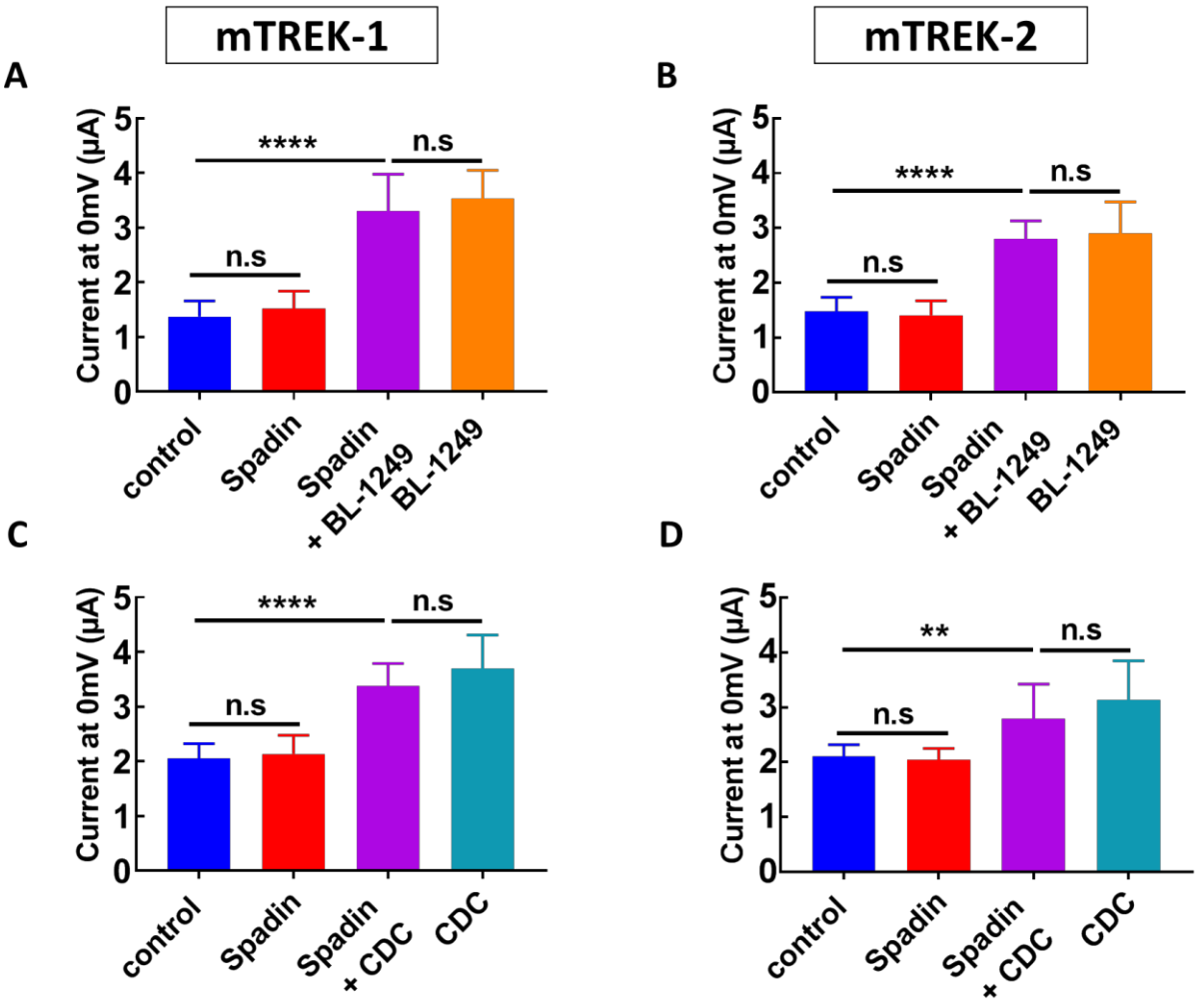


**Figure 6.10**. Effects of spadin on BL-1249/CDC-activation of mTREK-1 and mTREK-2 channels activity. Mean currents of mTREK-1 (**A,** *n* = 10) and mTREK-2 (**B,** *n* = 10) measured at 0 mV with bath conditions (control; 4 K) and following treatment with the agents spadin (1 µM); BL-1249 (1 µM in mTREK-1 and 3 µM in mTREK-2) + spadin (1 µM); and BL-1249 on its own (1 µM in mTREK-1 and 3 µM in mTREK-2). As above, currents of spadin + CDC (10 µM) at 0 mV were recorded before the activation of 10 µM CDC in mTREK-1 (**C**, *n* = 10) and mTREK-2 (**D**, *n* = 8). Error bars represent SD, ***P < 0.01*, *****P* < 0.0001, one-way ANOVA.

### 6.2.8 $Ba^{2+}$ blocks both AA and BL-1249 activation of mTREK-1 and mTREK-2 channels

To confirm that activated TREK-1 channels could be inhibited I applied $Ba^{2+}$ to AA and BL-1249 activated mTREK-1 and mTREK-2 currents. As expected, in mTREK-1 currents measured at 0 mV, 1 mM $Ba^{2+}$ significantly blocked AA-activated currents by 46.2 ± 5.3% (currents from 2.23 ± 0.1 µA reduced to 1.23 ± 0.1 µA, $n$ = 8, $p$ < 0.05, Student's paired t-test; **Figure 6.11 A1**) and BL-1249 activation by 39.1 ± 3.0 % (currents from 2.6 ± 0.1 µA reduced to 1.6 ± 0.1 µA, $n$ = 10, $p$ < 0.05, Student's paired t-test; **Figure 6.11 A2**). In mTREK-2 currents measured at 0 mV, 1 mM $Ba^{2+}$ significantly blocked AA-activation in 37.2 ± 5.5% (currents from 2.81 ± 0.1 µA reduced to 1.8 ± 0.1 µA, $n$ = 6, $p$ < 0.05, Student's paired t-test; **Figure 6.11 B1**) and BL-1249 activation in 35.5 ± 4.2% (currents from 2.1 ± 0.2 µA reduced to 1.3 ± 0.1 µA, $n$ = 9, $p$ < 0.05, Student's paired t-test; **Figure 6.11 B2**). These data confirm that the known pore blocker $Ba^{2+}$ is able to block both AA and BL-1249 activated mTREK-1 and mTREK-2 currents and helps to reinforce the notion that spadin is not a blocker of mTREK-1 channels.

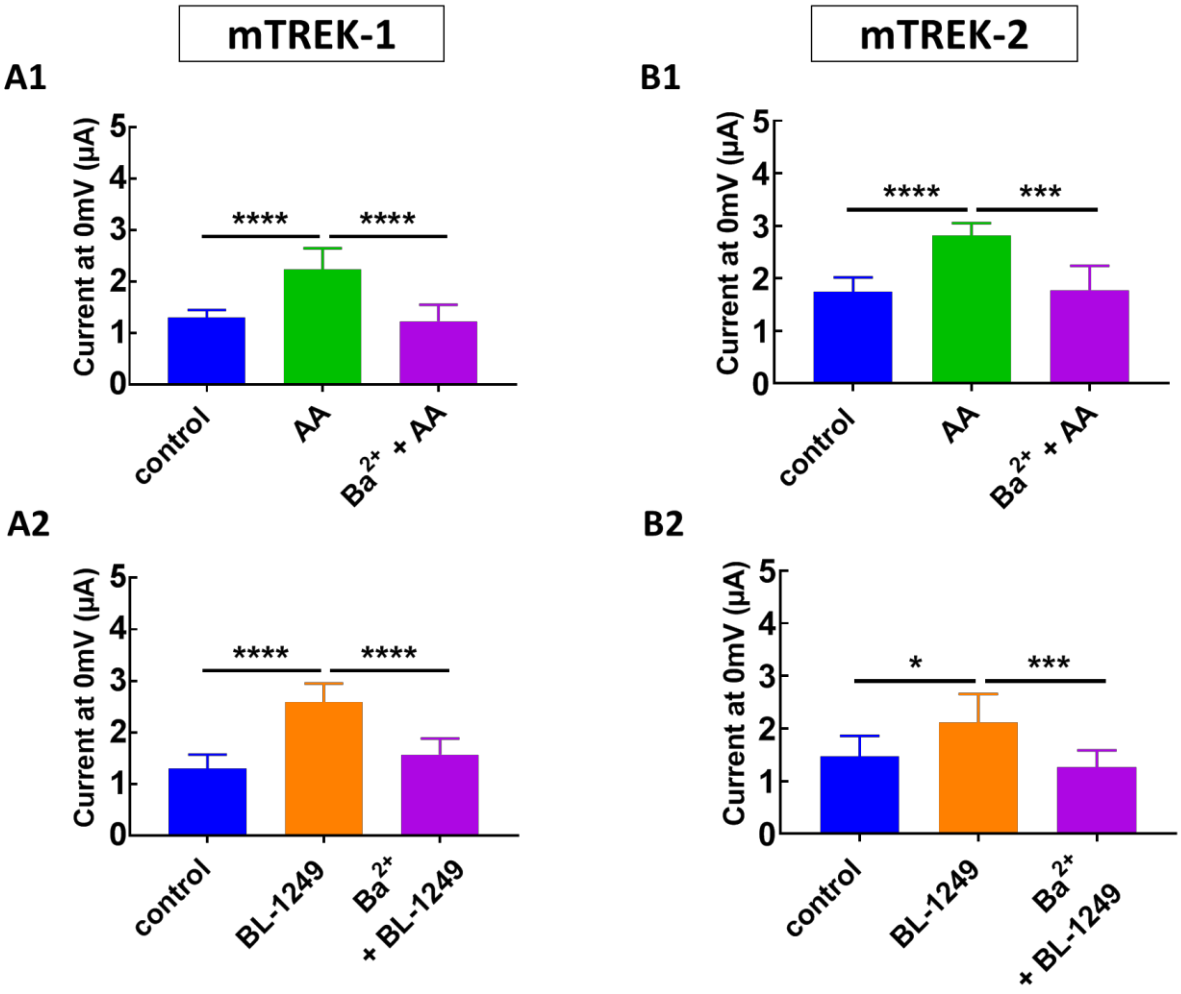


**Figure 6.11.** Effects of $Ba^{2+}$ on the mTREK-1 and mTREK-2 channel activity**.** Mean currents of $Ba^{2+}$ + AA and $Ba^{2+}$ + BL-1249 were measured at 0 mV after pre-activation of mTREK-1 by 10 µM AA (**A1,** *n* = 8) and 1 µM BL-1249 (**A2**, *n* = 10). Mean currents for mTREK-2 at 0 mV showing effects of 1 mM $Ba^{2+}$ after 10 µM AA (**B1**, *n* = 6) and 3 µM BL-1249 (**B2**, *n* = 9) activation. Error bars represent SD. * $P < 0.05$, *** $P < 0.001$, **** $P < 0.0001$, Student's paired *t*-test.

### 6.2.9 Spadin antagonism does not involve the C-terminus of mTREK-1

Gating stimuli detected by sensors in various parts of the channel converge on the $K_{2P}$ selectivity filter C-type gate (Schewe et al., 2016, Lolicato et al., 2017). Previous evidence suggests the C-terminal domain is the sensor for TREK-1 activation by both physiological and chemical activators (Honore et al., 2002, Lotshaw, 2007, Chemin et al., 2007). Notably, previous research infers AA binds on the proximal c-terminus to activate the TREK channels (Patel et al., 1998). Therefore, we hypothesised spadin may share the same/similar binding site as AA in order to specifically antagonise AA activation of TREK-1 channels. Given the insensitivity of mTREK-2 channels to spadin, I generated a mTREK-2/TREK-1 chimera construct consisting the N-terminus and 4 transmembranes of mTREK-2 and C-terminus of mTREK-1 (**Figure 6.12 A**). The hypothesis was that if spadin bound to the c-terminus of TREK-1 to antagonise AA-activation, transfer of this domain to the insensitive mTREK-2 channel should also transfer spadin sensitivity. TEVC experiments showed that this chimera formed a functional channel generating robust currents analogous to the parental mTREK-1 and mTREK-2 channels (**Figure 6.12 B, C**). Plotting reversal potential in different external $K^+$ concentrations generated a Nernstian slope of 43.7 ± 2.9 mV ($n$ = 6), which was close to that predicted by the Nernst equation for a highly selective $K^+$ channel. As expected, this chimera construct generated currents that were still significantly activated by 10 µM AA; 1.63 ± 0.1-fold ($n$ = 7, $p$ < 0.0001, one-way ANOVA; **Figure 6.12 D**) at 0mV. Similar to their parental channels, 1 µM spadin did not inhibit the pre-activated AA currents in this chimera, which were measured as 3.7 ± 0.2 µA (AA-activated current, $n$ = 7) and 4.0 ± 0.2 µA (AA-activated current + spadin, $n$ = 7; **Figure 6.12 D**). In addition, application of 1 µM spadin did not affect this chimera basal channel activity, with no significant change in

currents measured at 0 mV; 2.1 ± 0.2 µA (control, *n* = 8) and 2.2 ± 0.2 µA (in presence of spadin, *n* = 8; **Figure 6.12 E**). In contrast to mTREK-1 channels, 1 µM spadin failed to antagonise AA-activation of the mTREK-2-mTREK-1 c-terminal chimera currents with currents measuring at 0 mV; 4.2 ± 0.4 µA (AA activated current + spadin, *n* = 8) and 4.5 ± 0.4 µA (AA alone, *n* = 8, *p* = 0.67, one-way ANOVA; **Figure 6.12 E**). As AA activation is preserved, but spadin no longer antagonises AA activation I suggest that the C-terminal domain does not contribute directly to spadin activity.

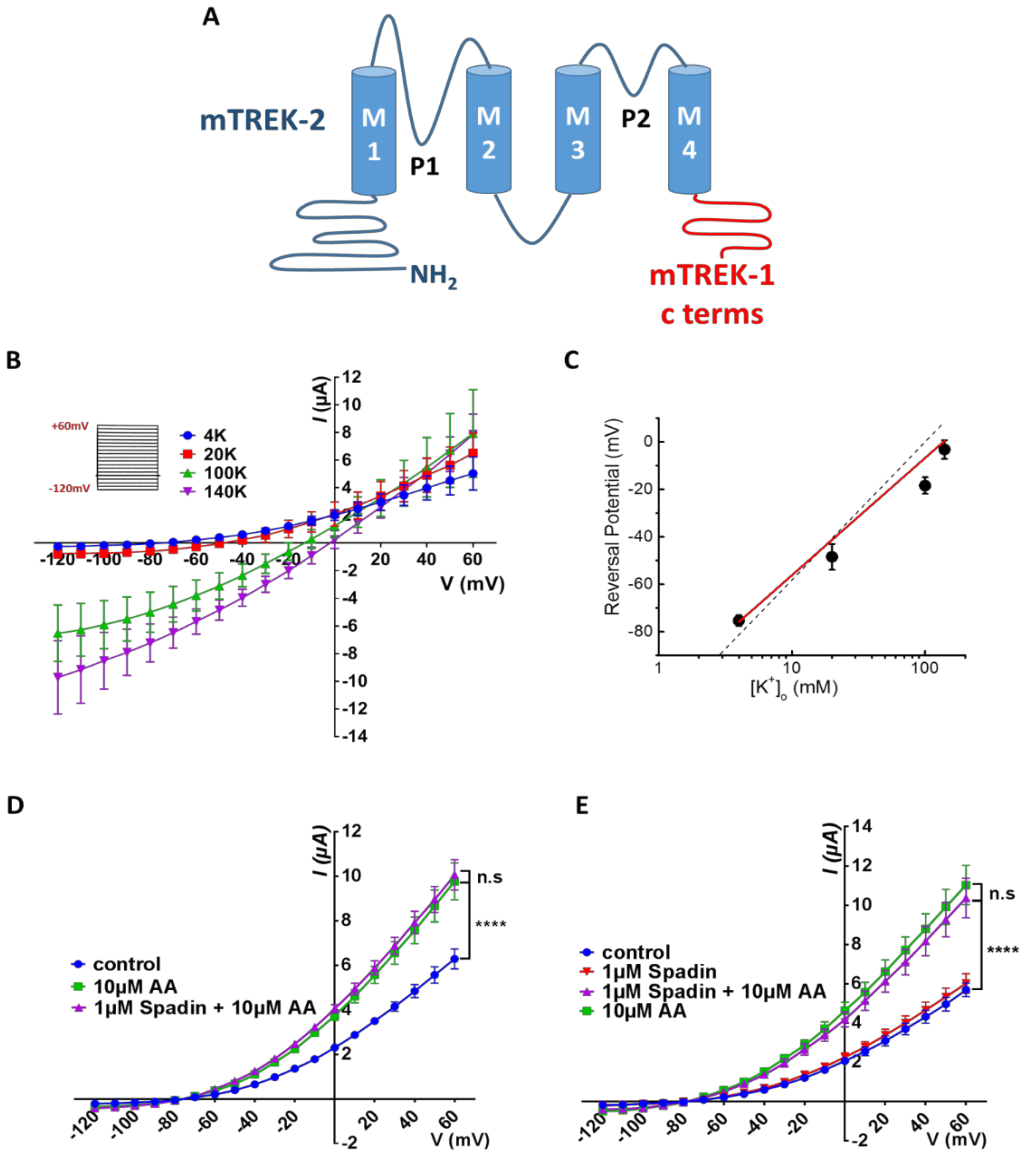


**Figure 6.12. (A)** shows the cartoon structure of the mTREK-2-mTREK-1-c-terminal chimera construct. **(B)** Mean current-voltage (I-V) relationships taken from steady-state currents in the presence of differing concentrations of extracellular K+; 4 mM (blue), 20 mM (red), 100 mM (green) and 140 mM (purple), *n* = 6. Currents of the chimera elicited by voltage pulses from -120 to +60 mV in 10 mV steps, 1 s in duration, from a holding potential of -80 mV, in low $K^+$ solutions (4 mM) or high $K^+$ solutions (140 mM). Reversal potentials of chimera currents **(C)** were plotted as a function of $[K+]_{out}$ (mean ± SEM). Data points are fitted with the Goldman-Hodgkin-Katz voltage equation (lines). Currents were measured in K+ solutions respectively 4 mM, 20 mM, 100 mM and 140 mM. Data points are fitted with a linear relationship (red line). Dashed line represents Nerstian theoretical linear relationship of $E_K$ with changing $[K^+]_o$ as calculated using the Nernst equation assuming $[K^+]_i$ is 140 mM (slope = -58.2 mV). **(D, E)** I-V plots for effects of spadin in chimera currents. **D,** currents were recorded after chimera AA-activation by 10 μM arachidonic acid (AA) and AA + spadin (1 μM) (*n* = 7). **E,** currents were recorded in absence (control) and in presence of spadin (1 μM), followed by AA (10 μM) + spadin (1 μM) and then AA (10 μM) (*n* = 8). Error bars represent SD, *****P* < 0.0001, one-way ANOVA.

Overall, these data suggest that spadin is an allosteric antagonist of mTREK-1 channels, preventing AA-activation. This antagonism is specific to TREK-1 channels and is specific to AA-activation. Moreover, the mechanism of spadin antagonism does not involve the C-terminus of mTREK-1.

## 6.3 Discussion

In my previous chapters, I demonstrated that mechano-gated TREK subfamily channels not only exhibit distinctive expression patterns in mouse intestinal smooth cells and enteric neurons, but also play a function role in regulating the mouse intestinal smooth muscle contractility. Hence, pharmacological manipulation of TREK subfamily channels could be a vital new therapeutic target for treating GI motility disorders. In order to understand the physiological roles of TREK channels in the mouse model, a pharmacological profile of different mouse TREK channels needs to be established, at least initially, through the application of known TREK channels activators and inhibitors, to isolated heterologously expressed mouse channels. These important details are currently lacking in the literature. So to allow comparison of TREK-1, TREK-2 and TRAAK channel properties in mouse tissue to previous reports, mouse homologues of TREK-1, TREK-2 and TRAAK were expressed in *Xenopus* oocytes and their biophysical properties and pharmacological phenotypes assessed through TEVC analysis. However, mTRAAK was failed to produce robust currents despite varying concentrations of cRNA, expression durations and creating de-sumoylated mutants. The data within this chapter show both TREK-1 and TREK-2 channels are sensitive to pharmacological activators of the mechano-gated $K_{2P}$ channels, with particular potency

exhibited by the fenamate, BL-1249. Investigation into the activity and specificity of spadin towards TREK-1 and TREK-2 channels suggested a structural component, such as the C-terminus, may be responsible for the mechanism of action of antagonism of AA-activation of TREK-1 channels. Transplant of the c-terminus from the spadin sensitive m TREK-1 channels to the spadin insensitive mTREK-2 channel failed to transfer spadin activity, suggesting spadin does not bind on the C-terminus to antagonise AA action in TREK-1 channels.

### 6.3.1 Heterologous expression of mTRAAK in *Xenopus laevis* oocytes

Injection of individual cloned mouse TREK channel cRNAs into *Xenopus* oocytes resulted in robust, measurable currents from mTREK-1 and mTREK-2 but not for mTRAAK, despite various attempts using altered concentrations and incubation times. There could be several reasons as to why mTRAAK failed to elicit substantial currents; 1) proteins were not efficiently translated; 2) proteins were translated but not efficiently trafficked to the cell membrane; 3) proteins may form functional expression by requiring accessory or regulatory subunits, such as SUMO, analogous to the $K_{2P}$ channel TWIK-1 (Rajan et al., 2005), or Mtap2, like the $K_{2P}$ channel TREK-1 (Sandoz et al., 2008); 4) channels have a low open probability; 5) TRAAK channels have a low single channel conductance (Soussia et al., 2018, Blin et al., 2016). Previous studies revealed that the silent $K_{2P}$ channel, TWIK-1, could be awakened by perturbing sumoylation via mutation of the binding site at K274 to either an arginine, glutamine, tyrosine or cysteine (Rajan et al., 2005, Plant et al., 2005). To test the hypothesis that sumoylation was involved in low TRAAK activity, high probability SUMO sites in TRAAK were mutated. Mutations at sites K38 and K330 failed to elicit a substantial

increase in currents suggesting mTRAAK activity is not regulated by sumoylation. Regulatory partners or accessory proteins play an important role in mammalian and plant $K_{2P}$ channel trafficking and regulation (Noel et al., 2011). Unlike TRAAK, TREK-1 and TREK-2 have protein partners regulating their channel activity, such as A-kinase-anchoring protein (AKAP150) and Microtubule-associated protein 2 (Mtap2) (Noel et al., 2011). AKAP150 binds to a major regulatory domain located in the C-terminus of TREK-1, promoting a drastic increase in channel currents which are unable to be further enhanced by polyunsaturated fatty acids, acidic pH, or stretch but can still be regulated by protein kinase (Sandoz et al., 2006). Mtap2 is another identified constituent protein of TREK channels in the brain, binding to TREK-1 and TREK-2 does not affect channel activity directly but increases channel surface expression and current density (Sandoz et al., 2008). The beta-coatomer protein complex (β-COP) as another interacting partner of TREK-1 binding on the N-terminus by enhancing the TREK-1 channel surface expression (Kim et al., 2010). It is not known if β-COP interacts with TREK-2 and TRAAK, however, this does present a potential probability for future investigation.

All these three TREK subfamily channels have a similar unitary conductance in physiological conditions (Fink et al., 1998, Patel et al., 1998), however, TREK-1 and TREK-2 display larger currents than TRAAK, when they are in the same expression conditions (Levitz et al., 2016), indicating differences in the number of channels at the membrane or open probability of individual channels. In this same study, it was demonstrated that co-assembly of TREK channels could occur, forming functional heterodimers (Levitz et al., 2016). When TREK-1 is co-expressed with TREK-2, heterodimers display voltage-dependent gating and open

probability similar to TREK-1 homodimers (Blin et al., 2016). TRAAK can form heterodimers with both TREK-1 and TREK-2 (Levitz et al., 2016). TREK-1/TRAAK heterodimers exhibit functional, regulatory and pharmacological differences from TRAAK homodimers. TREK-1/TRAAK heterodimers are stimulated by both intracellular acidification and alkalinisation, and regulated by the enzyme phospholipase D2 (Levitz et al., 2016). Activation of protein kinase A (PKA) down-regulates TREK-1 and TREK-1/TRAAK, although displays no effect to TRAAK (Blin et al., 2016). Moreover, heterodimerization also impacts channel pharmacology in TREK-1/TRAAK. TREK channels modulators such as fluoxetine and ML67 display different sensitivities towards TREK1/TRAAK heterodimers versus TREK-1 or TRAAK homodimers (Blin et al., 2016). This may suggest that TRAAK preferentially assembles with other TREK subfamily channels *in-vivo* rather than forming a homodimer. Given the distinct expression profiles of TREK-1 and TRAAK in mouse GI tract, functional studies of TREK-1/TRAAK heterodimers were not pursued.

Recently, the proximal C-terminal domain (pCt) of TREK channels has been reported as a key element in regulating the channel basal currents (Soussia et al., 2018). Notably, this pCt region exhibits opposite effects in TREK-1 and TRAAK, which stimulate activity in TREK-1 and impairs TRAAK activity. Deletion of this region dramatically decreased TREK-1 current amplitude whereas increased TRAAK current by 13-fold. Moreover, the same effects were observed when the two pCt were swapped (Soussia et al., 2018). Therefore, this could be another reason to explain why TRAAK is less active than other two channels and produces small currents in basal conditions.

### 6.3.2 mTREK-1 and mTREK-2 display comparable biophysical and pharmacological phenotypes as their human orthologues

To compare the properties of TREK-1 and TREK-2 channels in mouse tissue to previous organ bath studies, mouse homologues of TREK-1 (mTREK-1) and TREK-2 (mTREK-2) were characterised after expression in *Xenopus* oocytes. Expression of mTREK-1 in oocytes resulted in a conductance with similar electrophysiological properties as the human TREK-1 (hTREK-1) and a previously characterised colonic conductance postulated to be TREK-1 (Fink et al., 1996, Koh et al., 2001). There is no previous research documenting the properties of mouse TREK-2, therefore the results presented in this chapter provides new insight. My data reveals that mTREK-2 channels share very similar biophysical properties as its rat TREK-2 (rTREK-2) and human TREK-2 (hTREK-2) counterparts (Bang et al., 2000, Lesage et al., 2000).

Polyunsaturated fatty acids, including arachidonic acid (AA) have been revealed to activate all mechano-gated $K_{2P}$ channels (TREK-1, TREK-2 and TRAAK) (Fink et al., 1998, Bang et al., 2000, Kim et al., 2001a). BL-1249, a non-steroid anti-inflammatory drug has been shown to directly and reversibly activate TREK-1, TREK-2 and TRAAK channels (Veale et al., 2014, Pope et al., 2018), and the caffeic acid derivative, CDC, to activate TREK-1 (Danthi et al., 2004). All three compounds produced activation effects on both mTREK-1 and mTREK-2 channel currents. In addition, BL-1249 produced more potent activation of mTREK-1 than mTREK-2 echoing a previous study (Pope et al., 2018). However, a novel finding from my experiments was the activation of mTREK-2 by CDC, which displays a similar potency as mTREK-1. However, the mechanism of action of CDC has not been elucidated, and future

studies describing the binding site and mechanism of action should be sought. Furthermore, given the number of research studies conducted in mice, and their use as a model for many physiological processes and pathologies, the biophysical and pharmacological characterisation of two cloned mouse TREK channels here provides useful and timely information for future studies in this model.

### 6.3.3 Spadin specifically antagonizes the activation of TREK-1 channels by AA, but not other pharmacological activators

Recently, a new antidepressant peptide, spadin, was described as a blocker of TREK-1 channels, and a new potential therapeutic treatment for depression (Mazella et al., 2010, Borsotto et al., 2015). The authors showed that spadin was able to block TREK-1 activation stimulated by 10 µM AA ($IC_{50}$ = 71 nM) in COS-7 cells. The action of spadin on TREK-1 was also confirmed in brain slices by directly recording hippocampal CA3 pyramidal cells. Moreover, this inhibitory effect of spadin on AA stimulated current in CA3 neurons was absent in the same experimental conditions in the TREK-1 knock-out mice, which confirmed the specificity of spadin for TREK-1 channels (Mazella et al., 2010). However, I was unable to reproduce these findings in my oocyte expression system with either human or mouse TREK-1 channels. On the contrary, data from my study indicates that spadin does not block mTREK-1 currents under basal conditions, but rather antagonises mTREK-1 activation by AA. Given the stark contrast to previous findings, my experiments characterised the activity of spadin when applied after AA addition and also before AA addition, experiments not described in previous studies.

Taken together my data suggested spadin to be an antagonist of TREK-1 channel activation, rather than a "blocker" as previously perceived. In order to help understand the mechanisnm of action of spadin, and how it may act as an antagonist, it was important to establish whether this antagonism was modulator specific, i.e. prevented TREK-1 channel activation by any chemical modulator, or whether this was specific to lipid activation. My results clearly show that spadin was unable to antagonise the activation of TREK-1 channels by BL-1249 or CDC, or indeed by other lipid modulators such as DHA (Fink et al., 1998). These data led me to propose that spadin specifically antagonises the activation of mTREK-1 channels by AA, and not other pharmacological activators.

### 6.3.4 How does spadin antagonise TREK-1 channel activation by AA?

Spadin may antagonise AA-activation in TREK-1 channels by allosteric or orthosteric antagonism, meaning it may have a different binding site from AA on the channel protein and induce a change in the conformation of the protein that affects subsequent AA binding, or it may bind to the same site as AA and prevent AA activity directly. A recent set of studies investigating the state-depending binding of fluoxetine in TREK channels could possibly explain any potential allostery. Crystal structures of TREK-1 (Lolicato et al., 2017), TREK-2 (Dong et al., 2015) and TRAAK (Brohawn et al., 2012) channels in the up and down conformations have been reported, and suggest different conformational gating states, but provide no firm consensus about the structure of the active open state. The crystal structures of the hTREK-2 channel in complex with its inhibitor norfluoxetine suggests that conformational changes induced by drug binding can modulate channel activity (Dong et al., 2015). The authors proposed a gating mechanism of TREK-2 in which movement of the

pore-lining helices converts channel between ‘‘down’’ and ‘‘up’’ functional states. The ‘‘down’’ state represents a closed and poorly conductive state stabilized by inhibitors such as norfluoxetine binding within the fenestrations, whereas the ‘‘up’’ state can be induced by membrane stretch or AA activation and represents an open and more conductive state (Dong et al., 2015). Moreover, many physiological TREK activators, such as AA, $PIP_2$ and intracellular acidification, are thought to act on C-terminus and influence C-type gate through M4 (Dong et al., 2015, Bagriantsev et al., 2012, Lolicato et al., 2014), and shift the channel confirmation from outward rectifier mode to an ohmic ‘‘leak mode’’ (Schewe et al., 2016). In addition, norfluoxetine would access its binding site only when the TREK-2 channel is in the ‘‘down’’ state. TREK-2 shifts to the ‘‘up’’ functional state when activated by AA, and becomes resistant to norfluoxetine (as shown in **Figure 6.13 below**) (McClenaghan et al., 2016). Indeed, the inhibitory ability of norfluoxetine can been markedly reduced by the mutation Y315A locates in channel M4, which promotes a conformation of pore-lining the TREK-1, TREK-2 and TRAAK channel subfamily are thought to be similar, and thus like TREK-2, TREK-1 is proposed to be only sensitive to fluoxetine when it is in the ‘‘down’’ conformation, but not when TREK-1 is stimulated by AA and in the up state (Soussia et al., 2018). Both norfluoxetine and fluoxetine are clinically effective antidepressants which also have been reported as a blocker of TREK channel (Heurteaux et al., 2006). Interestingly, spadin has also been proposed to work as a potential antidepressant peptide for treating the depression. Therefore, I propose that spadin could possibly act in a similar way to fluoxetine, which only being effective when applied before AA. Spadin only binds to TREK-1 channels when the channel is in the so-called ‘‘down’’ conformation, and as such would inhibit subsequent activation by AA. Similarly, when pre-activated by AA and channel will change its confirmation to the “up” state, spadin is no

longer able to bind, and so this model would predict no activity of spadin in AA activated TREK-1 channels.

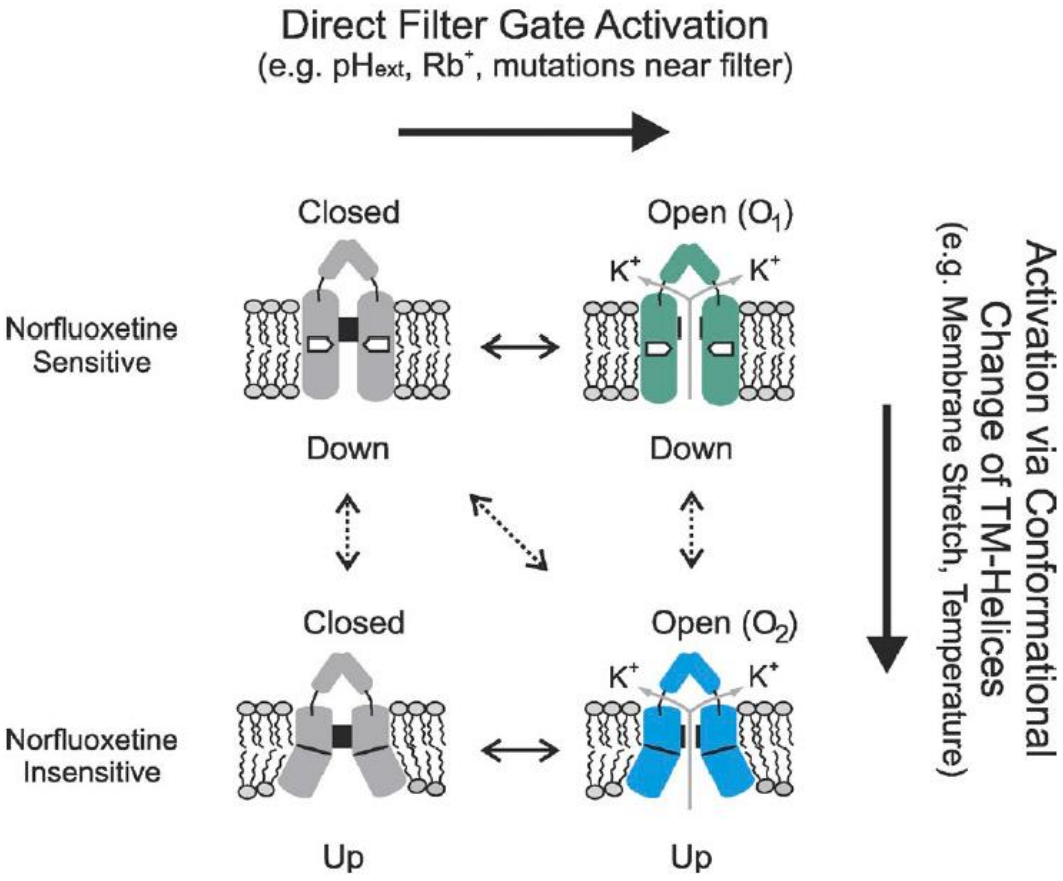


**Figure 6.13**: Expanded gating model for TREK-2 activation. This cartoon illustrates how structurally distinct open states (e.g., O1 and O2) can be produced by different activatory stimuli. The model allows for the filter to gate independently in both the up and down conformations. The dotted line illustrates how the major conformational changes in the TM helices caused by, e.g., membrane stretch and temperature can also influence the filter gating mechanism. The model also shows how the channel can interconvert between different open states in response to membrane stretch (McClenaghan et al., 2016).

Notably, TRAAK displays opposite activity to TREK-1 and TREK-2 in the state-depending binding of fluoxetine. TRAAK is not sensitive to fluoxetine when in the ‘‘down’’ conformation, whereas it becomes sensitive once activated by AA (Soussia et al., 2018). The authors suggest that this opposing behaviour of TRAAK and TREK-1 are due to their

proximal c-terminus (pCt), as swapping this section of the C-terminus between TRAAK and TREK-1 induces an exchange of their activity regarding fluoxetine sensitivity in the stimulated state. In addition, these new findings highlight the significance of the pCt (Soussia et al., 2018). These data suggest that the C-terminal domain plays an important role in influencing the conformational state of TREK-1 and TRAAK channels, and implies the pCt may critical to spadin sensitivity in TREK-1 channel.

### 6.3.5 The role of the C-terminus in AA sensitivity

The finding that spadin does not antagonise other known activators of TREK channels, implied that spadin may share the same binding site as AA in order to specifically antagonise AA activation of TREK-1 channels. A previous report identified that a charge cluster (RVISKKTKEE) in the C-terminal region (Arg297-Glu306) of TREK-1 was a critical binding site for AA sensitivity (Patel et al., 1998, Honore et al., 2002). Interestingly, progressive deletion of the C-terminal domain of TREK-1 reduced sensitivity to AA, but replacing the C-terminal region of TASK-1 and 3 (not stimulated by AA) with TREK-1 do not have any significant effect to AA (Patel et al., 1998, Honore et al., 2002). TREK-2 has been also reported that consist a region of 25 amino-acid between position Arg323 and Thr348, containing a charge cluster (KKTKEE), which are thought to be critical to AA sensitivity (Kim et al., 2001b). However, there is also evidence to suggest the C-terminus plays a less important role, as shown in TRAAK channel, where substitution of a homologous charge cluster results fails to effect of AA sensitivity (Kim et al., 2001a). Taken together with the significance of pCt in TREK-1, I predicted that the C-terminus of TREK-1 would be important in providing the sensitivity to spadin. Replacing the mTREK-2 C-terminal domain with that

from mTREK-1 creates a fully functional channel with biophysical attributes expected of a potassium selective channel, and similar to its parental channels, retains significant AA sensitivity. However, spadin did not antagonise AA stimulated chimera currents indicating that the C-terminal region of TREK-1 is not sufficient nor necessary to mediate the selective action of spadin.

### 6.3.6 Locating the binding site of spadin in TREK-1

It is possible that AA also binds to other regions in TREK-1 and not just in the c-terminus as previously suggested, as TRAAK also contains a cluster of charged amino acids (KVISKKTKEE) in its c terminus, but replacing it with that from TASK-1 or 3 channels still leaves AA sensitivity intact (Kim et al., 2001a). Spadin does not antagonise the effects of BL-1249, and so it is unlikely that spadin binds at this site. Veale *et al*., (2014) identified M1 (W44A), M2 (L174A) and M4 (W275S and W284A) mutations in TREK-1 affect fenamate activation (including BL-1249). Pope *et al*., (2018) suggest the M2/M3 transmembrane helix interface as a key site of BL-1249 sensitivity (Pope et al., 2018), but acknowledge a role for the c-terminus in BL-1249 activation, inferring co-operatively between the pore and c-terminus in determining gating states of the channel. I can rule out spadin as a classical pore blocker given its ineffectiveness on basal or activated currents, which were clearly demonstrated with the classical pore blocker barium. Spadin could possibly share a similar binding site as fluoxetine, since it may become accessible when the pore lining M4 helix adopts a ‘‘down’’ conformation as fluoxetine does. The molecular modelling data of TREK-2 with norfluoxetine shows that this inhibitor binds in a pocket underneath the P2 helix of the selectivity filter at a site that is framed by the M2, M3 and M4 transmembrane helices

(Dong et al., 2015). Notably, disruption of the binding site by the L320W mutation located in M4 helices, reduces the inhibition of TREK-2 by norfluoxetine. Furthermore, the structural data indicates that the primary amine of norfluoxetine is near to the lower side of the selectivity filter where it could influence ion conductivity by disturbing the electrostatic environment of the pore (Dong et al., 2015). These recent findings suggest transmembrane M4 or the channel modulator pocket could be a possible binding site of spadin, although to date no co-crystal structure of TREK with spadin have been studied. To further understand the mechanism action of spadin in TREK-1 channels two approaches could be undertaken; 1) the generation of a chimera by replacing the M2, M3 and M4 of TREK-2 by TREK-1 respectively, 2) utilise molecular modelling of the TREK-1 structure in complex with spadin to identify the highest probable binding site and use mutagenesis to demonstrate proof of principle. To this end, I am currently collaborating with Dr Paul Cox, University of Portsmouth, to identify the binding site of spadin in TREK-1 using molecular modelling technology.

In summary, application of known mechano-gated TREK activators, AA, BL-1249 and CDC resulted in the activation of both mTREK-1 and mTREK-2 channels. The previously proposed blocker of TREK-1 channels, spadin, was found to specifically antagonise AA-activation of TREK-1. Spaidin did not antagonise AA activation of mTREK-2, nor did it antagonise activation by other known TREK activators. Substitution of the C-terminus of mTREK-2 with that of mTREK-1 failed to transfer spadin sensitivity, suggesting its mechanism of action does not likely involve the C-terminus. Further definition of the action site of spadin

through chimera and molecular modelling studies will be crucial for defining how spadin controls TREK-1 activity.

# Chapter 7 – General discussion

## 7.1 Summary and key findings

The overall aim of this thesis was to provide an insight into potassium ion channel expression in the GI system and to understand the physiological contribution and function of mechano-gated $K_{2P}$ subtypes TREK-1, TREK-2 and TRAAK in intestinal smooth muscle. Smooth muscle plays an important role in controlling GI motility, forming mechanical and electrical junctions with neighbouring cells creating a functional syncytium that stimulates coordinated contractions, forcing the food, water and waste to move though the gut (Sanders et al., 2012b). The key findings within this thesis show; 1) many different potassium channel subtypes from $K_v$, $K_{ir}$ and $K_{2P}$ subfamilies are heterogeneously expressed along mouse ileum and colon; 2) $K_{2P}$ channels, TWIK-1 and TASK-2, transcripts and proteins are expressed at high levels across multiple cell types in the GI tract; 3) mechano-gated $K_{2P}$ channel proteins are differentially expressed in GI tract with TREK-1 exclusive to smooth muscle whereas TREK-2 and TRAAK are expressed only in enteric neurons; 4) pharmacological activation of mechano-gated channels is sufficient to induce significant relaxation of pre-contracted ileum and colon, suggesting an important role in GI physiology; 5) cloned mouse TREK-1, TREK-2 and TRAAK channels exhibit similar biophysical properties as their human homologues, with sensitivity to well-known $K_{2P}$ activators AA, CDC and BL-1249; 6) spadin is not a blocker of mTREK-1 or mTREK-2 channels, but specifically antagonises the activation of mTREK-1 channels by AA, and not that of other pharmacological activators; 7) the mechanism of action of spadin does not involve the C-terminus directly, and likely works via an allosteric mechanism distinct from the AA binding site. This study has provided a new insight into the potassium channel subtype expression profile and function in mouse intestine, and highlights the mechano-gated $K_{2P}$ channel

TREK-1 as a potential target for future drug development treating hypermotility GI disorders.

## 7.2 Could $K^+$ channels be a potential target for treating IBS?

Potassium channels are intimately involved in almost all aspects of physiology and play a critical role in diverse processes such as nerve and muscle relaxation, sensory transduction, regulation of blood pressure, and cell proliferation (Hille, 2001, Kew and Davies, 2010). Therefore, potassium channels have been reported as therapeutic targets for treating a wide range of diseases that include cardiac disorders (Diness et al., 2015, Doshi and Marx, 2009), neuropathic pain (Busserolles et al., 2016, Tsantoulas and McMahon, 2014), skeletal muscle disorders (Zhu et al., 2014) and kidney failure (Grgic et al., 2009, Mene and Pirozzi, 2013). Their membrane expression makes these proteins easy to target chemically, and their ability to establish and maintain an electrical membrane potential is key for controlling many aspects of cell physiology. L-type calcium channels have been previously targeted in GI tract to treat motility issues including IBS related diarrhoea by promoting relaxation of GI smooth muscle (Wegener et al., 2006, Radulovic et al., 2015). Alternatively, comparably little is known about the underlying potassium channels responsible for suppressing smooth muscle contractility and promoting GI tract relaxation, and represents and as yet unexplored mechanism for treating a range of GI motility disorders including IBS.

IBS is a disorder of the brain-gut axis causing disruption to the physiological process of motility involving the coordinated contractions of the circular and longitudinal smooth

muscle cells. Current treatments for IBS are often selected sympomatically, whether involving diarrhoea or constipation, while the treatment of pain remains a significant unmet need (Camilleri and Ford, 2017). Therefore, novel effective therapeutic targets are required which are able to target both motility and pain symptoms and improve prognosis.

Identification of distinct expression patterns and functional contributions of $K^+$ channel families in Chapter 3, 4 and 5 respectively within the mouse intestine, reveal the $K_{2P}$ channel family could become increasingly seen as valid therapeutic targets. For example, specific smooth muscle and ENS neuron expression patterns of different $K_{2P}$ subunits were apparent from my data. Given the finding that TREK-1 appears to be expressed only in smooth muscle and TREK-2 and TRAAK only in enteric neurons, the two main symptoms of IBS, motility and pain, could be targeted independently depending on the patients' presentation. A picture emerges of TREK-2, TRAAK, TASK-2/3 and TWIK-2 subunits being located only in ENS neurons and thus suggest they could be potential targets for treating visceral pain symptoms. Notably, both TREK-2 and TRAAK exhibits ChAT-immunopositive MP neurons labelling, which thought to be a primary afferent neurons as the sensor of the pain pathway (Furness, 2000). Indeed, TREK-2 has been reported as a major background $K^+$ current in dorsal root ganglion (DRG) neurons, which serves such an important role in limiting pain sensation (Kang and Kim, 2006). Moreover, molecules that activate TREK-2 channels have been found to stimulate $K^+$ currents in DRG neurons and limit calcium influx in order to reducing neuropathic pain (Dadi et al., 2017, Veale and Mathie, 2016). However, from my data presented here, I am not able to confirm whether these channels are directly involved in controlling abdominal pain sensation. Furthermore, ChAT positive neurons also

include excitatory motor neurons and interneurons which are involved in motility reflexes (Furness, 2000, Rao and Gershon, 2018, Costa et al., 2000), therefore TREK-2 could also be a target for indirectly treating contractile dysfunction. TREK-1 and TRAAK have also been shown to have strong immunoreactivity in small-sized DRG neurons (Viatchenko-Karpinski et al., 2018), and TREK-1 KO mice haven been found to be more sensitive to painful heat sensations compared to WT (Alloui et al., 2006). Thus, I believe further immunohistochemistry experiments of $K_{2P}$ subunits within specific ENS sensory neurons are required, for example using the calcium-binding proteins calbindin (CB) as a marker for identifying the sensory neurons in both MP and SP (Furness, 2000, Megias et al., 2003) and subsequent overlapping expression of TREK-2 and TRAAK.

On the basis of the combination of the immunolocalisation and organ bath pharmacology, I can conservatively conclude that since TREK-1 is exclusively expressed by smooth muscle, this channel is likely to be principally involved in the contractile functions of intestinal smooth muscle. Indeed, the block of neuronal action potentials by TTX suggests the relaxation induced by activation of mechano-gated $K_{2P}$ channels is independent of enteric neuron input. However, specific pharmacological modulators of TREK-1 channels are still lacking, and is an area of research that requires significant input if $K_{2P}$ channels are to be realised as therapeutic targets for various pathologies. Based on my pharmacology characterisation of $K_{2P}$ channels in Chapter 6, the potency of BL-1249 for different TREK subtypes was identified, thereby suggesting the relaxation induced by BL-1249 may also related to effects across enteric neurons though TREK-2 and TRAAK channels. Importantly, TREK-2 and TRAAK exhibit expression patterns in both inhibitory and excitatory enteric

motor neurons, as GI motility is directly controlled by those two motor neurons that innervate the layers of smooth muscle (Brookes, 1993). Thus, I believe that subunit-specific KO mice will need to be employed in future experiments. For instance, repeating organ bath experiments of BL-1249 using tissue from TREK-1, TREK-2 and TRAAK KO mice should be assessed.

Furthermore, GI motility involves co-ordinated activity between GI longitudinal and circular muscles. However, in my organ bath preparation, I essentially only measured longitudinal muscle activity. This was simply due to the availability of recording equipment. Therefore, repeating the experiments using the myograph preparation (Jepps et al., 2009) would allow direct analysis of circular muscle function and analysis of $K_{2P}$ pharmacology would address their roles in circular muscles.

## 7.3 Could $K^+$ channel as a cause of IBS

My results from Chapter 3 demonstrated, for the first time, the expression profile of whole potassium families within WT mouse intestine, and from Chapter 4 further focused on the localisation and physiological role of $K_{2P}$ subfamily channels. However, how this expression level of $K^+$ channel subtypes changes in GI disease (such as IBS & IBD) is remains to be elucidated. Although on the organ bath studies I identified several $K^+$ subtype channel play a functional role in regulating the intestinal contractility, I am not able to determine whether there is a cause-effect relationship from these channels. In addition, determining the onset of IBS could be important to human health and wellbeing. If particular $K^+$ subtypes

are found to have a direct role in GI disorder development, then early diagnoses and therapy with specific $K^+$ channel modulators are likely to offer clinical benefits. Therefore, to further investigate this, I will need to repeat these experiments in different animal models (such as IBS, stress or Parkinson's) or samples from patients to take this research to the next level.

To date little is known about the changes in expression level of the $K^+$ channels in GI disease model, especially in IBS model. TREK-1 expression has been recently reported to be down-regulated in Hirschsprung's disease (Tomuschat et al., 2016), which is an intestinal obstruction disease with symptoms characterised by the absence of ganglion cells in the colon. This disease presents similar symptoms with IBS, such as constipation. Apart from the $K^+$ channels, $Ca^{2+}$ channels has been well-studied in IBS and as a target of current treatment using otilonium bromide (OB) resulting in reducing abdominal pain frequency (Camilleri and Ford, 2017). In IBS patients, the T-type calcium channel $Ca_v$ 3.2 channels exhibits higher expression in colon compared to control (Scanzi et al., 2016). Furthermore, neither the protein nor mRNA expression of L-Type voltage-dependent $Ca^{2+}$ channel ($Ca_v$ 1.2) appears to change in colonic myocytes from IBD mouse whereas the calcium currents were reduced by almost 70% by inflammation (Kang et al., 2004c). Thus, various experiments in IBS mouse model can be conducted in the future to probe the role of $K^+$ channels in causation, quantified by mRNA expression using qPCR and protein levels by using western-blot, as well as recording isolated smooth muscle cell from an IBS model to observe changes in current density.

Recently, information suggests that association of IBS and psychiatric disorders may be more fundamental than was previously believed (Lydiard, 2001). A comprehensive body of research indicates that the mental disorders such as stress, anxiety and depression play an important role in the development, onset and symptom exacerbation of IBS (Wood, 2002, Drossman, 2004). In addition, on a functional level, stress leads to the inhibition of gastric emptying which is accompanied by an increase in the colonic motility, mucosal electrolyte secretion and faecal pellet discharge (Tache et al., 1999, Maillot et al., 2000). Furthermore, various clinical studies have shown as many as 30-40% IBS patients have co-morbid depression or anxiety disorder (Lydiard and Falsetti, 1999, Kabra and Nadkarni, 2013). Within the CNS, various types of $K^+$ channels are abundantly expressed and their activities are suggested to be altered during depression (Lodge and Li, 2008). In general, when activated, potassium channels inhibit excitability of cells and lower the effectiveness of excitatory inputs by hyperpolarizing cell membrane potential. For instance, $K_{2P}$ channels (such as TREK-1 and TASK-3) have been identified as a target for the treatment of depression (Borsotto et al., 2015). Moreover, deletion of the TREK-1 gene leads to resistance to depression in animal models (Heurteaux et al., 2006), and thus suggests this gene plays an important role in onset of depression. Notably, both TREK-1 and TASK-3 subunits exhibit specific localisation in smooth muscle and NOS neurons respectively in mouse intestine. Nevertheless, whether the stress-specific alterations in the expression of specific $K^+$ subunits are compensatory or pathological remain unclear. If such experiments were to be conducted in the future, the stress or depression animal model would be a useful model to utilise. Moreover, tracking motility directly through assessing faecal pellet transit through the gut in TREK-1 KO mice compared to WT would also be another approach to assess whether the TREK-1 channel plays an essential role in the symptomology of IBS.

Given the link between stress, anxiety and GI motility disorders, it may also be fruitful to conduct further immunohistochemistry studies of $K^+$ channel expression and corticotropin-releasing hormone (CRH) receptors in the gut. CRHRs are important mediators in the stress response. For example, exposure of rats to early life stress, in form of maternal separation, leads to an increase in CRH1 and CRH2 receptors within the colon at protein levels (O'Malley et al., 2010). Importantly, increase in CRH1 receptor expression within certain disorders of the GI tract such as IBS has been reported (Tache et al., 2004, Tache and Perdue, 2004).

IBS is one of the most commonly encountered functional GI disorders in the elderly (Bennett and Talley, 2002), but whether advancing age impacts on IBS remains unknown. Interestingly, an onset of IBS after the age of 65 years (elderly) is extremely rare, as in most cases, the incidence increases during adolescence and young adulthood (Kurniawan and Kolopaking, 2014). This information suggest ageing may act as an important role in onset of IBS, and thus whether changes in the expression of $K^+$ during ageing within the intestine could be conducted in the future. However, it is very difficult to relate the development or existence of IBS to ageing due to the usual co-existence of GI disorders with other age-related diseases such as Parkinson's disease (PD). Moreover, $K^+$ channels have been thought to be a new therapeutic target for PD, as $K^+$ channels such as $K_v7$ (Sander et al., 2012), $K_{ATP}$ (Dragicevic et al., 2015), SK (Dolga et al., 2014, Mourre et al., 2017) and A-type $K^+$ ($K_v4$) (Subramaniam et al., 2014) are widely expressed in the basal ganglia (especially in DAergic neurons) which play crucial roles in the pathophysiology of PD. Notably, these $K^+$ channels also exhibit high level expression within mouse intestine, as revealed from my

qPCR results. Thus, this interesting finding regarding expression patterns of specific $K^+$ subunits in both DAergic and intestine could provide the impetus for a new programme of work investigating the contributions of individual subunits to IBS/PD development and ageing.

## 7.4 Clinical implications of findings

Differential pharmacology between species, or speciation, is a common problem encountered during the course of drug discovery that can severely hamper efficient advancement of clinical candidates. However, in Chapter 6, mouse homologues of $K_{2P}$ channels display similar pharmacology as their human orthologues. More recently, $K_{2P}$ channels have been suggested as targets for treating CNS disorders especially depression (Borsotto et al., 2015, Mathie and Veale, 2007, Djillani et al., 2017), since activators of TREK subfamily have been demonstrated to be neuroprotective, such as riluzole, polyunsaturated fatty acids and lysophospholipids. Patients with IBS frequently suffer from anxiety and depression. Interestingly, treatments that relieve the mental health symptoms, often provide relief from secondary, co-existing GI symptoms (Fadgyas-Stanculete et al., 2014, Olden, 2005). For example, anti-anxiety drugs such as chlordiazepoxide, which belongs to the drug class of benzodiazepines, have also been used in the treatment of IBS. However, these drugs have not been very successful due to the unwanted central side-effects such as drowsiness and dizziness. The $K_{2P}$ channel inhibitor, spadin, displays particular antidepressant properties with a rapid onset of action and the absence of adverse effects on animal model (Moha Ou Maati et al., 2012, Devader et al., 2015) but was not reported to induce any GI side effects such as diarrhoea. Collectively, the data

within this thesis provide the scientific rationale for the re-evaluation of such agents with a view to reformulating them specifically for delivery to the GI tract.

In conclusion, the results presented in this thesis have achieved my stated aims and objectives and my PhD research will thus contribute to the body of knowledge regarding the expression and function of $K^+$ channels in gut. Nevertheless, the results created more questions than answers. I believe this to be advantageous, since the value of data often resides in the previously unknown complexity it unveils. Moreover, my findings lead to many further potential avenues of research that may be of interest and importance. The next phase of investigations will need to focus on the cause-effect relationship and exact roles of $K^+$ channels in these physiological processes and how they can be exploited. The thesis provides a solid foundation on which these future investigations can be built with the aim of developing therapies targeting the modulation of $K^+$ channels in GI motility pathologies.

# Reference


ABBOTT, G. W. 2016. KCNE1 and KCNE3: The yin and yang of voltage-gated K(+) channel regulation. *Gene,* 576**,** 1-13.

ABBOTT, G. W., BUTLER, M. H., BENDAHHOU, S., DALAKAS, M. C., PTACEK, L. J. & GOLDSTEIN, S. A. 2001. MiRP2 forms potassium channels in skeletal muscle with Kv3.4 and is associated with periodic paralysis. *Cell,* 104**,** 217-31.

ACOSTA, C., DJOUHRI, L., WATKINS, R., BERRY, C., BROMAGE, K. & LAWSON, S. N. 2014. TREK2 expressed selectively in IB4-binding C-fiber nociceptors hyperpolarizes their membrane potentials and limits spontaneous pain. *J Neurosci,* 34**,** 1494-509.

AL-HAZZA, A., LINLEY, J., AZIZ, Q., HUNTER, M. & SANDLE, G. 2016. Upregulation of basolateral small conductance potassium channels (KCNQ1/KCNE3) in ulcerative colitis. *Biochem Biophys Res Commun,* 470**,** 473-478.

AL-SHBOUL, O. A. 2013. The importance of interstitial cells of cajal in the gastrointestinal tract. *Saudi J Gastroenterol,* 19**,** 3-15.

ALLER, M. I., VEALE, E. L., LINDEN, A. M., SANDU, C., SCHWANINGER, M., EVANS, L. J., KORPI, E. R., MATHIE, A., WISDEN, W. & BRICKLEY, S. G. 2005. Modifying the subunit composition of TASK channels alters the modulation of a leak conductance in cerebellar granule neurons. *J Neurosci,* 25**,** 11455-67.

ALLOUI, A., ZIMMERMANN, K., MAMET, J., DUPRAT, F., NOEL, J., CHEMIN, J., GUY, N., BLONDEAU, N., VOILLEY, N., RUBAT-COUDERT, C., BORSOTTO, M., ROMEY, G., HEURTEAUX, C., REEH, P., ESCHALIER, A. & LAZDUNSKI, M. 2006. TREK-1, a K+ channel involved in polymodal pain perception. *EMBO J,* 25**,** 2368-76.

AMBERG, G. C., KOH, S. D., HATTON, W. J., MURRAY, K. J., MONAGHAN, K., HOROWITZ, B. & SANDERS, K. M. 2002. Contribution of Kv4 channels toward the A-type potassium current in murine colonic myocytes. *J Physiol,* 544**,** 403-15.

AMBERG, G. C., KOH, S. D., IMAIZUMI, Y., OHYA, S. & SANDERS, K. M. 2003. A-type potassium currents in smooth muscle. *Am J Physiol Cell Physiol,* 284**,** C583-95.

AMBUDKAR, I. S. 2009. Unraveling smooth muscle contraction: the TRP link. *Gastroenterology,* 137**,** 1211-4.

AN, W. F., BOWLBY, M. R., BETTY, M., CAO, J., LING, H. P., MENDOZA, G., HINSON, J. W., MATTSSON, K. I., STRASSLE, B. W., TRIMMER, J. S. & RHODES, K. J. 2000. Modulation of A-type potassium channels by a family of calcium sensors. *Nature,* 403**,** 553-6.

ANDERSEN, C. L., JENSEN, J. L. & ORNTOFT, T. F. 2004. Normalization of real-time quantitative reverse transcription-PCR data: a model-based variance estimation approach to identify genes suited for normalization, applied to bladder and colon cancer data sets. *Cancer Res,* 64**,** 5245-50.

ANDERSON, A. J., HARVEY, A. L., ROWAN, E. G. & STRONG, P. N. 1988. Effects of charybdotoxin, a blocker of Ca2+-activated K+ channels, on motor nerve terminals. *Br J Pharmacol,* 95**,** 1329-35.

ANDERSON, U. A., CARSON, C., JOHNSTON, L., JOSHI, S., GURNEY, A. M. & MCCLOSKEY, K. D. 2013. Functional expression of KCNQ (Kv7) channels in guinea pig bladder smooth muscle and their contribution to spontaneous activity. *Br J Pharmacol,* 169**,** 1290-304.

ANUMONWO, J. M. & LOPATIN, A. N. 2010. Cardiac strong inward rectifier potassium channels. *J Mol Cell Cardiol,* 48**,** 45-54.

ASHER, V., SOWTER, H., SHAW, R., BALI, A. & KHAN, R. 2010. Eag and HERG potassium channels as novel therapeutic targets in cancer. *World J Surg Oncol,* 8**,** 113.

BAGRIANTSEV, S. N., CLARK, K. A. & MINOR, D. L., JR. 2012. Metabolic and thermal stimuli control K(2P)2.1 (TREK-1) through modular sensory and gating domains. *EMBO J,* 31**,** 3297-308.

BAHRING, R., BARGHAAN, J., WESTERMEIER, R. & WOLLBERG, J. 2012. Voltage sensor inactivation in potassium channels. *Front Pharmacol,* 3**,** 100.

BAHRING, R., DANNENBERG, J., PETERS, H. C., LEICHER, T., PONGS, O. & ISBRANDT, D. 2001. Conserved Kv4 N-terminal domain critical for effects of Kv channel-interacting protein 2.2 on channel expression and gating. *J Biol Chem,* 276**,** 23888-94.

BANERJEE, A., GHATAK, S. & SIKDAR, S. K. 2016. l-Lactate mediates neuroprotection against ischaemia by increasing TREK1 channel expression in rat hippocampal astrocytes in vitro. *J Neurochem,* 138**,** 265-81.

BANG, H., KIM, Y. & KIM, D. 2000. TREK-2, a new member of the mechanosensitive tandem-pore K+ channel family. *J Biol Chem,* 275**,** 17412-9.

BARGHAAN, J., TOZAKIDOU, M., EHMKE, H. & BAHRING, R. 2008. Role of N-terminal domain and accessory subunits in controlling deactivation-inactivation coupling of Kv4.2 channels. *Biophys J,* 94**,** 1276-94.

BARHANIN, J., LESAGE, F., GUILLEMARE, E., FINK, M., LAZDUNSKI, M. & ROMEY, G. 1996. K(V)LQT1 and lsK (minK) proteins associate to form the I(Ks) cardiac potassium current. *Nature,* 384**,** 78-80.

BECK, E. J., BOWLBY, M., AN, W. F., RHODES, K. J. & COVARRUBIAS, M. 2002. Remodelling inactivation gating of Kv4 channels by KChIP1, a small-molecular-weight calcium-binding protein. *J Physiol,* 538**,** 691-706.

BEECH, D. J., MURAKI, K. & FLEMMING, R. 2004. Non-selective cationic channels of smooth muscle and the mammalian homologues of Drosophila TRP. *J Physiol,* 559**,** 685-706.

BENNETT, G. & TALLEY, N. J. 2002. Irritable bowel syndrome in the elderly. *Best Pract Res Clin Gastroenterol,* 16**,** 63-76.

BERG, A. P., TALLEY, E. M., MANGER, J. P. & BAYLISS, D. A. 2004a. Motoneurons express heteromeric TWIK-related acid-sensitive K+ (TASK) channels containing TASK-1 (KCNK3) and TASK-3 (KCNK9) subunits. *Journal of Neuroscience,* 24**,** 6693-6702.

BERG, A. P., TALLEY, E. M., MANGER, J. P. & BAYLISS, D. A. 2004b. Motoneurons express heteromeric TWIK-related acid-sensitive K+ (TASK) channels containing TASK-1 (KCNK3) and TASK-3 (KCNK9) subunits. *J Neurosci,* 24**,** 6693-702.

BEYDER, A. & FARRUGIA, G. 2012. Targeting ion channels for the treatment of gastrointestinal motility disorders. *Therap Adv Gastroenterol,* 5**,** 5-21.

BIERVERT, C., SCHROEDER, B. C., KUBISCH, C., BERKOVIC, S. F., PROPPING, P., JENTSCH, T. J. & STEINLEIN, O. K. 1998. A potassium channel mutation in neonatal human epilepsy. *Science,* 279**,** 403-6.

BILLINGTON, C. K., OJO, O. O., PENN, R. B. & ITO, S. 2013. cAMP regulation of airway smooth muscle function. *Pulm Pharmacol Ther,* 26**,** 112-20.

BITTNER, S., RUCK, T., SCHUHMANN, M. K., HERRMANN, A. M., MOHA OU MAATI, H., BOBAK, N., GOBEL, K., LANGHAUSER, F., STEGNER, D., EHLING, P., BORSOTTO, M., PAPE, H. C., NIESWANDT, B., KLEINSCHNITZ, C., HEURTEAUX, C., GALLA, H. J., BUDDE, T., WIENDL, H. & MEUTH, S. G. 2013. Endothelial TWIK-related potassium channel-1 (TREK1) regulates immune-cell trafficking into the CNS. *Nat Med,* 19**,** 1161-5.

BLEICH, M. & WARTH, R. 2000. The very small-conductance K+ channel KvLQT1 and epithelial function. *Pflugers Arch,* 440**,** 202-6.

BLIN, S., BEN SOUSSIA, I., KIM, E. J., BRAU, F., KANG, D., LESAGE, F. & BICHET, D. 2016. Mixing and matching TREK/TRAAK subunits generate heterodimeric K2P channels with unique properties. *Proc Natl Acad Sci U S A,* 113**,** 4200-5.

BLIN, S., CHATELAIN, F. C., FELICIANGELI, S., KANG, D., LESAGE, F. & BICHET, D. 2014. Tandem pore domain halothane-inhibited K+ channel subunits THIK1 and THIK2 assemble and form active channels. *J Biol Chem,* 289**,** 28202-12.

BOCKSTEINS, E. 2016. Kv5, Kv6, Kv8, and Kv9 subunits: No simple silent bystanders. *J Gen Physiol,* 147**,** 105-25.

BORSOTTO, M., VEYSSIERE, J., MOHA OU MAATI, H., DEVADER, C., MAZELLA, J. & HEURTEAUX, C. 2015. Targeting two-pore domain K(+) channels TREK-1 and TASK-3 for the treatment of depression: a new therapeutic concept. *Br J Pharmacol,* 172**,** 771-84.

BROHAWN, S. G., DEL MARMOL, J. & MACKINNON, R. 2012. Crystal structure of the human K2P TRAAK, a lipid- and mechano-sensitive K+ ion channel. *Science,* 335**,** 436-41.

BROOKE, R. E., MOORES, T. S., MORRIS, N. P., PARSON, S. H. & DEUCHARS, J. 2004. Kv3 voltage-gated potassium channels regulate neurotransmitter release from mouse motor nerve terminals. *Eur J Neurosci,* 20**,** 3313-21.

BROOKES, S. J. 1993. Neuronal nitric oxide in the gut. *J Gastroenterol Hepatol,* 8**,** 590-603.

BROOKES, S. J. 2001. Classes of enteric nerve cells in the guinea-pig small intestine. *Anat Rec,* 262**,** 58-70.

BRUEGGEMANN, L. I., KAKAD, P. P., LOVE, R. B., SOLWAY, J., DOWELL, M. L., CRIBBS, L. L. & BYRON, K. L. 2012. Kv7 potassium channels in airway smooth muscle cells: signal transduction intermediates and pharmacological targets for bronchodilator therapy. *Am J Physiol Lung Cell Mol Physiol,* 302**,** L120-32.

BULK, E., AY, A. S., HAMMADI, M., OUADID-AHIDOUCH, H., SCHELHAAS, S., HASCHER, A., ROHDE, C., THOENNISSEN, N. H., WIEWRODT, R., SCHMIDT, E., MARRA, A., HILLEJAN, L., JACOBS, A. H., KLEIN, H. U., DUGAS, M., BERDEL, W. E., MULLER-TIDOW, C. & SCHWAB, A. 2015. Epigenetic dysregulation of KCa 3.1 channels induces poor prognosis in lung cancer. *Int J Cancer,* 137**,** 1306-17.

BUSSEROLLES, J., TSANTOULAS, C., ESCHALIER, A. & LOPEZ GARCIA, J. A. 2016. Potassium channels in neuropathic pain: advances, challenges, and emerging ideas. *Pain,* 157 Suppl 1**,** S7-14.

BUTT, A. M. & KALSI, A. 2006. Inwardly rectifying potassium channels (Kir) in central nervous system glia: a special role for Kir4.1 in glial functions. *Journal of Cellular and Molecular Medicine,* 10**,** 33-44.

CADAVEIRA-MOSQUERA, A., RIBEIRO, S. J., REBOREDA, A., PEREZ, M. & LAMAS, J. A. 2011. Activation of TREK currents by the neuroprotective agent riluzole in mouse sympathetic neurons. *J Neurosci,* 31**,** 1375-85.

CALCATERRA, N. E., HOEPPNER, D. J., WEI, H., JAFFE, A. E., MAHER, B. J. & BARROW, J. C. 2016. Schizophrenia-Associated hERG channel Kv11.1-3.1 Exhibits a Unique Trafficking Deficit that is Rescued Through Proteasome Inhibition for High Throughput Screening. *Sci Rep,* 6**,** 19976.

CALLOE, K., SOLTYSINSKA, E., JESPERSEN, T., LUNDBY, A., ANTZELEVITCH, C., OLESEN, S. P. & CORDEIRO, J. M. 2010. Differential effects of the transient outward K(+) current activator NS5806 in the canine left ventricle. *J Mol Cell Cardiol,* 48**,** 191-200.

CAMILLERI, M. & FORD, A. C. 2017. Pharmacotherapy for Irritable Bowel Syndrome. *J Clin Med,* 6.

CAMPOMANES, C. R., CARROLL, K. I., MANGANAS, L. N., HERSHBERGER, M. E., GONG, B., ANTONUCCI, D. E., RHODES, K. J. & TRIMMER, J. S. 2002. Kv beta subunit oxidoreductase activity and Kv1 potassium channel trafficking. *J Biol Chem,* 277**,** 8298-305.

CANAVAN, C., WEST, J. & CARD, T. 2014. The epidemiology of irritable bowel syndrome. *Clin Epidemiol,* 6**,** 71-80.

CARL, A., BAYGUINOV, O., SHUTTLEWORTH, C. W., WARD, S. M. & SANDERS, K. M. 1995. Role of Ca(2+)-activated K+ channels in electrical activity of longitudinal and circular muscle layers of canine colon. *Am J Physiol,* 268**,** C619-27.

CHAVEZ, R. A., GRAY, A. T., ZHAO, B. B., KINDLER, C. H., MAZUREK, M. J., MEHTA, Y., FORSAYETH, J. R. & YOST, C. S. 1999. TWIK-2, a new weak inward rectifying member of the tandem pore domain potassium channel family. *J Biol Chem,* 274**,** 7887-92.

CHEMIN, J., PATEL, A. J., DUPRAT, F., SACHS, F., LAZDUNSKI, M. & HONORE, E. 2007. Up- and down-regulation of the mechano-gated K(2P) channel TREK-1 by PIP (2) and other membrane phospholipids. *Pflugers Arch,* 455**,** 97-103.

CHEN, M. X., GORMAN, S. A., BENSON, B., SINGH, K., HIEBLE, J. P., MICHEL, M. C., TATE, S. N. & TREZISE, D. J. 2004. Small and intermediate conductance Ca(2+)-activated K+ channels confer distinctive patterns of distribution in human tissues and differential cellular localisation in the colon and corpus cavernosum. *Naunyn Schmiedebergs Arch Pharmacol,* 369**,** 602-15.

CHENG, L. K., O'GRADY, G., DU, P., EGBUJI, J. U., WINDSOR, J. A. & PULLAN, A. J. 2010. Gastrointestinal system. *Wiley Interdiscip Rev Syst Biol Med,* 2**,** 65-79.

CHO, S. Y., BECKETT, E. A., BAKER, S. A., HAN, I., PARK, K. J., MONAGHAN, K., WARD, S. M., SANDERS, K. M. & KOH, S. D. 2005. A pH-sensitive potassium conductance (TASK) and its function in the murine gastrointestinal tract. *J Physiol,* 565**,** 243-59.

CHOI, J. H., YARISHKIN, O., KIM, E., BAE, Y., KIM, A., KIM, S. C., RYOO, K., CHO, C. H., HWANG, E. M. & PARK, J. Y. 2018. TWIK-1/TASK-3 heterodimeric channels contribute to the neurotensin-mediated excitation of hippocampal dentate gyrus granule cells. *Exp Mol Med,* 50**,** 145.

CLERC, N., FURNESS, J. B., BORNSTEIN, J. C. & KUNZE, W. A. 1998. Correlation of electrophysiological and morphological characteristics of myenteric neurons of the duodenum in the guinea-pig. *Neuroscience,* 82**,** 899-914.

CLEVERS, H. 2013. The intestinal crypt, a prototype stem cell compartment. *Cell,* 154**,** 274-84.

COSTA, M., BROOKES, S. J. & HENNIG, G. W. 2000. Anatomy and physiology of the enteric nervous system. *Gut,* 47 Suppl 4**,** iv15-9; discussion iv26.

COVARRUBIAS, M., WEI, A. A. & SALKOFF, L. 1991. Shaker, Shal, Shab, and Shaw express independent K+ current systems. *Neuron,* 7**,** 763-73.

CUI, Y., GIBLIN, J. P., CLAPP, L. H. & TINKER, A. 2001. A mechanism for ATP-sensitive potassium channel diversity: Functional coassembly of two pore-forming subunits. *Proc Natl Acad Sci U S A,* 98**,** 729-34.

CURRO, D. 2016. The Modulation of Potassium Channels in the Smooth Muscle as a Therapeutic Strategy for Disorders of the Gastrointestinal Tract. *Adv Protein Chem Struct Biol,* 104**,** 263-305.

CZIRJAK, B., TOTH, Z. E. & ENYEDI, P. 2004. The two-pore domain K+ channel, TRESK, is activated by the cytoplasmic calcium signal through calcineurin. *Journal of Biological Chemistry,* 279**,** 18550-18558.

CZIRJAK, G. & ENYEDI, P. 2002. Formation of functional heterodimers between the TASK-1 and TASK-3 two-pore domain potassium channel subunits. *J Biol Chem,* 277**,** 5426-32.

CZIRJAK, G. & ENYEDI, P. 2006. Zinc and mercuric ions distinguish TRESK from the other two-pore-domain K+ channels. *Mol Pharmacol,* 69**,** 1024-32.

DADI, P. K., VIERRA, N. C., DAYS, E., DICKERSON, M. T., VINSON, P. N., WEAVER, C. D. & JACOBSON, D. A. 2017. Selective Small Molecule Activators of TREK-2 Channels Stimulate Dorsal Root Ganglion c-Fiber Nociceptor Two-Pore-Domain Potassium Channel Currents and Limit Calcium Influx. *ACS Chem Neurosci,* 8**,** 558-568.

DAHLMANN, A., LI, M., GAO, Z., MCGARRIGLE, D., SACKIN, H. & PALMER, L. G. 2004. Regulation of Kir channels by intracellular pH and extracellular K(+): mechanisms of coupling. *J Gen Physiol,* 123**,** 441-54.

DANTHI, S., ENYEART, J. A. & ENYEART, J. J. 2004. Caffeic acid esters activate TREK-1 potassium channels and inhibit depolarization-dependent secretion. *Mol Pharmacol,* 65**,** 599-610.

DE LA PENA, E., MALKIA, A., VARA, H., CAIRES, R., BALLESTA, J. J., BELMONTE, C. & VIANA, F. 2012. The influence of cold temperature on cellular excitability of hippocampal networks. *PLoS One,* 7**,** e52475.

DEDEK, K. & WALDEGGER, S. 2001. Colocalization of KCNQ1/KCNE channel subunits in the mouse gastrointestinal tract. *Pflugers Arch,* 442**,** 896-902.

DELA PENA, I. C., YOON, S. Y., KIM, S. M., LEE, G. S., PARK, C. S., KIM, Y. C. & CHEONG, J. H. 2009. Inhibition of intestinal motility by the putative BK(Ca) channel opener LDD175. *Arch Pharm Res,* 32**,** 413-20.

DEVADER, C., KHAYACHI, A., VEYSSIERE, J., MOHA OU MAATI, H., ROULOT, M., MORENO, S., BORSOTTO, M., MARTIN, S., HEURTEAUX, C. & MAZELLA, J. 2015. In vitro and in vivo regulation of synaptogenesis by the novel antidepressant spadin. *Br J Pharmacol,* 172**,** 2604-17.

DINESS, J. G., BENTZEN, B. H., SORENSEN, U. S. & GRUNNET, M. 2015. Role of Calcium-activated Potassium Channels in Atrial Fibrillation Pathophysiology and Therapy. *J Cardiovasc Pharmacol,* 66**,** 441-8.

DIOCHOT, S., DRICI, M. D., MOINIER, D., FINK, M. & LAZDUNSKI, M. 1999. Effects of phrixotoxins on the Kv4 family of potassium channels and implications for the role of Ito1 in cardiac electrogenesis. *Br J Pharmacol,* 126**,** 251-63.

DJILLANI, A., PIETRI, M., MORENO, S., HEURTEAUX, C., MAZELLA, J. & BORSOTTO, M. 2017. Shortened Spadin Analogs Display Better TREK-1 Inhibition, In Vivo Stability and Antidepressant Activity. *Front Pharmacol,* 8**,** 643.

DOLGA, A. M., DE ANDRADE, A., MEISSNER, L., KNAUS, H. G., HOLLERHAGE, M., CHRISTOPHERSEN, P., ZISCHKA, H., PLESNILA, N., HOGLINGER, G. U. & CULMSEE, C. 2014. Subcellular expression and neuroprotective effects of SK channels in human dopaminergic neurons. *Cell Death Dis,* 5**,** e999.

DONG, Y. Y., PIKE, A. C., MACKENZIE, A., MCCLENAGHAN, C., ARYAL, P., DONG, L., QUIGLEY, A., GRIEBEN, M., GOUBIN, S., MUKHOPADHYAY, S., RUDA, G. F., CLAUSEN, M. V., CAO, L., BRENNAN, P. E., BURGESS-BROWN, N. A., SANSOM, M. S., TUCKER, S. J. & CARPENTER, E. P. 2015. K2P channel gating mechanisms revealed by structures of TREK-2 and a complex with Prozac. *Science,* 347**,** 1256-9.

DOSHI, D. & MARX, S. O. 2009. Ion channels, transporters, and pumps as targets for heart failure therapy. *J Cardiovasc Pharmacol,* 54**,** 273-8.

DOYLE, D. A., MORAIS CABRAL, J., PFUETZNER, R. A., KUO, A., GULBIS, J. M., COHEN, S. L., CHAIT, B. T. & MACKINNON, R. 1998. The structure of the potassium channel: molecular basis of K+ conduction and selectivity. *Science,* 280**,** 69-77.

DRAGICEVIC, E., SCHIEMANN, J. & LISS, B. 2015. Dopamine midbrain neurons in health and Parkinson's disease: emerging roles of voltage-gated calcium channels and ATP-sensitive potassium channels. *Neuroscience,* 284**,** 798-814.

DROSSMAN, D. A. 2004. Psychosocial factors and the disorders of GI function: what is the link? *Am J Gastroenterol,* 99**,** 358-60.

DUBYAK, G. R. 2004. Ion homeostasis, channels, and transporters: an update on cellular mechanisms. *Adv Physiol Educ,* 28**,** 143-54.

DUPRAT, F., GIRARD, C., JARRETOU, G. & LAZDUNSKI, M. 2005. Pancreatic two P domain K+ channels TALK-1 and TALK-2 are activated by nitric oxide and reactive oxygen species. *J Physiol,* 562**,** 235-44.

DUPRAT, F., LESAGE, F., FINK, M., REYES, R., HEURTEAUX, C. & LAZDUNSKI, M. 1997. TASK, a human background K+ channel to sense external pH variations near physiological pH. *EMBO J,* 16**,** 5464-71.

DUPRAT, F., LESAGE, F., PATEL, A. J., FINK, M., ROMEY, G. & LAZDUNSKI, M. 2000. The neuroprotective agent riluzole activates the two P domain K(+) channels TREK-1 and TRAAK. *Mol Pharmacol,* 57**,** 906-12.

ELLINGHAUS, P., SCHEUBEL, R. J., DOBREV, D., RAVENS, U., HOLTZ, J., HUETTER, J., NIELSCH, U. & MORAWIETZ, H. 2005. Comparing the global mRNA expression profile of human atrial and ventricular myocardium with high-density oligonucleotide arrays. *J Thorac Cardiovasc Surg,* 129**,** 1383-90.

ENYEART, J. J., XU, L., DANTHI, S. & ENYEART, J. A. 2002. An ACTH- and ATP-regulated background K+ channel in adrenocortical cells is TREK-1. *J Biol Chem,* 277**,** 49186-99.

ENYEDI, P. & CZIRJAK, G. 2010. Molecular Background of Leak K+ Currents: Two-Pore Domain Potassium Channels. *Physiological Reviews,* 90**,** 559-605.

EPPERSON, A., BONNER, H. P., WARD, S. M., HATTON, W. J., BRADLEY, K. K., BRADLEY, M. E., TRIMMER, J. S. & HOROWITZ, B. 1999. Molecular diversity of K(V) alpha- and beta-subunit expression in canine gastrointestinal smooth muscles. *Am J Physiol,* 277**,** G127-36.

ESCOUBAS, P., DIOCHOT, S., CELERIER, M. L., NAKAJIMA, T. & LAZDUNSKI, M. 2002. Novel tarantula toxins for subtypes of voltage-dependent potassium channels in the Kv2 and Kv4 subfamilies. *Mol Pharmacol,* 62**,** 48-57.

FADGYAS-STANCULETE, M., BUGA, A. M., POPA-WAGNER, A. & DUMITRASCU, D. L. 2014. The relationship between irritable bowel syndrome and psychiatric disorders: from molecular changes to clinical manifestations. *J Mol Psychiatry,* 2**,** 4.

FELICIANGELI, S., BENDAHHOU, S., SANDOZ, G., GOUNON, P., REICHOLD, M., WARTH, R., LAZDUNSKI, M., BARHANIN, J. & LESAGE, F. 2007. Does sumoylation control K2P1/TWIK1 background K+ channels? *Cell,* 130**,** 563-9.

FELICIANGELI, S., CHATELAIN, F. C., BICHET, D. & LESAGE, F. 2015. The family of K2P channels: salient structural and functional properties. *J Physiol,* 593**,** 2587-603.

FINK, M., DUPRAT, F., LESAGE, F., REYES, R., ROMEY, G., HEURTEAUX, C. & LAZDUNSKI, M. 1996. Cloning, functional expression and brain localization of a novel unconventional outward rectifier K+ channel. *EMBO J,* 15**,** 6854-62.

FINK, M., LESAGE, F., DUPRAT, F., HEURTEAUX, C., REYES, R., FOSSET, M. & LAZDUNSKI, M. 1998. A neuronal two P domain K+ channel stimulated by arachidonic acid and polyunsaturated fatty acids. *EMBO J,* 17**,** 3297-308.

FLYNN, E. R., MCMANUS, C. A., BRADLEY, K. K., KOH, S. D., HEGARTY, T. M., HOROWITZ, B. & SANDERS, K. M. 1999. Inward rectifier potassium conductance regulates membrane potential of canine colonic smooth muscle. *J Physiol,* 518**,** 247-56.

FOSTER, R. R., ZADEH, M. A., WELSH, G. I., SATCHELL, S. C., YE, Y., MATHIESON, P. W., BATES, D. O. & SALEEM, M. A. 2009. Flufenamic acid is a tool for investigating TRPC6-mediated calcium signalling in human conditionally immortalised podocytes and HEK293 cells. *Cell Calcium,* 45**,** 384-90.

FRANCHINI, L., LEVI, G. & VISENTIN, S. 2004. Inwardly rectifying K+ channels influence Ca2+ entry due to nucleotide receptor activation in microglia. *Cell Calcium,* 35**,** 449-59.

FUJITA, A., TAKEUCHI, T., SAITOH, N., HANAI, J. & HATA, F. 2001. Expression of Ca(2+)-activated K(+) channels, SK3, in the interstitial cells of Cajal in the gastrointestinal tract. *Am J Physiol Cell Physiol,* 281**,** C1727-33.

FURNESS, J. B. 2000. Types of neurons in the enteric nervous system. *J Auton Nerv Syst,* 81**,** 87-96.

FURNESS, J. B. 2007. Enteric nervous system. *Scholarpedia,* 2.

FURNESS, J. B. 2008. The enteric nervous system: normal functions and enteric neuropathies. *Neurogastroenterol Motil,* 20 Suppl 1**,** 32-8.

FURNESS, J. B., CALLAGHAN, B. P., RIVERA, L. R. & CHO, H. J. 2014. The enteric nervous system and gastrointestinal innervation: integrated local and central control. *Adv Exp Med Biol,* 817**,** 39-71.

FURNESS, J. B., KUNZE, W. A., BERTRAND, P. P., CLERC, N. & BORNSTEIN, J. C. 1998. Intrinsic primary afferent neurons of the intestine. *Prog Neurobiol,* 54**,** 1-18.

GABORIT, N., LE BOUTER, S., SZUTS, V., VARRO, A., ESCANDE, D., NATTEL, S. & DEMOLOMBE, S. 2007. Regional and tissue specific transcript signatures of ion channel genes in the non-diseased human heart. *J Physiol,* 582**,** 675-93.

GESSNER, G. & HEINEMANN, S. H. 2003. Inhibition of hEAG1 and hERG1 potassium channels by clofilium and its tertiary analogue LY97241. *Br J Pharmacol,* 138**,** 161-71.

GIJON, M. A. & LESLIE, C. C. 1999. Regulation of arachidonic acid release and cytosolic phospholipase A2 activation. *J Leukoc Biol,* 65**,** 330-6.

GIL, V., GALLEGO, D., MOHA OU MAATI, H., PEYRONNET, R., MARTINEZ-CUTILLAS, M., HEURTEAUX, C., BORSOTTO, M. & JIMENEZ, M. 2012. Relative contribution of SKCa and TREK1 channels

in purinergic and nitrergic neuromuscular transmission in the rat colon. *Am J Physiol Gastrointest Liver Physiol,* 303**,** G412-23.

GIRARD, C., DUPRAT, F., TERRENOIRE, C., TINEL, N., FOSSET, M., ROMEY, G., LAZDUNSKI, M. & LESAGE, F. 2001. Genomic and functional characteristics of novel human pancreatic 2P domain K(+) channels. *Biochem Biophys Res Commun,* 282**,** 249-56.

GOLDSTEIN, S. A., BOCKENHAUER, D., O'KELLY, I. & ZILBERBERG, N. 2001. Potassium leak channels and the KCNK family of two-P-domain subunits. *Nat Rev Neurosci,* 2**,** 175-84.

GOLDSTEIN, S. A., PRICE, L. A., ROSENTHAL, D. N. & PAUSCH, M. H. 1996. ORK1, a potassium-selective leak channel with two pore domains cloned from Drosophila melanogaster by expression in Saccharomyces cerevisiae. *Proc Natl Acad Sci U S A,* 93**,** 13256-61.

GONCZI, M., SZENTANDRASSY, N., JOHNSON, I. T., HEAGERTY, A. M. & WESTON, A. H. 2006. Investigation of the role of TASK-2 channels in rat pulmonary arteries; pharmacological and functional studies following RNA interference procedures. *Br J Pharmacol,* 147**,** 496-505.

GOPALAKRISHNAN, M., WHITEAKER, K. L., MOLINARI, E. J., DAVIS-TABER, R., SCOTT, V. E., SHIEH, C. C., BUCKNER, S. A., MILICIC, I., CAIN, J. C., POSTL, S., SULLIVAN, J. P. & BRIONI, J. D. 1999. Characterization of the ATP-sensitive potassium channels (KATP) expressed in guinea pig bladder smooth muscle cells. *J Pharmacol Exp Ther,* 289**,** 551-8.

GREENWOOD-VAN MEERVELD, B., JOHNSON, A. C. & GRUNDY, D. 2017. Gastrointestinal Physiology and Function. *Handb Exp Pharmacol,* 239**,** 1-16.

GREENWOOD, I. A. & OHYA, S. 2009. New tricks for old dogs: KCNQ expression and role in smooth muscle. *Br J Pharmacol,* 156**,** 1196-203.

GRGIC, I., KISS, E., KAISTHA, B. P., BUSCH, C., KLOSS, M., SAUTTER, J., MULLER, A., KAISTHA, A., SCHMIDT, C., RAMAN, G., WULFF, H., STRUTZ, F., GRONE, H. J., KOHLER, R. & HOYER, J. 2009. Renal fibrosis is attenuated by targeted disruption of KCa3.1 potassium channels. *Proc Natl Acad Sci U S A,* 106**,** 14518-23.

GRIBKOFF, V. K., LUM-RAGAN, J. T., BOISSARD, C. G., POST-MUNSON, D. J., MEANWELL, N. A., STARRETT, J. E., JR., KOZLOWSKI, E. S., ROMINE, J. L., TROJNACKI, J. T., MCKAY, M. C., ZHONG, J. & DWORETZKY, S. I. 1996. Effects of channel modulators on cloned large-conductance calcium-activated potassium channels. *Mol Pharmacol,* 50**,** 206-17.

GUEGUINOU, M., CHANTOME, A., FROMONT, G., BOUGNOUX, P., VANDIER, C. & POTIER-CARTEREAU, M. 2014. KCa and Ca(2+) channels: the complex thought. *Biochim Biophys Acta,* 1843**,** 2322-33.

GUINAMARD, R., SIMARD, C. & DEL NEGRO, C. 2013. Flufenamic acid as an ion channel modulator. *Pharmacol Ther,* 138.

GULBRANSEN, B. D. & SHARKEY, K. A. 2012. Novel functional roles for enteric glia in the gastrointestinal tract. *Nat Rev Gastroenterol Hepatol,* 9**,** 625-32.

GURNEY, A. M., OSIPENKO, O. N., MACMILLAN, D., MCFARLANE, K. M., TATE, R. J. & KEMPSILL, F. E. 2003. Two-pore domain K channel, TASK-1, in pulmonary artery smooth muscle cells. *Circ Res,* 93**,** 957-64.

HAGIWARA, S., MIYAZAKI, S. & ROSENTHAL, N. P. 1976. Potassium current and the effect of cesium on this current during anomalous rectification of the egg cell membrane of a starfish. *J Gen Physiol,* 67**,** 621-38.

HAN, H. J., LEE, S. W., KIM, G. T., KIM, E. J., KWON, B., KANG, D., KIM, H. J. & SEO, K. S. 2016. Enhanced Expression of TREK-1 Is Related with Chronic Constriction Injury of Neuropathic Pain Mouse Model in Dorsal Root Ganglion. *Biomol Ther (Seoul),* 24**,** 252-9.

HANANI, M., ERMILOV, L. G., SCHMALZ, P. F., LOUZON, V., MILLER, S. M. & SZURSZEWSKI, J. H. 1998. The three-dimensional structure of myenteric neurons in the guinea-pig ileum. *J Auton Nerv Syst,* 71**,** 1-9.

HANSEN, M. B. 2003. The enteric nervous system I: organisation and classification. *Pharmacol Toxicol,* 92**,** 105-13.

HANSEN, R. S., DINESS, T. G., CHRIST, T., DEMNITZ, J., RAVENS, U., OLESEN, S. P. & GRUNNET, M. 2006. Activation of human ether-a-go-go-related gene potassium channels by the diphenylurea 1,3-bis-(2-hydroxy-5-trifluoromethyl-phenyl)-urea (NS1643). *Mol Pharmacol,* 69**,** 266-77.

HATTON, W. J., MASON, H. S., CARL, A., DOHERTY, P., LATTEN, M. J., KENYON, J. L., SANDERS, K. M. & HOROWITZ, B. 2001. Functional and molecular expression of a voltage-dependent K(+) channel (Kv1.1) in interstitial cells of Cajal. *J Physiol,* 533**,** 315-27.

HEGINBOTHAM, L., LU, Z., ABRAMSON, T. & MACKINNON, R. 1994. Mutations in the K+ channel signature sequence. *Biophys J,* 66**,** 1061-7.

HEITZMANN, D. & WARTH, R. 2008. Physiology and pathophysiology of potassium channels in gastrointestinal epithelia. *Physiol Rev,* 88**,** 1119-82.

HENNIG, G. W., SPENCER, N. J., JOKELA-WILLIS, S., BAYGUINOV, P. O., LEE, H. T., RITCHIE, L. A., WARD, S. M., SMITH, T. K. & SANDERS, K. M. 2010. ICC-MY coordinate smooth muscle electrical and mechanical activity in the murine small intestine. *Neurogastroenterol Motil,* 22**,** e138-51.

HEURTEAUX, C., LUCAS, G., GUY, N., EL YACOUBI, M., THUMMLER, S., PENG, X. D., NOBLE, F., BLONDEAU, N., WIDMANN, C., BORSOTTO, M., GOBBI, G., VAUGEOIS, J. M., DEBONNEL, G. & LAZDUNSKI, M. 2006. Deletion of the background potassium channel TREK-1 results in a depression-resistant phenotype. *Nat Neurosci,* 9**,** 1134-41.

HIBINO, H., FUJITA, A., IWAI, K., YAMADA, M. & KURACHI, Y. 2004. Differential assembly of inwardly rectifying K+ channel subunits, Kir4.1 and Kir5.1, in brain astrocytes. *J Biol Chem,* 279**,** 44065-73.

HIBINO, H., INANOBE, A., FURUTANI, K., MURAKAMI, S., FINDLAY, I. & KURACHI, Y. 2010. Inwardly rectifying potassium channels: their structure, function, and physiological roles. *Physiol Rev,* 90**,** 291-366.

HILGEMANN, D. W. & BALL, R. 1996. Regulation of cardiac Na+,Ca2+ exchange and KATP potassium channels by PIP2. *Science,* 273**,** 956-9.

HILGEMANN, D. W., FENG, S. & NASUHOGLU, C. 2001. The complex and intriguing lives of PIP2 with ion channels and transporters. *Sci STKE,* 2001**,** re19.

HILLE, B. 2001. *Ion channels of excitable membranes,* Sunderland, Mass., Sinauer.

HIRST, G. D., HOLMAN, M. E. & SPENCE, I. 1974. Two types of neurones in the myenteric plexus of duodenum in the guinea-pig. *J Physiol,* 236**,** 303-26.

HO, I. H. & MURRELL-LAGNADO, R. D. 1999. Molecular determinants for sodium-dependent activation of G protein-gated K+ channels. *J Biol Chem,* 274**,** 8639-48.

HOLZER, P. 2002. Sensory neurone responses to mucosal noxae in the upper gut: relevance to mucosal integrity and gastrointestinal pain. *Neurogastroenterol Motil,* 14**,** 459-75.

HONG, S. H., SUNG, R., KIM, Y. C., SUZUKI, H., CHOI, W., PARK, Y. J., JI, I. W., KIM, C. H., MYUNG, S. C., LEE, M. Y., KANG, T. M., YOU, R. Y., LEE, K. J., LIM, S. W., YUN, H. Y., SONG, Y. J., XU, W. X., KIM, H. S. & LEE, S. J. 2013. Mechanism of Relaxation Via TASK-2 Channels in Uterine Circular Muscle of Mouse. *Korean J Physiol Pharmacol,* 17**,** 359-65.

HONG, S. J., ROAN, Y. F. & CHANG, C. C. 1997. Spontaneous activity of guinea pig ileum longitudinal muscle regulated by Ca(2+)-activated K+ channel. *Gastrointestinal and Liver physiology,* 272**,** G962-G971.

HONORE, E. 2007. The neuronal background K2P channels: focus on TREK1. *Nat Rev Neurosci,* 8**,** 251-61.

HONORE, E., MAINGRET, F., LAZDUNSKI, M. & PATEL, A. J. 2002. An intracellular proton sensor commands lipid- and mechano-gating of the K(+) channel TREK-1. *EMBO J,* 21**,** 2968-76.

HOPKINS, W. F. 1998. Toxin and subunit specificity of blocking affinity of three peptide toxins for heteromultimeric, voltage-gated potassium channels expressed in Xenopus oocytes. *J Pharmacol Exp Ther,* 285**,** 1051-60.

HRISTOV, K. L., CHEN, M., SODER, R. P., PARAJULI, S. P., CHENG, Q., KELLETT, W. F. & PETKOV, G. V. 2012. KV2.1 and electrically silent KV channel subunits control excitability and contractility of guinea pig detrusor smooth muscle. *Am J Physiol Cell Physiol,* 302**,** C360-72.

HU, H., TIAN, J., ZHU, Y., WANG, C., XIAO, R., HERZ, J. M., WOOD, J. D. & ZHU, M. X. 2010. Activation of TRPA1 channels by fenamate nonsteroidal anti-inflammatory drugs. *Pflugers Arch,* 459**,** 579-92.

HUANG, C. L., FENG, S. & HILGEMANN, D. W. 1998. Direct activation of inward rectifier potassium channels by PIP2 and its stabilization by Gbetagamma. *Nature,* 391**,** 803-6.

HUR, C. G., KIM, E. J., CHO, S. K., CHO, Y. W., YOON, S. Y., TAK, H. M., KIM, C. W., CHOE, C., HAN, J. & KANG, D. 2012. K(+) efflux through two-pore domain K(+) channels is required for mouse embryonic development. *Reproduction,* 143**,** 625-36.

HWANG, E. M., KIM, E., YARISHKIN, O., WOO, D. H., HAN, K. S., PARK, N., BAE, Y., WOO, J., KIM, D., PARK, M., LEE, C. J. & PARK, J. Y. 2014. A disulphide-linked heterodimer of TWIK-1 and TREK-1 mediates passive conductance in astrocytes. *Nat Commun,* 5**,** 3227.

HWANG, P. M., FOTUHI, M., BREDT, D. S., CUNNINGHAM, A. M. & SNYDER, S. H. 1993. Contrasting immunohistochemical localizations in rat brain of two novel K+ channels of the Shab subfamily. *J Neurosci,* 13**,** 1569-76.

IPAVEC, V., MARTIRE, M., BARRESE, V., TAGLIALATELA, M. & CURRO, D. 2011. KV7 channels regulate muscle tone and nonadrenergic noncholinergic relaxation of the rat gastric fundus. *Pharmacol Res,* 64**,** 397-409.

ISHIKAWA, T., NAKAMURA, Y., SAITOH, N., LI, W. B., IWASAKI, S. & TAKAHASHI, T. 2003. Distinct roles of Kv1 and Kv3 potassium channels at the calyx of Held presynaptic terminal. *J Neurosci,* 23**,** 10445-53.

JACKSON, W. F. 2005. Potassium channels in the peripheral microcirculation. *Microcirculation,* 12**,** 113-27.

JEPPS, T. A., GREENWOOD, I. A., MOFFATT, J. D., SANDERS, K. M. & OHYA, S. 2009. Molecular and functional characterization of Kv7 K+ channel in murine gastrointestinal smooth muscles. *Am J Physiol Gastrointest Liver Physiol,* 297**,** G107-15.

JEPPS, T. A., OLESEN, S. P. & GREENWOOD, I. A. 2013. One man's side effect is another man's therapeutic opportunity: targeting Kv7 channels in smooth muscle disorders. *Br J Pharmacol,* 168**,** 19-27.

JIN, W. & LU, Z. 1998. A novel high-affinity inhibitor for inward-rectifier K+ channels. *Biochemistry,* 37**,** 13291-9.

JIN, X., MALYKHINA, A. P., LUPU, F. & AKBARALI, H. I. 2004. Altered gene expression and increased bursting activity of colonic smooth muscle ATP-sensitive K+ channels in experimental colitis. *Am J Physiol Gastrointest Liver Physiol,* 287**,** G274-85.

JOSEPH, B. K., THAKALI, K. M., MOORE, C. L. & RHEE, S. W. 2013. Ion channel remodeling in vascular smooth muscle during hypertension: Implications for novel therapeutic approaches. *Pharmacol Res,* 70**,** 126-38.

KABRA, N. & NADKARNI, A. 2013. Prevalence of depression and anxiety in irritable bowel syndrome: A clinic based study from India. *Indian J Psychiatry,* 55**,** 77-80.

KANG, D., CHOE, C. & KIM, D. 2005a. Thermosensitivity of the two-pore domain K+ channels TREK-2 and TRAAK. *J Physiol,* 564**,** 103-16.

KANG, D., HAN, J., TALLEY, E. M., BAYLISS, D. A. & KIM, D. 2004a. Functional expression of TASK-1/TASK-3 heteromers in cerebellar granule cells. *J Physiol,* 554**,** 64-77.

KANG, D., MARIASH, E. & KIM, D. 2004b. Functional expression of TRESK-2, a new member of the tandem-pore K+ channel family. *J Biol Chem,* 279**,** 28063-70.

KANG, J., CHEN, X. L., WANG, H., JI, J., CHENG, H., INCARDONA, J., REYNOLDS, W., VIVIANI, F., TABART, M. & RAMPE, D. 2005b. Discovery of a small molecule activator of the human ether-a-go-go-related gene (HERG) cardiac K+ channel. *Mol Pharmacol,* 67**,** 827-36.

KANG, M., MORSY, N., JIN, X., LUPU, F. & AKBARALI, H. I. 2004c. Protein and gene expression of Ca2+ channel isoforms in murine colon: effect of inflammation. *Pflugers Arch,* 449**,** 288-97.

KAZAMA, I. 2015. Roles of lymphocyte Kv1.3-channels in gut mucosal immune system: Novel therapeutic implications for inflammatory bowel disease. *Med Hypotheses,* 85**,** 61-3.

KENNARD, L. E., CHUMBLEY, J. R., RANATUNGA, K. M., ARMSTRONG, S. J., VEALE, E. L. & MATHIE, A. 2005. Inhibition of the human two-pore domain potassium channel, TREK-1, by fluoxetine and its metabolite norfluoxetine. *Br J Pharmacol,* 144**,** 821-9.

KESHAVAPRASAD, B., LIU, C., AU, J. D., KINDLER, C. H., COTTEN, J. F. & YOST, C. S. 2005. Species-specific differences in response to anesthetics and other modulators by the K2P channel TRESK. *Anesth Analg,* 101**,** 1042-9, table of contents.

KESSARIS, N., FOGARTY, M., IANNARELLI, P., GRIST, M., WEGNER, M. & RICHARDSON, W. D. 2006. Competing waves of oligodendrocytes in the forebrain and postnatal elimination of an embryonic lineage. *Nat Neurosci,* 9**,** 173-9.

KETCHUM, K. A., JOINER, W. J., SELLERS, A. J., KACZMAREK, L. K. & GOLDSTEIN, S. A. N. 1995. A new family of outwardly rectifying potassium channel proteins with two pore domains in tandem. *Nature,* 376**,** 690.

KEW, J. & DAVIES, C. 2010. *Ion channels from structure to function,* New York, Oxford University Press Inc.

KEYNES, R. D., AIDLEY, D. J. & HUANG, C. L. H. 2011. *Nerve and muscle,* Cambridge ; New York, Cambridge University Press.

KIM, D., CAVANAUGH, E. J., KIM, I. & CARROLL, J. L. 2009. Heteromeric TASK-1/TASK-3 is the major oxygen-sensitive background K+ channel in rat carotid body glomus cells. *J Physiol,* 587**,** 2963-75.

KIM, E., HWANG, E. M., YARISHKIN, O., YOO, J. C., KIM, D., PARK, N., CHO, M., LEE, Y. S., SUN, C. H., YI, G. S., YOO, J., KANG, D., HAN, J., HONG, S. G. & PARK, J. Y. 2010. Enhancement of TREK1 channel surface expression by protein-protein interaction with beta-COP. *Biochem Biophys Res Commun,* 395**,** 244-50.

KIM, Y., BANG, H., GNATENCO, C. & KIM, D. 2001a. Synergistic interaction and the role of C-terminus in the activation of TRAAK K+ channels by pressure, free fatty acids and alkali. *Pflugers Arch,* 442**,** 64-72.

KIM, Y., GNATENCO, C., BANG, H. & KIM, D. 2001b. Localization of TREK-2 K+ channel domains that regulate channel kinetics and sensitivity to pressure, fatty acids and pHi. *Pflugers Arch,* 442**,** 952-60.

KNOX, A. J. & TATTERSFIELD, A. E. 1995. Airway smooth muscle relaxation. *Thorax,* 50**,** 894-901.

KOH, S. D., BRADLEY, K. K., RAE, M. G., KEEF, K. D., HOROWITZ, B. & SANDERS, K. M. 1998. Basal activation of ATP-sensitive potassium channels in murine colonic smooth muscle cell. *Biophys J,* 75**,** 1793-800.

KOH, S. D., MONAGHAN, K., SERGEANT, G. P., RO, S., WALKER, R. L., SANDERS, K. M. & HOROWITZ, B. 2001. TREK-1 regulation by nitric oxide and cGMP-dependent protein kinase. An essential role in smooth muscle inhibitory neurotransmission. *J Biol Chem,* 276**,** 44338-46.

KOH, S. D. & SANDERS, K. M. 2001. Stretch-dependent potassium channels in murine colonic smooth muscle cells. *J Physiol,* 533**,** 155-63.

KOH, S. D., SANDERS, K. M. & CARL, A. 1996. Regulation of smooth muscle delayed rectifier K+ channels by protein kinase A. *Pflugers Arch,* 432**,** 401-12.

KOH, S. D., WARD, S. M., DICK, G. M., EPPERSON, A., BONNER, H. P., SANDERS, K. M., HOROWITZ, B. & KENYON, J. L. 1999. Contribution of delayed rectifier potassium currents to the electrical activity of murine colonic smooth muscle. *J Physiol,* 515 ( Pt 2)**,** 475-87.

KOH, S. D., WARD, S. M. & SANDERS, K. M. 2012. Ionic conductances regulating the excitability of colonic smooth muscles. *Neurogastroenterol Motil,* 24**,** 705-18.

KUBOTA, K., OHTAKE, N., OHBUCHI, K., MASE, A., IMAMURA, S., SUDO, Y., MIYANO, K., YAMAMOTO, M., KONO, T. & UEZONO, Y. 2015. Hydroxy-alpha sanshool induces colonic

motor activity in rat proximal colon: a possible involvement of KCNK9. *Am J Physiol Gastrointest Liver Physiol,* 308**,** G579-90.

KUNTAMALLAPPANAVAR, G. & DOPICO, A. M. 2016. Alcohol modulation of BK channel gating depends on beta subunit composition. *J Gen Physiol,* 148**,** 419-440.

KUNZE, W. A. & FURNESS, J. B. 1999. The enteric nervous system and regulation of intestinal motility. *Annu Rev Physiol,* 61**,** 117-42.

KUO, H. C., CHENG, C. F., CLARK, R. B., LIN, J. J., LIN, J. L., HOSHIJIMA, M., NGUYEN-TRAN, V. T., GU, Y., IKEDA, Y., CHU, P. H., ROSS, J., GILES, W. R. & CHIEN, K. R. 2001. A defect in the Kv channel-interacting protein 2 (KChIP2) gene leads to a complete loss of I(to) and confers susceptibility to ventricular tachycardia. *Cell,* 107**,** 801-13.

KURNIAWAN, I. & KOLOPAKING, M. S. 2014. Management of irritable bowel syndrome in the elderly. *Acta Med Indones,* 46**,** 138-47.

LARSEN, C. K., PRAETORIUS, H. A., LEIPZIGER, J. & SORENSEN, M. V. 2017. Intact colonic KCa1.1 channel activity in KCNMB2 knockout mice. *Physiol Rep,* 5.

LEI, Q., PAN, X. Q., CHANG, S., MALKOWICZ, S. B., GUZZO, T. J. & MALYKHINA, A. P. 2014. Response of the human detrusor to stretch is regulated by TREK-1, a two-pore-domain (K2P) mechano-gated potassium channel. *J Physiol,* 592**,** 3013-30.

LEMBRECHTS, R., PINTELON, I., SCHNORBUSCH, K., TIMMERMANS, J. P., ADRIAENSEN, D. & BROUNS, I. 2011. Expression of mechanogated two-pore domain potassium channels in mouse lungs: special reference to mechanosensory airway receptors. *Histochem Cell Biol,* 136**,** 371-85.

LENGYEL, M., CZIRJAK, G. & ENYEDI, P. 2016. Formation of Functional Heterodimers by TREK-1 and TREK-2 Two-pore Domain Potassium Channel Subunits. *J Biol Chem,* 291**,** 13649-61.

LERCHE, C., BRUHOVA, I., LERCHE, H., STEINMEYER, K., WEI, A. D., STRUTZ-SEEBOHM, N., LANG, F., BUSCH, A. E., ZHOROV, B. S. & SEEBOHM, G. 2007. Chromanol 293B binding in KCNQ1 (Kv7.1) channels involves electrostatic interactions with a potassium ion in the selectivity filter. *Mol Pharmacol,* 71**,** 1503-11.

LESAGE, F., GUILLEMARE, E., FINK, M., DUPRAT, F., LAZDUNSKI, M., ROMEY, G. & BARHANIN, J. 1996. TWIK-1, a ubiquitous human weakly inward rectifying K+ channel with a novel structure. *EMBO J,* 15**,** 1004-11.

LESAGE, F., TERRENOIRE, C., ROMEY, G. & LAZDUNSKI, M. 2000. Human TREK2, a 2P domain mechano-sensitive K+ channel with multiple regulations by polyunsaturated fatty acids, lysophospholipids, and Gs, Gi, and Gq protein-coupled receptors. *J Biol Chem,* 275**,** 28398-405.

LEVITZ, J., ROYAL, P., COMOGLIO, Y., WDZIEKONSKI, B., SCHAUB, S., CLEMENS, D. M., ISACOFF, E. Y. & SANDOZ, G. 2016. Heterodimerization within the TREK channel subfamily produces a diverse family of highly regulated potassium channels. *Proc Natl Acad Sci U S A,* 113**,** 4194-9.

LEWIS, A., HARTNESS, M. E., CHAPMAN, C. G., FEARON, I. M., MEADOWS, H. J., PEERS, C. & KEMP, P. J. 2001. Recombinant hTASK1 is an O(2)-sensitive K(+) channel. *Biochem Biophys Res Commun,* 285**,** 1290-4.

LEWIS, L. M., BHAVE, G., CHAUDER, B. A., BANERJEE, S., LORNSEN, K. A., REDHA, R., FALLEN, K., LINDSLEY, C. W., WEAVER, C. D. & DENTON, J. S. 2009. High-throughput screening reveals a small-molecule inhibitor of the renal outer medullary potassium channel and Kir7.1. *Mol Pharmacol,* 76**,** 1094-103.

LI, G., SHI, R., WU, J., HAN, W., ZHANG, A., CHENG, G., XUE, X. & SUN, C. 2016. Association of the hERG mutation with long-QT syndrome type 2, syncope and epilepsy. *Mol Med Rep,* 13**,** 2467-75.

LI, M., ZHANG, Z., KOH, H., LU, R., JIANG, Z., ALIOUA, A., GARCIA-VALDES, J., STEFANI, E. & TORO, L. 2013. The beta1-subunit of the MaxiK channel associates with the thromboxane A2 receptor and reduces thromboxane A2 functional effects. *J Biol Chem,* 288**,** 3668-77.

LIU, C., AU, J. D., ZOU, H. L., COTTEN, J. F. & YOST, C. S. 2004. Potent activation of the human tandem pore domain K channel TRESK with clinical concentrations of volatile anesthetics. *Anesth Analg,* 99**,** 1715-22, table of contents.

LIU, D. H., HUANG, X., GUO, X., MENG, X. M., WU, Y. S., LU, H. L., ZHANG, C. M., KIM, Y. C. & XU, W. X. 2014. Voltage dependent potassium channel remodeling in murine intestinal smooth muscle hypertrophy induced by partial obstruction. *PLoS One,* 9**,** e86109.

LIU, M., SEINO, S. & KIRCHGESSNER, A. L. 1999. Identification and characterization of glucoresponsive neurons in the enteric nervous system. *J Neurosci,* 19**,** 10305-17.

LIVAK, K. J. & SCHMITTGEN, T. D. 2001. Analysis of relative gene expression data using real-time quantitative PCR and the 2(-Delta Delta C(T)) Method. *Methods,* 25**,** 402-8.

LODGE, N. J. & LI, Y. W. 2008. Ion channels as potential targets for the treatment of depression. *Curr Opin Drug Discov Devel,* 11**,** 633-41.

LOLICATO, M., ARRIGONI, C., MORI, T., SEKIOKA, Y., BRYANT, C., CLARK, K. A. & MINOR, D. L., JR. 2017. K2P2.1 (TREK-1)-activator complexes reveal a cryptic selectivity filter binding site. *Nature,* 547**,** 364-368.

LOLICATO, M., RIEGELHAUPT, P. M., ARRIGONI, C., CLARK, K. A. & MINOR, D. L., JR. 2014. Transmembrane helix straightening and buckling underlies activation of mechanosensitive and thermosensitive K(2P) channels. *Neuron,* 84**,** 1198-212.

LOMAX, A. E. & FURNESS, J. B. 2000. Neurochemical classification of enteric neurons in the guinea-pig distal colon. *Cell Tissue Res,* 302**,** 59-72.

LONG, S. B., CAMPBELL, E. B. & MACKINNON, R. 2005a. Crystal structure of a mammalian voltage-dependent Shaker family K+ channel. *Science,* 309**,** 897-903.

LONG, S. B., CAMPBELL, E. B. & MACKINNON, R. 2005b. Voltage sensor of Kv1.2: structural basis of electromechanical coupling. *Science,* 309**,** 903-8.

LOPES, C. M., ZHANG, H., ROHACS, T., JIN, T., YANG, J. & LOGOTHETIS, D. E. 2002. Alterations in conserved Kir channel-PIP2 interactions underlie channelopathies. *Neuron,* 34**,** 933-44.

LOTSHAW, D. P. 2007. Biophysical, pharmacological, and functional characteristics of cloned and native mammalian two-pore domain K+ channels. *Cell Biochem Biophys,* 47**,** 209-56.

LU, W., LI, J., GONG, L., XU, X., HAN, T., YE, Y., CHE, T., LUO, Y., LI, J., ZHAN, R., YAO, W., LIU, K., CUI, S. & LIU, C. 2014. H2 S modulates duodenal motility in male rats via activating TRPV1 and K(ATP) channels. *Br J Pharmacol,* 171**,** 1534-50.

LUNDBY, A., JESPERSEN, T., SCHMITT, N., GRUNNET, M., OLESEN, S. P., CORDEIRO, J. M. & CALLOE, K. 2010. Effect of the I-to activator NS5806 on cloned K(v)4 channels depends on the accessory protein KChIP2. *British Journal of Pharmacology,* 160**,** 2028-2044.

LUNDBY, A. & OLESEN, S. P. 2006. KCNE3 is an inhibitory subunit of the Kv4.3 potassium channel. *Biochem Biophys Res Commun,* 346**,** 958-67.

LYDIARD, R. B. 2001. Irritable bowel syndrome, anxiety, and depression: what are the links? *J Clin Psychiatry,* 62 Suppl 8**,** 38-45; discussion 46-7.

LYDIARD, R. B. & FALSETTI, S. A. 1999. Experience with anxiety and depression treatment studies: implications for designing irritable bowel syndrome clinical trials. *Am J Med,* 107**,** 65S-73S.

MA, L., XIE, Y. P., ZHOU, M. & CHEN, H. 2012. Silent TWIK-1 potassium channels conduct monovalent cation currents. *Biophys J,* 102**,** L34-6.

MA, X. Y., YU, J. M., ZHANG, S. Z., LIU, X. Y., WU, B. H., WEI, X. L., YAN, J. Q., SUN, H. L., YAN, H. T. & ZHENG, J. Q. 2011. External Ba2+ block of the two-pore domain potassium channel TREK-1 defines conformational transition in its selectivity filter. *J Biol Chem,* 286**,** 39813-22.

MACKINNON, R. 2004. Potassium channels and the atomic basis of selective ion conduction (Nobel Lecture). *Angew Chem Int Ed Engl,* 43**,** 4265-77.

MACKINNON, R., ALDRICH, R. W. & LEE, A. W. 1993. Functional stoichiometry of Shaker potassium channel inactivation. *Science,* 262**,** 757-9.

MAILLOT, C., MILLION, M., WEI, J. Y., GAUTHIER, A. & TACHE, Y. 2000. Peripheral corticotropin-releasing factor and stress-stimulated colonic motor activity involve type 1 receptor in rats. *Gastroenterology,* 119**,** 1569-79.

MAINGRET, F., LAURITZEN, I., PATEL, A. J., HEURTEAUX, C., REYES, R., LESAGE, F., LAZDUNSKI, M. & HONORE, E. 2000a. TREK-1 is a heat-activated background K(+) channel. *EMBO J,* 19**,** 2483-91.

MAINGRET, F., PATEL, A. J., LAZDUNSKI, M. & HONORE, E. 2001. The endocannabinoid anandamide is a direct and selective blocker of the background K(+) channel TASK-1. *EMBO J,* 20**,** 47-54.

MAINGRET, F., PATEL, A. J., LESAGE, F., LAZDUNSKI, M. & HONORE, E. 1999. Mechano- or acid stimulation, two interactive modes of activation of the TREK-1 potassium channel. *J Biol Chem,* 274**,** 26691-6.

MAINGRET, F., PATEL, A. J., LESAGE, F., LAZDUNSKI, M. & HONORE, E. 2000b. Lysophospholipids open the two-pore domain mechano-gated K(+) channels TREK-1 and TRAAK. *J Biol Chem,* 275**,** 10128-33.

MANE, V. P., HEUER, M. A., HILLYER, P., NAVARRO, M. B. & RABIN, R. L. 2008. Systematic method for determining an ideal housekeeping gene for real-time PCR analysis. *J Biomol Tech,* 19**,** 342-7.

MARYNOWSKI, M., LIKONSKA, A., ZATORSKI, H. & FICHNA, J. 2015. Role of environmental pollution in irritable bowel syndrome. *World J Gastroenterol,* 21**,** 11371-8.

MATHIE, A. & VEALE, E. L. 2007. Therapeutic potential of neuronal two-pore domain potassium-channel modulators. *Curr Opin Investig Drugs,* 8**,** 555-62.

MATSUBARA, H., SUZUKI, J. & INADA, M. 1993. Shaker-related potassium channel, Kv1.4, mRNA regulation in cultured rat heart myocytes and differential expression of Kv1.4 and Kv1.5 genes in myocardial development and hypertrophy. *J Clin Invest,* 92**,** 1659-66.

MAUDLEJ, N. & HANANI, M. 1992. Modulation of dye coupling among glial cells in the myenteric and submucosal plexuses of the guinea pig. *Brain Res,* 578**,** 94-8.

MAZELLA, J., PETRAULT, O., LUCAS, G., DEVAL, E., BERAUD-DUFOUR, S., GANDIN, C., EL-YACOUBI, M., WIDMANN, C., GUYON, A., CHEVET, E., TAOUJI, S., CONDUCTIER, G., CORINUS, A., COPPOLA, T., GOBBI, G., NAHON, J. L., HEURTEAUX, C. & BORSOTTO, M. 2010. Spadin, a sortilin-derived peptide, targeting rodent TREK-1 channels: a new concept in the antidepressant drug design. *PLoS Biol,* 8**,** e1000355.

MCCLAIN, J. L., FRIED, D. E. & GULBRANSEN, B. D. 2015. Agonist-evoked Ca(2+) signaling in enteric glia drives neural programs that regulate intestinal motility in mice. *Cell Mol Gastroenterol Hepatol,* 1**,** 631-645.

MCCLENAGHAN, C., SCHEWE, M., ARYAL, P., CARPENTER, E. P., BAUKROWITZ, T. & TUCKER, S. J. 2016. Polymodal activation of the TREK-2 K2P channel produces structurally distinct open states. *J Gen Physiol,* 147**,** 497-505.

MCCLOSKEY, C., RADA, C., BAILEY, E., MCCAVERA, S., VAN DEN BERG, H. A., ATIA, J., RAND, D. A., SHMYGOL, A., CHAN, Y. W., QUENBY, S., BROSENS, J. J., VATISH, M., ZHANG, J., DENTON, J. S., TAGGART, M. J., KETTLEBOROUGH, C., TICKLE, D., JERMAN, J., WRIGHT, P., DALE, T., KANUMILLI, S., TREZISE, D. J., THORNTON, S., BROWN, P., CATALANO, R., LIN, N., ENGLAND, S. K. & BLANKS, A. M. 2014. The inwardly rectifying K+ channel KIR7.1 controls uterine excitability throughout pregnancy. *EMBO Mol Med,* 6**,** 1161-74.

MCHUGH, D. & BEECH, D. J. 1995. Inhibition of delayed rectifier K(+)-current by levcromakalim in single intestinal smooth muscle cells: effects of cations and dependence on K(+)-flux. *Br J Pharmacol,* 114**,** 391-9.

MCPHERSON, G. A. & ANGUS, J. A. 1990. Characterization of responses to cromakalim and pinacidil in smooth and cardiac muscle by use of selective antagonists. *Br J Pharmacol,* 100**,** 201-6.

MEADOWS, H. J., BENHAM, C. D., CAIRNS, W., GLOGER, I., JENNINGS, C., MEDHURST, A. D., MURDOCK, P. & CHAPMAN, C. G. 2000. Cloning, localisation and functional expression of the human orthologue of the TREK-1 potassium channel. *Pflugers Arch,* 439**,** 714-22.

MEDHURST, A. D., RENNIE, G., CHAPMAN, C. G., MEADOWS, H., DUCKWORTH, M. D., KELSELL, R. E., GLOGER, II & PANGALOS, M. N. 2001. Distribution analysis of human two pore domain potassium channels in tissues of the central nervous system and periphery. *Brain Res Mol Brain Res,* 86**,** 101-14.

MEGIAS, M., ALVAREZ-OTERO, R. & POMBAL, M. A. 2003. Calbindin and calretinin immunoreactivities identify different types of neurons in the adult lamprey spinal cord. *J Comp Neurol,* 455**,** 72-85.

MENE, P. & PIROZZI, N. 2013. Potassium channels, renal fibrosis, and diabetes. *Diabetes,* 62**,** 2648-50.

MEVES, H. 2008. Arachidonic acid and ion channels: an update. *Br J Pharmacol,* 155**,** 4-16.

MITCHESON, J. S., CHEN, J. & SANGUINETTI, M. C. 2000. Trapping of a methanesulfonanilide by closure of the HERG potassium channel activation gate. *J Gen Physiol,* 115**,** 229-40.

MITTAL, R., DEBS, L. H., PATEL, A. P., NGUYEN, D., PATEL, K., O'CONNOR, G., GRATI, M., MITTAL, J., YAN, D., ESHRAGHI, A. A., DEO, S. K., DAUNERT, S. & LIU, X. Z. 2017. Neurotransmitters: The Critical Modulators Regulating Gut-Brain Axis. *J Cell Physiol,* 232**,** 2359-2372.

MOHA OU MAATI, H., VEYSSIERE, J., LABBAL, F., COPPOLA, T., GANDIN, C., WIDMANN, C., MAZELLA, J., HEURTEAUX, C. & BORSOTTO, M. 2012. Spadin as a new antidepressant: absence of TREK-1-related side effects. *Neuropharmacology,* 62**,** 278-88.

MONAGHAN, K., BAKER, S. A., DWYER, L., HATTON, W. C., SIK PARK, K., SANDERS, K. M. & KOH, S. D. 2011. The stretch-dependent potassium channel TREK-1 and its function in murine myometrium. *J Physiol,* 589**,** 1221-33.

MONTELL, C., BIRNBAUMER, L. & FLOCKERZI, V. 2002. The TRP channels, a remarkably functional family. *Cell,* 108**,** 595-8.

MORAIS-CABRAL, J. H., ZHOU, Y. & MACKINNON, R. 2001. Energetic optimization of ion conduction rate by the K+ selectivity filter. *Nature,* 414**,** 37-42.

MORIMURA, K., YAMAMURA, H., OHYA, S. & IMAIZUMI, Y. 2006. Voltage-dependent Ca2+-channel block by openers of intermediate and small conductance Ca2+-activated K+ channels in urinary bladder smooth muscle cells. *J Pharmacol Sci,* 100**,** 237-41.

MOURRE, C., MANRIQUE, C., CAMON, J., AIDI-KNANI, S., DELTHEIL, T., TURLE-LORENZO, N., GUIRAUDIE-CAPRAZ, G. & AMALRIC, M. 2017. Changes in SK channel expression in the basal ganglia after partial nigrostriatal dopamine lesions in rats: Functional consequences. *Neuropharmacology,* 113**,** 519-532.

NA, J. S., HONG, C., KIM, M. W., PARK, C. G., KANG, H. G., WU, M. J., JIAO, H. Y., CHOI, S. & JUN, J. Y. 2017. ATP-sensitive K(+) channels maintain resting membrane potential in interstitial cells of Cajal from the mouse colon. *Eur J Pharmacol,* 809**,** 98-104.

NADAL, M. S., AMARILLO, Y., VEGA-SAENZ DE MIERA, E. & RUDY, B. 2001. Evidence for the presence of a novel Kv4-mediated A-type K(+) channel-modifying factor. *J Physiol,* 537**,** 801-9.

NADAL, M. S., OZAITA, A., AMARILLO, Y., VEGA-SAENZ DE MIERA, E., MA, Y., MO, W., GOLDBERG, E. M., MISUMI, Y., IKEHARA, Y., NEUBERT, T. A. & RUDY, B. 2003. The CD26-related dipeptidyl aminopeptidase-like protein DPPX is a critical component of neuronal A-type K+ channels. *Neuron,* 37**,** 449-61.

NAUSCH, B., RODE, F., JORGENSEN, S., NARDI, A., KORSGAARD, M. P., HOUGAARD, C., BONEV, A. D., BROWN, W. D., DYHRING, T., STROBAEK, D., OLESEN, S. P., CHRISTOPHERSEN, P., GRUNNET, M., NELSON, M. T. & RONN, L. C. 2014. NS19504: a novel BK channel activator with relaxing effect on bladder smooth muscle spontaneous phasic contractions. *J Pharmacol Exp Ther,* 350**,** 520-30.

NERBONNE, J. M. 2000. Molecular basis of functional voltage-gated K+ channel diversity in the mammalian myocardium. *J Physiol,* 525 Pt 2**,** 285-98.

NEYLON, C. B., NURGALI, K., HUNNE, B., ROBBINS, H. L., MOORE, S., CHEN, M. X. & FURNESS, J. B. 2004. Intermediate-conductance calcium-activated potassium channels in enteric

neurones of the mouse: pharmacological, molecular and immunochemical evidence for their role in mediating the slow afterhyperpolarization. *J Neurochem,* 90**,** 1414-22.

NEZAMI, B. G. & SRINIVASAN, S. 2010. Enteric nervous system in the small intestine: pathophysiology and clinical implications. *Curr Gastroenterol Rep,* 12**,** 358-65.

NIE, X., ARRIGHI, I., KAISSLING, B., PFAFF, I., MANN, J., BARHANIN, J. & VALLON, V. 2005. Expression and insights on function of potassium channel TWIK-1 in mouse kidney. *Pflugers Arch,* 451**,** 479-88.

NIEL, J. P., BYWATER, R. A. & TAYLOR, G. S. 1983. Apamin-resistant post-stimulus hyperpolarization in the circular muscle of the guinea-pig ileum. *J Auton Nerv Syst,* 9**,** 565-9.

NIEMEYER, M. I., CID, L. P., BARROS, L. F. & SEPULVEDA, F. V. 2001. Modulation of the two-pore domain acid-sensitive K+ channel TASK-2 (KCNK5) by changes in cell volume. *J Biol Chem,* 276**,** 43166-74.

NISHI, S. & NORTH, R. A. 1973. Intracellular recording from the myenteric plexus of the guinea-pig ileum. *J Physiol,* 231**,** 471-91.

NOEL, J., SANDOZ, G. & LESAGE, F. 2011. Molecular regulations governing TREK and TRAAK channel functions. *Channels (Austin),* 5**,** 402-9.

O'MALLEY, D., DINAN, T. G. & CRYAN, J. F. 2010. Alterations in colonic corticotropin-releasing factor receptors in the maternally separated rat model of irritable bowel syndrome: differential effects of acute psychological and physical stressors. *Peptides,* 31**,** 662-70.

OKUNO, Y., KONDO, T., SAEKI, A., UCHIDA, E., TERAOKA, H. & KITAZAWA, T. 2011. Colon-specific contractile responses to tetrodotoxin in the isolated mouse gastrointestinal tract. *Auton Autacoid Pharmacol,* 31**,** 21-30.

OLDEN, K. W. 2005. The use of antidepressants in functional gastrointestinal disorders: new uses for old drugs. *CNS Spectr,* 10**,** 891-6.

OONUMA, H., IWASAWA, K., IIDA, H., NAGATA, T., IMUTA, H., MORITA, Y., YAMAMOTO, K., NAGAI, R., OMATA, M. & NAKAJIMA, T. 2002. Inward rectifier K(+) current in human bronchial smooth muscle cells: inhibition with antisense oligonucleotides targeted to Kir2.1 mRNA. *Am J Respir Cell Mol Biol,* 26**,** 371-9.

OPIE, L. H. 1997. Pharmacological differences between calcium antagonists. *Eur Heart J,* 18 Suppl A**,** A71-9.

ORDOG, B., BRUTYO, E., PUSKAS, L. G., PAPP, J. G., VARRO, A., SZABAD, J. & BOLDOGKOI, Z. 2006. Gene expression profiling of human cardiac potassium and sodium channels. *Int J Cardiol,* 111**,** 386-93.

ORTNER, N. J. & STRIESSNIG, J. 2016. L-type calcium channels as drug targets in CNS disorders. *Channels (Austin),* 10**,** 7-13.

OSAWA, M., YOKOGAWA, M., MURAMATSU, T., KIMURA, T., MASE, Y. & SHIMADA, I. 2009. Evidence for the direct interaction of spermine with the inwardly rectifying potassium channel. *J Biol Chem,* 284**,** 26117-26.

OTTSCHYTSCH, N., RAES, A., VAN HOORICK, D. & SNYDERS, D. J. 2002. Obligatory heterotetramerization of three previously uncharacterized Kv channel alpha-subunits identified in the human genome. *Proc Natl Acad Sci U S A,* 99**,** 7986-91.

PARELKAR, N. K., SILSWAL, N., JANSEN, K., VAUGHN, J., BRYAN, R. M., JR. & ANDRESEN, J. 2010. 2,2,2-trichloroethanol activates a nonclassical potassium channel in cerebrovascular smooth muscle and dilates the middle cerebral artery. *J Pharmacol Exp Ther,* 332**,** 803-10.

PARK, K. J., BAKER, S. A., CHO, S. Y., SANDERS, K. M. & KOH, S. D. 2005. Sulfur-containing amino acids block stretch-dependent K+ channels and nitrergic responses in the murine colon. *Br J Pharmacol,* 144**,** 1126-37.

PATEL, A. J., HONORE, E., LESAGE, F., FINK, M., ROMEY, G. & LAZDUNSKI, M. 1999. Inhalational anesthetics activate two-pore-domain background K+ channels. *Nature Neuroscience,* 2**,** 422-426.

PATEL, A. J., HONORE, E., MAINGRET, F., LESAGE, F., FINK, M., DUPRAT, F. & LAZDUNSKI, M. 1998. A mammalian two pore domain mechano-gated S-like K+ channel. *EMBO J,* 17**,** 4283-90.

PATEL, A. J., LAZDUNSKI, M. & HONORE, E. 2001. Lipid and mechano-gated 2P domain K(+) channels. *Curr Opin Cell Biol,* 13**,** 422-8.

PATEL, A. J., MAINGRET, F., MAGNONE, V., FOSSET, M., LAZDUNSKI, M. & HONORE, E. 2000. TWIK-2, an inactivating 2P domain K+ channel. *J Biol Chem,* 275**,** 28722-30.

PEIRSON, S. N., BUTLER, J. N. & FOSTER, R. G. 2003. Experimental validation of novel and conventional approaches to quantitative real-time PCR data analysis. *Nucleic Acids Res,* 31**,** e73.

PENG, I. F. & WU, C. F. 2007. Differential contributions of Shaker and Shab K+ currents to neuronal firing patterns in Drosophila. *J Neurophysiol,* 97**,** 780-94.

PETKOV, G. V., BONEV, A. D., HEPPNER, T. J., BRENNER, R., ALDRICH, R. W. & NELSON, M. T. 2001. Beta1-subunit of the Ca2+-activated K+ channel regulates contractile activity of mouse urinary bladder smooth muscle. *J Physiol,* 537**,** 443-52.

PFAFFL, M. W. 2001. A new mathematical model for relative quantification in real-time RT-PCR. *Nucleic Acids Res,* 29**,** e45.

PLANT, L. D., RAJAN, S. & GOLDSTEIN, S. A. 2005. K2P channels and their protein partners. *Curr Opin Neurobiol,* 15**,** 326-33.

PLANT, L. D., ZUNIGA, L., ARAKI, D., MARKS, J. D. & GOLDSTEIN, S. A. N. 2012. SUMOylation Silences Heterodimeric TASK Potassium Channels Containing K2P1 Subunits in Cerebellar Granule Neurons. *Science Signaling,* 5.

POPE, L., ARRIGONI, C., LOU, H., BRYANT, C., GALLARDO-GODOY, A., RENSLO, A. R. & MINOR, D. L., JR. 2018. Protein and Chemical Determinants of BL-1249 Action and Selectivity for K2P Channels. *ACS Chem Neurosci*.

POST, J. M., STEVENS, R. J., SANDERS, K. M. & HUME, J. R. 1991. Effect of cromakalim and lemakalim on slow waves and membrane currents in colonic smooth muscle. *Am J Physiol,* 260**,** C375-82.

POST, M. A., KIRSCH, G. E. & BROWN, A. M. 1996. Kv2.1 and electrically silent Kv6.1 potassium channel subunits combine and express a novel current. *FEBS Lett,* 399**,** 177-82.

POTIER, M., JOULIN, V., ROGER, S., BESSON, P., JOURDAN, M. L., LEGUENNEC, J. Y., BOUGNOUX, P. & VANDIER, C. 2006. Identification of SK3 channel as a new mediator of breast cancer cell migration. *Mol Cancer Ther,* 5**,** 2946-53.

POUOKAM, E., BADER, S., BRUCK, B., SCHMIDT, B. & DIENER, M. 2013. ATP-sensitive K(+) channels in rat colonic epithelium. *Pflugers Arch,* 465**,** 865-77.

PREISIG-MULLER, R., SCHLICHTHORL, G., GOERGE, T., HEINEN, S., BRUGGEMANN, A., RAJAN, S., DERST, C., VEH, R. W. & DAUT, J. 2002. Heteromerization of Kir2.x potassium channels contributes to the phenotype of Andersen's syndrome. *Proc Natl Acad Sci U S A,* 99**,** 7774-9.

PRESTON, P., WARTOSCH, L., GUNZEL, D., FROMM, M., KONGSUPHOL, P., OUSINGSAWAT, J., KUNZELMANN, K., BARHANIN, J., WARTH, R. & JENTSCH, T. J. 2010. Disruption of the K+ channel beta-subunit KCNE3 reveals an important role in intestinal and tracheal Cl- transport. *J Biol Chem,* 285**,** 7165-75.

QUAYLE, J. M., STANDEN, N. B. & STANFIELD, P. R. 1988. The voltage-dependent block of ATP-sensitive potassium channels of frog skeletal muscle by caesium and barium ions. *J Physiol,* 405**,** 677-97.

RADULOVIC, M., ANAND, P., KORSTEN, M. A. & GONG, B. 2015. Targeting Ion Channels: An Important Therapeutic Implication in Gastrointestinal Dysmotility in Patients With Spinal Cord Injury. *J Neurogastroenterol Motil,* 21**,** 494-502.

RAJAN, S., PLANT, L. D., RABIN, M. L., BUTLER, M. H. & GOLDSTEIN, S. A. 2005. Sumoylation silences the plasma membrane leak K+ channel K2P1. *Cell,* 121**,** 37-47.

RAJAN, S., WISCHMEYER, E., KARSCHIN, C., PREISIG-MULLER, R., GRZESCHIK, K. H., DAUT, J., KARSCHIN, A. & DERST, C. 2001. THIK-1 and THIK-2, a novel subfamily of tandem pore domain K+ channels. *J Biol Chem,* 276**,** 7302-11.

RAMAKERS, C., VOS, M. A., DOEVENDANS, P. A., SCHOENMAKERS, M., WU, Y. S., SCICCHITANO, S., IODICE, A., THOMAS, G. P., ANTZELEVITCH, C. & DUMAINE, R. 2003. Coordinated down-regulation of KCNQ1 and KCNE1 expression contributes to reduction of I(Ks) in canine hypertrophied hearts. *Cardiovasc Res,* 57**,** 486-96.

RAO, M. & GERSHON, M. D. 2016. The bowel and beyond: the enteric nervous system in neurological disorders. *Nat Rev Gastroenterol Hepatol,* 13**,** 517-28.

RAO, M. & GERSHON, M. D. 2018. Enteric nervous system development: what could possibly go wrong? *Nat Rev Neurosci,* 19**,** 552-565.

RAO, M., NELMS, B. D., DONG, L., SALINAS-RIOS, V., RUTLIN, M., GERSHON, M. D. & CORFAS, G. 2015. Enteric glia express proteolipid protein 1 and are a transcriptionally unique population of glia in the mammalian nervous system. *Glia,* 63**,** 2040-2057.

RAO, M., RASTELLI, D., DONG, L., CHIU, S., SETLIK, W., GERSHON, M. D. & CORFAS, G. 2017. Enteric Glia Regulate Gastrointestinal Motility but Are Not Required for Maintenance of the Epithelium in Mice. *Gastroenterology,* 153**,** 1068-1081 e7.

RASBAND, M. N. 2010. Ion Channels and Excitable Cells. *Nature Education,* 3**,** 41.

REED, K. K. & WICKHAM, R. 2009. Review of the gastrointestinal tract: from macro to micro. *Semin Oncol Nurs,* 25**,** 3-14.

REYES, R., DUPRAT, F., LESAGE, F., FINK, M., SALINAS, M., FARMAN, N. & LAZDUNSKI, M. 1998. Cloning and expression of a novel pH-sensitive two pore domain K+ channel from human kidney. *Journal of Biological Chemistry,* 273**,** 30863-30869.

RICHARDSON, D., ALIBHAI, K. N. & HUIZINGA, J. D. 1992. On the pharmacological and physiological role of glibenclamide-sensitive potassium channels in colonic smooth muscle. *Pharmacol Toxicol,* 71**,** 365-70.

RICHARDSON, F. C. & KACZMAREK, L. K. 2000. Modification of delayed rectifier potassium currents by the Kv9.1 potassium channel subunit. *Hear Res,* 147**,** 21-30.

RINNE, S., KIPER, A. K., SCHLICHTHORL, G., DITTMANN, S., NETTER, M. F., LIMBERG, S. H., SILBERNAGEL, N., ZUZARTE, M., MOOSDORF, R., WULF, H., SCHULZE-BAHR, E., ROLFES, C. & DECHER, N. 2015. TASK-1 and TASK-3 may form heterodimers in human atrial cardiomyocytes. *J Mol Cell Cardiol,* 81**,** 71-80.

ROBBINS, J. 2001. KCNQ potassium channels: physiology, pathophysiology, and pharmacology. *Pharmacol Ther,* 90**,** 1-19.

ROSATI, B., PAN, Z., LYPEN, S., WANG, H. S., COHEN, I., DIXON, J. E. & MCKINNON, D. 2001. Regulation of KChIP2 potassium channel beta subunit gene expression underlies the gradient of transient outward current in canine and human ventricle. *J Physiol,* 533**,** 119-25.

ROUX, B. & MACKINNON, R. 1999. The cavity and pore helices in the KcsA K+ channel: electrostatic stabilization of monovalent cations. *Science,* 285**,** 100-2.

SAHA, L. 2014. Irritable bowel syndrome: pathogenesis, diagnosis, treatment, and evidence-based medicine. *World J Gastroenterol,* 20**,** 6759-73.

SANDER, S. E., LEMM, C., LANGE, N., HAMANN, M. & RICHTER, A. 2012. Retigabine, a K(V)7 (KCNQ) potassium channel opener, attenuates L-DOPA-induced dyskinesias in 6-OHDA-lesioned rats. *Neuropharmacology,* 62**,** 1052-61.

SANDERS, K. M., KITO, Y., HWANG, S. J. & WARD, S. M. 2016. Regulation of Gastrointestinal Smooth Muscle Function by Interstitial Cells. *Physiology (Bethesda),* 31**,** 316-26.

SANDERS, K. M., KOH, S. D., RO, S. & WARD, S. M. 2012a. Regulation of gastrointestinal motility--insights from smooth muscle biology. *Nat Rev Gastroenterol Hepatol,* 9**,** 633-45.

SANDERS, K. M., KOH, S. D., RO, S. & WARD, S. M. 2012b. Regulation of gastrointestinal motility—insights from smooth muscle biology. *Nature Reviews Gastroenterology &Amp; Hepatology,* 9**,** 633.

SANDERS, K. M., KOH, S. D. & WARD, S. M. 2006. Interstitial cells of cajal as pacemakers in the gastrointestinal tract. *Annu Rev Physiol,* 68**,** 307-43.

SANDERS, K. M. & WARD, S. M. 2006. Interstitial cells of Cajal: a new perspective on smooth muscle function. *J Physiol,* 576**,** 721-6.

SANDOZ, G., TARDY, M. P., THUMMLER, S., FELICIANGELI, S., LAZDUNSKI, M. & LESAGE, F. 2008. Mtap2 is a constituent of the protein network that regulates twik-related K+ channel expression and trafficking. *J Neurosci,* 28**,** 8545-52.

SANDOZ, G., THUMMLER, S., DUPRAT, F., FELICIANGELI, S., VINH, J., ESCOUBAS, P., GUY, N., LAZDUNSKI, M. & LESAGE, F. 2006. AKAP150, a switch to convert mechano-, pH- and arachidonic acid- sensitive TREK K+ channels into open leak channels. *Embo Journal,* 25**,** 5864-5872.

SANGUINETTI, M. C. & TRISTANI-FIROUZI, M. 2006. hERG potassium channels and cardiac arrhythmia. *Nature,* 440**,** 463-9.

SANKARANARAYANAN, A., RAMAN, G., BUSCH, C., SCHULTZ, T., ZIMIN, P. I., HOYER, J., KOHLER, R. & WULFF, H. 2009. Naphtho[1,2-d]thiazol-2-ylamine (SKA-31), a new activator of KCa2 and KCa3.1 potassium channels, potentiates the endothelium-derived hyperpolarizing factor response and lowers blood pressure. *Mol Pharmacol,* 75**,** 281-95.

SANO, Y., INAMURA, K., MIYAKE, A., MOCHIZUKI, S., KITADA, C., YOKOI, H., NOZAWA, K., OKADA, H., MATSUSHIME, H. & FURUICHI, K. 2003. A novel two-pore domain K+ channel, TRESK, is localized in the spinal cord. *J Biol Chem,* 278**,** 27406-12.

SANTINI, E. & PORTER, J. T. 2010. M-type potassium channels modulate the intrinsic excitability of infralimbic neurons and regulate fear expression and extinction. *J Neurosci,* 30**,** 12379-86.

SCANZI, J., ACCARIE, A., MULLER, E., PEREIRA, B., AISSOUNI, Y., GOUTTE, M., JOUBERT-ZAKEYH, J., PICARD, E., BOUDIEU, L., MALLET, C., GELOT, A., ARDID, D., CARVALHO, F. A. & DAPOIGNY, M. 2016. Colonic overexpression of the T-type calcium channel Cav 3.2 in a mouse model of visceral hypersensitivity and in irritable bowel syndrome patients. *Neurogastroenterol Motil,* 28**,** 1632-1640.

SCHENZER, A., FRIEDRICH, T., PUSCH, M., SAFTIG, P., JENTSCH, T. J., GROTZINGER, J. & SCHWAKE, M. 2005. Molecular determinants of KCNQ (Kv7) K+ channel sensitivity to the anticonvulsant retigabine. *J Neurosci,* 25**,** 5051-60.

SCHEWE, M., NEMATIAN-ARDESTANI, E., SUN, H., MUSINSZKI, M., CORDEIRO, S., BUCCI, G., DE GROOT, B. L., TUCKER, S. J., RAPEDIUS, M. & BAUKROWITZ, T. 2016. A Non-canonical Voltage-Sensing Mechanism Controls Gating in K2P K(+) Channels. *Cell,* 164**,** 937-49.

SCHROEDER, B. C., WALDEGGER, S., FEHR, S., BLEICH, M., WARTH, R., GREGER, R. & JENTSCH, T. J. 2000. A constitutively open potassium channel formed by KCNQ1 and KCNE3. *Nature,* 403**,** 196-9.

SEEBOHM, G., LERCHE, C., PUSCH, M., STEINMEYER, K., BRUGGEMANN, A. & BUSCH, A. E. 2001. A kinetic study on the stereospecific inhibition of KCNQ1 and I(Ks) by the chromanol 293B. *Br J Pharmacol,* 134**,** 1647-54.

SEIFI, M., BROWN, J. F., MILLS, J., BHANDARI, P., BELELLI, D., LAMBERT, J. J., RUDOLPH, U. & SWINNY, J. D. 2014. Molecular and functional diversity of GABA-A receptors in the enteric nervous system of the mouse colon. *J Neurosci,* 34**,** 10361-78.

SEMENOV, I., WANG, B., HERLIHY, J. T. & BRENNER, R. 2011. BK channel beta1 subunits regulate airway contraction secondary to M2 muscarinic acetylcholine receptor mediated depolarization. *J Physiol,* 589**,** 1803-17.

SHAW, R. M. & COLECRAFT, H. M. 2013. L-type calcium channel targeting and local signalling in cardiac myocytes. *Cardiovasc Res,* 98**,** 177-86.

SHI, W., WANG, H. S., PAN, Z., WYMORE, R. S., COHEN, I. S., MCKINNON, D. & DIXON, J. E. 1998. Cloning of a mammalian elk potassium channel gene and EAG mRNA distribution in rat sympathetic ganglia. *J Physiol,* 511 ( Pt 3)**,** 675-82.

SHIEH, C. C. & KIRSCH, G. E. 1994. Mutational analysis of ion conduction and drug binding sites in the inner mouth of voltage-gated K+ channels. *Biophys J,* 67**,** 2316-25.

SIROIS, J. E., LEI, Q. B., TALLEY, E. M., LYNCH, C. & BAYLISS, D. A. 2000. The TASK-1 two-pore domain K+ channel is a molecular substrate for neuronal effects of inhalation anesthetics. *Journal of Neuroscience,* 20**,** 6347-6354.

SKERN, R., FROST, P. & NILSEN, F. 2005. Relative transcript quantification by quantitative PCR: roughly right or precisely wrong? *BMC Mol Biol,* 6**,** 10.

SMITH, T. K., BURKE, E. P. & SHUTTLEWORTH, C. W. 1999. Topographical and electrophysiological characteristics of highly excitable S neurones in the myenteric plexus of the guinea-pig ileum. *J Physiol,* 517 ( Pt 3)**,** 817-30.

SOBEY, C. G. 2001. Potassium channel function in vascular disease. *Arterioscler Thromb Vasc Biol,* 21**,** 28-38.

SODER, R. P., PARAJULI, S. P., HRISTOV, K. L., ROVNER, E. S. & PETKOV, G. V. 2013. SK channel-selective opening by SKA-31 induces hyperpolarization and decreases contractility in human urinary bladder smooth muscle. *Am J Physiol Regul Integr Comp Physiol,* 304**,** R155-63.

SORENSEN, M. V., MATOS, J. E., SAUSBIER, M., SAUSBIER, U., RUTH, P., PRAETORIUS, H. A. & LEIPZIGER, J. 2008. Aldosterone increases KCa1.1 (BK) channel-mediated colonic K+ secretion. *J Physiol,* 586**,** 4251-64.

SOUSSIA, I. B., CHOVEAU, F. S., BLIN, S., KIM, E. J., FELICIANGELI, S., CHATELAIN, F. C., KANG, D., BICHET, D. & LESAGE, F. 2018. Antagonistic Effect of a Cytoplasmic Domain on the Basal Activity of Polymodal Potassium Channels. *Front Mol Neurosci,* 11**,** 301.

STOTT, J. B., JEPPS, T. A. & GREENWOOD, I. A. 2014. K(V)7 potassium channels: a new therapeutic target in smooth muscle disorders. *Drug Discov Today,* 19**,** 413-24.

STROBAEK, D., TEUBER, L., JORGENSEN, T. D., AHRING, P. K., KJAER, K., HANSEN, R. S., OLESEN, S. P., CHRISTOPHERSEN, P. & SKAANING-JENSEN, B. 2004. Activation of human IK and SK Ca2+ -activated K+ channels by NS309 (6,7-dichloro-1H-indole-2,3-dione 3-oxime). *Biochim Biophys Acta,* 1665**,** 1-5.

SUBRAMANIAM, M., ALTHOF, D., GISPERT, S., SCHWENK, J., AUBURGER, G., KULIK, A., FAKLER, B. & ROEPER, J. 2014. Mutant alpha-synuclein enhances firing frequencies in dopamine substantia nigra neurons by oxidative impairment of A-type potassium channels. *J Neurosci,* 34**,** 13586-99.

SUN, X. P., SCHLICHTER, L. C. & STANLEY, E. F. 1999. Single-channel properties of BK-type calcium-activated potassium channels at a cholinergic presynaptic nerve terminal. *J Physiol,* 518 ( Pt 3)**,** 639-51.

SUN, Y. D. & BENISHIN, C. G. 1994. K+ channel openers relax longitudinal muscle of guinea pig ileum. *Eur J Pharmacol,* 271**,** 453-9.

SUZUKI, Y., TSUTSUMI, K., MIYAMOTO, T., YAMAMURA, H. & IMAIZUMI, Y. 2017. Heterodimerization of two pore domain K+ channel TASK1 and TALK2 in living heterologous expression systems. *PLoS One,* 12**,** e0186252.

TACHE, Y., MARTINEZ, V., MILLION, M. & RIVIER, J. 1999. Corticotropin-releasing factor and the brain-gut motor response to stress. *Can J Gastroenterol,* 13 Suppl A**,** 18A-25A.

TACHE, Y., MARTINEZ, V., WANG, L. & MILLION, M. 2004. CRF1 receptor signaling pathways are involved in stress-related alterations of colonic function and viscerosensitivity: implications for irritable bowel syndrome. *Br J Pharmacol,* 141**,** 1321-30.

TACHE, Y. & PERDUE, M. H. 2004. Role of peripheral CRF signalling pathways in stress-related alterations of gut motility and mucosal function. *Neurogastroenterol Motil,* 16 Suppl 1**,** 137-42.

TAKAHIRA, M., SAKURAI, M., SAKURADA, N. & SUGIYAMA, K. 2005. Fenamates and diltiazem modulate lipid-sensitive mechano-gated 2P domain K(+) channels. *Pflugers Arch,* 451**,** 474-8.

TALLEY, E. M., SOLORZANO, G., LEI, Q., KIM, D. & BAYLISS, D. A. 2001a. Cns distribution of members of the two-pore-domain (KCNK) potassium channel family. *J Neurosci,* 21**,** 7491-505.

TALLEY, E. M., SOLORZANO, G., LEI, Q. B., KIM, D. & BAYLISS, D. A. 2001b. CNS distribution of members of the two-pore-domain (KCNK) potassium channel family. *Journal of Neuroscience,* 21**,** 7491-7505.

TALLEY, N. J. 2003. Evaluation of drug treatment in irritable bowel syndrome. *Br J Clin Pharmacol,* 56**,** 362-9.

TANG, Y. R., YANG, W. W., WANG, Y., GONG, Y. Y., JIANG, L. Q. & LIN, L. 2015. Estrogen regulates the expression of small-conductance Ca-activated K+ channels in colonic smooth muscle cells. *Digestion,* 91**,** 187-96.

TATULIAN, L., DELMAS, P., ABOGADIE, F. C. & BROWN, D. A. 2001. Activation of expressed KCNQ potassium currents and native neuronal M-type potassium currents by the anti-convulsant drug retigabine. *J Neurosci,* 21**,** 5535-45.

TERTYSHNIKOVA, S., KNOX, R. J., PLYM, M. J., THALODY, G., GRIFFIN, C., NEELANDS, T., HARDEN, D. G., SIGNOR, L., WEAVER, D., MYERS, R. A. & LODGE, N. J. 2005. BL-1249 [(5,6,7,8-tetrahydro-naphthalen-1-yl)-[2-(1H-tetrazol-5-yl)-phenyl]-amine]: a putative potassium channel opener with bladder-relaxant properties. *J Pharmacol Exp Ther,* 313**,** 250-9.

THOMPSON-VEST, N., SHIMIZU, Y., HUNNE, B. & FURNESS, J. B. 2006. The distribution of intermediate-conductance, calcium-activated, potassium (IK) channels in epithelial cells. *J Anat,* 208**,** 219-29.

TIAN, C., ZHU, R., ZHU, L., QIU, T., CAO, Z. & KANG, T. 2014. Potassium channels: structures, diseases, and modulators. *Chem Biol Drug Des,* 83**,** 1-26.

TODA, N. & HERMAN, A. G. 2005. Gastrointestinal function regulation by nitrergic efferent nerves. *Pharmacol Rev,* 57**,** 315-38.

TOMUSCHAT, C., O'DONNELL, A. M., COYLE, D., DREHER, N., KELLY, D. & PURI, P. 2016. Altered expression of a two-pore domain (K2P) mechano-gated potassium channel TREK-1 in Hirschsprung's disease. *Pediatr Res,* 80**,** 729-733.

TORTORA, G. J. & DERRICKSON, B. H. 2009. *Principles of anatomy and physiology,* Hoboken, John Wiley & Sons, (Asia) Pte Ltd.

TSANTOULAS, C. & MCMAHON, S. B. 2014. Opening paths to novel analgesics: the role of potassium channels in chronic pain. *Trends Neurosci,* 37**,** 146-58.

TSVILOVSKYY, V. V., ZHOLOS, A. V., ABERLE, T., PHILIPP, S. E., DIETRICH, A., ZHU, M. X., BIRNBAUMER, L., FREICHEL, M. & FLOCKERZI, V. 2009. Deletion of TRPC4 and TRPC6 in mice impairs smooth muscle contraction and intestinal motility in vivo. *Gastroenterology,* 137**,** 1415-24.

VEALE, E. L., AL-MOUBARAK, E., BAJARIA, N., OMOTO, K., CAO, L., TUCKER, S. J., STEVENS, E. B. & MATHIE, A. 2014. Influence of the N terminus on the biophysical properties and pharmacology of TREK1 potassium channels. *Mol Pharmacol,* 85**,** 671-81.

VEALE, E. L. & MATHIE, A. 2016. Aristolochic acid, a plant extract used in the treatment of pain and linked to Balkan endemic nephropathy, is a regulator of K2P channels. *Br J Pharmacol,* 173**,** 1639-52.

VIATCHENKO-KARPINSKI, V., LING, J. & GU, J. G. 2018. Characterization of temperature-sensitive leak K(+) currents and expression of TRAAK, TREK-1, and TREK2 channels in dorsal root ganglion neurons of rats. *Mol Brain,* 11**,** 40.

VILLARROEL, A. 1993. Suppression of neuronal potassium A-current by arachidonic acid. *FEBS Lett,* 335**,** 184-8.

VOGALIS, F. 2000. Potassium channels in gastrointestinal smooth muscle. *J Auton Pharmacol,* 20**,** 207-19.

WANG, H. S., PAN, Z., SHI, W., BROWN, B. S., WYMORE, R. S., COHEN, I. S., DIXON, J. E. & MCKINNON, D. 1998. KCNQ2 and KCNQ3 potassium channel subunits: molecular correlates of the M-channel. *Science,* 282**,** 1890-3.

WANG, W., HUANG, H., HOU, D., LIU, P., WEI, H., FU, X. & NIU, W. 2010. Mechanosensitivity of STREX-lacking BKCa channels in the colonic smooth muscle of the mouse. *Am J Physiol Gastrointest Liver Physiol,* 299**,** G1231-40.

WARTH, R., GARCIA ALZAMORA, M., KIM, J. K., ZDEBIK, A., NITSCHKE, R., BLEICH, M., GERLACH, U., BARHANIN, J. & KIM, S. J. 2002. The role of KCNQ1/KCNE1 K(+) channels in intestine and pancreas: lessons from the KCNE1 knockout mouse. *Pflugers Arch,* 443**,** 822-8.

WEBB, R. C. 2003. Smooth muscle contraction and relaxation. *Adv Physiol Educ,* 27**,** 201-6.

WEGENER, J. W., SCHULLA, V., KOLLER, A., KLUGBAUER, N., FEIL, R. & HOFMANN, F. 2006. Control of intestinal motility by the Ca(v)1.2 L-type calcium channel in mice. *FASEB J,* 20**,** 1260-2.

WEISER, M., VEGA-SAENZ DE MIERA, E., KENTROS, C., MORENO, H., FRANZEN, L., HILLMAN, D., BAKER, H. & RUDY, B. 1994. Differential expression of Shaw-related K+ channels in the rat central nervous system. *J Neurosci,* 14**,** 949-72.

WETTWER, E., AMOS, G., GATH, J., ZERKOWSKI, H. R., REIDEMEISTER, J. C. & RAVENS, U. 1993. Transient outward current in human and rat ventricular myocytes. *Cardiovasc Res,* 27**,** 1662-9.

WICKENDEN, A. D., ZOU, A., WAGONER, P. K. & JEGLA, T. 2001. Characterization of KCNQ5/Q3 potassium channels expressed in mammalian cells. *Br J Pharmacol,* 132**,** 381-4.

WITZEL, K., FISCHER, P. & BAHRING, R. 2012. Hippocampal A-type current and Kv4.2 channel modulation by the sulfonylurea compound NS5806. *Neuropharmacology,* 63**,** 1389-403.

WOO, D. H., BAE, J. Y., NAM, M. H., AN, H., JU, Y. H., WON, J., CHOI, J. H., HWANG, E. M., HAN, K. S., BAE, Y. C. & LEE, C. J. 2018. Activation of Astrocytic mu-opioid Receptor Elicits Fast Glutamate Release Through TREK-1-Containing K2P Channel in Hippocampal Astrocytes. *Front Cell Neurosci,* 12**,** 319.

WOOD, J. D. 2002. Neuropathophysiology of irritable bowel syndrome. *J Clin Gastroenterol,* 35**,** S11-22.

WOOD, J. D. 2012. Nonruminant Nutrition Symposium: Neurogastroenterology and food allergies. *J Anim Sci,* 90**,** 1213-23.

WOOD, J. D., ALPERS, D. H. & ANDREWS, P. L. 1999. Fundamentals of neurogastroenterology. *Gut,* 45 Suppl 2**,** II6-II16.

XU, H., LI, H. & NERBONNE, J. M. 1999. Elimination of the transient outward current and action potential prolongation in mouse atrial myocytes expressing a dominant negative Kv4 alpha subunit. *J Physiol,* 519 Pt 1**,** 11-21.

YANG, D., SWAMINATHAN, A., ZHANG, X. & HUGHES, B. A. 2008. Expression of Kir7.1 and a novel Kir7.1 splice variant in native human retinal pigment epithelium. *Exp Eye Res,* 86**,** 81-91.

YARISHKIN, O., LEE, D. Y., KIM, E., CHO, C. H., CHOI, J. H., LEE, C. J., HWANG, E. M. & PARK, J. Y. 2014. TWIK-1 contributes to the intrinsic excitability of dentate granule cells in mouse hippocampus. *Mol Brain,* 7**,** 80.

YELLEN, G. 2002. The voltage-gated potassium channels and their relatives. *Nature,* 419**,** 35-42.

YEUNG, S. Y., PUCOVSKY, V., MOFFATT, J. D., SALDANHA, L., SCHWAKE, M., OHYA, S. & GREENWOOD, I. A. 2007. Molecular expression and pharmacological identification of a role for K(v)7 channels in murine vascular reactivity. *Br J Pharmacol,* 151**,** 758-70.

YEUNG, S. Y., THOMPSON, D., WANG, Z., FEDIDA, D. & ROBERTSON, B. 2005. Modulation of Kv3 subfamily potassium currents by the sea anemone toxin BDS: significance for CNS and biophysical studies. *J Neurosci,* 25**,** 8735-45.

YONEDA, S., KADOWAKI, M., SUGIMORI, S., SEKIGUCHI, F., SUNANO, S., FUKUI, H. & TAKAKI, M. 2001. Rhythmic spontaneous contractions in the rat proximal colon. *Jpn J Physiol,* 51**,** 717-23.

YUAN, X. J., WANG, J., JUHASZOVA, M., GOLOVINA, V. A. & RUBIN, L. J. 1998. Molecular basis and function of voltage-gated K+ channels in pulmonary arterial smooth muscle cells. *Am J Physiol,* 274**,** L621-35.

ZHANG, H., HE, C., YAN, X., MIRSHAHI, T. & LOGOTHETIS, D. E. 1999. Activation of inwardly rectifying K+ channels by distinct PtdIns(4,5)P2 interactions. *Nat Cell Biol,* 1**,** 183-8.

ZHOU, M., MORAIS-CABRAL, J. H., MANN, S. & MACKINNON, R. 2001a. Potassium channel receptor site for the inactivation gate and quaternary amine inhibitors. *Nature,* 411**,** 657-61.

ZHOU, M., XU, G., XIE, M., ZHANG, X., SCHOOLS, G. P., MA, L., KIMELBERG, H. K. & CHEN, H. 2009. TWIK-1 and TREK-1 are potassium channels contributing significantly to astrocyte passive conductance in rat hippocampal slices. *J Neurosci,* 29**,** 8551-64.

ZHOU, Y., MORAIS-CABRAL, J. H., KAUFMAN, A. & MACKINNON, R. 2001b. Chemistry of ion coordination and hydration revealed by a K+ channel-Fab complex at 2.0 A resolution. *Nature,* 414**,** 43-8.

ZHOU, Z., GONG, Q., YE, B., FAN, Z., MAKIELSKI, J. C., ROBERTSON, G. A. & JANUARY, C. T. 1998. Properties of HERG channels stably expressed in HEK 293 cells studied at physiological temperature. *Biophys J,* 74**,** 230-41.

ZHU, Y. & HUIZINGA, J. D. 2008. Nitric oxide decreases the excitability of interstitial cells of Cajal through activation of the BK channel. *J Cell Mol Med,* 12**,** 1718-27.

ZHU, Z., SIERRA, A., BURNETT, C. M., CHEN, B., SUBBOTINA, E., KOGANTI, S. R., GAO, Z., WU, Y., ANDERSON, M. E., SONG, L. S., GOLDHAMER, D. J., COETZEE, W. A., HODGSON-ZINGMAN, D. M. & ZINGMAN, L. V. 2014. Sarcolemmal ATP-sensitive potassium channels modulate skeletal muscle function under low-intensity workloads. *J Gen Physiol,* 143**,** 119-34.

# FORM UPR16

**Research Ethics Review Checklist**

Please include this completed form as an appendix to your thesis (see the Research Degrees Operational Handbook for more information

| Postgraduate Research Student (PGRS) Information | | | | Student ID: | 456122 |
|---|---|---|---|---|---|
| PGRS Name: | Ruolin Ma | | | | |
| Department: | PHBM | First Supervisor: | Dr Anthony Lewis | | |
| Start Date: (or progression date for Prof Doc students) | 01/02/2015 | | | | |
| Study Mode and Route: | Part-time ☐ | MPhil ☐ | MD ☐ | | |
| | Full-time ☒ | PhD ☒ | Professional Doctorate ☐ | | |

| Title of Thesis: | Identification and functional characterisation of potassium channels in mouse GI tract |
|---|---|
| Thesis Word Count: (excluding ancillary data) | 50,213 |

If you are unsure about any of the following, please contact the local representative on your Faculty Ethics Committee for advice. Please note that it is your responsibility to follow the University's Ethics Policy and any relevant University, academic or professional guidelines in the conduct of your study

Although the Ethics Committee may have given your study a favourable opinion, the final responsibility for the ethical conduct of this work lies with the researcher(s).

**UKRIO Finished Research Checklist:**
(If you would like to know more about the checklist, please see your Faculty or Departmental Ethics Committee rep or see the online version of the full checklist at: http://www.ukrio.org/what-we-do/code-of-practice-for-research/)

| | |
|---|---|
| a) Have all of your research and findings been reported accurately, honestly and within a reasonable time frame? | YES ☒ NO ☐ |
| b) Have all contributions to knowledge been acknowledged? | YES ☒ NO ☐ |
| c) Have you complied with all agreements relating to intellectual property, publication and authorship? | YES ☒ NO ☐ |
| d) Has your research data been retained in a secure and accessible form and will it remain so for the required duration? | YES ☒ NO ☐ |
| e) Does your research comply with all legal, ethical, and contractual requirements? | YES ☒ NO ☐ |

**Candidate Statement:**

I have considered the ethical dimensions of the above named research project, and have successfully obtained the necessary ethical approval(s)

| Ethical review number(s) from Faculty Ethics Committee (or from NRES/SCREC): | N/A |
|---|---|

If you have *not* submitted your work for ethical review, and/or you have answered 'No' to one or more of questions a) to e), please explain below why this is so:

| Signed *(PGRS)*: | Date: 16/01/2019 |
|---|---|

**UPR16** – April 2018